Application of Advanced Oxidation Processes for Organic Compound Removal from Saline Water

Pradip Saha

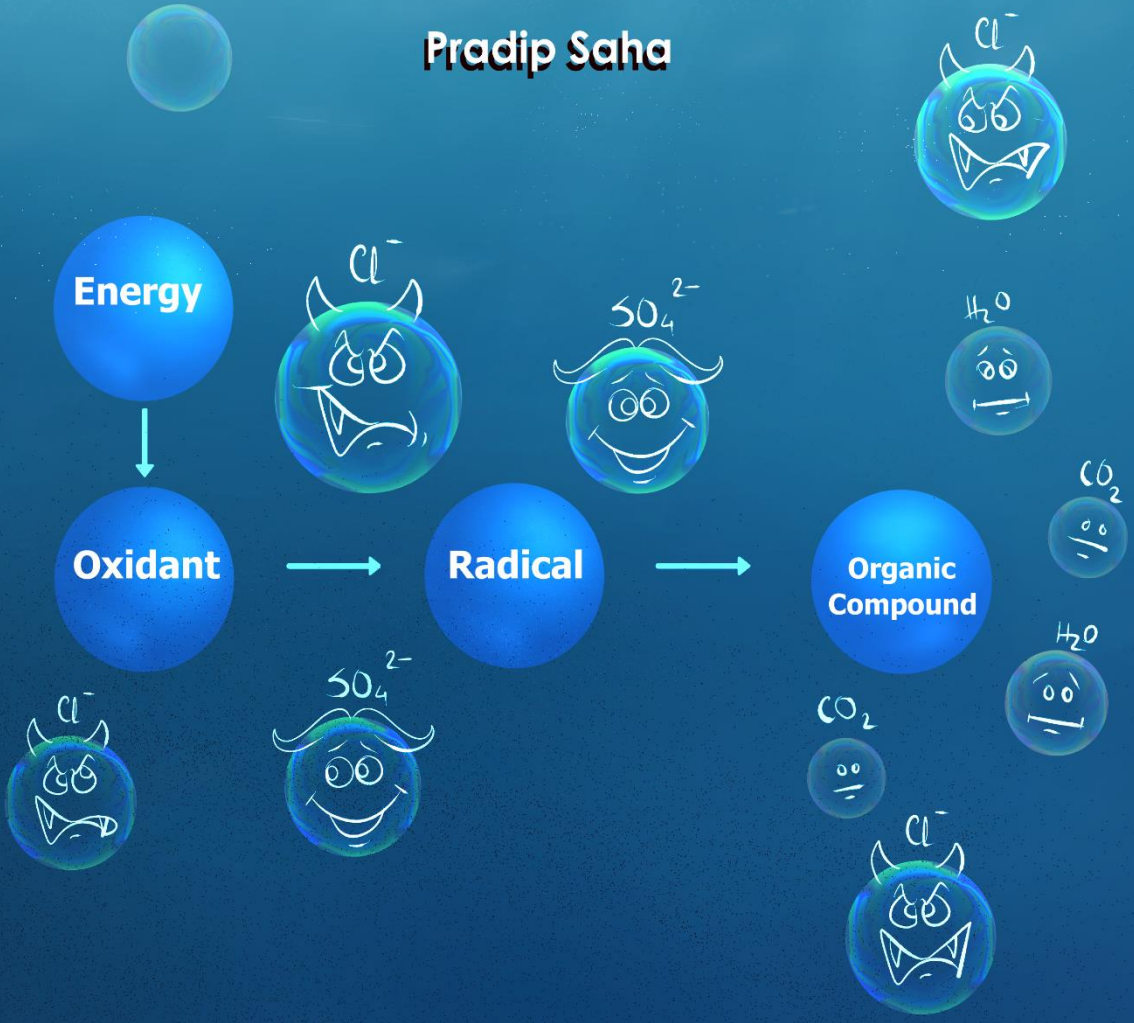

Propositions

1. Peroxydisulfate and Ultraviolet-based advanced oxidation processes effectively remove organic compound without toxic by-products formation in saline wastewater.
   (this thesis)

2. Electrochemical oxidation is only applicable when toxic by-product formation can be avoided. (this thesis)

3. In research articles overestimation and non-addressed uncertainty concerning real applications mislead the fellow researcher and the society.

4. In the scientific community technology readiness level is inversely proportional to research novelty.

5. An empathy-driven society is happier than a power-driven society.

6. Socio-economic conditions dictate the aim in life of individuals in developing countries.

Propositions belonging to the thesis, entitled

Application of Advanced Oxidation Processes for Organic Compound Removal from Saline Water

Pradip Saha
Wageningen, 16 February 2022

Application of Advanced Oxidation Processes for Organic Compound Removal from Saline Water

Pradip Saha

Thesis committee

Promotor

Prof. Dr H.H.M. Rijnaarts

Professor of Environmental Technology

Wageningen University & Research

Co-promotor

Dr H. Bruning

Assistant Professor, Environmental Technology

Wageningen University & Research

Other members

Prof. Dr J.H. Bitter, Wageningen University & Research

Prof. Dr S.Van Hulle, Ghent University, Belgium

Dr L.C.P.M. de Smet, Wageningen University & Research

Dr N.C. Boelee, Nijhuis Saur Industries, Doetinchem

This research was conducted under the auspices of the Graduate School for Socio-Economic and Natural Sciences of the Environment (SENSE)

Application of Advanced Oxidation Processes for Organic Compound Removal from Saline Water

Pradip Saha

Thesis
submitted in fulfillment of the requirements for the degree of doctor
at Wageningen University
by the authority of the Rector Magnified,
Prof. Dr A.P.J. Mol,
in the presence of the
Thesis Committee appointed by the Academic Board
to be defended in public
on Wednesday 16 February 2022
at 1.30 p.m. in the Aula.

Pradip Saha

Application of Advanced Oxidation Processes for Organic Compound Removal from Saline Water, 344 pages.

PhD thesis, Wageningen University, Wageningen, The Netherlands (2022)

With references, with summary in English and Dutch.

ISBN: 978-94-6447-045-1
DOI: https://doi.org/10.18174/558913

to my son and my soulmate

Table of contents

Chapter 1. *General introduction*

Cooling tower water: Quantity, quality, and advanced oxidation processes for organic compound removal.

1.1 INTRODUCTION: INDUSTRIAL WATER CONSUMPTION SCENARIO

Climate change has become visible by causing extreme water-related weather events like droughts and floods, directly affecting water quantity and quality. Water consumption increases two times faster than the population and is related to economic activity, energy and agricultural production, and domestic activity [1]. The united nations' organization emphasizes the interconnection of climate change and water in efforts needed to reach the Sustainable Development Goals (SDGs) and the Paris Agreement on Climate Change [1]. Several SDGs -for instance, zero hunger (SDG 2), accessibility to clean water and sanitation (SDG 6), clean energy production (SDG 7), sustainable industrialization (SDG 9 and 12), combat to climate change (SDG 13), and ecosystem services (SDG 15)- are directly linked to freshwater [2]. By 2050 more than 685 million people are projected to live in cities and urban areas with a sharp decline in freshwater availability. This freshwater availability may shrink by 30 to 50% for some cities like Cape Town, Melbourne, or Santiago. Global water demand will increase with 40% by 2030 and 55% by 2050 [3]. Industrial, energy generation and domestic water demand will increase with 400%, 140%, and 130%, respectively, between 2000 and 2050 [4]. Energy and industrial sectors are the other two water-intensive sectors responsible for 19% of total freshwater withdraw, which may increase to 24% by 2050 [1]. The energy sector was responsible for 10% of global water use. Globally 69% (2,769 km^3/yr.) of total freshwater withdrawal is going to be used for irrigation, which may increase another 5.5% by 2050 [5]. These huge water uses create massive pressures on the local and regional water cycles. Circular water management, including the 5Rs - reduce, reuse, recycle, restore, and recovery- are proposed to be part of the solution to overcome future water problems [6].

1.2 RESEARCH CONTEXT: WATER NEXUS PROJECT

Delta areas are considered as the world's economic hub because of accessibility to resources, transportation, land fertility, and industrial activity. Around one-third of the global population lives in the delta areas, which will increase with 50% to 4 billion by 2050. All these delta areas' industrial, agricultural, and domestic activities

heavily depend on an adequate freshwater supply. Freshwater is becoming severely scarce day by day due to increasing population, industrial and economic growth, and climate change [1, 7, 8]. The NWO-STW Water Nexus (WN) program aims to develop an integrated solution to deal with the water scarcity problems of delta areas worldwide by developing water quality and quantity management tools.

According to the program proposal, "The Water Nexus program aims at developing integral solutions for problems with freshwater scarcity in delta areas worldwide. The central paradigm shift within Water Nexus is to consider saline water as a resource instead of a threat: saline water where possible, freshwater where essential." [9]. Fig. 1-1. depicted that the saline water would be used where possible, and freshwater would only be extracted when it is the only option. In addition, an integrated treatment system would be incorporated within the water cycle to close the loop.

Fig. 1-1. *Illustration of water nexus project [9]*

The program consists of three interdependent research lines focusing on materializing the water nexus project motto "*saline water where possible, freshwater where essential.*" These research lines are:

Research line 1: Resource management and control

This research line was aimed to develop mapping and modeling tools to analyze the fresh and saline water distribution at the global to the local level. Essential tools were developed and studied to facilitate strategic and operational water management

based on the information. In addition, possibilities and limitations of saline water use at the plant root zone level were explored.

Research line 2: Treatment technologies

This research line was aimed to develop sustainable, selective, cost-effective biological and physical-chemical technologies to facilitate the (re)use of saline (waste)water as an alternative to a freshwater source. Anaerobic and aerobic granulation to remove organic substances at elevated salinity was studied. A stable anode was developed for electrochemical oxidation to remove persistent organic compounds in saline conditions. A new membrane was fabricated to selectively remove the organic (micro)pollutants and monovalent ions. Plant-microbial cells (PMC) were examined as a sensor for real-time monitoring of constructed wetlands (CWs) operation (also part of research line 3). The PhD project described in this thesis contributed to this research line and developed electrochemical and advanced oxidation processes to remove organic pollutants (anthropogenic and natural origin) from water as part of a treatment train to clean industrial saline waters and make these reusable. Based on the findings, an integrated treatment concept was proposed.

Research line 3: Integral blueprints

This research line was aimed to develop a dynamic demand and supply model to provide decision-making tools. In addition, a nature-based solution to treat saline industrial wastewater, constructed wetlands (CWs), was studied. In the end, an adaptive treatment train was studied to treat cooling tower water as a practical case provided by the end-uses of the water nexus project.

This Ph.D. thesis is part of research line 2 and contributed to research line 3 by studying the integration and application of the technologies studied in research lines 2 and 3 in offering an adaptive treatment for industrial water reuse, connected to an industrial case study.

1.3 DOW CASE STUDY

The DOW chemicals company is one of the three largest chemical industries globally and has the second-largest production facility in Dow Benelux Terneuzen, The Netherlands. This production site requires 22 million m^3 freshwater each year. Dow Benelux uses water from different freshwater sources, including 30% from

internal condensate, 25% from local surface water, 20% from large storage basins located in the Biesbosch nature area, 15% from DOW's treated wastewater, and 10% from treated municipal wastewater. Freshwater from Biesbosch is transported to the DOW location via a 120 km pipeline [10].

One of the four pillars of Dow's desire is to meet the sustainable development goals (SDG 9: sustainable industrialization). To do so, Dow aims to reduce their freshwater consumption by 20% and recycle 100% treated wastewater as an alternative to freshwater water sources before 2025 [10]. In this way, DOW wants to become independent of the water supply from the Biesbosch basins. In future scenarios of extreme drought, these basins may temporarily be made unavailable for industrial use. In addition, climate change and the competition between local agricultural, domestic, and industrial sectors may cause additional pressure on freshwater supply in the near future. Several water sources are available around the DOW location; however, water quality and quantities vary due to source and seasonal variation. Thus, treating them to make them usable is challenging. Fortunately, DOW produces large amounts of wastewater internally, which are not reused yet. The quality and quantities of this wastewater do not vary a lot over time [11]. The cooling tower of the Elsta power plant at the DOW complex discharges a large volume of wastewater during the operation. This discharge is called cooling tower blowdown water (CTBD). The quality and quantity of this CTBD remain stable for longer times [11]. This case study aims to develop and select an appropriate technology to treat the CTBD to be able to reuse the recovered water in the cooling tower as make-up water (feed water). The coming section of this chapter will give a general overview of a cooling system, cooling water, CTBD, and their treatment possibilities and challenges.

1.4 QUANTITY AND QUALITY OF COOLING TOWER WATER

1.4.1 Introduction to cooling tower system

Power generation, oil, gas, coal refineries, metals, and chemical industries are the major freshwater user in the industrial sector. The cooling system plays a vital role in these water-intensive industries [12]. 60%–70% of total industrial water is used in cooling systems [13]. In 2015, 290 km^3 of freshwater was withdrawn for

thermal power plants worldwide, whereas consumption was 18 km^3 [14]. In Europe, power plant cooling systems were responsible for 44 % of total freshwater abstraction [15]. In 2018 in The Netherlands, 5.8 km^3 freshwater was used for cooling systems in manufacturing and power generation companies, whereas the total water abstraction was 8.1 km^3 [16]. Reducing and reusing freshwater in cooling systems could significantly reduce the water footprint of the industries.

1.4.2 Cooling system and cooling tower:

Cooling systems are used to remove heat from industrial processes. Traditionally cooling system consists of two units (Fig. 1-2). i) a heat exchanger, where hot process liquid loses its heat to cooling water. ii) a cooling tower where hot cooling water is sprayed from the top of the tower and (cold) air passes from the bottom of the tower. Heat is dissipated as water vapor during the contact between hot water and air in the cooling tower. Due to water evaporation, the water temperature drops. Typically, one percent of the total cooling water is evaporated for each 5.5°C of cooling. The rest of the cooled water is sent back to the cooling loop. Water, called make-up water, is added to the cooling tower to compensate for the water loss due to evaporation and other losses, such as leakages.

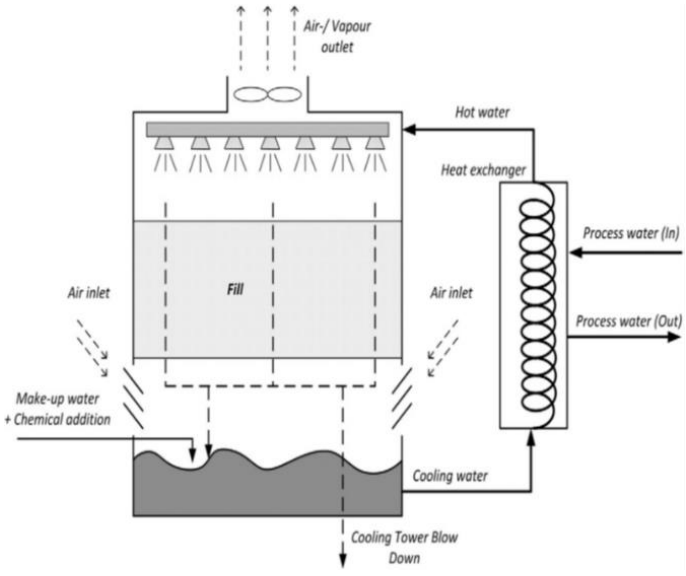

Fig. 1-2. *Schematic diagram of water flow across a counterflow cooling tower (figure from J. Löwenberg et al. (2015))[11].*

1.4.3 Operation challenges of cooling towers

Water evaporation increases the concentration of dissolved solids, suspended solids, microbes, and naturally occurring organic matter (NOM) in the cooling tower. The addition of make-up water reduces the concentration of the contaminant, but contaminants are also added. In continuous operation, the concentration of the pollutant in the circulating cooling water will increase, which eventually creates operational problems in the form of scaling, corrosion, and (bio)fouling [11].

Deposition of salts on the heat transfer surface causes scaling. Several ions are present in the cooling tower water, for instance, calcium and magnesium [17]. The precipitation of salts on the surface occurs due to increasing salts concertation, elevated temperature in the cooling tower, and local elevation of pH due to corrosion on the metal surface.

Deposition of suspended solids on the surface also causes fouling. Sand, silt, and iron oxides are potential solids causing fouling in the cooling tower. In addition, bacteria, algae, and fungi are the main microbes present in the cooling tower. The growth of these microbes forms biofilms on the heating surface. Continuous input of nutrients and minerals with make-up water, extensive heat transfer area, and warm temperatures favoring microbial growth in the cooling tower accelerate the biofouling problem.

Loss of mass or damage to a metal surface is called corrosion. Chemical and electrochemical reactions and microbial growth in the metal surface cause corrosion. Corrosion, biofouling, and scaling processes occur independently and mutually influence each other.

Due to scaling and (bio) fouling, the pipelines could clog. The heat transfer area could be covered by biofilms or mineral layers, decreasing heat transfer efficiency, increasing hydraulic resistance, increasing energy consumption, equipment breakdown, increasing operation and maintenance costs. Therefore, different physical and chemical mitigation methods are applied to reduce scaling, corrosion, and (bio)fouling. Chemical mitigation includes the addition of biocides, corrosion inhibitors, antiscalants and dispersants, and surfactants to the cooling tower water [18]. Biocides, used to mitigate biofouling, are divided into oxidative and non-oxidative biocides. Various inorganic and organic chemicals are used in the cooling

tower as corrosion inhibitors, including chromate, nitrate, zinc, (ortho, poly)phosphate, copolymers, and benzotriazole. A detailed list of conditioning chemicals used in cooling towers is reported elsewhere [18].

Continuous evaporation of cooling water increases the electrical conductivity due to increasing salts concentration. During recirculating water in the cooling tower operation, electrical conductivity is maintained to a threshold value (4500 μS/cm) [17]. When the circulating water reaches a conductivity higher than the threshold value, the concentrated water is discharged as cooling tower blowdown water (CTBD) to maintain the salt concentration below the threshold level. Typically 10%-20% cooling water is discharged as CTBD [11]. In order to maintain the constant water level in the cooling tower, make-up water is added. In most cases, make-up water is collected from a freshwater source. Environmental regulations restrict the industries from discharging the CTBD in the water body without proper treatment. Because of its large volume, this CTBD, when recovered and treated, could be an attractive water source to reduce industrial freshwater consumption. This is very attractive to industries in fresh water-stressed areas. The reuse of treated CTBD can decrease up to 15% of the make-up water uptake, significantly reducing the industrial water footprint [19].

1.4.4 Cooling tower water quality

The CTBD mainly contains salts and organic compounds. Characteristics of different CTBD are given in Table 1-1. The CTBD composition differ significantly based on the source of make-up water used and the cycle of concentration (CoC)-the ratio of total dissolved solids in the CTBD and the make-up water. A cooling tower using surface water as make-up water is operated at 3 to 5 CoC. CTBD shows neutral to slightly alkaline properties. Conductivity, one vital marker for operating the cooling tower, varies between 600 to 4500 μS/cm. CTBD contains dissolved chloride, sulfate, phosphate, sodium, calcium, magnesium ionic species, and organic compounds. The primary source of the organic compounds in the CTBD is the natural organic matter (NOM) present in the make-up water and the conditioning chemicals added to the cooling tower during operation [18].

Table 1-1. *Composition of different CTBD water*

Parameter	Unit	Kim et al. (2001) [20]	Wang et al. (2006) [13]	Zhang et al. (2007; 2008) [21, 22]	Löwenberg et al. (2015) [11]	Groot et al. (2015) [17]	Davood Farahani et al. (2016) [23]	Pinel et al. 2020 [24]	Paranjape et al. 2020 [25]	H.I. Abdel-Shafy et al. (2020) [26]	X. Li, et al. (2020) [27]
Temperature	ºC	-	4-40	5-21	19±1.2	20-30		15-25	9-29	-	-
pH	-	8.2	7.8-9.3	8.2-8.75	7.9±0.2	7.5-8.5	6.7-7.2	7.5-7.9	8.2-8.9	7.8	8.1-8.5
COD	mg/L	-	0-10	3-4.8	-	-	181			-	63-68
TOC	mg/L	-	-	-	59±1.5	40-60		34-56	6-41	-	-
Electrical conductivity	µs/cm	2150	1650-2100	1300-2000	3620±810	3500-4500	2928	3000-3500	600-1400	-	3120-3209
Turbidity	NTU	-	-	5-23	7±1	-	73.6	1-13	1-58	6.5	-
Total suspended solids (TSS)	mg/L	-	5-80	7-22	12±4.6	<15	-	-	<100	1100 (TDS)	-
Calcium	mg/L	544	-	-	487±12	350-600	-	-	-	365	-
Magnesium	mg/L	236	-	-	63±1.4	40-80	-	-	-	260	-
Alkalinity	mg/L $CaCO_3$	-	-	350-370	-	-	1350	800-1300	-	100	189-493
Chloride	mg/L	188	-	-	500	400-600	-	400-550	-	151	-
Phosphate	mg/L	404	-	1.1	5±1	5-15	-	6-9	<3	6	5.6-6.3
Silica	mg/L SiO_2	-	-	50-200	0.9±0.2	-	-	-	-	24	-

To reuse the CTBD in the cooling tower itself, treated CTBD needs to meet the make-up water quality requirements. C. K. Groot et al. (2015) propose that electrical conductivity, total suspended solids, chloride, phosphate, and total organic carbon (TOC) concentration of the treated CTBD should be less than 1000 µS/cm, one mg/L, 150 mg/L, and 15 mg/L, respectively [17]. The extent of treatment (EoT) depends on the CoC and can be calculated as EoT (%) = (1-1/CoC)×100. Table 1-2 shows the EoT required at different CoC in terms of electrical conductivity. The DOW cooling tower operates at a CoC of 4; therefore, the extent of treatment and recovery should be around 75% of the CTBD to meet the make-up water quality.

Table 1-2. *relation of CoC with the extent of treatment*

Water	Electrical conductivity	Extent of treatment (EoT)
make-up	1000 µS/cm	-
CoC: 2	2000 µS/cm	50%
CoC: 3	3000 µS/cm	66%
CoC: 4	4000 µS/cm	75%
CoC: 5	5000 µS/cm	80%
CoC: 10	10000 µS/cm	90%

1.5 COOLING TOWER WATER TREATMENT TECHNOLOGIES

1.5.1 Desalination technologies and necessity of organic compounds removal before desalination

Salinity is the vital parameter needed to achieve a conductivity <1000 µs/cm to enable the reuse of the CTBD in the cooling tower itself [17]. Several desalination techniques have been studied to remove the salts from CTBD and reduce the conductivity to the desired level.

The traditional desalination processes are soda-lime softening [28] and brine evaporation [29]. In the Soda-lime process, lime and soda ash are added to the blowdown water to precipitate Ca^{2+}, $Mg^{2+,}$ and silica. However, other ions such as Na^{+}, K^{+}, SO_4^{2-}, and Cl^{-} remain in the blowdown water. Thus it is not suitable for reuse after the Soda-lime process. Besides, a large sludge formation is a major drawback of this process. Brine evaporation is capable of producing high-quality water with over 98% recovery. Unfortunately, this process consumes 26-83 kWh

energy per cubic meter of water treated, while a typical membrane desalination process consumes 2-20 kWh energy per cubic meter water treatment [30, 31].

Over the last few decades, membrane technologies have developed a lot and have become commonly used desalination processes because of their reliability and economic feasibility. Different membrane technologies, including nanofiltration (NF), reverse osmosis (RO), electrodialysis, membrane capacitive deionization, and membrane distillation, have been studied for CTBD water desalination [11, 17, 19, 22, 23, 32-34]. Among those, nanofiltration and reverse osmosis are more mature and are used for desalination in different sectors. However, electrodialysis, membrane capacitive deionization, and membrane distillation are more recently developed technologies and need further improvement to ensure reliability, economic/energy efficiency, and environmental sustainability [17].

Several authors studied nanofiltration, electrodialysis, capacitive deionization, and membrane desalination to treat DOW CTBD [11, 17, 33, 34], the same CTBD used in this thesis. Experimental results show that all the processes could produce water at required conductivity suitable to reuse as make-up water in the cooling water. However, electrodialysis and capacitive deionization were unable to meet the required TOC level [35]. In addition, the nanofiltration methods faced fouling problems due to accumulated NOM in the water and required pretreatment [35]. In membrane distillation, the membranes show outstanding stability with respect to NOM and produce water with conductivity less than 100 μS/cm [34]. Membrane distillation can use waste heat to operate, which reduces the loading in the cooling tower and reduce overall water intake by 37%. In comparison, nanofiltration could reduce only 15%. However, the flux of membrane distillation is 10 to 20 times lower than pressure-driven membrane desalination, such as nanofiltration and reverse osmosis [34, 35]. This is one of the significant bottlenecks of membrane distillation application. In addition, L.D. Tijing et al. (2015) reported that membrane distillation also encountered organic fouling because of NOM, even though N.E. Koeman-Stein et al. (2016) found otherwise [34, 36]. Normally, hydrophobic microfilter membranes are used in membrane distillation, which is prone to organic fouling due to NOM [37]. However, the membrane distillation fouling mechanisms would differ from the pressure-driven process because of different membrane configurations and operating conditions [36, 37]. Moreover, pressure-driven processes undergo regular backwash and chemical cleaning to control fouling, which is impossible in

membrane distillation. Thus, the fouling in the membrane distillation and its mitigation needs further study before large-scale application. Nevertheless, all membrane processes encounter problems with membrane fouling, including organic/mineral abiotic fouling and biofouling, due to natural organic matter (NOM) and conditioning chemicals in the CTBD water [38]. These fouling problems ultimately reduce the membrane performance and hinder the application membrane processes.

The detailed characteristics of the NOM are described elsewhere and given in Fig. 1-3 [39]. In short, the NOM consists of humic acid, fulvic acid, protein-like recalcitrant polymeric substances, polysaccharides, and other compounds. Humic acids are comparatively higher molecular fractions, and fulvic acids are moderate molecular weight fractions of the NOM. Humic substances, a combination of humic and fulvic acids, comprise aromatic and aliphatic hydrocarbons containing carboxylic and phenolic groups. This fraction of the humic substance is also called allochthonous NOM. The adsorption of the humic substance on the membrane surface depends on chemical interactions, electrostatic forces, and hydrophobicity of the membrane [40]. Based on the adsorption mechanisms involved, the humic substances can block the pores of the membranes, aggregate on the surface to form a gel-like layer, and bind with particles to form a particle/humic substance layer on top of the membrane. At low pH, humic macromolecules show affinity to hydrophobic membranes because acidic moieties are associated with protons at lower pH, i.e., making the compounds neutral or even positively charged when the pH is below the iso-electric point of the humic substances [32].

Studies show that microfiltration membrane, used in membrane distillation, is more prone to fouling due to NOM than the UF membranes. Also, MF is less suitable for backwash [40]. Water with high molecular weight polysaccharides, high hydrophilic, protein-like and low humic compounds shows the organic fouling tendency to all membrane types. This organic fouling is hydraulically irreversible [36, 37, 41-44]. Aggressive chemicals like sodium hydroxy can remove the organic fouling initiated by the polysaccharides and protein-like substances. In contrast, washing with hypochlorite is required for removing the humic substrate-based fouling [36]. Chemical cleaning of the membrane reduces the lifetime of the membrane and needs more frequent replacement.

.

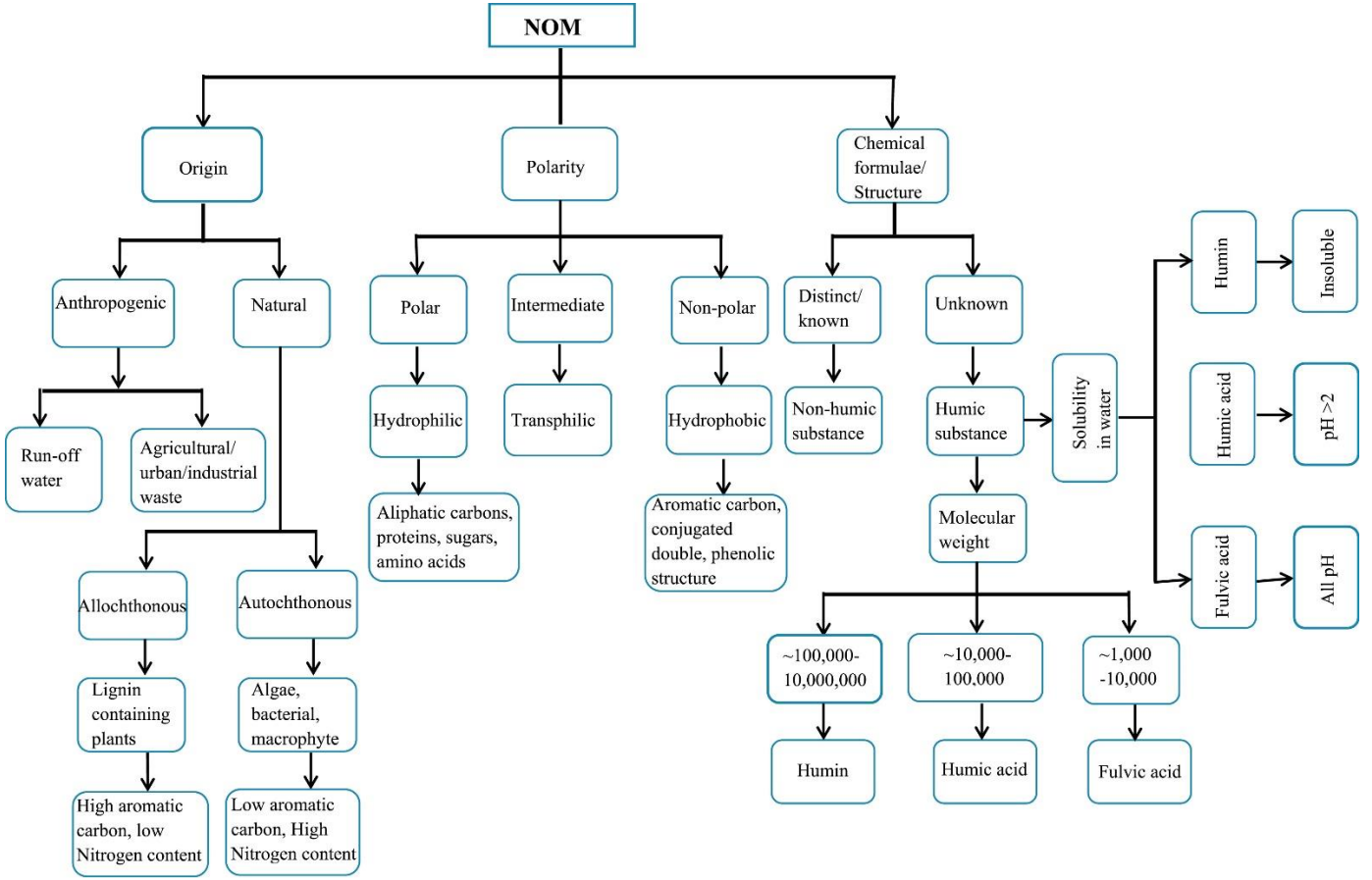

Fig. 1-3. *An overview of NOM characterization (figure from J. Adusei-Gyamfi et al. (2019))[39.]*

Ion exchange membranes used in electrodialysis and capacitive deionization are also vulnerable to organic fouling due to NOM [43, 45]. Kobus and Heertjes (1973) show that negatively charged humic acids could sorb on positively charged anion exchange membrane surfaces, increasing membrane resistance. Low molecular weight multivalent humic acids fractions were more prone to sorb on the ion exchange membrane [46]. The activated carbon electrode, the main component of the capacitive deionization technology, is challenged by fouling with humic acid. Humic acid is adsorbed in the electrode's active side (mesopores) and does not desorb during the discages/regeneration step [41]. Thus the electrode loses its capacity to remove ions, specially monovalent ions. In addition, flux through the membrane is reduced, and the energy consumption increases due to humic acid fouling. M. Mossad L. Zou (2013) recommended pretreatment to remove the humic substance before capacitive deionization to maintain maximum performance [41].

In addition to NOM, conditioning chemicals were also shown to trigger membrane fouling [18]. Scale and corrosion inhibitors can adsorb on the membrane surface, leading to a change in the surface charge and hydrophobicity. In addition, excess free chlorine, ozone, and hydrogen peroxide added as biocide could damage the membrane structure. Moreover, phosphorus-based organic conditioning chemicals are a suitable feed for microbial growth, which leads to biofouling on the membrane surface [47]. Therefore, effective pretreatment is essential before membrane-based desalination technology to retain membrane performance, increase the membrane lifetime, and reduce operational and maintenance costs.

1.5.2 Cooling tower blowdown (CTBD) pre-treatment technologies

A pretreatment of CTDB, removing NOM and the conditioning chemicals before the membrane process, is a prerequisite to reduce the membrane fouling, energy consumption, operational cost, maintenance cost, and increasing the membrane lifetime. Several studies have been conducted to pretreat CTBD before the water enters membrane units. For instance, microfiltration (MF) [48], integrated sand filtration- MF [13], coagulation (Polyaluminium chloride, $FeCl_3$), powdered activated carbon (PAC) adsorption [11, 23], and ultrafiltration (UF) has been investigated as pretreatment for RO or NF [21-23, 49, 50]. All the studied pretreatment processes can remove particles and turbidity from CTBD water and

improve the reverse osmosis (RO) or nanofiltration (NF) desalination performance. J. Zhang et al. (2007and 2008) and Huiming Zeng (2009) showed that MF and UF could maintain water quality suitable for RO treatment. However, CTBD in those studies contains very little organic compounds (< 5mg/L COD) [21, 22, 49]. Z. Liao et al. (2009) and H.I. Abdel-Shafy et al. (2020) only focused on removing hardness and silica [26, 51]. J. Löwenberg et al.(2015) studied different pretreatment technologies, including adsorption with powdered activated carbon (PAC), coagulation with ferric chloride, and ultrafiltration (UF) to remove the organic contaminants from CTBD [11]. The CTBD used in that study contained 59 mg/L dissolved organic carbon (DOC) comprised of 4 mg/L biopolymers, 37 mg/L humic substances, 6 mg/L building blocks, and 5 mg/L low molecular weight (LMW) substances. Results show that UF was able to remove the turbidity and the suspended solids. PAC and UF showed a limited capacity to remove humic substances. It was concluded that both the humic substance and the conditioning compounds were smaller than the pore size of the UF membrane. A thin irreversible fouling layer of biopolymers faction was found on the UF surface. Biopolymers are the largest fraction of the NOM. Only a tiny fraction of the low molecular fraction of the DOC was removed by the PAC. This indicates that CTBD may contain hydrophobic compounds which hinder the humic substance's adsorption on the PAC [11]. Coagulation with 20 mg/L Fe^{3+} at pH 5.5 yielded a complete removal for biopolymers, partial for humic substances, and building block chemicals. However, the turbidity of the treated CTBD was higher than the untreated CTBD due to the complexation of hydroxylated iron and the organic substance like antiscalants. Thereby, the high-pressure membrane process still faces the challenge of fouling caused by the OC in the CTBD water [11, 35]. Over the last few decades, advanced oxidation processes (AOPs) have become attractive to remove organic compounds, including NOM and the recalcitrant compound like benzotriazole, added as a corrosion inhibitor in the cooling tower [52, 53].

1.6 ADVANCED OXIDATION PROCESS FOR ORGANIC COMPOUNDS REMOVAL

1.6.1 Principle of Advance oxidation process for OCs removal

According to Glaze et al. (1987), Advance oxidation processes (AOPs) are defined as "near ambient temperature and pressure water treatment processes which involve the generation of hydroxyl radicals in sufficient quantity to affect water purification" [54]. However, high temperature or pressure is also used to generate hydroxyl radicals nowadays. So AOPs can be defined as a water treatment process in which highly reactive hydroxyl radicals ($HO^{\bullet}$) form, facilitating the degradation of organic compounds to CO_2 and water. AOPs have gained much attention as an advanced water treatment technology to remove all kinds of organic compounds and disinfection methods. Numerous AOPs studies have been reported to remove persistence, toxic, non-biodegradable, micropollutants, pesticides, dyes, pharmaceuticals, personal care products, hormones, and industrial organic pollutants [55-57]. Hydroxyl radicals ($HO^{\bullet}$) have a standard oxidation potential of 2.7V/SHE and 2.3 V/SHE (standard hydrogen electrode) at pH 7. Several processes can be applied to generate $HO^{\bullet}$, such as Fenton-based, photochemical, photocatalytic, photolytic, electrochemical, Ozon-based, sonolytic, gamma-ray/electron beam-based, persulfate based and super-critical processes (Fig. 1-4) [55].

In general, AOPs can be used as pretreatment to remove organics before the membrane-based process to protect the membrane or increase the biodegradability of non-biodegradable compounds before a biological treatment (prior to membrane treatment). Also, AOPs could be used as post-treatment to remove micropollutants, pathogens, and toxic compounds [58]. The application of AOPs in saline conditions faces challenges because the presence of chloride can lead to the formation of unwanted chlorinated by-products and transformation products [59].

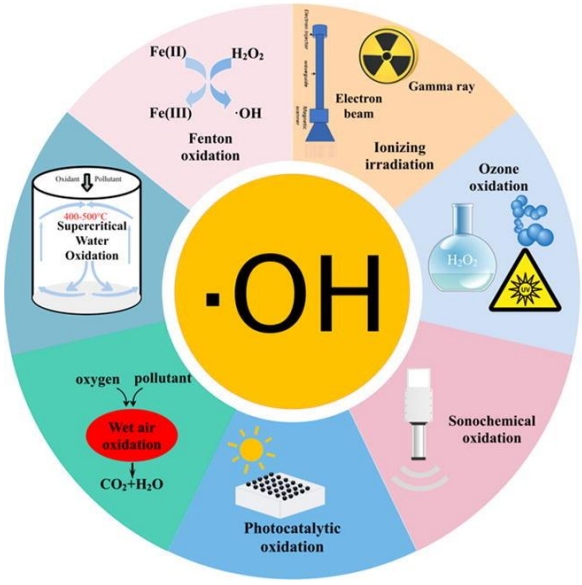

Fig. 1-4. *Possible hydroxyl radicals ($HO^{\bullet}$)-based advanced oxidation processes (figure from J. Wang, R. Zhuan (2020)) [57].*

These by-products can be even more toxic or more persistent than the parent compounds. Several factors influence the harmful by-product formation, including the composition of reactive chlorine species formed in the AOPs, their interaction with the organic compounds, and operating conditions [60].

Thus, a proper understanding of the chloride chemistry for each AOPs is essential for their application in saline conditions. In the following section, electrochemical oxidation (EO), photocatalytic degradation (PCD), persulfate-based oxidation (PS), ultraviolet-based processes (UVC), and UVC/vacuum UV (UVC/VUV) are elaborated. In this thesis, special attention is given to the EO.

1.6.2 Electrochemical oxidation

The electrochemical oxidation (EO) process is considered a robust clean, and powerful technique for treating a wide range of pollutants, including persistent organic compounds in various wastewater streams. EO process has several advantages over other methods, such as no external chemicals are needed, and the process can run at normal temperature and pressure [61]. Moreover, this robust

technology can withstand variations of incoming wastewater quality and quantity and can be easily integrated with other treatment technologies [62].

In the EO process, electrons are transferred to the electrode. In this process, in-situ generated strong oxidizing species; for instance, hydroxyl radical ($HO^{\bullet}$), peroxydisulfate, active chlorine species can degrade a wide variety of compounds [63, 64]. In recent years, EO has been applied to remove organic compounds, including dyes, pesticides and herbicides, pharmaceuticals, hormones, plasticizers, perfluorinated chemicals, and industrial chemicals [65-68]. The degradation of the organic compounds can take place in anode surface (direct oxidation) and/or in the bulk solution (mediated oxidation) depending on the anode material and electrolyte properties (Fig. 1-5) [69]. For an effective EO system, a proper selection of electrode material and operational conditions should be made [70].

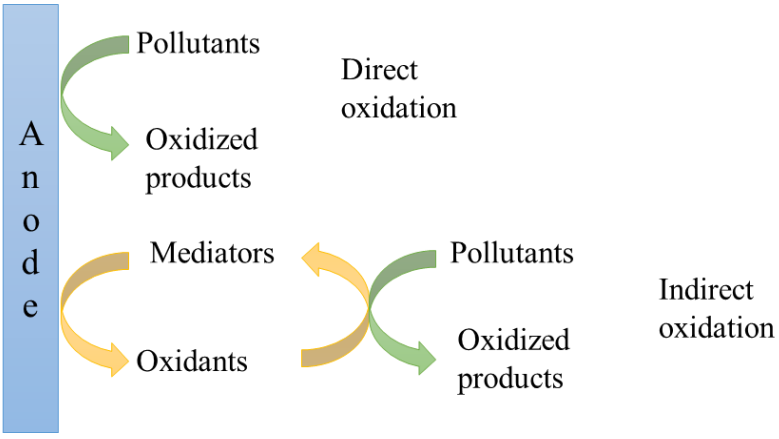

Fig. 1-5. *Schematic of a direct and indirect electrochemical oxidation process*

The selection of anode material is the most important since it directly affects the process selectivity, efficiency, partial/complete conversion, and toxic by-product formation [71]. Electrodes are divided into active and nonactive anodes based on the interaction between hydroxyl radical and anode surface. The hydroxyl radical is covalently attached to the active anode surface, whereas hydroxyl radical is physisorbed on the nonactive anode [72]. Most of the anodes show mixed behavior [69]. For the last couple of decades, mixed metal oxide (MMO; e.g., RuO_2, IrO_2, PbO_2, SnO_2) electrodes, known as dimensionally stable anodes (DSA), have been used for the EO process [73]. IrO_2 and RuO_2, considered active anodes, have a low overpotential for O_2 evolution and, therefore, low current efficiency and only partial

oxidation of recalcitrant organic compounds can be reached [69]. However, because of their corrosion resistance, IrO_2 and RuO_2 electrodes are still attractive for wastewater treatment.

On the other hand, PbO_2 and SnO_2 are considered nonactive anodes and have a high O_2 evolution overpotential. Therefore, those electrodes can achieve higher current efficiency with complete oxidation of persistent organic compounds at lower energy costs [69]. Industrial applications of PbO_2 and SnO_2 electrodes are limited because of the short service life of the SnO_2 electrode and the dissolution of Pb ions in the treated water during electrochemical oxidation with PbO_2 electrodes [66]. Magneli phase suboxides of TiO_2 and doped-TiO_2 are attractive electrode materials for water treatment due to their high overpotential for O_2 evolution, low-cost starting materials, excellent corrosion resistance, and electrical conductivity [66]. However, more studies need to be carried out to understand electron transfer mechanisms at the surface, increasing their stability and application in wastewater treatment.

Boron-doped diamond (BDD) electrodes are the most widely studied electrodes for the EO process. Compared with MMO anodes, BDD anodes have high O_2 evolution overpotential, making them better for the direct oxidation of contaminants with high current and removal efficiency [63]. The operational potential window of the BDD anode may exceed 3V/SHE since the hydrogen and oxygen evaluation takes place at about -1.25V and +2.3V/SHE, respectively [74]. In addition, high corrosion resistance, low adsorption properties, and being less prone to deactivation make BDD anode suitable for treating a large variety of organic compounds [71]. However, due to the high production costs and poor mechanical stability of the diamond film (film delamination), the large-scale application of BDD anode is still limited [66]. The selection of the suitable electrode for particular conditions on a theoretical basis is still challenging due to the complexity of the electrode performance [75]. Therefore, extended studies at actual conditions need to be carried out to select the electrode material properly.

As mentioned previously, the organic compounds can be oxidized directly or indirectly (Fig. 1.5). In direct oxidation, organic compounds are oxidized on the anode surface by physically absorbing active oxygen or chemically adsorbed active oxygen in the oxide lattice [76, 77].

The substrate limits direct oxidation efficiency since the concentration of the targeted compound at the anode surface is very low [78]. In addition, a poisonous effect is observed during direct oxidation due to the formation of a polymer layer on the electrode surface. This polymer layer formation depends on the electrode surface property, concentration, and properties of the organic compound and their intermediates formed during oxidation. Polymer layer formation can be prevented by oxidizing at a high potential [69, 79, 80]. However, current efficiency in high potential decreases due to the oxygen evolution reaction [69]. In the indirect process, the oxidation of organic pollutants takes place in the bulk solution through the in-situ anodic generation of hydroxyl radicals, free chlorine/active chlorine species [81], peroxodisulfuric [82], ozone [70], or cathodic generation of hydrogen peroxide [83]. Active chlorine is the common oxidant present in the electrochemical process because of the direct oxidation of chloride [80]. The extensive formation of active chlorine is due to chloride's abundant presence in wastewaters [84]. However, the role of active chlorine is controversial in the oxidation of organic pollutants [70]. Different research reported that EO of NaCl containing wastewater produces active chlorine species such as hypochlorite, chlorine dioxide, and chlorine, which could significantly improve the overall electrochemical removal of organic pollutants. The active chlorine oxidizing power and their concentration are dependent on EO operation conditions such as solution pH, operation time, and electrode material [81, 85]. Several researchers have shown that the EO of chloride-containing wastewater forms perchlorate (ClO_4^-). Active chlorine reacts with an organic compound and forms chlorinated organic compounds measured as adsorbable organic compounds (AOX) [86]. Those by-products are more toxic than the mother organic compounds [75]. Very few studies have been focusing on the formatting of AOX. However, Anglada et al. speculate that the pH greatly influences AOX formation, applied current density, and electrolytes concentration and composition [70]. A. Donaghue and co-authors mention that the formation of ClO_4^- is significantly slower, and optimum operating conditions could potentially reduce ClO_4^- formation in the EO process [87]. According to the above discussion and literature, it can be concluded that electrode material, operating conditions, concentration, and the chemical properties of the targeted organic compounds affect the performance of EO of organics in saline wastewater [79]. In addition, different authors mention that degradation of organic compounds can follow different routes, which makes it even

more complicated to predict the actual influence of operating parameters [81]. In addition, the impact of parameters is interconnected; thus, process optimization is a challenging task.

Nowadays, integrating the EO process with other technologies (electrodialysis reversal (EDR), biological and membrane process) has become a hot topic within the scientific world [88]. For instance, integrating the EO process with secondary treatment (concentration of organics) is required when organic chemicals are present at very low concentrations. Because in low concentration conditions, the EO process is economically and technically unfeasible due to mass transfer limitations. If these wastewaters contain chloride, then the oxidation of the organic compounds can take place in the bulk solution by the active chlorine produced during EO. However, when a high concentration of chloride is present in the wastewater, there is a possibility to form chlorate and perchlorates. In addition, AOX is formed during the EO of organic compounds in the presence of chloride in the wastewater. In these cases, the removal of chloride is suggested before the EO of an organic compound. A couple of studies show that integrating membrane filtration with EO technology could be an interesting strategy for improving the EO treatment of wastewater polluted with organics [84, 89]. However, more study is required for EO and membrane process integration. Case-specific integrated scenarios need to be built before applying EO and get the maximum benefit of the process. To the best of our knowledge, the application and integration of EO for CTBD treatment have not been studied yet.

1.6.3 Sulfate radical based oxidation

In recent years, sulfate radical-based ($SO_4^{\bullet -}$) oxidation has become attractive for persistent organic compound removal because of the high $SO_4^{\bullet -}$oxidation potential (E^o=2.60 V/SHE) and strong reactivity with organic compounds. Also, it performs well at a wide pH range as compared with the $HO^{\bullet}$ radical-based process. Peroxydisulfate (PDS) and peroxymonosulfate (PMS) are the most suitable oxidants for sulfate radical formation. PDS and PMS properties are listed in Table 1-3. PDS and PMS can be activated in different ways, including the use of heat, ultraviolet light, ultrasound, transition metal ions, phenol, carbonaceous materials, quinones, and alkaline conditions [90]. From an application point of view, heating is an effective way to activate PDS and PMS. Because each mole of PDS and PMS yields

two moles of radicals during heat activation, while transition metal activation yields only one mole of radicals (Eq. 1.1).

$$S_2O_8^{2-} + M^{n+} \rightarrow SO_4^{2-} + SO_4^{\bullet-} + M^{n-1} \quad (1.1)$$

Additionally, the competitive reaction of $SO_4^{\bullet-}$ with the excess catalyst and organic compounds reduces the available radicals and reduces performance [91]. Moreover, waste heat from industry, abundant in the case of CTBD, can be used to activate the PDS and PMS, reducing the energy requirement during application. Furthermore, no additional chemicals are required in the heat activation process, making this process simple and easy to operate. No extra post-treatment step is necessary to remove the catalyst.

Table 1-3. *Peroxydisulfate (PDS) and peroxymonosulfate (PMS) properties*

Properties	**PDS**	**PMS**
Molecular formula	$Na_2S_2O_8$	$2KHSO_5 \cdot KHSO_5 \cdot K2SO_5$
Structure	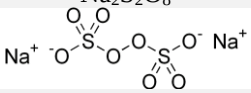	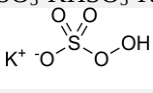
Molecular Weight	238.092 g/mol	614.738 g/mol
Solubility	73 g/100 g of H_2O at 25°C	25.6 g/100 g of H_2O at 20°C
Redox potential	2.01V	1.82V

At temperatures above 50℃, the O-O Bond bonds in PDS and PMS are equally broken down to form radicals (Eqs. 1.2-1.3) [90]. At a further temperature increase, the radical formation rate increases [92, 93]. Several studies show that alkaline conditions promote the reaction between PDS with the hydroxyl ion to produce $SO_4^{\bullet-}$, which can be further transformed into $HO^{\bullet}$, given in Eqs. (1.4) – (1.6) [90, 92, 94].

$$S_2O_8^{2-} + \Delta \rightarrow 2SO_4^{\bullet-} \quad (1.2)$$

$$SO_4\text{-}OH^- + \Delta \rightarrow 2SO_4^{\bullet-} + HO^{\bullet} \quad (1.3)$$

$$S_2O_8^{2-} + 3OH^- \rightarrow 2SO_4^{2-} + HO_2^- + H_2O \quad (1.4)$$

$$S_2O_8^{2-} + HO_2^- \rightarrow SO_4^{2-} + SO_4^{\bullet-} + O_2^{\bullet-} + H^+ \quad (1.5)$$

$$SO_4^{\bullet-} + OH^- \rightarrow SO_4^{2-} + HO^{\bullet} \quad (1.6)$$

As indicated above, the solution pH influences the sulfate radical formation. Sulfate radicals become dominating oxidative species at acidic conditions (pH <6). At pH between 7 and 9, both sulfate and hydroxyl radicals coexist, and hydroxyl radicals become dominating at pH higher than 9 (Fig. 1-6) [91, 95]. At higher pH, sulfate radicals react with hydroxyl ions to produce hydroxyl radicals shown in Eqs. (1.7) and (1.8) [96]. However, the sulfate and hydroxyl radical reactions can form PMS, ultimately reducing the available radical count Eq. (1.9).

$$SO_4^{\bullet-} + H_2O \rightarrow HO^{\bullet} + HSO_4^- \quad (1.7)$$

$$SO_4^{\bullet-} + OH^- \rightarrow HO^{\bullet} + SO_4^{2-} \quad (1.8)$$

$$SO_4^{\bullet-} + HO^{\bullet} \rightarrow HSO_5^- \quad (1.9)$$

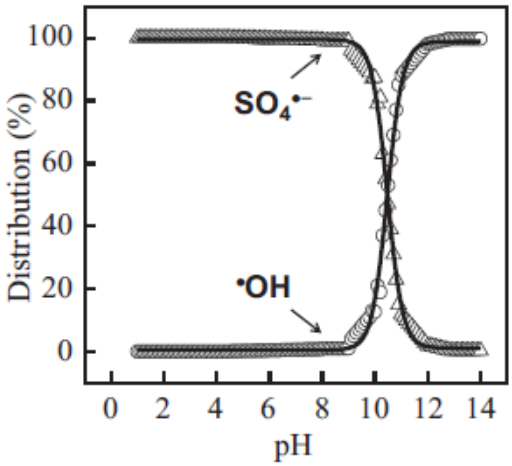

Fig. 1-6. *pH effect on radical species distribution in pure water (Figure from G.-D. Fang et al. (2012))[95].*

Hydroxyl radicals react with a wide range of organic compounds, whereas sulfate radicals are more selective. Sulfate radicals predominantly undergo electron transfer reactions with an organic compound, whereas hydroxyl radicals prefer hydrogen atom transformation and addition reactions [97]. Carbon-carbon double bond and aromatic ring with the reactive functional group show higher reactivity with sulfate radical in persulfate-based oxidation. However, saturated and halogenated hydrocarbon remain stable in the same condition. Sulfate radical-based

oxidation effectively degrades perfluorinated compounds, which remain stable in hydroxyl-based processes [98].

Chloride ions can influence the sulfate radical-based oxidation more compared to hydroxyl radical-based oxidation. The reaction between chloride and sulfate radical, producing chloride radical atoms ($Cl^{\bullet}$) (Eq. 1.10), is not influenced by pH, whereas reaction with hydroxyl radical dominates at acidic conditions. During AOPs, organic compounds are oxidized and broken down into low molecular compounds. These compounds can react with reactive chlorine radicals to form AOX. In addition, chloride ions can react directly with PDS and PMS to form free chlorine, which also reacts with organic substances and forms AOX. AOX can be toxic to ecosystems and human health [99, 100]. With active radicals, chloride can be converted to toxic ClO_3^- and ClO_4^- (Eq. 1.11) [101]. Most of the sulfate radical based-AOPs studies were conducted on a lab-scale with mostly synthetic wastewater. In this thesis, sulfate radical-based -AOPs are studied with synthetic and real water to understand the influence and mechanism of chloride ions on the sulfate radical-based AOPs.

$$SO_4^{\bullet-} + Cl^- \rightarrow Cl^{\bullet} + SO_4^{2-} \quad (1.10)$$

$$PDS/PMS + Cl^- \rightarrow ClO^- \rightarrow ClO_3^- \rightarrow ClO_4^- \quad (1.11)$$

1.6.4 Photocatalytic degradation

In 1972 Fujishima & Honda first observed that TiO_2 could absorb photon energy to initiate photolysis of water [102]. This observation led to a photocatalytic process to treat organic contaminants in an aqueous environment. TiO_2 has been used and studied extensively for contaminants removal from air and water for photocatalytic studies [103]. TiO_2 has become attractive among many semiconducting materials because of its low cost, low toxicity, high efficiency, and high chemical stability. During the photocatalytic process, TiO_2 absorbs UV photon energy. When the absorbed energy is equal to or higher than the TiO_2 bandgap energy, electrons in the valence band (VB) get excited and move to the conduction band (CB) (Eq. 1.12). In this way, a hole (empty state) is created in the valence band. The excited electron and the hole can either recombine to release energy (Eq.1.13) or migrate to the material's surface, where several redox reactions are taking place. The hole has a

potential of +2.53 V/SHE at pH 7, directly reacting with the targeted pollutants absorbed in the surface. It can also produce a hydroxyl radical from water or hydroxyl ion (Eqs. 1.14-1.15) [103, 104].

The excited electrons can generate reactive oxygen species, such as superoxide radical ions and hydrogen peroxide (Eqs. 1.16-1.19) [105]. All these in-situ reactive oxygen species are capable of reacting with organic compounds to produce intermediates. When those intermediates are exposed to photocatalytic conditions for a longer time, they are mineralized to carbon dioxide, water, and inorganic salts [105, 106].

$$TiO_2 + h\nu \rightarrow e^-_{CB} + h^+_{VB} \quad (1.12)$$

$$e^-_{CB} + h^+_{VB} \rightarrow \text{energy} \quad (1.13)$$

$$H_2O + h^+_{VB} \rightarrow H^+ + HO^\bullet \quad (1.14)$$

$$HO^- + h^+_{VB} \rightarrow HO^\bullet \quad (1.15)$$

$$e^-_{CB} + O_2 \rightarrow O_2^{\bullet -} \quad (1.16)$$

$$O_2^{\bullet -} + H^+ \rightarrow HOO^\bullet \quad (1.17)$$

$$HOO^\bullet + e^-_{CB} \rightarrow HO_2^- \xrightarrow{H^+} H_2O_2 \quad (1.18)$$

$$O_2^{\bullet -} \rightarrow {}^1O_2 + e^- \quad (1.19)$$

Like other AOPs, photocatalytic AOPs are influenced by water quality, including turbidity, bulk pH, natural organic matter, and inorganic salts. pH influences the surface charge of the TiO_2, which affects the catalyst surface's absorption property [97, 104]. Maintaining a pH that would provide a point of zero charges (pH_{pzc}) of the catalyst surface is vital. The pH_{pzc} of TiO_2 is between pH 4 to 7. If the pH is less than pH_{pzc}, the catalyst surface will be positively charged, and a negatively charged compound can attach to the surface. In contrast, when the pH is higher than the pH_{pzc}, the catalyst surface will be negatively charged and suitable to attach positively charged compounds [107]. The presence of salts can affect the process efficiency in different ways, including absorption of the light, scavenging the reactive oxygen species and holes, blocking the active sites by attaching to the surface [108]. In the case of TiO_2, maintaining the pH around 6-7 can minimize the

surface blocking by the charged ions like chloride since the surface is charged neutral.

1.6.5 Ultraviolet-based (UV) technologies: UVC and VUV process

Ultraviolet-based (UV) technologies have been used worldwide to remove organic (micro)pollutants and disinfect in full-scale water treatment plants. UV-based technology is flexible to integrate with existing water treatment technology and has high removal capacity [60, 109-111]. UV technology can be divided into UVA, UVB, UVC, and VUV processes according to their UV wavelength. The technology used wavelength between 315 to 400 nm is called UVA, between 280 to 315 is called UVB, between 200 to 280 is called UVC, and between 200 to 100 is called VUV (vacuum ultraviolet). In this part, only UVC and VUV technology are discussed. Many organic compounds can absorb UVC light and degrade to small molecules compounds, called photolysis [112]. The photolysis performance largely depends on the pollutants absorption capacity called molar absorption coefficient, which depends on the physicochemical properties of organic compounds [113]. The higher the absorption coefficient, the greater the quantum yield. However, often pollutants are present in small concentrations so that a tiny fraction of the light is absorbed by the targeted compound. In addition, some contaminants do not absorb direct light and remain stable under UV light [114]. In many cases, oxidants like H_2O_2, O_3, and persulfate are added to produce reactive oxygen species by photolysis. Normally, UVC level light is unable to mineralize many organic pollutants. However, contaminants like ibuprofen could be removed under the UVC light [109, 115, 116]. In this thesis, the potential of UVC for CTBD treatment is investigated.

Several studies show that pH influences the organic compound removal in the UVC process. Studies show that the benzotriazole and sulfamethoxazole removal rate decreased with the increasing pH under the UVC treatment [117, 118]. With the increase of pH, organics compounds get deprotonated, which leads to a decrease in molecular absorption capacity. Bahnmuller, Loi [109] studied that benzotriazole and 2-hydroxybenzothiazole deprotonated in the alkaline conditions, leading to lower photo-reactivity than the parent compounds. In addition, the humic substance also influences the UVC process. Several functional groups in the humic substance are photoactive and absorb light at 254 nm wavelength [119]. Thus, organic pollutants

removal is hampered. Also, absorption of UV light by the humic substance may alter the organic pollutant solubility and hinder their removal [120]. NO_3^- ions in the water matrix also influence the UVC process. Nitrate ions have a 4 $M^{-1}cm^{-1}$ molar absorbed coefficient at 254nm. Photolysis of nitrate can produce nitrite with a strong radical scavenging tendency (Eq. 1.20)(1.1 x 10^{10} M^{-1} S^{-1}) [111].

$$NO_3^- + h\nu\ (>200\ nm) \rightarrow NO_2^- + 1/2O_2 \quad (1.20)$$

Vacuum ultraviolet (VUV) AOPs have become attractive in degrading and mineralizing water pollutants in recent years. A low-pressure mercury-vapor lamp is used in VUV AOPs studies. This type of lamp emits around 90% light at 253.7nm and 10% at 184.9 nm wavelength. During VUV AOP, pollutants can absorb light and degrade, similar to the UVC process. However, organic pollutants have higher absorption coefficients for VUV light compared to UVC. For instance, perfluorinated compounds (PFCs) are resistant to reacting with hydroxyl radicals; thus, conventional hydroxyl radical-based AOPs were ineffective for perfluorinated compound removal. In addition, the UVC process does not show any removal of PFCs, whereas VUV does. However, most of the VUV radiation is absorbed by water. For instance, water has an absorption coefficient of 1.46-1.80 cm^{-1} at 185nm at 25ºC. When water absorbs photons at VUV length, homolysis and photo-ionization of water take place (Eq. 1.21). During the photolysis, $HO^\bullet$, $H^\bullet$, and aqueous electrons (e_{aq}^-) are formed (Eq. 1.22) [121].

$$H_2O + VUV \rightarrow H^\bullet + HO^\bullet \text{ (Homolysis)} \quad (1.21)$$

$$H_2O + VUV \rightarrow e^-_{aq} + HO^\bullet + H^+ \text{ (Ionization)} \quad (1.22)$$

$$2HO^\bullet \rightarrow H_2O_2 \quad (1.23)$$

$$H_2O_2 + h\nu \rightarrow 2HO^\bullet \quad (1.24)$$

$$HO^\bullet + H_2O_2 \rightarrow H_2O + HO_2^\bullet \quad (1.25)$$

$$2HO_2^\bullet \rightarrow H_2O_2 + O_2^\bullet \quad (1.26)$$

$$HO_2^\bullet + HO^\bullet \rightarrow H_2O + O_2^\bullet \quad (1.27)$$

$$HO_2^\bullet + H_2O_2 \rightarrow HO^\bullet + H_2O + O_2^\bullet \quad (1.28)$$

Usually, e_{aq^-} concentration is very low in the system; thus, their contribution to the total performance is negligible. $HO^\bullet$ attacks most organic molecules and breaks

down their structures [122]. The $HO^{\bullet}$ and $H^{\bullet}$ radicals are accumulated in the bulk phase, which initiates recombination reactions to produce H_2O_2, O_2, and H_2O, as shown in Eq. (1.23) [123]. These reactions occur at a diffusion control rate (10^9 $M^{-1}.s^{-1}$). Dissolved oxygen can react with $H^{\bullet}$ and decreases the recombination reaction of hydroxyl radical and $H^{\bullet}$ radicals, which ultimately increases the hydroxyl radical concentration. In addition, UVC light, emitting with VUV, can activate the H_2O_2 to form $HO^{\bullet}$ (Eq. (1.24). Furthermore, $HO^{\bullet}$ can react with H_2O_2 to produce $HO_2^{\bullet}$ (Eq. 1.25). Several studies have reported that VUV AOPs can successfully remove organic pollutants [124, 125].

Besides that, dissolved oxygen helps to reduce the hydroxyl radical recombination; it can also absorb VUV photons and produce ozone. Introducing ozone in the reactor can increase the treatment efficiency; however, partial absorption of VUV light can reduce the direct photolysis of organic compounds and the water so that overall process efficiency can be hampered [126, 127]. Thus, it is very important to control the dissolved oxygen concentration in the VUV AOPs. Relevant reactions are given in Eqs. (1.29-30).

$$O_2 + VUV \rightarrow 2O \quad (1.29)$$

$$O_2 + O \rightarrow O_3 \quad (1.30)$$

The pH influences the VUV process via two different pathways [18, 128, 129]. i) pH influences the radical formation and accumulation. At basic conditions, H_2O_2 self-decomposes and produces H_2O and O_2, Which ultimately facilitated more hydroxyl radical recombination reaction to form H_2O_2 [128].ii) at basic conditions, HO^- ion absorbs a significant fraction of the 185nm light; therefore, direct degradation of the organic compounds gets inhibited [18]. Thus, the acidic conditions may favor the VUV-AOPs performance. In addition, similar to UVC, pH influences the molar absorption coefficient of organic compounds by influencing the molecular structure. This leads to a change in the removal performance. For example, a study showed that ciprofloxacin removal performance was optimal at neutral conditions compared to acidic and basic conditions. Ciprofloxacin has both electrophilic and nucleophilic functional groups, which charge distribution was influenced by the solution pH. Neutral pH help to maintain the electron clouds in an equilibrium condition in the ciprofloxacin, which has a maximum affinity to react with the hydroxyl radical [18, 130]. However, several research reports also claim

that pH has a negligible influence on VUV AOPs. For instance, the propranolol degradation rate was not influenced by the pH between 5 to 9 during VUV AOP [131].

Similar to other AOPs, chloride ions have an influence on the VUV AOPs. VUV radiation is absorbed by chloride ions and produces chlorine radicals and aqueous electrons (Eq. 1.31). The chloride radicals reacted with organic compounds and formed AOX [124]. In addition, inorganic ions such as NO_3^- and CO_3^{2-}, absorb VUV and also consume radicals. Absorption and the reaction between radicals produce corresponding fewer active radicals. However, the reaction rate between inorganic ions and hydroxyl radicals is orders of magnitude lower than the rate with organic compounds. Thus, the influence of the inorganic ions becomes dominating at higher concentration Eqs. (1.32-1.37) [92, 123, 124]. Because NO_3^- and CO_3^{2-} can scavenge strong radicals ($H^\bullet$ and $HO^\bullet$) to form less-active radicals, they may impede the treatment efficiency of VUV-AOP.

$$Cl^- + VUV \rightarrow Cl^\bullet + e^-_{aq} \quad (1.31)$$

$$NO_3^- + H^\bullet \rightarrow NO_3H^{\bullet-} \quad (1.32)$$

$$NO_3^- + e^-_{aq} \rightarrow (NO_3^\bullet)^{2-} \quad (1.33)$$

$$(NO_3^\bullet)^{2-} + H^+ \rightarrow NO_3H^{\bullet-} \quad (1.34)$$

$$(NO_3^\bullet)^{2-} + H_2O \rightarrow NO_2^\bullet + 2OH^- \quad (1.35)$$

$$2NO_2^\bullet + H_2O \rightarrow NO_3^- + NO_2^- + 2H^+ \quad (1.36)$$

$$OH^\bullet + CO_3^{2-} \rightarrow OH^- + CO_3^{\bullet-} \quad (1.37)$$

1.7 RESEARCH SCOPE AND THESIS OUTLINE

As discussed, CTBD contains a mixture of organic compounds, including humic substances and conditioning chemicals. The removal of the organic compounds by AOPs is case-specific. In addition, different conditioning chemicals in the CTBD have different degradation mechanisms in different AOPs. Salts, like chloride, presence in the CTBD influences the AOPs and chlorinated by-produced formation. It is very important to understand the degradation mechanism of the OCs in AOPs and the formation, accumulation, and environmental impact of chlorinated by-

products. As described in the overviews above, such insights were still missing in the literature. Thus, the overall objective of this thesis is to provide a better understanding as well as further development of AOPs for the removal of organic compounds from cooling tower blowdown in saline conditions. Particular emphasis has been given to the following aspects of AOPs: 1) development of electrochemical oxidation methods to improve the removal efficiency of organic carbon (of natural and anthropogenic origin) 2) understanding the oxidation and chlorinated by-product formation pathway in different AOPs in saline conditions, and 3) minimize toxic by-product formation in these processes, and 4) to design process trains in which these processes are integrated in an effective way to treatment CTBD.

In this thesis, the following specific research questions were addressed:

- What are the possibility and limitations of electrochemical oxidation (EO) for CTBD OCs removal? (Chapter 2)
- What is the influence of integrating electrochemical oxidation with different technology (constructed wetland (CW) and nanofiltration (NF)) with respect to removal efficiency and toxicity minimization? (chapters 3, 4, and 7).
- What are the differences in the influence of salinity on OCs degradation pathway, by-product formation, and toxicity during electrochemical oxidation, persulfate, photocatalytic, and UV-based AOPs treatments treatment? (chapters 5 and 6)

In Chapter 2, the feasibility and the limitation of electrochemical AOPs to remove organic compounds present in the cooling tower blowdown water are described. The influence of operational parameters on process performance, chlorinated by-product formation, and toxicity is highlighted. The change of the humic substance profile is monitored, and the degradation mechanism is explained.

Based on the outcome of chapter 2, two approaches are followed: 1) to study the strategies to minimize the limitations of the electrochemical oxidation process **(Chapter 3 and Chapter 4)**. 2) to study alternative AOPs to elucidate the difference in oxidation and chlorinated by-production formation mechanism **(Chapter 5 and Chapter 6)** (Fig. 1.7).

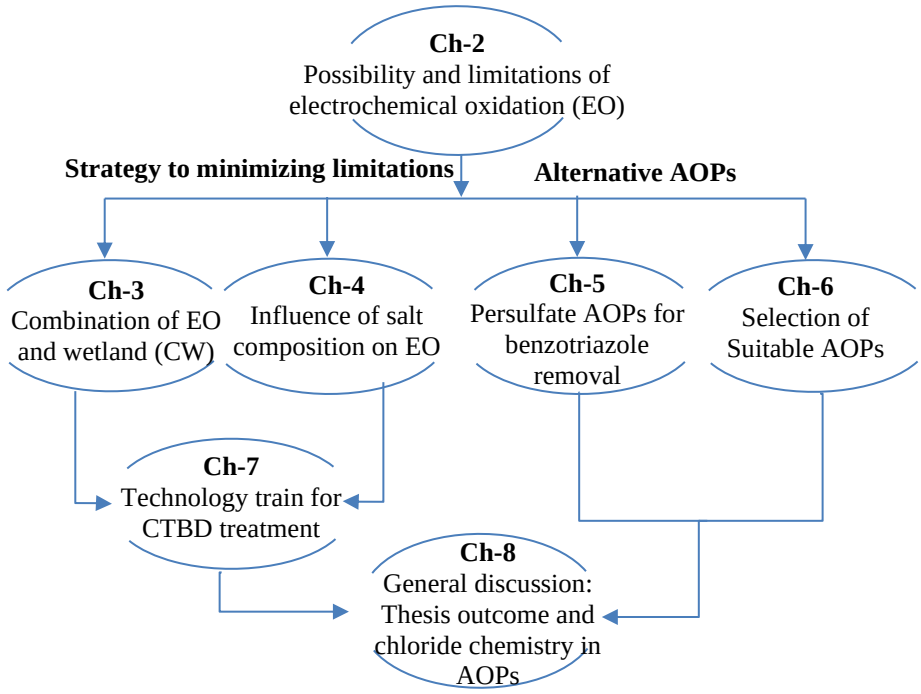

Fig. 1-7. *Thesis outline: Advanced oxidations processes (AOPs) for cooling tower blowdown (CTBD) or saline water treatment*

In Chapter 3, the combination of electrochemical oxidation and a vertical-flow constructed wetlands system is studied to understand the organic compounds removal, accumulation of adsorbable organic halogens, chlorite, and perchlorate. The fate of the benzotriazole is watched as a model compound.

In Chapter 4, the reactive oxidation species formation pathway during an electrochemical process in different electrolytes compositions is studied. In particular, sulfate radical formation pathways are illustrated in detail. It shows how the electrolytes' composition influences the process performance and degradation by-products distribution.

In Chapter 5, the influence of saline conditions on the heat-activated sulfate radical-based oxidation is studied as an alternative to electrochemical oxidation. To understand the chloride chemistry in different oxidative conditions, the degradation and undesired chlorinated by-product formation mechanisms are studied. Peroxydisulfate and peroxymonosulfate are used as the source of sulfate radicals.

In Chapter 6, four types of AOPs are studied to understand better the humic substances' degradation mechanism present in the cooling tower blowdown. An in-depth analysis of humic substance is presented to monitor the humic substance degradation pathway. Moreover, chlorinated by-products are analyzed to see the influence of the AOPs. The distribution of chlorinated by-produce in different AOPs is described based on literature. The best AOPs are recommended for saline water treatment based on the outcome.

In Chapter 7, knowledge obtained from Chapters 2,3, 4, and research line 3 are applied to develop a comprehensive technology train to treat CTBD to meet the desired quality for reuse in the cooling tower itself. In this study, wetland, nanofiltration, and reverse osmosis are combined in series. All the critical parameters of the CTBD are monitored in each step. The nanofiltration would change electrolytes composition of the nanofiltration concentrated. Chapter 4 highlighted the effect of electrolytes composition on the EO for a synthetic solution. The outcome of chapter 4 is evaluated on real conditions in chapter 7. To do so, the nanofiltration concentrated has been treated with electrochemical oxidation to remove concentrated organic compounds. Based on the outcome, strengths and points of concern are highlighted in chapter 7.

In Chapter 8, three aspects are highlighted, 1) a summary of the research outcome described in the previous chapters, 2) possible application of AOPs in a bigger context, 3) comparative understanding of chloride chemistry in state-of-the-art AOPs to provide essential knowledge to select suitable AOPs in saline conditions. In addition, recommendations and future research niches are pointed out.

Chapter 2.

Removal of organic compounds from cooling tower blowdown by electrochemical oxidation: Role of electrodes and operational parameters.

This chapter has been published as:
Saha, Pradip, Harry Bruning, Thomas V. Wagner, and Huub H.M. Rijnaarts. "Removal of organic compounds from cooling tower blowdown by electrochemical oxidation: Role of electrodes and operational parameters." Chemosphere 259 (2020): 127491.

Abstract

The reuse of cooling tower blowdown (CTBD) in the cooling tower itself requires CTBD deionization and a pre-treatment before deionization to remove organic compounds (OCs) that induce membrane fouling. This study assesses the potential of electrochemical oxidation (EO) with a boron-doped diamond (BDD) and a Ti/RuO_2 mixed-metal oxide (MMO) anode for CTBD pre-treatment. Also, the influence of the applied current density (*j*), initial pH, hydrodynamic conditions, and supporting electrolytes on the process performance was evaluated. Results show that COD and TOC removal were 85 and 51%, respectively, with the BDD-anode; however, they were 50 and 12% with MMO-anode at a *j*-value of 8.7 $mA.cm^{-2}$ and neutral pH. An increased *j*-value increased the COD and TOC removal; however, different pHs, hydrodynamic conditions, and the addition of supporting electrolytes had a minor impact on the removal with both anodes. Liquid chromatography-organic carbon detection analysis showed that the OCs in CTBD mainly consisted of humic substances (HS). EO with the BDD-anode resulted in 35% HS mineralization, while the rest of the HS was partially oxidized into low molecular weight compounds and building blocks. However, HS mineralization was limited with the MMO-anode. The mineralization and oxidation were accompanied by the formation of organic and inorganic chlorinated species. These species increased the toxicity to *Vibrio fischeri* 20-fold compared to the initially low-toxic CTBD. Thus, EO with a BDD-anode is a promising pre-treatment technology for removing OCs before CTBD deionization. Still, before its application, measures to minimize the chlorinated species formation are required.

Keywords

Boron-doped diamond anode; Mixed-metal oxide anode; Applied current density; Humic substances; Chlorinated by-products.

2.1 INTRODUCTION

The reuse of discharged cooling tower water in the cooling tower itself can substantially lower the industrial freshwater footprint. This is especially relevant in fresh water-stressed areas where freshwater stress is expected to increase due to climate change and droughts [132]. In 2015, the United States withdrew 102 km^3 of freshwater for the cooling systems of thermal power plants [14]. During the operation of the cooling tower, the concentration of salts and organic compounds (OCs) in the cooling water increases due to evaporation. Increased salt concentrations eventually create operational problems, such as scaling. To prevent operational problems, the concentrated cooling water is discharged regularly as cooling tower blowdown (CTBD) when too high salt concentrations are reached [19, 133]. Subsequently, fresh make-up water needs to be added to the cooling system to compensate for the water loss. To reuse CTBD as make-up water and lower the freshwater footprint of the cooling tower, the deionization of the CTBD is required.

Different membrane technologies for CTBD deionization have been assessed, such as nanofiltration, reverse osmosis [17], electrodialysis combined with electrodialysis reversal [134], capacitive deionization [135], and membrane distillation [34, 136]. All these membrane-based deionization technologies encounter fouling through pore-clogging and gel formation due to organic compounds (OCs) present in the CTBD [137, 138]. Fouling ultimately reduces the deionization efficiency of the membranes. Therefore, a pre-treatment method that removes OCs before membrane deionization would enhance the CTBD deionization efficiency and make the reuse of CTBD in the cooling tower economically more attractive. Several pre-treatment technologies for the removal of OCs from CTBD before membrane deionization have been studied, such as microfiltration [48], integrated sand filtration/nanofiltration [13], coagulation [139], powdered activated carbon (PAC) [11], ultrafiltration [21, 22, 49] and constructed wetlands [140]. The incomplete removal of recalcitrant OCs is a reoccurring issue with the abovementioned pre-treatment technologies. However, during the last decade, electrochemical oxidation (EO) has proven itself as a suitable technology for the removal of recalcitrant OCs from wastewater streams [141-143], such as wastewater from textile industries [144], petrochemical industries [145], pulp and paper mills [146], tanneries [147], chemical industries [148], municipal secondary effluent

[149], domestic wastewater [2, 150] and landfill leachates [151-154]. A distinct advantage of EO is that no additional chemicals are required, processes are operated in mild conditions, and processes can easily be automated [155-157].

In the present study, the application of EO as a CTBD pre-treatment method before CTBD deionization was studied. EO was performed with two different anodes: a Ti/RuO_2 mixed-metal oxide (MMO) anode and a boron-doped diamond (BDD) anode. Both MMO-anodes and BDD-anodes are capable of oxidizing OCs efficiently [158-160]. During the EO of OCs, various mechanisms are responsible for the degradation of OCs. OCs are directly oxidized on the MMO-anode or BDD-anodes surface. In addition, water oxidation results in the formation of hydroxyl radicals ($HO^{\bullet}$) with both anodes (Fig. S2-1). Furthermore, with the MMO-anode, higher oxidation complexes (MMO_{x+1}) are formed. Additionally, $HO^{\bullet}$ is capable of forming sulfate radicals and active chlorine species from their corresponding anions present in the water. Moreover, chloride ions can directly be oxidized to chlorine. Chlorine is subsequently converted to hypochlorite. These reactive oxygen species (ROS) can indirectly oxidize the OCs. All the corresponding processes can be expressed as reactions Eqs. (2.1)–(2.8) [161-164].

$$BDD + H_2O \rightarrow BDD(HO^{\bullet}) + H^+ + e^- \quad (2.1)$$

$$MMO_X + H_2O \rightarrow MMO_X(HO^{\bullet}) + H^+ + e^- \quad (2.2)$$

$$MMO_X(HO^{\bullet}) \rightarrow MMO_{X+1} + H^+ + e^- \quad (2.3)$$

$$SO_4^{2-} + HO^{\bullet} \rightarrow SO_4^{\bullet -} + OH^- \quad (2.4)$$

$$Cl^- + HO^{\bullet} \rightarrow ClO^{\bullet -} + H^+ + e^- \quad (2.5)$$

$$2Cl^- \rightarrow Cl_2 + 2e^- \quad (2.6)$$

$$Cl_2 + 2H_2O \rightarrow HClO/ClO^- + Cl^- + H^+/2H^+ \quad (2.7)$$

$$\text{Organic compounds} + ROS \rightarrow CO_2 + \text{Intermediates} + H_2O \quad (2.8)$$

In this study, the treatment performance of the MMO-anode and BDD-anode was compared in terms of COD and TOC removal efficiency, average oxidation state (AOS), instantaneous current efficiency (ICE), and energy consumption (EC). Besides, the overall efficiency of EO depends on the applied current density (j), pH, hydrodynamic conditions, and electrolyte composition, and these were varied in the present study to determine their impact on the process efficiency. In addition, the

composition of the OCs in CTBD before and after EO-treatment was assessed by liquid chromatography-organic carbon detection (LC-OCD). Furthermore, the formation of adsorbable organic halides (AOX) and chlorinated inorganic species was monitored, and the toxicity of the EO-treated CTBD was assessed because AOX and chlorinated inorganic species are potentially toxic and can accumulate in the environment.

2.2 MATERIALS AND METHODS

2.2.1 Chemicals

Potassium ferrocyanide ($K_4Fe(CN)_6$, ≥98.5%); Potassium ferricyanide ($K_3Fe(CN)_6$, ≥99%); sulfuric acid (H_2SO_4, 95%); sodium hydroxide (NaOH, ≥99%); sodium nitrate ($NaNO_3$, 99%); sodium sulfate (Na_2SO_4, ≥99%), sodium chloride (NaCl, ≥99%), calcium chloride ($CaCl_2$, ≥96%), potassium nitrate (KNO_3, ≥99%), and copper sulfate ($CuSO_4$, ≥99%) were obtained from Sigma Aldrich (The Netherlands).

2.2.2 Cooling tower blowdown composition

CTBD was collected from a cooling tower of Dow Benelux BV (Terneuzen, The Netherlands). During normal operation of this cooling tower, H_2SO_4 is dosed for pH adjustment, Nalco 3DT187 and Nalco 3DT199 are dosed as a corrosion inhibitor, Nalsperse 7348 is dosed as bio-dispersant, and NaClO is dosed as a disinfectant [34]. The collected CTBD was stored at 4^{o}C to minimize microbial activity and growth. Subsequently, the CTBD was used for the experiments without any physical-chemical pre-treatment. The composition of the CTBD is provided in the supplementary info (SI) (Table S2-1).

2.2.3 Experimental set-up

EO experiments were performed in batch recirculation mode using 350 mL CTBD. The electrochemical cell comprises a single flow chambered flat plate reactor assembly with an active electrodes surface area of 22.4 cm^2 (L: 11.2cm × W: 2.0 cm) (Fig. S2-2). The inter-electrode distance was 1.5 cm. A platinum-coated

titanium electrode was used as the cathode, and a Ti/RuO_2 mixed-metal oxide (MMO) or boron-doped diamond (BDD) electrode was used as the working anode (Magneto Special Anodes, Schiedam, The Netherlands). A silver/silver chloride (Ag/AgCl) electrode (QM711X/Gel, Prosense, The Netherlands) served as a reference electrode, and it was ionically plugged into the EO cell using Haber-Lugging capillaries filled up with a 1M potassium nitrate solution. A peristaltic pump circulates the CTBD through the cell at different flow rates. On-line pH, conductivity, and temperature sensors were installed in the setup. The system's temperature was maintained at 21-23ºC EO experiments were conducted galvanostatically using an IviumStat.h potentiostat (Ivium Technologies B.V. The Netherlands). The potentiostat was attached in a three-electrode conformation (anode, cathode, and reference electrode). Iviumstat software was used to record and analyze the experimental electrochemical data. The system was polarized at 2.7 $mA.cm^{-2}$ for 30 min using a 0.1M sulfuric acid solution prior to the experiments. The mass transfer coefficient of the EO cell was measured by the oxidation and reduction of ferrocyanide and ferricyanide. The detailed protocol of this method is reported in [165]. At a recirculation flow rate of 30 L h^{-1}, the mass transfer coefficient (K_m, $m.s^{-1}$) was 1.7 (±0.06) $\times 10^{-5}$ $m.s^{-1}$. The limiting current density (I_{lim}) for the CTBD was 3 $mA.cm^{-2}$, which was calculated according to the Eq. (2.9) [164]:

$$I_{lim} = 4FAK_m COD_0 \quad (2.9)$$

Where, A is the surface area of the electrode (m^2), COD_0 the initial CTBD (mol O_2 m^{-3}), and F the Faraday's constant (96485 C mol^{-1}).

Na_2SO_4 and $NaNO_3$ were separately added to the CTBD to assess the effect of the supporting electrolyte on the EO performance. In addition, 96% H_2SO_4 and NaOH solution were added to the CTBD to evaluate the impact of an acidic or basic initial pH on the EO performance.

To determine the COD removal rate and removal efficiency, seven samples of 2 mL were taken for COD analysis during the 3 h EO treatment. In addition, a 50 mL sample was collected after the 3 h EO-treatment to determine free chlorine (FC, the total concentration of Cl_2 and $HOCl/OCl^-$), the TOC concentration, the ionic composition, the composition of the OCs, and the toxicity of the treated CTBD.

2.2.4 Analytical methods

The CTBD OCs concentration was measured as COD using Hach kit LCK-314/ LCK-1414 and a Hach DR/3900 spectrophotometer (Hach Lange GmbH, Germany). The degree of OCs mineralization was measured as TOC removal using a TOC-$L_{CPH/CPN}$ analyzer equipped with an ASI-L autosampler (Shimadzu, The Netherlands). The OCs were catalytically oxidized to CO_2 at a temperature of 680°C, and non-dispersive infrared detection was used to detect the CO_2. Anions were measured with a Dionex ICS-2100 ion chromatography (IC) (Dionex, The Netherlands) connected with a Dionex IonPac AS19 column (4x250 mm). A Perkin Elmer ICP-OES AVIO 500 plasma atomic emission spectroscopy (ICP) was used to determine the cations. The composition of the OCs in the CTBD samples was analyzed with a size-exclusion liquid chromatography-organic carbon detector (LC-OCD) (Model 8, DOC-Labor, Germany), according to the method described in Ajao et al. (2019). In short, the analyzer was equipped with a non-dispersive infrared detector together with an organic nitrogen detector (UV 220 nm) and a UV detector (254 nm). Each sample was separated according to their molecular weight into biopolymers, HS, low molecular weight (LMW) acids, and LMW neutrals in the size-exclusion column [166, 167]. The sample was filtered with a 0.45µm polytetrafluoroethylene filter before analysis. Free chlorine (FC) concentrations were measured using a Hach DPD free and total chlorine test reagent and a Hach DR/3900 spectrophotometer (Hach Lange GmbH, Germany). According to the manufacturer's protocol, the AOX concentrations were measured with the Hach LCK-390 cuvette test (Hach Lange GmbH, Germany). The acute toxicity of the initial and treated samples was measured by Microtox® toxicity test kits model 500 (Microloan, the Netherlands).

2.2.5 Data analysis

2.2.5.1 Performance evaluation

The performance of the EO process was monitored by following the %COD removal, %TOC removal, instantaneous current efficiency (%ICE), and energy consumption (EC in $kWh.kg^{-1}$ COD). All the corresponding performances are calculated according to the following Eqs. (2.10)– (2.13) [164, 168, 169].

$$\%\text{COD reoval} = \frac{\text{COD}_{\text{in}} - \text{COD}_{\text{out}}}{\text{COD}_{\text{in}}} \times 100\% \quad (2.10)$$

$$\%\text{TOC removal} = \frac{\text{TOC}_{\text{in}} - \text{TOC}_{\text{out}}}{\text{TOC}_{\text{in}}} \times 100\% \quad (2.11)$$

$$\%\text{ICE} = \text{FV}_{\text{S}}\left(\frac{\text{COD}_{\text{in}} - \text{COD}_{\text{out}}}{\text{mI}\Delta\text{t}}\right) \times 100\% \quad (2.12)$$

$$\text{EC} = \frac{\Delta\text{E}_{\text{cell}}\text{It}}{(\text{V}_{\text{s}} \times \Delta\text{COD})} \quad (2.13)$$

Where: COD_{in} and COD_{out} in $gO_2.L^{-1}$ are respectively the initial and final COD obtained before and after EO treatment. TOC_{in} and TOC_{out} in $g.L^{-1}$ are, respectively, the initial and final TOC obtained before and after EO treatment. F is Faraday's constant (96485 $C.mol^{-1}$), V_S is electrolyte volume (L), I is the applied current (A), Δt is the electrolysis time (s), t is the electrolysis time (h), m=8= oxygen equivalent mass (gO_2 $eq.mol^{-1}$) and ΔE_{cell} is the average cell voltage (V).

2.2.5.2 Average oxidation state (AOS)

The change of oxidation state of the organic carbon is expressed as the average oxidation state (AOS) of the organic carbon in the treated CTBD, which was evaluated using Eq. (2.14) [170].

Where TOC and COD are expressed in molar units, the AOS value varies from +4 to -4. +4 implies the highest oxidation state of the carbon, such as CO_2 or CCl_4. -4 indicates the lowest oxidation stated of the carbon, such as methane.

$$\text{AOS} = 4\frac{(\text{TOC}_{\text{out}} - \text{COD}_{\text{out}})}{\text{TOC}_{\text{out}}} \quad (2.14)$$

2.3 RESULTS AND DISCUSSION

2.3.1 Influence of applied current density (j) on OCs oxidation

The COD removal efficiency increased with an increasing applied current density (*j*) for both anodes (Fig. 2-1). The applied current density is an important parameter that governs the removal kinetics [146]. More ROS are formed at a higher *j*-value [161, 162, 164]. These ROS indirectly oxidize the COD present in the CTBD. An increase of the *j*-value with the BDD-anode from 2.3 to 5.5 and 8.7 mA.cm^{-2} enhanced the COD removal from 45 to 77 and 85%, respectively. (Fig. 2-1a). With a *j*-value of 2.3 mA.cm^{-2}, the COD removal was controlled by ROS formation since this *j*-value is lower than the limiting current density [171]. With a higher *j*-value, the EO of the COD in the CTBD was limited by mass transport, leading to only an 8% increase in COD removal with an increase of the *j*-value from 5.5 to 8.7 mA.cm^{-2}. In addition to mass transfer limitation, a higher *j*-value also facilitates undesired oxygen evolution reactions and reduces energy efficiency [172].

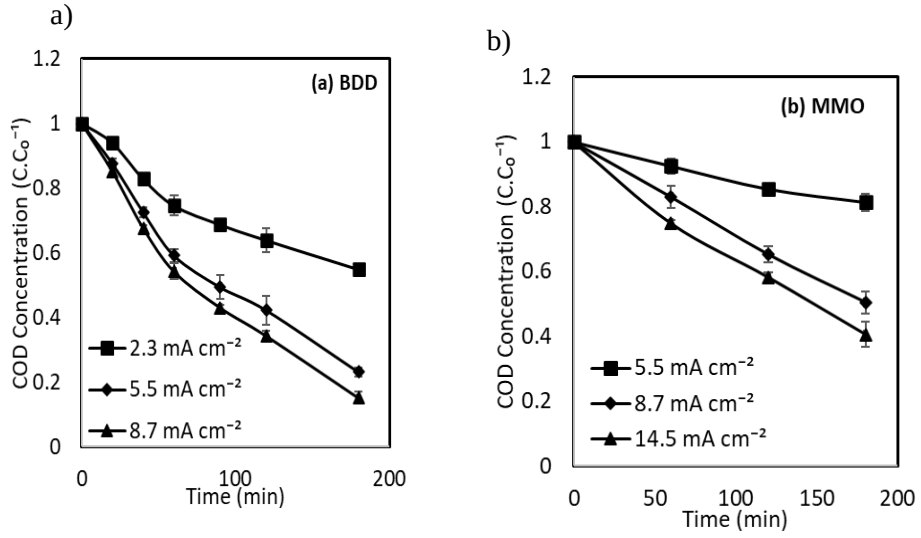

Fig. 2-1. *Influence of applied current density (j) on COD removal with (a) BDD-anode and (b) MMO- anode. Experimental conditions: T=21-23°C, Conductivity = 3.7 mS cm-1, pH = 6.9, recirculation flow rate = 30 L h-1.*

The COD removal over time with the BDD-anode has a two-phase removal profile with a decreasing removal rate after 60 minutes (Fig. 2-1a). The simultaneous occurrence of three processes results in this two-phase removal profile: 1) the reaction kinetics of OCs at the surface of the anode; 2) mass-transfer of OCs by diffusion; 3) the transformation of OCs into intermediates with a different reactivity or diffusivity than the parent compound. During the first 60 minutes, the reaction kinetics are controlled by the $HO^{\bullet}$ formed at the anode surface, and OCs can be supplied at a high enough diffusion rate not to become rate-limiting. After 60 minutes, the reaction kinetics decrease, possibly by diffusive mass transfer limitation because of the decreased OCs concentration. In addition, the two-phase removal profile might be explained by the production of OC intermediates that are unfavorable to oxidation. [173] reported a similar COD removal profile. In their study, the removal of COD from phenolic wastewaters was faster during the first 0.5 h of treatment, after which the removal slowed down due to mass transfer limitation at the surface of the BDD-anode [173].

EO with the MMO-anode resulted in incomplete COD removal that is substantially lower than with the BDD-anode for all *j* values (Fig. 2-1b). Several competitive processes occur during EO with the MMO-anode, which could explain the lower COD removal compared to the BDD-anode. Firstly, MO_{x+1} active higher oxidation complexes are formed at the MMO-anode surface that less efficiently oxidize OCs than the $HO^{\bullet}$ produced by the BDD-anode. Also, MO_{x+1} proceeds to oxygen evaluation reactions [146]. Secondly, 80, 205, and 310 $mg.L^{-1}$ hypochlorite is formed with a *j* of 5.5, 8.7, and 14.5 $mA.cm^{-2}$ with the MMO-anode (Table 2-3), and hypochlorite has less oxidation potential compared to the $HO^{\bullet}$ formed by the BDD-anode [73]. Lastly, the low water oxidation overpotential of the MMO-anode (+1.50 V/SHE) compared to the BDD-anode (+ 2.3 V/SHE) results in a loss of applied energy to undesired water oxidation [73, 164].

2.3.2 Effect of applied current on the performance of the electrochemical oxidation process

During EO, the OCs in CTBD are oxidized and partially mineralized to carbon dioxide. Only part of the applied energy is used for the desired oxidation reactions. Thus, analysis of the TOC removal, the OCs average oxidation state (AOS),

instantaneous current efficiency (ICE), and energy consumption allows determining the process efficiency.

An increasing *j* led to increased removal of TOC with both anodes. A similar phenomenon was observed for COD removal (section 2.3.1; Table 2-1). TOC removal represents the complete mineralization of OCs. The higher COD than TOC removal (Table 2-1) indicates that partial oxidation of OCs occurred, resulting in OC's with a higher oxidation state (Bilińska et al., 2016). Evaluation of the OCs AOS over time confirms this partial oxidation phenomenon since the AOS-values substantially increased after 180 min EO of CTBD with the BDD-anode and the MMO-anode (Table 2-1). A fraction of the OCs was most likely oxidized into smaller organic molecules, especially organic acids, alcohols and aldehydes, and possibly chlorinated OCs (Oller et al., 2011). Several studies indicated that the breakdown of large molecules into smaller and more oxidized organic intermediates corresponds with higher AOS values (Reyes et al., 2006; Orts et al., 2017).

Table 2-1. *EO performance in terms of COD and TOC removal, average oxidation state (AOS) of the OCs, instantaneous current efficiency (ICE) and energy consumption per kg of COD at different applied current densities (j). Experimental conditions: T=21-23°C, conductivity = 3.7 mS cm-1, pH = 6.9, recirculation flow rate = 30L h-1, treatment time = 3 h.*

Anode	*j* ($mA.cm^{-2}$)	% COD removal (±)	%TOC removal (±)	AOS*, †	%ICE†	EC (kWh kg^{-1} COD) †
BDD	2.3	45 (1)	39 (1)	+1.5	48	12
	5.5	77 (2)	42 (1)	+2.8	31	24
	8.7	85 (3)	51 (1)	+3.0	20	47
MMO	5.5	19 (3)	9 (1)	+0.9	5.0	119
	8.7	50 (3)	12 (0)	+1.5	7.0	125
	14.5	60 (4)	15 (2)	+2.3	8.0	142

* Initial AOS of CTBD: +0.8; †AOS, ICE, and EC were calculated based on average COD and TOC value.

The ICE declined with increasing *j*-values with the BDD-anode (Table 2-1). At a low *j*-value, most of the applied energy is used to oxidize the OCs. Higher *j*-value

results in decreasing ICE because more energy is used for the oxidation of water. The ICE was substantially lower with the MMO-anode than the BDD-anode (Table 2-1). Consequently, significantly more energy is consumed to oxidize a kg of COD with the MMO-anode than with the BDD-anode (Table 2-1). Hence, the performance efficiency of the BDD-anode is higher than that of the MMO-anode.

2.3.3 Influence of electrochemical oxidation on the dissolved organic carbon profile

LC-OCD analysis showed that the dissolved organic carbon (DOC) profile of the CTBD changed during EO with the BDD-anode and MMO-anode (Fig.2-2). During the EO process, the AOS of the OCs changes, likely because of the conversion of large organic molecules to smaller oxidized organic molecules (section 2-3.2).

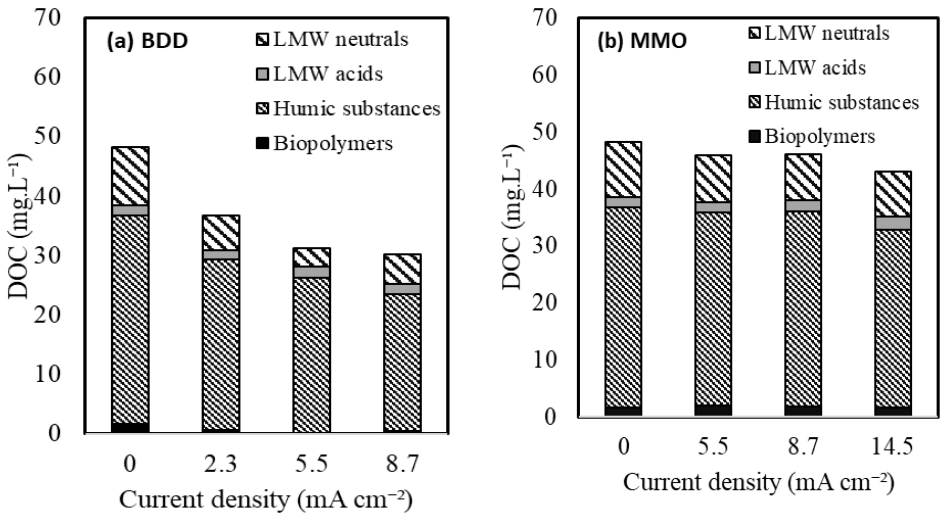

Fig. 2-2. *The DOC-profile of CTBD OCs after EO at different j-values with (a) BDD-anode and (b) MMO-anode. Experimental conditions: T=21-23°C, conductivity = 3.7 mS cm-1, pH = 6.9, recirculation flow rate = 30 L h-1, treatment time = 3 h.*

Before EO, the CTBD is composed of 35.1 $mg.L^{-1}$ HS, 1.6 $mg.L^{-1}$ biopolymers, 1.8 $mg.L^{-1}$ low molecular weight (LMW) acids, and 9.8 $mg.L^{-1}$ LMW-neutrals (Fig. 2-2), which agrees with the earlier described composition of CTBD from the same

site [11]. EO with the BDD-anode at the highest applied *j*-value resulted in the removal of HS, while this removal was less apparent with the MMO-anode (Fig. 2-2). A shoulder appears on the HS peak after EO-treatment with the BDD-anode in the total ion chromatogram of the LC-OCD analysis (Fig. S2-3). This shoulder indicates the formation of a low molecular weight fraction, building blocks, during the oxidation of HS [167]. The concentration of the LMW-acids also increased after EO with the BDD-anode. The formation of building blocks and LMW-acids corroborates that HS is partially oxidized and broken down into smaller fragments, leading to higher COD removal than TOC removal and an increased AOS, as was discussed in sections 2-3.1 and 2-3.2.

The ineffective removal of HS with the MMO-anode can be attributed to the less effective oxidation because of the formation of $HClO/ClO^-$. $HClO/ClO^-$ produced by a SnO_2-Sb_2O_4 (MMO)-anode has shown to indirectly oxidize HS in sanitary landfill leachate, resulting in 66% COD and 15% DOC removal at a *j*-value of 30 mA cm^{-2} and eight hours of treatment in the presence of 2.5 g L^{-1} chloride [152]. The low DOC removal compared to the COD removal shows that the MMO-anode is ineffective for the breakdown and mineralization of HS.

2.3.4 Influence of hydrodynamic conditions on OCs oxidation

Varying the flowrate (linear flow velocity) between 18 $L.h^{-1}$ (0.84 $cm.s^{-1}$), 30 $L.h^{-1}$ (2.8 $cm.s^{-1}$) or 46 $L.h^{-1}$ (4.25 $cm.s^{-1}$) at 8.7 $mA.cm^{-2}$ for the BDD-anode and 14.5 $mA.cm^{-2}$ for the MMO-anode did not result in substantial changes in the COD removal efficiency or removal rate (Fig. 2-3).

Varying the flowrate (linear flow velocity) between 18 $L.h^{-1}$ (0.84 $cm.s^{-1}$), 30 $L.h^{-1}$ (2.8 $cm.s^{-1}$) or 46 $L.h^{-1}$ (4.25 $cm.s^{-1}$) at 8.7 $mA.cm^{-2}$ for the BDD-anode and 14.5 $mA.cm^{-2}$ for the MMO-anode did not result in substantial changes in the COD removal efficiency or removal rate (Fig. 2-3).

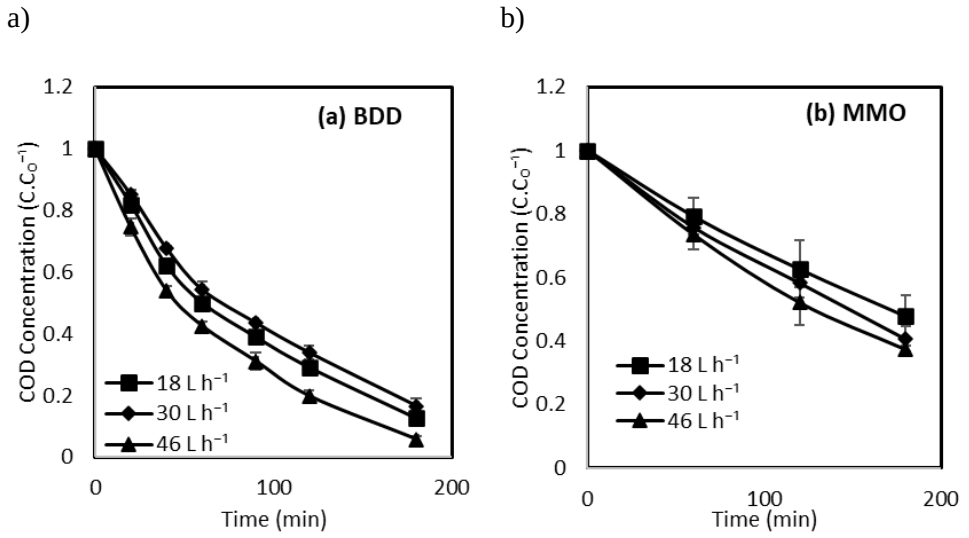

Fig. 2-3. *COD removal at different flowrates with a) BDD-anode and b) MMO-anode. Experimental conditions: T=21-23^{o}C ; conductivity = 3.7 mS cm-1; pH = 6.9; treatment time = 3 h.*

Generally, the removal of OCs by EO depends on the dynamics of the flow regime [172]. Approximately 10% variation in the COD removal efficiency was observed for the different flow rates with both anodes. The TOC removal also did not change substantially because of the flow rate variation (Table S2-2). It was expected that increasing the flow rate would reduce the mass transfer limitation by reducing the diffusion layer thickness and increasing the reaction rate [172], and in this way improving the COD removal efficiency. The unaffected COD removal efficiency at varying flowrates shows that the COD removal is not only limited by mass transfer and reaction kinetics of the parent OCs, as was discussed in section 2-3.1 but also by the oxidation rate of the OCs intermediates with the reactive oxidative species formed in the EO system.

2.3.5 Influence of pH and supporting electrolyte on OCs oxidation

Varying the initial pH between 3.0, 6.9, and 11.5 did not affect the COD and TOC removal efficiency of both anodes (Table 2-2)

Table 2-2. *The effect of different initial pHs and supporting electrolytes on COD and TOC removal, instantaneous current efficiency (ICE) and energy consumption. Experimental conditions: j = 8.7 mA cm-2 (BDD) and 14.5 mA cm-2 (MMO), T = 21-23°C, conductivity = 3.7 mS cm-1, recirculation flow rate = 30 L h-1, treatment time = 3 h.*

Anode	Parameters	% COD removal (±)	% TOC removal (±)	% ICE*	EC (kWh.kg^{-1} COD) *
BDD	pH=6.9 (CTBD)	85 (3)	51 (1)	20	47
	pH=3.0	88 (1)	49 (5)	21	42
	pH=11.5	92 (4)	53 (3)	22	40
	28 mM Na_2SO_4	90 (3)	50 (3)	22	31
	48 mM $NaNO_3$	75 (2)	35 (1)	19	37
MMO	pH=6.9 (CTBD)	60 (4)	15 (2)	8.0	142
	pH=3.0	54 (4)	20 (2)	8.7	124
	pH=11.5	56 (1)	17 (1)	8.9	122
	28 mM Na_2SO_4	54 (2)	20 (1)	8.8	109
	48 mM $NaNO_3$	51 (3)	21 (2)	7.0	135

* The ICE and EC were calculated based on average COD value.

EO with the BDD-anode results in the formation of $HO^{\bullet}$ Their oxidation power is unaffected by different pH values, as was previously shown during the treatment of ferulic acid [174], paper mill wastewater [146], and sinapinic acid-containing wastewater [175]. During EO with the MMO-anode, active chlorine species are responsible for the oxidation of OCs. The pH does influence the formation of active chlorine species. HOCl is the dominating species at an acidic pH and has a higher oxidation potential (1.63 V/SHE) compared to ClO^- (0.89 V/SHE) [149]. Therefore, the OCs removal with the MMO-anode was expected to be higher at pH 3 than at

pH 11.5. Nevertheless, the COD and TOC removal were comparable at both pHs (Table 2-2). This resulted from a fast increase of pH 3 to pH 6.5 during the first h of EO with the MMO-anode, which is similar to the initial CTBD pH. Hence, CTBD can be electrochemically treated without adjusting the pH.

The addition of $NaNO_3$ electrolyte lowered the COD and TOC removal with the BDD-anode, while these were unaffected by the addition of Na_2SO_4 electrolyte (Table 2-2). With the MMO-anode, the COD and TOC removal were not affected by either electrolyte (Table 2-2). Supporting electrolytes enhance electric conductivity and electron transfer [175]. $NaNO_3$ may increase the surface covering and lower the ROS formation on the BDD-anode surface. In contrast, Na_2SO_4 leads to the formation of strong oxidants, such as sulfate radicals and persulfate, which can improve the removal efficiency. Several researchers indicated that the EO of OCs with a BDD-anode is faster in sulfate electrolyte than in nitrate electrolyte because of the formation of active sulfate species together with $HO^{\bullet}$ [162, 176]. The original CTBD contains around 1.1 $g.L^{-1}$ sulfate salts, and thus additional sulfate did not improve the process performance. Nevertheless, the supporting electrolyte lowers the EC by reducing the internal resistance of the system (Table 2-2). The addition of electrolyte increases the CTBD electrical conductivity from 3.4 to 8.0 $mS.cm^{-1}$ and decreases the overall cell voltage by lowering the voltage drop (iR drop) [160]. Hence, Na_2SO_4 electrolytes can be added during the EO of CTBD to reduce the EC without affecting the OCs removal efficiency.

2.3.6 Formation of chlorinated species and their effect on the acute toxicity

EO of the chloride-containing CTBD by the BDD-anode and MMO-anode at different *j*-values resulted in the formation of various organic and inorganic chlorinated species (Table 2-3). This resulted in an increase in the acute toxicity of the treated CTBD to *Vibrio fisheri*, as evidenced by the % bioluminescence inhibition (BI) (Table 2-3).

$HO^{\bullet}$ formed during EO with the BDD anode may oxidize Cl^- to ClO_4^- via the ($OCl^- \xrightarrow{HO^{\bullet}} ClO_2^- \xrightarrow{HO^{\bullet}} ClO_3^- \xrightarrow{HO^{\bullet}} ClO_4^-$) pathway [163]. The MMO-anode mainly forms HClO/ClO^- during EO, and the absence of $HO^{\bullet}$ leads to less oxidation towards

ClO_3^-. Therefore, less ClO_3^- was produced with the MMO-anode compared to the BDD-anode, and no ClO_4^- was produced with the MMO-anode (Table 2-3). However, the AOX production with the MMO-anode was higher than with the BDD-anode (Table 2-3) due to the chlorination of OCs with the produced HClO/ClO^- (section 2-3.1) [177].

Table 2-3. *Chlorinated by-products and bioluminescence inhibition (BI) before and after EO of CTBD with the BDD-anode and MMO-anode at different j-values. Experimental conditions: T = 21-23°C, conductivity = 3.7 mS cm^{-1}, pH = 6.9, recirculation flow rate = 30 L h^{-1}, treatment time = 3 h.*

	Applied current (mA cm^{-2})	Cl^- (mg L^{-1})	ClO^- (mg L^{-1})	ClO_3^- (mg L^{-1})	ClO_4^- (mg L^{-1})	AOX (mg Cl^- L^{-1})	% BI
Initial CTBD	-	505 (12)	-	-	-	1.78	<5
BDD	2.3	400 (9)	35 (2)	55 (3)	15 (1)	16 (3)	>80
	5.5	312 (12)	78 (2)	192 (1)	44 (3)	15 (1)	> 90
	8.7	290 (10)	152 (6)	302 (5)	82 (2)	17 (1)	> 90
MMO	5.5	426 (3)	80 (3)	18 (1)	-	19 (2)	> 90
	8.7	387 (7)	205 (5)	56 (3)	-	23 (4)	> 90
	14.5	346 (1)	310 (3)	109 (4)	-	20 (3)	> 90

EO of the CTBD with both anodes significantly enhanced the acute toxicity of the initially non-toxic CTBD to *Vibrio fisheri* (Table 2-3), likely because of the production of the inorganic and organic chlorinated species. To determine the cause of the toxicity, EO with a synthetic solution without OCs (Table S2-3) based on the real CTBD (Table S2-1) was performed. EO-treatment of 3 h with a *j*-value of 5.5 mA.cm^{-2} with both anodes resulted in a BI of 80%, indicating that ClO^-, ClO_3^- and

ClO_4^- were responsible for the increase in BI, and not the production of chlorinated organic by-products (AOX) from the OCs. Another indication that chlorinated organic by-products from the OCs do not contribute to the acute toxicity of the EO-treated CTBD is that despite differences in TOC removal efficiency with different *j*-values, the toxicity is similar (Table 2-3). Also, similar AOX production but low ClO_3^- and ClO_4^- production at the lowest *j*-value of 2.3 $mA.cm^{-2}$ with the BDD-anode resulted in the lowest BI (Table 2-3). A similar increase in toxicity as a result of the production of ClO_3^- and ClO_4^- was observed by Wang et al. (2016) and Garcia-Espinoza et al. (2018) [178, 179]

Preventing inorganic chlorinated species evolution is essential for the viability of EO as a pre-treatment technology for CTBD for reuse as make-up water in the cooling tower. The production of hypochlorite ($HClO/ClO^-$) is somewhat beneficial since it can act as a disinfectant in the cooling tower system and as a continuous cleaning agent for the membranes in the deionization step [180, 181] reported that RO (RE8040-UE) and NF (TFC-SR3) membranes remove 60 to 90% ClO_4^- from water containing a mixture of salts and natural organic matter. Therefore, from an application perspective, inorganic chlorinated species formation and toxicity do not make EO of CTBD an immediate bottleneck, as long as the emission of reactive chlorine and AOX species to the environment is prevented, accumulation in the cooling tower system is carefully monitored and EO is smartly integrated with other CTBD treatment technologies.

2.4 CONCLUSIONS

Cooling tower blowdown (CTBD) needs a pre-treatment that removes recalcitrant organic compounds (OCs) before they can be desalinated and reused in the cooling tower itself. The present study shows that electrochemical oxidation (EO) is a potential pre-treatment technology to remove OCs from CTBD, especially when employing a boron-doped diamond (BDD) anode. With this anode, 51% of the OCs were mineralized with an applied current density of 8.3 $mA.cm^{-2}$, while the remaining OCs were partially oxidized. Increasing the applied current density enhanced the OCs removal efficiency, while acidic and basic pHs, different hydrodynamic conditions, and the addition of supporting electrolytes effect on the OCs removal efficiency were limited. The OCs in CTBD mainly consisted of humic

substances (HS), and 35% of these humic substances were mineralized after EO-treatment with the BDD-anode. The remaining humic substances were transformed into low-molecular-weight substances and building blocks after EO-treatment with the BDD-anode. The mineralization and transformation of OCs are accompanied by the formation of ClO^-, ClO_3^-, ClO_4^- and adsorbable organic halides (AOX). As a result of the formation of these products, the toxicity of the initially non-toxic CTBD to Vibrio fischeri increased 20-fold after EO-treatment. From an application perspective, the production of chlorinated by-product hypochlorite (ClO^-) can be advantageous because it can act as a disinfectant in the cooling tower system. However, toxic by-product formation and accumulation need to be critically monitored when applying EO with the BDD-anode for CTBD-treatment.

Chapter 3.

Cooling tower water treatment using a combination of electrochemical oxidation and constructed wetlands.

This chapter has been published as:
Saha, Pradip, Thomas V. Wagner, Jiahao Ni, Alette AM Langenhoff, Harry Bruning, and Huub H.M. Rijnaarts. "Cooling tower water treatment using a combination of electrochemical oxidation and constructed wetlands." Process Safety and Environmental Protection 144 (2020): 42-51.

Abstract

A substantial part of the freshwater used in the industry is consumed in cooling towers. Cooling towers discharge saline cooling tower blowdown (CTBD), and the reuse of CTBD in the cooling tower can lower the industrial freshwater footprint. This reuse requires CTBD desalination and a pre-treatment that removes organic chemicals before physico-chemical desalination technologies can be applied efficiently. In the present study, the pre-treatment of CTBD by a combination of electrochemical oxidation (EO) with a boron-doped diamond (BDD) or mixed-metal oxide (MMO) anode and a vertical flow constructed wetland (VFCW) was assessed in both possible configurations. The integrated VFCW-EO systems removed more organic chemicals, such as COD, TOC, and the corrosion inhibitor benzotriazole than the EO-VFCW systems. However, the EO resulted in highly toxic effluent to *Vibrio fischeri* and the plants in the VFCW. This toxicity was the result of the production of unwanted chlorinated organic compounds and ClO_3^- and ClO_4^- by both the BDD- and MMO-anode during EO. These toxic EO by-products were removed substantially in the VFCW during EO-VFCW treatment but did impact the removal efficiency and viability of the VFCW. Moreover, significant water loss was observed in the VFCW due to evapotranspiration. In conclusion, the negative impact of EO effluent on the VFCW and evapotranspiration of the VFCW should be considered during application.

Keywords

Boron-doped diamond anode; Mixed-metal oxide anode; Vertical-flow constructed wetland; Benzotriazole; Chlorinated by-products.

3.1 INTRODUCTION

The reuse of discharged cooling tower water in the industry itself lowers the industrial freshwater footprint and alleviates the pressure on natural freshwater resources. Approximately 25% of the worldwide freshwater withdrawal is used for industrial processes [182], and approximately 40-60% of the water used in refineries is consumed in cooling towers [183]. Due to evaporation in the cooling tower, the concentration of salts in the cooling tower water increases. After a salt concentration threshold is reached, cooling tower water is discharged as so-called cooling tower blowdown (CTBD) and replaced that with fresh water. The reuse of this CTBD in the cooling tower itself could allow the industries to reduce their freshwater consumption [19, 34].

CTBD mainly contains salts and organic compounds (OCs). The primary sources of OCs in the CTBD are conditioning chemicals, such as benzotriazole, added to the cooling tower water during operation [34], and humic substances originating from groundwater and surface water that is used to compensate for the discharged CTBD [184]. The salts result in a CTBD electrical conductivity of approximately 1.5-4.0 mS/cm, and this should be lower than 1.0 mS/cm to enable the reuse of CTBD in the cooling tower [11, 33, 139]. Hence, desalination is required before the reuse of the CTBD in the cooling tower. Several mild physico-chemical desalination technologies for CTBD-treatment have been studied, such as nano-filtration, reverse osmosis, membrane distillation, and electrodialysis [11, 34, 137, 138, 185]. These studies reported that the performance of physico-chemical desalination technologies was hampered due to too high concentrations of OCs in the CTBD. For instance, the OCs create fouling on the nano-filtration or reverse osmosis membranes and scaling on the electrode surface of the electrodialysis reversal system [137, 138]. Therefore, a pre-treatment that removes OCs before physico-chemical desalination is required to improve the performance and lifetime of these technologies.

Various pre-treatment methods were studied to remove OCs from CTBD before physico-chemical desalination, such as powdered activated carbon, sand filtration, coagulation, ultrafiltration, and biologically active carbon [11, 186]. Recently, constructed wetlands (CWs) have been proposed as an attractive alternative pre-treatment method [187, 188]. CWs are man-made wetlands systems in which various

biological, physical, and chemical removal mechanisms function simultaneously to remove compounds from wastewater [189, 190]. In addition to the removal of compounds, CWs offer additional benefits: providing the storage of large volumes of treated CTBD that can be used during droughts, increasing the local biodiversity, and lower operation and maintenance costs. However, various factors limit the application of CWs for CTBD treatment. For instance, CWs cannot remove some recalcitrant compounds to biodegradation and do not adsorb to the CW substrate. Also, OCs in CTBD can cause toxic effects on the microbial communities that are responsible for the degradation of OCs in the CW. For instance, commonly used biocides glutaraldehyde and DBNPA in concentrations that are relevant for cooling tower application can inhibit the biodegradation of OCs by CW microorganisms [191]. Therefore, an additional treatment step combined with CW treatment is necessary to remove OCs from CTBD before physico-chemical desalination completely.

Combined biological and chemical treatment systems are promising for industrial wastewater, which is not susceptible to a single treatment [192]. Electrochemical oxidation (EO) is of interest among chemical treatments because of its versatility, controllability, and enhanced removal efficiency for recalcitrant and toxic OCs [70]. During EO, electrical energy is applied to form hydroxyl radicals and reactive chlorine species on an anode surface that can subsequently oxidize OCs [163]. EO by boron-doped diamond (BDD) and mixed-metal oxide (MMO) anodes is effective for the removal of humic substances [152] and biocides [193]. The integration of CWs with EO has successfully been applied for the treatment of olive pomace leachate [190], olive washing wastewater [194], blackwater [195], and surface water [196]. However, several researchers reported that a substantial amount of organic halides (AOX), chlorite, and perchlorates are formed during EO of chloride-containing wastewaters [163, 184, 197]. These organic and inorganic chlorinated compounds may hamper the pre-treatment efficiency of CTBD.

In the present study, we assessed the effectiveness of a hybrid system combining EO with a vertical-flow CW system (VFCW) and vice versa for the removal of OCs from CTBD. The performance of two anodes was assessed: a BDD- and an MMO-anode. The process performance was determined according to the COD and TOC removals in the standalone EO and VFCW systems and combined EO-VFCW and VFCW-EO systems. Benzotriazole, which was already present in the CTBD, was

used in both systems as a model compound for the recalcitrant OCs fraction. Furthermore, CTBD contains chloride, and therefore the production of organic and inorganic chlorinated compounds may have an adverse effect on the CTBD pre-treatment efficiency of CWs. Therefore, the concentrations of AOX, chlorite, and perchlorate were monitored. Additionally, micro-toxicity tests were carried out using *Vibrio fischeri* to assess the toxicity of effluents of the different treatments.

3.2 MATERIALS AND METHODS

3.2.1 Chemicals

H_2SO_4, $CuSO_4$, methanol, and acetic acid were obtained from Sigma Aldrich (Zwijndrecht, The Netherlands). K_2PO_4, $CaCl_2.2H_2O$, $MgSO_4.7H_2O$, and urea were obtained from Merck KGaA (Darmstadt, Germany). NaCl was obtained from VWR chemicals (Leuven, Belgium).

3.2.2 Treatment scenarios

Two different scenarios were used to evaluate and compare the performance of the standalone and combined systems:

Scenario 1: VFCW treatment followed by EO with two different anodes (VFCW-EO) (Fig. 3-1a and 3-1b).

Scenario 2: EO with two different anodes, followed by VFCW treatment (EO-VFCW) (Fig. 3-1c and 3-1d).

EO was performed with either a ruthenium oxide – mixed metal oxide (MMO) or boron-doped diamond (BDD) electrode as the anode; hence the combined systems will be referred to as VFCW-EO/BDD, VFCW-EO/MMO, EO/BDD-VFCW, and EO/MMO-VFCW.

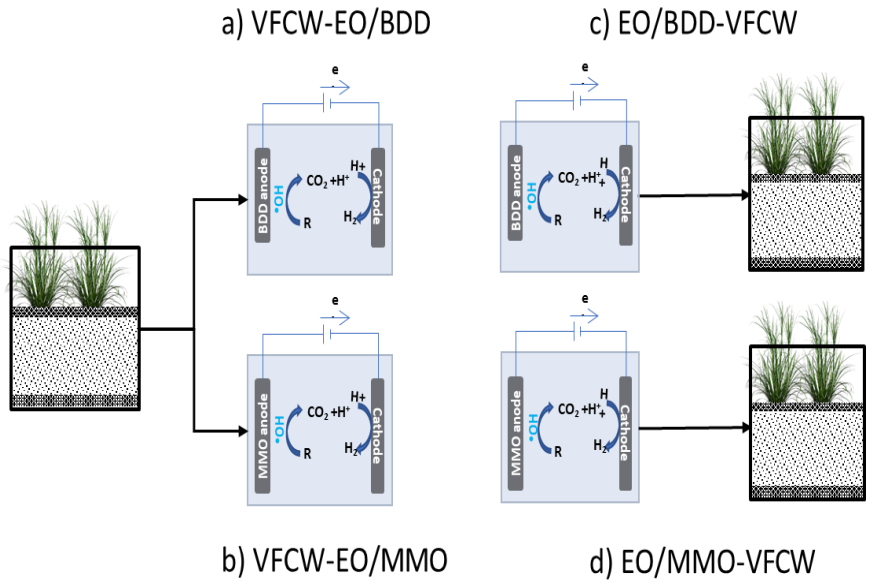

Fig. 3-1. *Treatment scenarios for cooling tower blowdown. a) Vertical-flow constructed wetland (VFCW) followed by electrochemical oxidation (EO) by boron-doped diamond (BDD)-anode; b) VFCW followed by EO by mixed-metal oxide (MMO)-anode; c) EO by BDD-anode followed by VFCW; d) EO by MMO-anode followed by VFCW.*

3.2.3 Electrochemical oxidation experiments

The EO experiments were conducted in an undivided flat plate reactor with a 22.4 cm^2 (11.2 cm × 2.0 cm) electrode surface area. A MMO- or BDD-electrode was used as the anode. Platinum-coated titanium- (Pt) electrode was employed as the cathode. Magneto Special Anodes BV provided both the anodes and the cathode (Schiedam, The Netherlands). The distance between the anode and cathode was 1.5 cm. A peristaltic pump was used to recirculate the CTBD in the cell at 10 mL/sec flow rate. Based on a previous study of our research group [198], all EO experiments were carried out with a current density of 5.5 mA/cm^2 in the EO/BDD cell and 8.7 mA/cm^2 in the EO/MMO cell for 3 hours. Before the EO experiment, the system was anodically polarized for 30 min at 2.7 mA/cm^2 using a 0.1M H_2SO_4 electrolyte solution. All experiments were carried out at room temperature without any additional supporting electrolyte. Original CTBD and day-3 effluent of VFCW were electrochemically treated in duplicate for kinetic study.

3.2.4 Vertical-flow constructed wetlands (VFCW)

Three lab-scale VFCWs were built based on the design of [199] and used for treating the raw CTBD, effluent from EO/BDD, and EO/MMO cell treatment. The VFCWs (Fig. 3-1) were built-in glass aquariums with a volume of 0.015 m^3 (0.25 × 0.25 × 0.25 m), of which the sides were covered with a fabric that was impenetrable by light to prevent algae growth. The VFCWs were composed of three layers. The top and bottom layers consisted of 4 cm of 8-16 mm gravel (GAMMA, Wageningen, the Netherlands) that allowed proper distribution of the influent and drainage of the effluent. The middle part consisted of a 16 cm thick layer of sand with an average diameter of 0.2 mm (GAMMA, Wageningen, the Netherlands). The VFCWs were planted with *Phragmites australis* since this plant species grow well in CWs fed with CTBD [187]. The VFCWs were kept in a climate chamber (Heraeus Vötsch MC 785-KLIMA) operated at 18 (±1)^{o}C, relative humidity of 75 (±5)%, and 10 hours of daily light exposure by fluorescent lamps (58 W, 400-800 nm, 645 lx).

Before the addition of CTBD, the VFCWs were fed with synthetic municipal wastewater composed of urea (30 mg/L), K_2PO_4 (28 mg/L), NaCl (7 mg/L), $CaCl_2.2H_2O$ (4 mg/L), and $MgSO_4.7H_2O$ (2 mg/L) for two months to enable the development of a microbial community capable of degrading OCs. Subsequently, all VFCWs were fed with raw CTBD for 15 days to acclimatize to CTBD, after which the performance assessment and date counting started. For scenario 1 (VFCW-EO), one of the VFCWs was fed with untreated CTBD for 90 days. For scenario 2 (EO-VFCW), the EO/BDD-VFCW and EO/MMO-VFCW systems were fed with the effluent of the EO experiments for 42 days. For the EO-VFCW experiments, EO treated CTBD every 3-day to obtain fresh EO-treated CTBD with a consistent composition. All the VFCWs were fed manually and completely emptied every 3-days to obtain a hydraulic retention time of 3 days. This 3-day hydraulic retention time was based on earlier experience of our research group with CWs treating CTBD [140, 187]. The VFCW effluent volume was compared with the influent volume to determine the evapotranspiration of the CWs during the entire experiment period (Table S3-1). Samples for COD and TOC measurements were taken every three days.

3.2.5 Cooling tower blowdown (CTBD) composition

Real CTBD was obtained from a cooling tower of Dow Benelux BV (Terneuzen, The Netherlands). During the operation of the cooling tower, cooling tower water is prepared from local surface water by sand filtration. Sulfuric acid is added to the treated surface water to adjust the pH. Benzotriazole is added to the treated surface water to prevent corrosion. Additionally, phosphonate antiscalants are added to prevent scaling, and biocides are added to inhibit microbiological activity [34]. After a salt concentration threshold is reached, the treated surface water is discharged as CTBD. The CTBD used in the present study was obtained during a regular discharge episode. The obtained CTBD was stored at 4°C to prevent the growth of microorganisms and was subsequently used in all experiments without any pre-treatment. The characteristics of the CTBD are provided in Table 3-1.

Table 3-1. *Characteristics of cooling tower blowdown (CTBD) used in this study.*

Parameter	Avg.	SD (±)	Unit
Conductivity	3.4	0.1	mS/cm
Cl^-	458	10	mg/L
NO_3^-	57	1.8	mg/L
SO_4^{2-}	1043	52	mg/L
Na^+	334	2.9	mg/L
Ca^{2+}	338	7.6	mg/L
Mg^{2+}	58	2.4	mg/L
K^+	75	1.3	mg/L
TOC	41	1.3	mg/L
COD	107	6.4	mg/L
Benzotriazole	0.8	0.1	mg/L
AOX	3.2	0.2	mg Cl^-/L
Bioluminescence inhibition	<5%		(%)
pH	6.8	0.2	

3.2.6 Analytical methods

3.2.6.1 COD and TOC

Chemical oxygen demand (COD) and total organic carbon (TOC) of every effluent batch were measured for both scenarios. COD was measured by Hach Lange

kit LCK-314 (Hach Lange GmbH, Düsseldorf, Germany), and TOC was analyzed by a TOC-L_{CPH} analyzer connected to an ASI-L autosampler (Shimadzu, 's Hertogenbosch, The Netherlands). A catalytic oxidation – non-dispersive infrared detection method was used.

3.2.6.2 Ions determination

Cl^-, ClO_3^-, ClO_4^-, NO_3^-, and SO_4^{2-} were measured by ion chromatography (IC) on an ICS 2100 (Dionex, Breda, The Netherlands) equipped with a Dionex IonPac AS19 column (4×250 mm) using a hydroxide gradient. ICP-OES AVIO 500 (Perkin Elmer, USA) was used for Na^+, Ca^{2+}, Mg^{2+}, and K^+ analysis.

3.2.6.3 Benzotriazole

Benzotriazole was measured by LC-MS/MS. The sample injection volume was 20 µl. Chromatographic separation was achieved with a Shim-pack XR-ODSIII C18-column (50×2 mm with a particle size of 1.6µm) (Shimadzu, 'S-Hertogenbosch, the Netherlands) installed in a Prominence LC consisting of two LC-20AD XR pumps, a SIL-20AC XR auto-sampler, and a CTO-20AC column oven. The mobile phase consisted of solvent A: H_2O with 0.1% acetic acid and solvent B: methanol. A 4.5 min gradient elution method was used with an increase from 10% B to 100% B in 2.5 min, 100% B for 1.5 min, and a decrease from 100% B to 10% B in 0.5 min. The flow rate was 0.3 ml/min, and the column temperature was 35°C. The system was allowed to equilibrate for 2.5 min prior to each sample injection. Mass spectrometry was performed on a 4000 QTRAP MS/MS system (AB Sciex, MA, USA) coupled to an ESI interface operating in positive mode. Data acquisition and analysis were performed with AB Sciex Analyst software (version 1.5.1, AB Sciex, USA). Benzotriazole was identified and quantified by multiple reaction monitoring (MRM) using fragment ions 120/65 and 120/92 and an 11-point external calibration line (0.1 – 20 µg/L). The lowest point of the calibration line (0.1 µg/L) corresponded with the limit of quantification for benzotriazole.

3.2.6.4 Adsorbable organic halides (AOX)

The formation of AOX was determined with the LCK 390 AOX Cuvette Test (Lange GmbH, Düsseldorf, Germany) according to the test protocol provided by the manufacturer. In short, AOX compounds were adsorbed on a carbon disk, after

which it was rinsed with solvent to remove the inorganic carbon before digestion for two hours at 100ºC. Finally, the AOX concentration was measured by a DR 3900 spectrophotometer (Lange GmbH, Düsseldorf, Germany).

3.2.6.5 Microtox toxicity tests

The bioluminescence inhibition of marine bacteria *Vibrio fischeri* was done by Microtox® test kits (Microlan, the Netherlands) and an M200 Infinite Pro Microplate Reader (Tecan, Switzerland). The bacteria were exposed to the effluent samples of the different scenarios for 15 min at room temperature and in darkness. $CuSO_4$ as Cu (II) and raw CTBD were used as negative control and blank control, respectively.

3.2.7 Data analysis

3.2.7.1 Removal efficiencies

A distinction was made between the mass-based removal efficiency (mbRE) and concentration-based removal efficiency (cbRE) for the different treatment systems. The cbRE for COD and TOC was calculated according to Eq. (3.1):

$$\mathrm{cbRE} = (\mathrm{C_{inf}} - \mathrm{C_{eff}})/\mathrm{C_{inf}} \times 100\% \quad (3.1)$$

In Eq. (1), C_{inf} and C_{eff} are the influent and effluent concentrations in mg/L.

The mbRE for COD and TOC were calculated according to Eq. (3.2):

$$\mathrm{mbRE} = (\mathrm{m_{inf}} - \mathrm{m_{eff}})/\mathrm{m_{inf}} \times 100\ \% \quad (3.2)$$

In Eq. (2), m_{inf} is the influent mass in mg, derived from the volume and concentration of the influent, and m_{eff} is the effluent mass derived from the volume and concentration of the effluent.

The combined mass-based removal efficiency ($\mathrm{mbRE_c}$) of the treatment-combinations is expressed as Eq. (3.3) (supporting calculations are provided in the SI text 3-1):

$$\mathrm{mbRE_C} = \mathrm{mbRE_1} + \mathrm{mbRE_2} - (\mathrm{mbRE_1} \times \mathrm{mbRE_2}) \quad (3.3)$$

In Eq. (3.3), $mbRE_1$ is the 1st step removal efficiency and $mbRE_2$ is the 2nd step removal efficiency.

3.2.7.2 Energy consumption during electrochemical oxidation

The energy consumption by EO (kWh/kg COD) was calculated according to Eq. (3.4)

$$\text{Energy consumption} = \frac{\Delta E_{cell} I t}{(1000 \times V_s \times \Delta COD)} \quad (3.4)$$

Where: V_S is electrolyte volume (m^3), I is the applied current (A), t is the electrolysis time (h), ΔE_{cell} is the average cell voltage (V), and ΔCOD is the cbCOD removal during the oxidation time (kg COD/m^3)

3.3 RESULTS AND DISCUSSION

The treatment efficiency of the integrated EO-CW systems will be discussed in the following sections according to the two scenarios described in section 3.2.2.

3.3.1 Constructed wetland treatment followed by electrochemical oxidation

In Scenario 1, raw CTBD was fed to the VFCWs, after which it was treated by EO with a BDD- or an MMO-anode. The performance of this scenario is provided in Table 3-2.

Table 3-2. *Performance of treatment scenario 1: Vertical-flow constructed wetland (VFCW) followed by electrochemical oxidation (EO) with boron-doped diamond (BDD) or mixed-metal oxide (MMO) anodes. mbRE = mass-based removal efficiency.*

Performance evaluation parameter	CW followed by EO/BDD			CW followed by EO/MMO		
	CW Step (±SD)	EO step (±SD)	Combine CW-EO/BDD	CW step (±SD)	EO step (±SD)	Combine CW-EO/MMO
COD mbRE (%)	47 (11)*	95 (5)†	97	47 (11)*	55 (5)†	76
TOC mbRE (%)	46 (9)*	28 (6)†	61	46 (9)*	8 (1)†	50
† Benzotriazole (%)	97 (0.1)	100	100	97 (0.1)	100	100
† Bioluminescence inhibition (%)	10 (3)	>95	-	10 (3)	>95	-
† AOX (mg Cl^-/L)	2.4 (1)	18 (2)	-	2.4 (1)	19 (2)	-
† ClO_3^- (mg/L)	0	197 (14)	-	0	79 (3)	-
† ClO_4^- (mg/L)	0	39 (3)	-	0	0	-

**Average of 15 measurements (3-45 days); † Average of 3 measurements (3-15 days)*

3.3.1.1 COD and TOC removal in the vertical-flow constructed wetland

During the first two weeks of operation, the cbRE for COD was around 60% (Fig. 3-2a). However, the cbRE decreased in the subsequent 45 days. The COD concentration in the VFCW effluent was higher than the VFCW influent concentration after 51 days of operation, probably due to a substantial amount of evapotranspiration by *Phragmites australis* in the VFCW, resulting in a concentrated VFCW effluent. On average, 32 (±3)% of the influent water evaporated from the VFCW under controlled climate conditions (Table S3-1). A similar declining trend of the COD cbRE caused by evapotranspiration in a VFCW was reported by Grafias et al. (2010) for the treatment of olive pomace leachate by VFCW-EO [190]. In that study, the COD cdRE also dropped substantially after initial removal, and effluent COD concentrations became similar to the influent COD concentration within 60 days of operation. A substantial amount of evapotranspiration of CTBD in the VFCW would result in a lower CTBD reuse efficiency and should, therefore, be avoided.

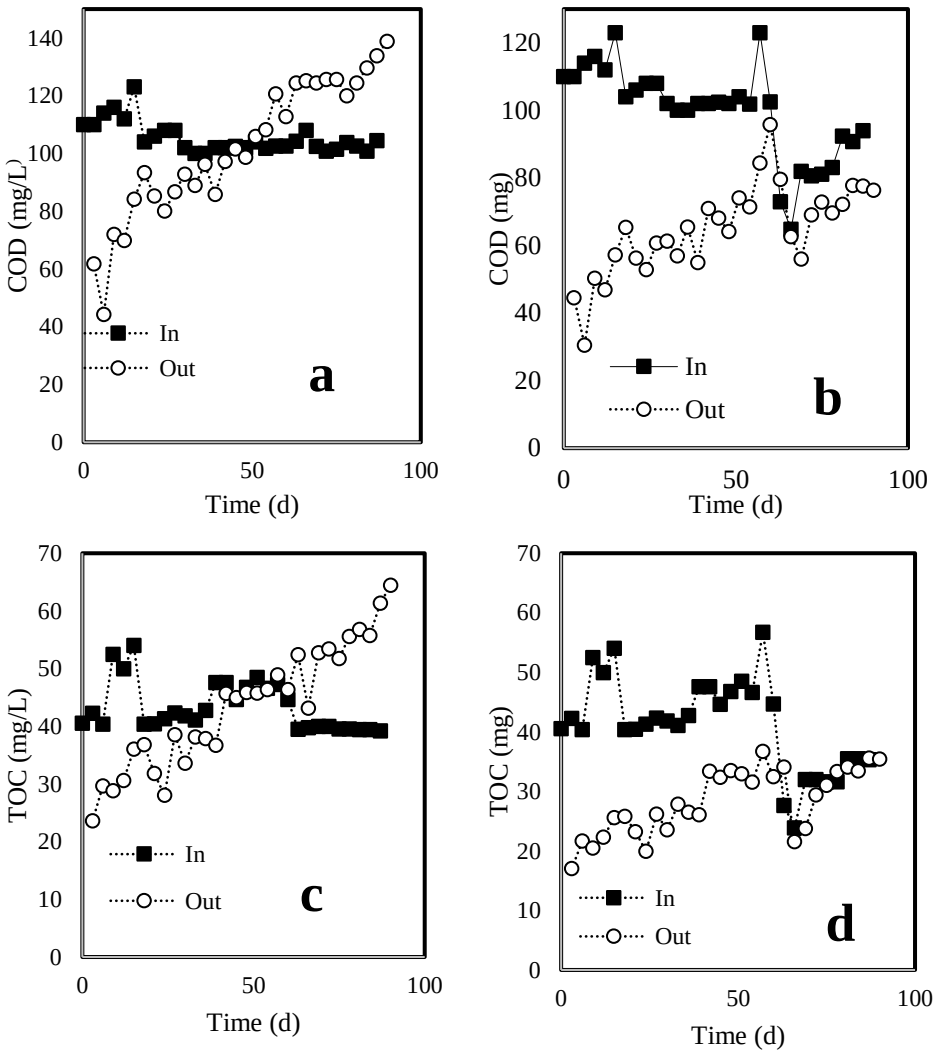

Fig. 3-2. *Vertical-flow constructed wetlands (VFCW) performance during original CTBD treatment. (a) concentration-based COD; (b) mass-based COD; (c) concentration-based TOC; (d) mass-based TOC.*

The mbRE of COD was calculated (Fig. 3-2b) to correct the COD concentrations for the evaporation. The mbRE decreased from ~65% during the first week of operation to ~10% after 45 days of operation (Fig 3-2b). After 60 days, the CTBD loading was varied to observe the response in the removal efficiency of the VFCW. The effluent COD concentration continued to increase, while the mbRE of COD fluctuated with the loading, indicating that part of the COD was removed but that

evapotranspiration caused a higher effluent concentration than influent concentration.

The TOC removal showed similar trends in cbRE and mbRE as the removal of COD (Fig. 3-2c; 3-2d). The TOC cbRE was ~50% during the first days of operation. However, the TOC cbRE decreased day by day, and the effluent TOC concentration became higher than the influent TOC concentration after 60 days (Fig 3-2c). The mbRE of TOC decreased from ~60% during the first 15 days to ~0% after 60 days (Fig 3-2d).

The removal of TOC/COD in CWs is the result of various removal processes and mainly depends on the form of the organic fraction [189]. The dissolved organic fraction can be removed by biodegradation, adsorption, and plant uptake, while the particulate organic matter fraction is retained in a CW by physical filtration. The TOC of the CTBD in the present study mainly consists of humic acids [11]. It was observed by Wagner et al. (2020a) that the particulate humic acid fraction of synthetic CTBD was retained by physical filtration [187]. However, the humic acids in the real CTBD in the present study were better dissolved and thus needed to be removed by biological and chemical rather than physical removal mechanisms, such as biodegradation and adsorption to the CW substrate. However, humic acid is recalcitrant to biodegradation [200], and this would explain the low mbRE of COD/TOC consisting of humic acids in the VFCW system.

The benzotriazole cbRE of the VFCW was 97 (±0.1)% (Table 3-2), despite the substantial impact of the evapotranspiration on the COD and TOC removal efficiencies. This benzotriazole removal from CTBD in subsurface CWs is the result of simultaneously occurring adsorption and biodegradation [140]. The complexation of benzotriazole and Ca^{2+} ions that are present in the CTBD (Table 3-1) increases the adsorption of benzotriazole to the sediment [140]. VFCWs have a higher benzotriazole removal efficiency than horizontal flow CWs [188, 201, 202] as a result of the prevailing aerobic conditions in the VFCW allowing aerobic biodegradation to occur.

3.3.1.2 COD removal by electrochemical oxidation post-treatment

VFCW pre-treated CTBD was treated by EO with a BDD or MMO anode, and the COD cbRE with the BDD-anode was 95 (±5)% after 3 hours of oxidation (Fig.

3-3). With the MMO-anode, the COD cbRE was only 55 (±5)% after the same time of operation (Fig. 3-3). The COD removal occurred with the first-order reaction kinetics with a linear regression coefficient of >0.99 for both anodes (Fig. S3-1). The rate constants were 1.3×10^{-2} /min for the BDD-anode and 4.8×10^{-3} /min for the MMO-anode.

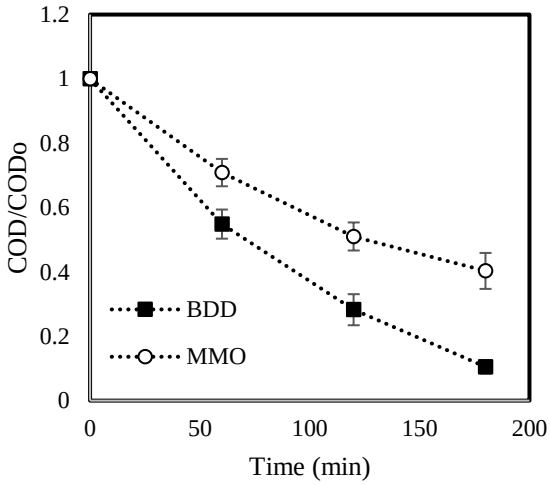

Fig. 3-3. *COD removal during the electrochemical oxidation (EO) of Day-3 VFCW effluent. COD: 61 mg/L, Conductivity: 4.8 mS/cm, pH: 7.08, Applied current density: 5.5 mA/cm2 for BDD anode and 8.7 mA/cm2 for MMO anode.*

The calculated rate constants show that the BDD-anode performed better than the MMO-anode. The water oxidation potential of the BDD-anode is 2.3 V/SHE (standard hydrogen electrode), whereas it is 1.47 V/SHE for a MMO-anode [164]. Therefore, the active hydroxyl, sulfate, and chlorine radicals' formation according to Eqs. (3.5)-(3.7) (Table 3-3) is more efficient with the BDD-anode. These radicals can quickly oxidize the OCs in the CTBD, which reduces the COD concentration [163].

In contrast, the radical formation with the MMO-anode is limited due to the low water oxidation potential. However, it was reported by different authors that active chlorinated species, such as hypochlorite, can be formed in the bulk liquid with the MMO-anode according to reaction Eqs. (3.8)-(3.10) (Table 3-3) [203, 204]. However, the oxidation potential of these active chlorinated species is lower than the oxidation potential of the radicals. Therefore, the COD removal was slower with the MMO-anode than with the BDD-anode, which was also reflected in the energy

consumption (Table S3-2) during the EO. The energy consumption was 19 kWh/kg COD for the EO/BDD system, whereas it was 64 kWh/kg COD for the EO/MMO system.

Table 3-3. *Possible radicals and active chlorinated species formed during electrochemical oxidation.*

Equation No	Reaction	Reference
(3.5)	$H_2O \rightarrow HO^{\bullet} + H^+ + e^-$	Lan et al. (2017)
(3.6)	$SO_4^{2-} + HO^{\bullet} \rightarrow SO_4^{\bullet -} + OH^-$	
(3.7)	$Cl^- + HO^{\bullet} \rightarrow Cl^{\bullet} + OH^-$	
(3.8)	$2Cl^{\bullet} \rightarrow Cl_2$	
(3.9)	$Cl_2 + H_2O \rightarrow HOCl + Cl^- + H^+$	
(3.10)	$HOCl \rightleftarrows ClO^- + H^+$	

3.3.1.3 The overall treatment performance of scenario 1

The COD mbRE of the integrated VFCW-EO/BDD system was 97%, while the TOC mbRE was 61% (Table 3-2). The VFCW-EO/MMO system had a COD mbRE of 55 (±5)% and a TOC mbRE of 50% (Table 3-2). EO-treatment after the VFCW by both anodes was capable of removing the remaining benzotriazole (Table 3-2). Hence, VFCW-EO/BDD treatment removed a substantial amount of OCs from the CTBD that could hinder physico-chemical CTBD desalination, despite the large loss in water volume as a result of evapotranspiration in the VFCW.

The toxicity of the CTBD in terms of bioluminescence inhibition of *Vibrio fischeri* showed an increase after VFCW-EO treatment. The untreated CTBD had a bioluminescence inhibition of ~5%. After VFCW-treatment, the bioluminescence inhibition increased to 10 (±3)% (Table 3-2), demonstrating a slight increase in toxicity of the VFCW-treated CTBD to *Vibrio fischeri*. This might have been a result of evapotranspiration and a corresponding increase of the electrical conductivity from 3.4 mS/cm to ~4.8 mS/cm. In contrast, the bioluminescence inhibition increased to 95% (Table 3-2) after the EO-treatment with both anodes, which indicated high toxicity of the treated CTBD to *Vibrio fischeri* as a result of EO. This increased toxicity was the result of the formation of chlorinated organic compounds (AOX) and chlorinated inorganic compounds that are toxic to *Vibrio fischeri* [205]. The AOX concentration increased from 2.4 (±1) to 18-19 mg Cl^-/L after EO-treatment by both anodes (Table 3-2). Also, 197 (±14) mg/L of ClO_3^- and 39 (±3)

mg/L ClO_4^- were formed with the BDD-anode. With the MMO-anode, only 79 (±3) mg/L of ClO_3^- was produced (Table 3-2). De Moura et al. (2014) showed that EO of chloride-containing water with RuO_2-MMO-anodes could produce hypochlorite (ClO^-) and ClO_3^- from chloride [203]. Perchlorate (ClO_4^-) was found during the EO of chlorinated wastewater with a BDD-anode according to the following steps [163].

$$Cl^- \rightarrow OCl^- \xrightarrow{HO^\bullet} ClO_2^- \xrightarrow{HO^\bullet} ClO_3^- \xrightarrow{HO^\bullet} ClO_4^-$$

Similarly, Garcia-Segura et al. (2015) observed that high concentrations of ClO_3^-, ClO_4^-, and lower concentrations of AOX were formed during EO-treatment of secondary effluent with a BDD-anode [149]. AOX, ClO_3^-, and ClO_4^- are responsible for increasing the toxicity of the treated CTBD [205]. In conclusion, VFCW-EO treatment does result in substantial OCs removal but produces undesired chlorinated products that increase the CTBD toxicity. Therefore, these undesirable chlorinated products need to be removed during subsequent physico-chemical desalination steps before reuse.

3.3.2 Scenario 2: Electrochemical oxidation followed by vertical-flow constructed wetlands

In Scenario 2, raw CTBD was electrochemically treated with the BDD-anode or the MMO-anode for 3 hours, after which EO effluent was fed to the VFCWs. The performance of this scenario is provided in Table 3-4.

Table 3-4. *Performance of treatment scenario 2: Electrochemical oxidation (EO) with boron-doped diamond (BDD) and mixed-metal oxide (MMO) anodes followed by vertical-flow constructed wetland (VFCW). mbRE = mass-based removal efficiency*

Performance evaluation parameter	EO_BDD followed by CW			EO_MMO followed by CW		
	EO step (±SD)	CW Step (±SD)	Combine EO/BDD-CW	EO step (±SD)	CW step (±SD)	Combine EO/MMO-CW
*COD mbRE (%)	81 (5)	-25 (31)	76	47 (6)	18 (32)	57
*TOC mbRE (%)	41 (5)	12 (23)	48	11 (4)	18 (29)	27
† Benzotriazole (%)	100	-	100	75 (10)	100	100
† Bioluminescence inhibition (%)	>95	27(17)	-	>95	14 (16)	-
† AOX (mg Cl^-/L)	15 (2)	3 (1)	-	24 (2)	5 (2)	
† ClO_3^- (mg/L)	183 (4)	118 (7)	-	99 (11)	29 (6)	-
† ClO_4^- (mg/L)	35 (1)	24 (1)	-	0	0	-

** Average of 14 measurements (3-42 days); † Average of 3 measurements (3-15 days)*

3.3.2.1 COD removal during electrochemical oxidation of original CTBD

EO-treatment with the BDD-anode resulted in a COD mbRE of 81 (±5)%, while the COD mbRE with the MMO-anode was 47 (±6)% (Fig. 3-4). Similar to scenario 1 (section 3.3.1), the BDD-anode has a higher COD mbRE than the MMO-anode due to the efficient formation of radicals with the BDD-anode.

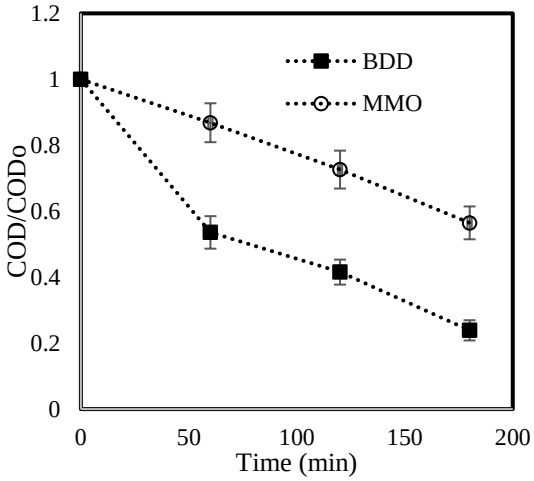

Fig. 3-4. *COD concentration over time during electrochemical oxidation (EO) of original CTBD. Average COD: 107 mg/L, Conductivity: 3.4 mS/cm, pH: 6.8, Applied current density: 5.5 mA/cm2 for BDD anode and 8.7 mA/cm2 for MMO anode.*

The COD removal with the BDD-anode was a two-phase process in which COD was quickly removed during the first hour, after which the removal rate decreased (Fig. 3-4). This two-phase phenomenon, which was also seen in our earlier study [198], can be explained by the radical formation process at the anode surface and the diffusion of the OCs towards the anode surface. Several researchers stated that radicals are formed very close to the BDD-anode surface [206]. Therefore, the reaction between the radicals and the OCs occurs only on the surface of the BDD-anode [207]. As a result, the oxidation of OCs is mass transfer limited and depends on the OCs concentration. It can be assumed that the radical formation controlled the first-hour reaction rate in the present study and that the OCs transport was fast enough to prevent mass transfer limitation in the system. As the reaction proceeds, OCs are oxidized, and the OCs concentration decreases, after which mass transfer limitation slows down the OCs oxidation rate. A similar phenomenon was observed during COD removal from phenolic wastewater with a BDD-anode [173]. Another reason for the two-phase OCs removal process might be that the OCs are oxidized into different intermediates during the oxidation, such as organic acids and chlorinated organics [208]. These intermediates are less favorable for oxidation, which ultimately causes a complicated COD removal profile with the BDD-anode [209, 210].

For the MMO-anode, the COD mbRE from untreated CTBD was similar to the COD mbRE from VFCW pre-treated CTBD. The COD removal by the MMO-anode was facilitated by active chlorinated species, such as hypochlorite (ClO^-). In our previous study, 205 (±5) mg/L of hypochlorite expressed as Cl_2 was formed during direct EO of CTBD with an MMO-anode at 8.7 mA/cm^2 current density, which was three times higher than the formation of ClO^- with a BDD-anode at 5.5 mA/cm^2 current density [198]. Thus, with the MMO-anode, the OC removal was dominated by active chlorine species, which have two times less oxidation potential than the hydroxyl radical produced by the BDD-anode.

The benzotriazole mbRE of the BDD-anode was 100%, while the MMO-anode had a benzotriazole mbRE of 75 (±10)%. Wu et al. (2015) showed that benzotriazole degradation by a BDD-anode was faster than by a PbO_2 (MMO)-anode because the BDD-anode has higher catalytical activity, and the hydroxyl radical has a lower affinity to be adsorbed to the electrode surface as compared to the PbO_2-anode [211]. The same authors also showed that not only hydroxyl radicals but also other active species were responsible for benzotriazole removal in the EO system. Hence, a substantial amount of benzotriazole was removed by the active chlorine species produced with the MMO-anode.

The energy consumption by EO before VFCW-treatment was higher than the energy consumption by EO after VFCW-treatment (Table S3-2). The energy consumption was 19% higher in the EO stage of EO-VFCW compared with the VFCW-EO system for both anodes. Lower energy consumption of EO-system treating VFCW-treated CTBD was attributed to the increased CTBD electrical conductivity after VFCW-treatment as a result of evapotranspiration, which decreased the internal resistance in the EO cell [212].

3.3.2.2 Treatment of electrochemically oxidized CTBD by the VFCW

The COD mbRE did not increase after VFCW-treatment of EO-treated CTBD (Fig. 3-5a) for the BDD-anode. The COD concentration in the VFCW effluent was higher than in the influent except for the first 15 days. The COD mbRE from the BDD-treated CTBD in the VFCW ranged from -85% to 29% (Fig. 3-5a). The TOC

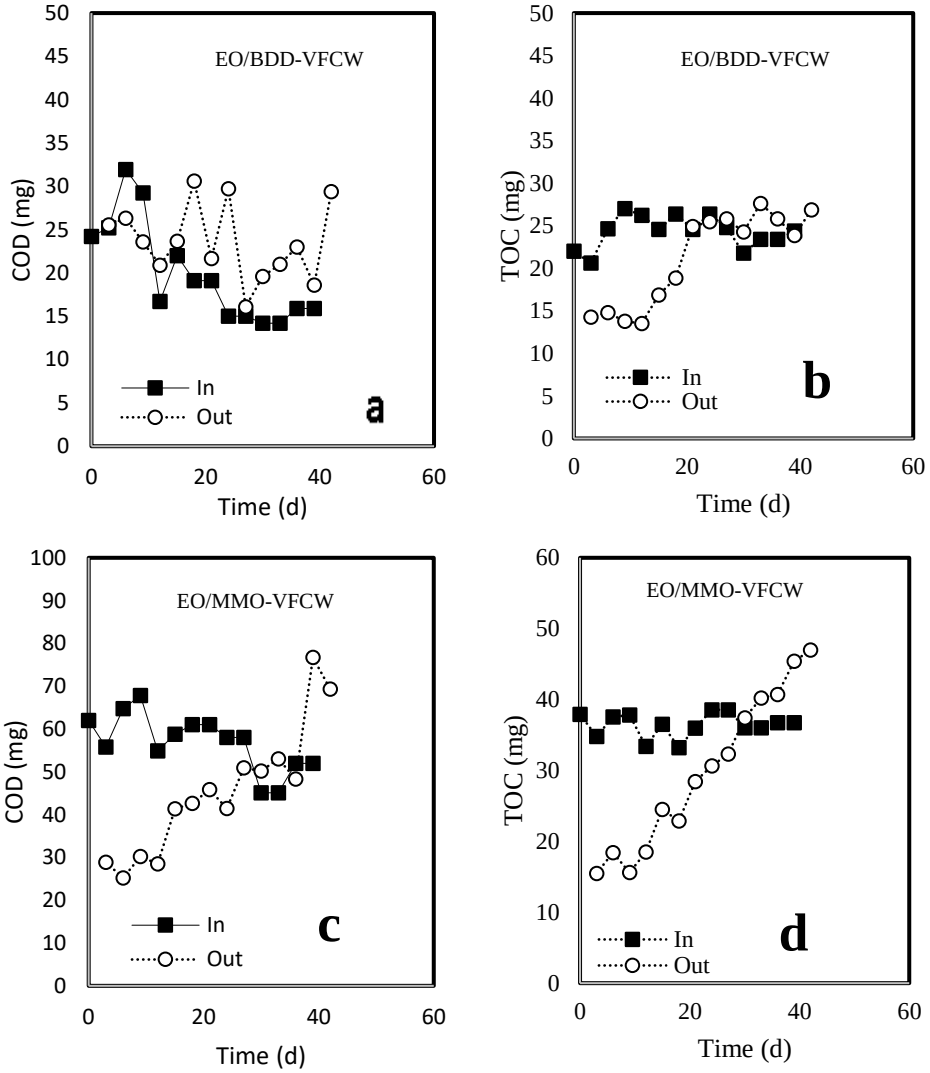

Fig. 3-5. *Vertical-flow constructed wetland (VFCW) performance during electrochemically pre-treated CTBD treatment. (a) mass-based COD and (b) mass-based TOC for EO/BDD-VFCW system ; (c) mass-based COD and (d) mass-based TOC for EO/MMO-VFCW system.*

mbRE in the VFCW ranged from -30% to 50% (Fig 3-5b). This illustrates that VFCW treatment does not contribute substantially to OCs removal after EO/BDD. The COD mbRE in the VFCW treating MMO-treated CTBD decreased from 55% to -48% during the 42-day experimental period, while the TOC mbRE decreased

from 60% to -28% (Fig 3-5c; 3-5d). Apparently, EO by both anodes does not result in an OCs fraction that is more readily biodegradable for microorganisms in the VFCW than the initial OCs fraction of the CTBD.

3.3.2.3 The overall treatment performance of scenario 2

The average overall COD mbRE in the EO/BDD-VFCW was 76%, while the average TOC mbRE was 48% during 42 days of operation (Table 3-4). In the EO/MMO-VFCW, the average overall COD mbRE was 57%, while the average TOC mbRE was only 27% (Table 3-4). During direct CTBD treatment by the VFCW in scenario 1, the mbRE of COD and TOC were not negative during the entire experiment period (Table 3-2). In contrast, the VFCW mbRE for COD and TOC became negative after 20 – 30 days of operation in scenario 2. The lower VFCW mbRE can be attributed to the formation of chlorinated organic and inorganic by-products during EO treatment that hampers normal VFCW functioning. Chlorinated compounds are toxic and may inhibit the microbial activity in the CW [213], resulting in a lower biodegradation efficiency. Besides, EO by-products could be less susceptible to biodegradation in VFCWs than the original OCs in the CTBD. However, this would not explain a negative COD mbRE. The negative mbRE might be attributed to the decay and leaching of plant root material and microbial biofilms that died due to the toxicity of EO pre-treated CTBD, thus increasing the COD concentration in the effluent.

An additional hint for an increase in the toxicity of the EO treated CTBD is the bioluminescence inhibition of *Vibrio fischeri*, which increased drastically from 5% to >95% for both anodes after EO. As described in section 3.3.1.3, the bioluminescence inhibition was triggered by the production of AOX, ClO_3^- and ClO_4^- during the EO treatment. Direct EO treatment of CTBD with the BDD-anode indeed produced 15 (±2) mg Cl^-/L AOX, 182 (±4) mg/L ClO_3^- and 35 (±1) mg/L ClO_4^-. The MMO-anode produced 24 (±2) mg Cl^-/L AOX and 99 (±11) mg/L of ClO_3^-. The formation of chlorinated compounds during direct EO of CTBD and EO of VFCW effluent was comparable. Due to the co-existence of all chlorinated species, it was not possible to determine the origin of toxicity.

The VFCW-treatment after EO significantly decreased the bioluminescence inhibition % to 27 (±17)% for the EO/BDD-VFCW system and 14 (±16)% for the

EO/MMO-VFCW system. The concentrations of AOX, ClO_3^- and ClO_4^- decreased substantially after VFCW treatment (Table 3-4). This was because of the reaction of the AOX and chlorinated inorganic species with the substrate of the CW and because of the detoxification capacity of naturally existing microorganisms in CWs through biodegradation reactions [213-215]. However, the *Phragmites australis* in the VFCWs were not able to cope with the EO-treated CTBD. Plants grown in untreated CTBD did not show visual abnormalities during the experimental period. However, the plants fed with EO/MMO and EO/BDD treated CTBD showed signs of discoloration and eventually died. The plant's death was likely the result of the toxicity of the electrogenerated chlorinated intermediate compounds. The plants in the VFCW were in the first stage of their development. More studies are needed to determine whether electrogenerated chlorinated species have a similar impact on more mature VFCW systems with better-developed plants. In addition, unplanted VFCW systems might be used as a first treatment step in a multi-component CW to deactivate the toxic chlorinated intermediates.

3.4 CONCLUSIONS

The reuse of cooling tower blowdown (CTBD) in the cooling tower itself requires physico-chemical desalination preceded by a proper pre-treatment that removes organic chemicals (OCs). In this research, the removal of OCs from CTBD using combined systems of electrochemical oxidation (EO) with boron-doped diamond (BDD)- and mixed-metal oxide (MMO)-anodes and vertical-flow constructed wetlands (VFCWs) were evaluated. The VFCW was effective in removing specific conditioning chemicals, such as benzotriazole, from CTBD. However, the removal of bulk OCs in VFCWs was low since the OCs in CTBD consisted of recalcitrant humic substances. EO-treatment after VFCW-treatment increased the OCs removal, especially with the BDD-anode. However, the EO of the VFCW effluent resulted in the production of toxic chlorinated organic and inorganic species, and therefore the VFCW-EO effluent should be further treated to reduce its toxicity. Direct EO of the CTBD followed by VFCW-treatment resulted in the death of the plants in the CTBD as a result of the production of unwanted toxic by-products, but a decrease in the toxicity of the combined effluent. Future research recommends identifying the exact source of the toxic effect to VFCW plants and identifying ways to mitigate this effect because EO-VFCW produces a less toxic

final product. Besides, EO methods that do not produce toxic chlorinated by-products should be developed to avoid related toxicity problems. Also, evapotranspiration should be minimized for maximal water recovery.

Chapter 4.

Effect of electrolyte composition on electrochemical oxidation: Active sulfate formation, benzotriazole degradation, and chlorinated by-products distribution.

This chapter has been submitted for publication as:
Saha, Pradip, Jiamin Wang, Yinong Zhou, Livio Carlucci, Adriaan W. Jeremiasse, Huub HM Rijnaarts, Harry Bruning, Effect of electrolyte composition on electrochemical oxidation: active sulfate formation, benzotriazole degradation, and chlorinated by-products distribution." (submitted).

Abstract

Electrochemical oxidation is an effective technique for treating persistent organic pollutants, which are hardly removed in conventional wastewater treatment plants. Sulfate and chloride salts commonly used and present in natural wastewater influence the electrochemical degradation process. In this study, the effect of electrolyte composition on the active sulfate species ($SO_4^{\bullet-}$ and $S_2O_8^{2-}$) formation, benzotriazole degradation- a model organic compound, and chlorinated by-products distribution have been investigated while using a boron-doped diamond (BDD) anode. The electrogenerated $SO_4^{\bullet-}$ and $S_2O_8^{2-}$ formation were faster in 10:1 and 2:1 Na_2SO_4:$NaNO_3$ ratios than in the 1:0 ratio. The $HO^{\bullet}$-mediated $SO_4^{\bullet-}$ production has prevailed in 10:1 and 2:1 ratios. However, $HO^{\bullet}$-mediated $SO_4^{\bullet-}$ production has hindered in 1:0 ratio due to excess chemisorption of SO_4^{2-} on the BDD anode. Similarly, the faster benzotriazole degradation, mineralization, and lowest energy consumption were achieved in the 10:1 Na_2SO_4:$NaNO_3$ and Na_2SO_4:NaCl ratio. Besides, chlorinated organic by-product concentration (AOX) was lower in the 10:1 Na_2SO_4:NaCl ratio but increased with the increasing chloride ratio in the electrolyte. LC-MS analysis shows that number of chlorinated organic transformation products were produced in 0:1 to 2:1 ratios which were not found in the 10:1 Na_2SO_4:NaCl ratio. A comparatively higher amount of ClO_4^- was formed in the 10:1 ratio than in 2:1 to 0:1 ratios. This ClO_4^- formation train evidences the effective $HO^{\bullet}$ generation in sulfate-enriched conditions because the ClO_4^- formation is positively correlated to $HO^{\bullet}$ concentration. Overall results show that sulfate-enriched electrolytes are suitable for electrochemical oxidation of organic pollutants. Nanofiltration is a widely used technique to concentrate wastewater effluents. Hence the combination of electrochemical and nanofiltration could be an appropriate technology train for treating sulfate-containing wastewaters with biorecalcitrant organic pollutants.

Keywords

Sulfate radical; Hydroxyl radical; Active chlorine species; Chlorinated transformation products; Boron-doped diamond anode; Benzotriazole.

4.1 INTRODUCTION

In the past few decades, an increasing number of persistent organic pollutants (POPs) have been detected in the aquatic environment due to the rising anthropogenic activities such as rapid industrialization, continuous development of agricultural operations, and excessive population growth [97]. Some of those pollutants have shown resistance to conventional biological wastewater treatment processes and enter the aquatic environments through effluents and sludges of wastewater treatment plants, causing threats to the ecosystem and human health [216]. Thus, appropriate technology needs to be developed to remove and degrade these bio recalcitrant organic pollutants.

Over the last decade, electrochemical oxidation (EO) with boron-doped diamond (BDD) anode has been considered an attractive technology for the removal of POPs from water because of its high removal efficiency, moderate operating conditions, in-situ oxidant generation, and automatability [69, 79]. The EO process can produce in-situ radicals potent to degrade and mineralize POPs, including pharmaceuticals, pesticides, plasticizers, dyes, industrial and municipal contaminants [217-220]. With the BDD anode, besides hydroxyl radicals ($HO^{\bullet}$), reactive sulfate and chloride species can be generated from their corresponding salts dissolved in the water matrix [217, 221]. Those reactive species were demonstrated to facilitate fast degradation of the pollutants close to the anode and/or in the bulk solution [222, 223].

Sulfate (SO_4^{2-}) is extensively used to support electrolytes in EO experiments and is present in natural and wastewaters. In sulfate-containing electrolytes, sulfate radicals ($SO_4^{\bullet-}$) and peroxydisulfate ($S_2O_8^{2-}$) can be electrochemically generated with the BDD anode [162, 224, 225]. Several studies show that $SO_4^{\bullet-}$ and $S_2O_8^{2-}$ can significantly boost POPs' degradation [156, 162, 226, 227]. Three $SO_4^{\bullet-}/S_2O_8^{2-}$ formation pathways have been reported in the literature, as shown in Fig. 4-1 [156, 162, 224, 225, 228-231].

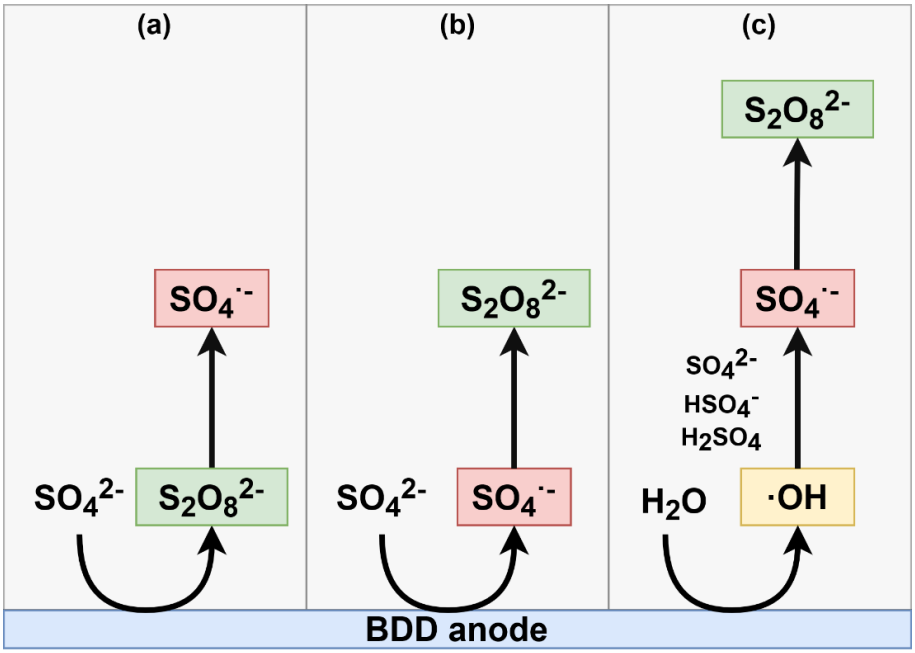

Fig. 4-1. *Possible mechanisms of peroxydisulfate formation with BDD anode.*

The relevant reactions of the pathways are described below:

$$2SO_4^{2-} \rightarrow S_2O_8^{2-} + 2e^- \quad (4.1)$$

$$S_2O_8^{2-} \rightleftarrows 2SO_4^{\bullet-} \quad (4.2)$$

$$SO_4^{2-} \rightarrow SO_4^{\bullet-} + e^- \quad (4.3)$$

$$SO_4^{2-} + HO^{\bullet} \rightarrow SO_4^{\bullet-} + OH^- \quad (4.4)$$

$$HSO_4^- + HO^{\bullet} \rightarrow SO_4^{\bullet-} + H_2O \quad (4.5)$$

$$H_2SO_4 + HO^{\bullet} \rightarrow SO_4^{\bullet-} + H_3O^+ \quad (4.6)$$

In pathway (a), SO_4^{2-} is directly oxidized to $S_2O_8^{2-}$ on the anode surface (Eq. 4.1), which is radically or non-radically activated to $SO_4^{\bullet-}$ (Eq. 4.2) [230, 232-234]. In this way, the increase of SO_4^{2-} concentration improves the generation of $S_2O_8^{2-}$. In pathway (b), SO_4^{2-} is directly oxidized to $SO_4^{\bullet-}$ by a one-electron transfer persulfate ion on the BDD anode (Eq. 4.3) [184]. Excessive SO_4^{2-} will facilitate more $SO_4^{\bullet-}$ formation, which is transferred to $S_2O_8^{2-}$ according to a recombination

reaction (the reverse reaction of Eq. 4.2) [235]. Regarding activation energy with BDD anode, direct oxidation of SO_4^{2-} is the easiest among direct oxidation of H_2O, SO_4^{2-}, HSO_4^- and H_2SO_4 [229]. In pathway (c), $HO^\bullet$ generated from water oxidation, mediated electrolysis of SO_4^{2-} to $SO_4^{\bullet-}$, which subsequently is converted to $S_2O_8^{2-}$ (Eq. (4.4)-(46)) [92, 184, 223, 233, 236, 237]. Studies show that a large proportion of $SO_4^{\bullet-}$ was generated by pathway (c) because $HO^\bullet$ had a higher oxidative ability, which could also react with HSO_4^- and H_2SO_4 [228, 234]. Thus, the $SO_4^{\bullet-}$ formation rate is related to $HO^\bullet$ formation, and an increasing number of $HO^\bullet$ will facilitate more $SO_4^{\bullet-}$ and $S_2O_8^{2-}$ formation via pathway (c).

The SO_4^{2-} concentration influenced the competitive $HO^\bullet$ and $S_2O_8^{2-}$ formation reactions [238]. At high SO_4^{2-} concentration, two slopes were found in the linear sweep curves corresponding to the transformation of SO_4^{2-} to $S_2O_8^{2-}$ and $HO^\bullet$ formation on the electrode surface [224, 238]. Surface-mediated oxidation of SO_4^{2-} was responsible for $S_2O_8^{2-}$ formation at concentrated SO_4^{2-} electrolytes [239]. However, the impact of electrolyte composition on $SO_4^{\bullet-}$ formation pathways is still unclear and needs more illustration to maximize the active oxidants formation.

The ubiquitous present chloride (Cl^-) of which its concentration varies from around 0.5 g/L in ground/surface water to 30 g/L in industrial or municipal wastewater discharge, and exceptionally even to higher concentrations. Thus, among other salts, Cl^- is also commonly studied in the EO process. Cl^- can be oxidized to different reactive chlorine species (Cl_2, $HOCl/ClO^-$) and chlorine radicals ($Cl^\bullet$, $Cl_2^{\bullet-}$, $ClOH^{\bullet-}$) during EO. In many cases, Cl^- presence boosts the organic compound degradation rate due to these reactive species. On the contrary, Cl^- itself will negatively affect the degradation rate of the organic compound. At high Cl^- concentration, $HO^\bullet$ is scavenged, and chlorine radicals are formed. Chlorine radicals subsequently convert to dichloride radical ions and causing an inefficient oxidation process [240]. In the complex transformation process, the formation of active chlorine species and chlorine radicals are considered as the crucial intermediate for the chlorinated (in general unwanted) by-product formation, including chlorinated organic transformation products (COTPs), chlorate, and perchlorate [223], that often have toxic or environmental harmful effects when discharge to the natural aquatic environment.

Moreover, several $SO_4^{\bullet-}$ based advanced oxidation process studies have shown that Cl^- reacts with $SO_4^{\bullet-}$ to form chlorine radicals, which subsequently would participate in the COTPs formation reactions. Sometimes, these COTPs are more toxic than the parent compounds, and their presence in discharge effluents and sludges should be avoided. An $SO_4^{\bullet-}$ base oxidation study showed that the low concentration of Cl^- (1 and 10 mM) increased the degradation rate of benzotriazole. In comparison, a higher concentration of Cl^- (100 mM) decreased the degradation rate because of $SO_4^{\bullet-}$ scavenging by Cl^- [92]. Thus, the Cl^- concentration in the electrolyte needs to be regulated to achieve the best degradation performance and stop or minimize the toxic COTPs formation.

EO's large-scale application is still limited because of mass transfer-controlled reaction kinetics, high energy consumption, and chlorinated by-product formation. Membrane separation, including reverse osmosis (RO) and nanofiltration (NF), becomes a promising pre-treatment before EO. Membrane separation increases organic compounds and salts' concentration in concentrate, reducing the transfer limitations and lowering the energy consumption. However, increasing salts concentration also increases the Cl^- concentration, ultimately facilitating undesired chlorinated by-product formation. Recently, research shows that nanofiltration can selectively reject SO_4^{2-} at a higher rate than Cl^- so that the concentrate would be rich in SO_4^{2-} and low in Cl^- [241]. Because of the larger molecular diameter, SO_4^{2-} could be blocked by the nanofiltration membrane while Cl^- could pass through it. Thus, integrating EO with nanofiltration may tune the SO_4^{2-} and Cl^- ratio, thereby altering the treatment performance. For instance, EO of bisphenol A in 0.008 M NaCl+0.047 M Na_2SO_4 solution shows better degradation and mineralization than 0.070 M NaCl+0.050 M Na_2SO_4. Also, excess SO_4^{2-} in the electrolyte subsides COTPs formation [242]. However, the appropriate explanation of this better degradation rate and mineralization still needs further research. Whether an optimum electrolyte composition will benefit the degradation rate and reduce the toxic by-product formation remains unknown.

Therefore, this study focused on the elucidation of the effect of electrolytes composition, in terms of Na_2SO_4:$NaNO_3$ (SN) ratio at constant conductivity, on electrogenerated active sulfate species ($SO_4^{\bullet-}$ and $S_2O_8^{2-}$) formation with boron-doped diamond (BDD) anode. $NaNO_3$ is used in the experiments because $NaNO_3$ is considered inert during electrochemical oxidation [108] and would cause negligible

interference in the $S_2O_8^{2-}$ detection [243]. Benzotriazole is chosen as a model organic biorecalcitrant pollutant often found in industrial and other wastewater effluents. The influence of Na_2SO_4:$NaNO_3$ (SN) and Na_2SO_4:NaCl (SCl) ratios on benzotriazole degradation kinetics, mineralization efficiency, energy consumption, and synergistic degree are also reported. The influence of the SCl ratio on chlorinated organic transformation products (COTPs) as AOX, chlorate, and perchlorate formation are also monitored. Finally, the effect of SCl ratios on possible COTPs distribution has been analyzed by LC-MS. Based on experimental results and existing literature, the reaction mechanisms are discussed.

4.2 MATERIALS AND METHODS

4.2.1 Chemicals

Benzotriazole ($C_6H_5N_3$, ≥96%) and sulfuric acid (H_2SO_4, ≥95.0%) were purchased from Sigma Aldrich Chemie BV (the Netherlands). Sodium chloride (NaCl, ≥99.0%), sodium sulfate (Na_2SO_4, ≥99.0%), sodium nitrate ($NaNO_3$, ≥99.0%), sodium peroxydisulfate ($Na_2S_2O_8$, ≥99.0%), disodium hydrogen phosphate dihydrate ($Na_2HPO_4{\cdot}2H_2O$, ≥99.0%), monosodium phosphate dihydrate ($NaH_2PO_4{\cdot}2H_2O$, ≥99.0%), and N,N-diethyl-p-phenylenediamine (DPD) was purchased from VWR chemicals (Leuven Belgium). Milli-Q™ water was used to prepare and dilute all samples unless otherwise stated.

4.2.2 Electrochemical oxidation experimental set-up

All experiments were performed in an undivided flat cell with an effective projected electrode surface area of 22.4 cm^2, described elsewhere [198]. A BDD electrode was employed as the anode, and a platinum-coated titanium electrode was used as the cathode (Magneto Special Anodes, the Netherlands). The distance between the electrodes was 1.5 cm. A silver/silver chloride (Ag/AgCl) electrode connected with Haber Lugging capillaries filled with 10% (W/V) potassium nitrate solution was employed as reference (QM711X/Gel, Prosense, The Netherlands). An IviumStat.h potentiostat with Iviumstat software (Ivium Technologies B.V., the Netherlands) was used to control the voltage and record the experimental data. The cell was continuously circulated with a 10 mg/L benzotriazole solution with different

electrolyte ratios of Na_2SO_4:NaCl (SCl) and Na_2SO_4:$NaNO_3$ (SN) at a flow rate of 580 mL/min from a 350 mL recirculation bottle (Table 4-1). The OLI Studio 9.6 software was used to calculate the amount of salts required to keep the conductivity of the electrolyte at 10 mS/cm (Table 4-1). Samples were collected at given time intervals for benzotriazole analysis. Samples were also taken for quantification of total organic carbon (TOC), anions (Cl^-, ClO_3^-, ClO_4^-), free chlorine, COTPs as AOX (adsorbable organic halides), and for the identification of COTPs.

Table 4-1. *Electrolyte composition with 10 (±0.1) mS/cm constant conductivity*

	Ratio	Na_2SO_4 (M)	NaCl (M)	$NaNO_3$ (M)
Na_2SO_4:$NaNO_3$ (SN)	1:0	0.064	-	0
	10:1	0.06	-	0.006
	2:3	0.034	-	0.051
	0:1	0	-	0.1
Na_2SO_4:NaCl (SCl)	1:0	0.064	0	-
	10:1	0.06	0.006	-
	2:1	0.060048	0.024	-
	2:3	0.032	0.047	-
	0:1	0	0.095	-

4.2.3 Analytical methods

Benzotriazole concentration was analyzed by high-performance liquid chromatography (HPLC, Thermo Scientific) connected with a fluorescence detector with a wavelength set to 278 nm. An ACQUITY UPLC CSH Phenyl-Hexyl column (1.7µm, 2.1×150mm) was used and kept at a constant temperature of 35°C. The eluents (A 0.1% formic acid in Milli-Q water and B 0.1% formic acid in acetonitrile) were pumped with a constant flow rate of 0.2 mL/min. The injected volume was 50.00 µL. The instruments were controlled by Chromeleon 6.8. A TOC-$L_{CPH/CPN}$ analyzer connected with an ASI-L autosampler (Shimadzu Corporation (Kyoto, Japan)) was used for TOC measurements. The sample was first acidified by the mean of H_2SO_4 to remove all inorganic carbon; the solution was then introduced in a compartment where the organic carbon was oxidized to CO_2 at 720°C, and last detected by mean of non-dispersive infrared detection. Anions (Cl^-, ClO_3^-, ClO_4^-) concentration was measured by ion chromatography (IC) on Dionex ICS-2100 (Dionex, Breda, The Netherlands), equipped with a Dionex IonPac AS19 column model (4x250 mm). Free chlorine concentrations were measured with Hach chlorine

DPD test reagent (USEPA-DPD 330.5 method) and a Hach DR/3900 spectrophotometer (Hach Lange GmbH, Düsseldorf, Germany). According to the instructions on the kit test, the Hach LCK390 cuvette and Hach DR/3900 spectrophotometer were used to analyze the AOX concentrations (Hach Lange GmbH, Düsseldorf, Germany). Peroxydisulfate ($S_2O_8^{2-}$) concentration was measured by the DPD-spectrophotometric method described in Gokulakrishnan, Mohammed [243]. 1 mL sample, 5 mL (50 mM) phosphate buffer, 0.1 mL (2.5 mM) DPD solutions, and 3.9 mL Milli-Q water were mixed and incubated for 10 min at room temperature. After that, the mixed solution's absorption spectra were measured at 510 nm and 551nm by Hach DR/3900 spectrophotometer. Detailed of the TOC, anions, free chlorine, and peroxydisulfate determination methods were reported elsewhere [244]

The chlorinated organic transformation products (COTPs) were identified by liquid chromatography combined with high-resolution-accurate-mass mass spectrometry detection (LC-HRAM-MS). The UHPLC Dionex Ultimate 3000 was equipped with an auto-sampler and a temperature-controlled oven compartment coupled with the orbitrap mass spectrometer Q-Executive (Thermo Fisher Scientific, US). After injection of 50 µL sample, the chromatographic separation was obtained by an Acuity UHPLC CSH Phenyl-Hexyl column (1.7µm, 2.1×150mm) (Waters, US) with a guard column (Waters, US) with the same phase. The chromatographic and mass spectrometric conditions are the same described by [245]. Data were collected in a full scan from 65 to 900 Da in positive and from 65 to 450 Da in negative modes for further analysis. The data analysis was done with Compound Discoverer (CD) v. 3.1 (Thermo Scientific, USA).

4.2.4 Data analysis

4.2.4.1 Performance evaluation

To evaluate EO process performance, benzotriazole degradation efficiency (η_{BTA}), mineralization efficiency (η_{TOC}), and energy consumption (EC in kWh/g benzotriazole) was followed and calculated according to the equations shown below Eqs. (4.7)-(4.9) [198].

$$\eta_{BTA} = \left(1 - \frac{c_f}{c_i}\right) \times 100\% \quad (4.7)$$

$$\eta_{TOC} = \left(1 - \frac{TOC_f}{TOC_i}\right) \times 100\% \quad (4.8)$$

$$EC = \frac{\sum_t V_t I_t \Delta t \times 10^{-3}}{m_f - m_i} \quad (4.9)$$

Where: c_i and c_f are the initial and final benzotriazole concentrations, respectively, in mg/L. TOC_i and TOC_f are the initial and final TOC concentrations, respectively, in mg/L. V_t is the cell voltage in V and I_t is the current at time t. Δt is the time interval in h. m_i and m_f are the initial and final benzotriazole masses, in g.

4.2.4.2 Synergistic effect

The synergistic effect of the electrolyte composition was evaluated by the synergy degree according to the equation (Eq. 4.10), where, k_{ab} and k_a are benzotriazole removal rates constants, in min^{-1}, for mixed and individual salts, respectively [246]. a is for sulfate and b is for chloride or nitrate.

$$S = \left(\frac{k_{ab} - k_a}{k_{ab}}\right) \times 100\% \quad (4.10)$$

4.2.4.3 Degradation by-products analysis

The raw LC-HRAM-MS data were processed by Compound Discoverer (CD) v. 3.1 (Thermo Scientific, USA). The COTPs were identified with the workflow template "Environmental w Stats Unknown ID w Online and Local Database Searches." The program used the differences between injected blanks and samples to select relevant peaks based on a minimum intensity (10^6 counts), mass tolerance (5 ppm), and retention time shift (0.2 min). The selected peaks were then assigned to the same compound with the same retention time (within the mentioned tolerance), the same measured mass (within the mentioned mass tolerance), matching the expected natural occurring isotope intensity, or the measured mass adducts formation. The extracted ion chromatogram (XIC) of these compounds was grouped together. The molecular formula was assigned according to the accurate mass and maximum element counts. The most matching compounds were selected from the ChemSpider database based on composition and mass lists. This resulted

in a list of potential components evaluated by peak shape, peak area, and relevance to the parent compound.

4.3 RESULTS AND DISCUSSION

4.3.1 Effect of Na_2SO_4:$NaNO_3$ (SN) ratios on reactive sulfate species formation

The peroxydisulfate ($S_2O_8^{2-}$) formation rate at different Na_2SO_4:$NaNO_3$ (SN) ratios is presented in Fig. 4-2. The experiment aimed to elucidate the electrolyte composition impact on dominating active sulfate species formation pathways. In the 10:1 and 2:3 ratio, the $S_2O_8^{2-}$ formation rates are similar, around 60 μM/min, while the rate is only 17 μM/min in the 1:0 ratio (Fig. 4-2a). The low $S_2O_8^{2-}$ formation rate in the highest SN ratio (1:0), the highest SO_4^{2-} concentration, excludes that pathways (a) and (b) from dominating. Besides, surface blocking by SO_4^{2-} hinders the $HO^{\bullet}$ the formation, ultimately inhibiting the pathway (c). This blocking can be explained by the chemisorption phenomenon of SO_4^{2-} on the electrode surface. NO_3^- belonged to class IA adsorbates, which had coulombic attraction or solvent-structure breaking effects when binding to the surface. In contrast, SO_4^{2-} belonged to class IB adsorbates, which formed a covalent bond when attaching to the surface [247]. For SO_4^{2-}, electrons were transferred from SO_4^{2-} to unoccupied orbitals to the electrode surface [248]. Therefore, SO_4^{2-} has a stronger adsorption ability to the electrode than NO_3^-. Studies also show that the electro-oxidation rate constant of 2,4-DCP with BDD anode was low at high SO_4^{2-} concentration (0.9 h^{-1} in 0.3 M and 0.4 M Na_2SO_4) compared to the low SO_4^{2-} concentration (1.4 h^{-1} in 0.2 M Na_2SO_4) [228]. This indicates that the high SO_4^{2-} concentration blocks the active radical formation, which decreases the rate constants.

The high $S_2O_8^{2-}$ formation rate in 10:1 and 2:3 ratios in Fig. 4-2a is noteworthy, which increases the possibility of the dominating pathway (c). $HO^{\bullet}$ generated on the surface participates in the electrolysis of SO_4^{2-} to $SO_4^{\bullet-}$, converting to $S_2O_8^{2-}$ [224, 228, 234, 238]. According to Fig. 4-2b, cyclic voltammetry shows that the water oxidation overpotential was around 1.74V (vs. Ag/AgCl) in the highest SO_4^{2-} ratio (1:0) and shifted to 1.55 to 1.50V (vs. Ag/AgCl) in the lower SO_4^{2-} ratios (10:1 and 1:10). The current density increases sharply with the decreasing SO_4^{2-} ratio in the

electrolyte, similar to the thiourea electrochemical oxidation study in sodium sulfate on a gold electrode, which shows that the current density decreased rapidly due to SO_4^{2-} chemisorbed [248]. Thus, the mixing of salts can reduce surface blocking by SO_4^{2-} and increase the direct water oxidation to $HO^{\bullet}$ on the active sides of the BDD anode. The similar $S_2O_8^{2-}$ formation rates in 10:1 and 2:3 might be attributed to little influence of surface blocking by SO_4^{2-} and maximum $HO^{\bullet}$ formation. The 1:10 ratio has the lowest $S_2O_8^{2-}$ formation rate because of the lowest initial SO_4^{2-} concentration and $HO^{\bullet}$ scavenged by NO_3^-.

Moreover, the electrolyte's initial pH was 5.7. pH changed to 12.3 in 10:1 and 2:3 ratios during the experiments, whereas 10.9 in 1:0 ratio (Fig. S4-1). SO_4^{2-} reaction with $HO^{\bullet}$ formed $SO_4^{\bullet-}$ and OH^- (Eq. 4.4). The generation of OH^- contributes to the increase of pH.

These results indicate that increasing $HO^{\bullet}$ facilitates more $SO_4^{\bullet-}$ formation (Eqs. (4.4)-(4.6)), subsequently forming $S_2O_8^{2-}$. Thus, pathway (c) is more likely to be dominant, and $SO_4^{\bullet-}$ and $S_2O_8^{2-}$ formation can be boosted by mixing the SO_4^{2-} with IA anions similar to NO_3^- or Cl^- in a certain ratio range (10:1 to 2:3).

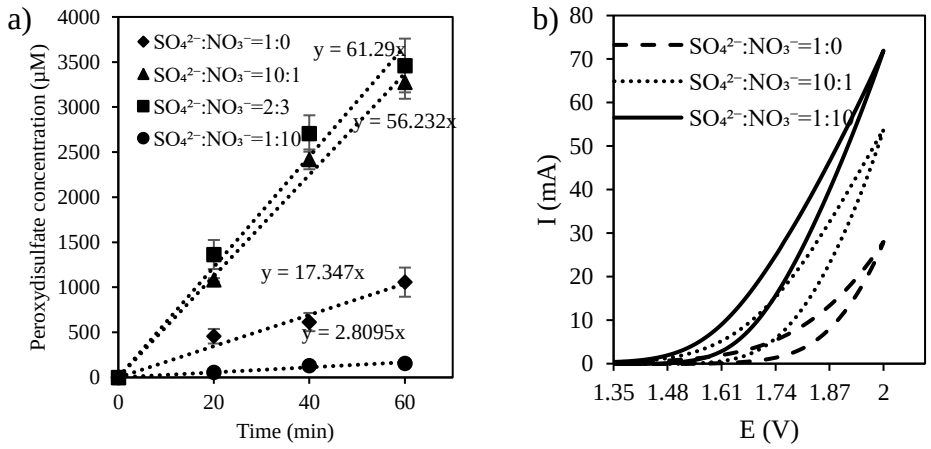

Fig. 4-2. *(a) Peroxydisulfate concentration (μM) changing with reaction time (min) in different Na_2SO_4:$NaNO_3$ ratios. Experimental conditions: T = 25-30°C, applied potential = 4.3 V (vs. Ag/AgCl), conductivity = 10 mS/cm, flow rate = 580 mL/min. (b) cyclic voltammetry tests in different Na_2SO_4:$NaNO_3$ ratios; scan rate 50 mV/s, applied potential 0-2-0 (vs. Ag/AgCl), conductivity 10 mS/cm.*

4.3.2 Effect of Na_2SO_4:$NaNO_3$ (SN) ratios on benzotriazole degradation

The electrochemical oxidation of benzotriazole with BDD anode was performed with different SN ratios, and benzotriazole concentration changed with reaction time is shown in Fig. 4-3. The degradation of benzotriazole was close to an exponential decrease. It is assumed that the benzotriazole removal was a first-order reaction, and the rate constants in different ratios are given in Table 4-2.

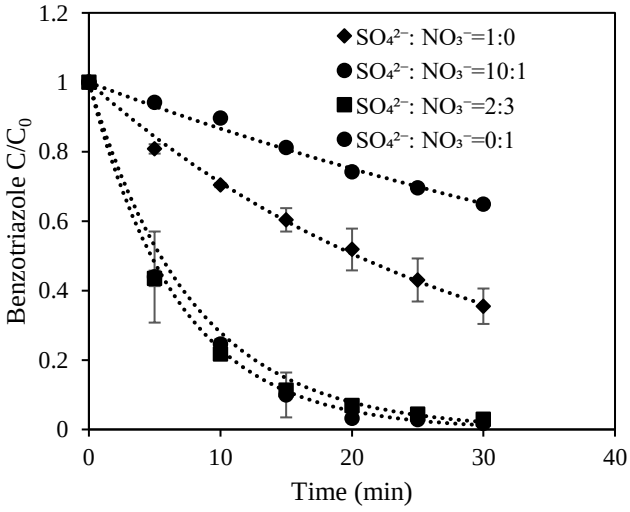

Fig. 4-3. *Benzotriazole concentration changing with reaction time (min) in different Na_2SO_4:$NaNO_3$ (SN) ratios. Experimental conditions: 10 mg/L benzotriazole, different electrolyte ratios, T = 25-30℃, applied potential = 4.3 V (vs. Ag/AgCl), conductivity = 10 mS/cm, flow rate = 580 mL/min.*

The benzotriazole degradation rate reached 0.15 min^{-1} and 0.13 min^{-1} in 10:1 and 2:3 ratios. Like maximum $S_2O_8^{2-}$ formation, the faster benzotriazole degradation rate in 10:1 and 2:3 SN ratios can be explained by less SO_4^{2-} accumulation on the anode surface and more radicals ($HO^{\bullet}$, $SO_4^{\bullet-}$ and $S_2O_8^{2-}$) formation is described in the previous section (3.1). Moreover, the benzotriazole degradation rate in the 1:0 (only in SO_4^{2-}) ratio was three times higher than the rate in the 0:1 ratio (only in NO_3^-) (Fig. S4-2). In the 1:0 ratio, $HO^{\bullet}$, $SO_4^{\bullet-}$ and $S_2O_8^{2-}$ participated in benzotriazole degradation, whereas $HO^{\bullet}$ was the only dominating reactive oxidant in the 0:1 ratio. Besides, the scavenging role of NO_3^- can also explain the benzotriazole degradation

inhibition in the nitrate-rich electrolyte (0:1). Experiments showed that humic acid removal efficiency by electron beam irradiation was reduced from 50% (no NO_3^-) to around 15% (100 mg/L NO_3^-) due to $HO^\bullet$ scavenging by NO_3^- [249]. Another literature reference also reported that NO_3^- interfered with the degradation pathway and scavenged $HO^\bullet$ during electrochemical degradation of diuron in a microreactor [250].

Furthermore, the initial pH changed from 6.9 to 9.6 in 1:0, 4.6 in 0:1, and 12.3 in 10:1 and 2:3 ratios (Fig. S4-3). This pH change indicates that SO_4^{2-} reaction with $HO^\bullet$ generates $SO_4^{\bullet-}$ and OH^- in solutions with 1:0, 10:1, and 2:3 SN ratios but was absent in an electrolyte with a 0:1 SN ratio (Eq. 4.4). In addition, benzotriazole (pKa2=8.27) tends to lose one proton under alkaline conditions [228]. This change of the benzotriazole molecular structure increases the electron density of the benzene ring in the molecule, making it more accessible for $SO_4^{\bullet-}$ to oxidize [92, 228, 237]. This explains why the benzotriazole degradation rate was the highest in 10:1 and 2:3 SN ratios.

Table 4-2. *Comparison of benzotriazole degradation rate constant and degree of synergy, TOC removal efficiency and energy consumption in different Na_2SO_4:$NaNO_3$ (SN) ratios. Experimental conditions: 10 mg/L benzotriazole, T = 25-30°C, applied potential = 4.3 V (vs. Ag/AgCl), conductivity = 10 mS/cm, flow rate = 580 mL/min. reaction time = 30 min for rate constant, degree of synergy, energy consumption calculation and 60 min for TOC removal efficiency calculation.*

SN ratio Na_2SO_4:$NaNO_3$	Chemical kinetic constant k (min^{-1})	Degree of synergy S (%)	TOC removal efficiency η_{TOC} (%) (±SD)	Energy consumption EC (kWh/g benzotriazole) (±SD)
1:0	0.034	-	56 (3)	0.82 (0.3)
10:1	0.15	77	71 (1)	0.43 (0.01)
2:3	0.13	74	62 (7)	0.58 (0.1)
0:1	0.014	-143	52 (2)	1.78 (0.01)

The degree of synergy, energy consumption, and mineralization are shown in Table 4-2. The highest degree of synergy (57%) and mineralization efficiency (71%) was found in ratio 10:1. The energy consumption (0.43 kWh/g benzotriazole) was also the lowest in this ratio. Higher reaction rates increased the amount of degradation and decreased reaction time, thereby reducing energy consumption.

This result demonstrates that the 10:1 to 2:3 SN ratio was an optimum range to maximize the synergistic effect for reactive species formation.

4.3.3 Effect of Na_2SO_4:NaCl (SCl) ratios on benzotriazole degradation

The electrochemical oxidation of benzotriazole was also studied in different SCl ratios with BDD anodes. Benzotriazole concentration changed with reaction time is shown in Fig. 4-4. Same as section 3.2, it is assumed that the reaction was a first-order reaction, and the rate constants in different SCl ratios are listed in Table 4-3.

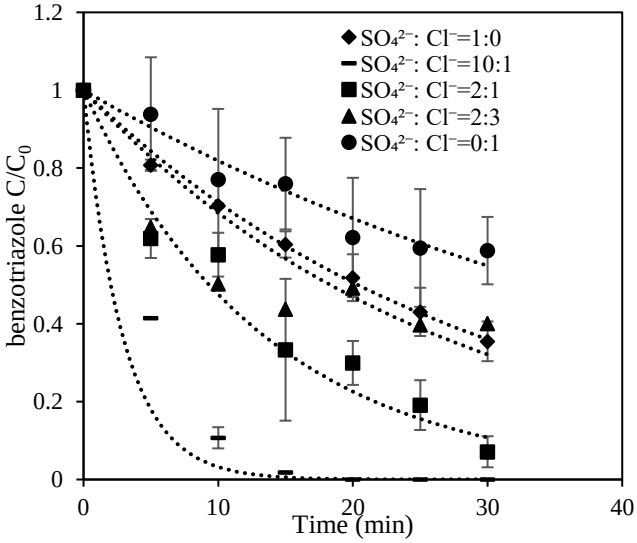

Fig. 4-4. *Benzotriazole concentration changing with reaction time (min) in different Na_2SO_4:NaCl (SCl) ratios. Experimental conditions: 10 mg/L benzotriazole, T = 25-30℃, applied potential = 4.3 V (vs. Ag/AgCl), conductivity = 10 mS/cm, flow rate = 580 mL/min.*

Like in the Na_2SO_4:$NaNO_3$ (SN) electrolyte, the 10:1 Na_2SO_4:NaCl (SCl) ratio also has the highest benzotriazole degradation rate. In SCl electrolyte, the degradation rate in the 10:1 ratio reached 0.34 min^{-1}, ten times faster than in the 1:0 SCl ratio and seventeen times faster than in the 0:1 SCl ratio (Fig. S4-4). It agrees with the investigation in sections 4.3.1 and 4.3.2. The addition of Cl^-, IA anion like NO_3^- reduces the excess surface blocking by chemisorption of SO_4^{2-} on the electrode.

Which promotes the $HO^{\bullet}$ and subsequent $SO_4^{\bullet-}$ formation (pathway c). The initial pH changed from 6.9 to 9.6-9.9 in 1:0, 2:3, 0:1 ratios and 12.0 in 10:1 ratio (Fig. S4-5). A similar reason has been explained in section 4.3.2. It is worth mentioning that the benzotriazole degradation rate was two times faster in the 10:1 Na_2SO_4:NaCl ratio than in the 10:1 SN ratio (Fig. S4-2). The high reaction rate in the 10:1 SCl ratio can be explained by $Cl^{\bullet}$, and free chlorine (active chlorine species) mediated oxidation together with $HO^{\bullet}$, $SO_4^{\bullet-}$ and $S_2O_8^{2-}$ mediated oxidation. Other experiments also reported that Cl^- accelerated the perfluorooctanesulfonate degradation with BDD anode due to the active chlorine species formation [251].

However, the benzotriazole degradation rate decreases with the increase of the Cl^- ratio in the electrolyte. The inhibiting effect becomes predominant with the increasing of Cl^- concentration. The $SO_4^{\bullet-}$ is scavenged by Cl^- to generate $Cl^{\bullet}$ and continue to react with Cl^- to generate less active radicals $Cl_2^{\bullet-}$ according to Eq. (11-12) [92, 97, 184]. Previous research on resorcinol removal by EO with BDD anodes found that in Na_2SO_4 electrolyte, the rate constant decreased from 2.4 ± 0.18 h^{-1} to 0.51 ± 0.05 h^{-1} when Cl^- increased from 0 mM to 20 mM [184]. Another research also concluded that Cl^- had a more significant influence on the $SO_4^{\bullet-}$ oxidation than $HO^{\bullet}$ oxidation because of $SO_4^{\bullet-}$ scavenging by Cl^- according to Eqs. (4.11)-(4.12) [252].

$$SO_4^{\bullet-} + Cl^- \rightarrow SO_4^{2-} + Cl^{\bullet} \qquad k = 3.1 \times 10^8\ M^{-1}s^{-1} \qquad (4.11)$$

$$Cl^{\bullet} + Cl^- \rightarrow Cl_2^{\bullet-} \qquad k = 1.4 \pm 0.2 \times 10^5\ M^{-1} \qquad (4.12)$$

Furthermore, the degree of synergy, energy consumption, and mineralization are listed in Table 4-3. Same as in SN, the highest synergy degree (92 %), benzotriazole mineralization efficiency (83 %), and lowest energy consumption (0.40 kWh/g benzotriazole) are in the 10:1 SCl ratio. For the same reason in section 3.2, the high reaction rate decreases reaction time and reduces energy consumption. During the EO of anaerobically treated landfill leachate with BDD anode, the highest COD removal (93 %) was achieved at 1:1 SO_4^{2-}: Cl^- molar ratio among 0.5:1 and 0.25:1 ratios [235]. Although this ratio is different from the ratio of this experiment, it can be seen that there is a trend that the sulfate-rich ratios improve the degradation of pollutants and decreases energy consumption.

Table 4-3. *Comparison of benzotriazole degradation rate constant and degree of synergy, TOC removal efficiency and energy consumption in different Na_2SO_4:NaCl(SCl) ratios. Experimental conditions: 10 mg/L benzotriazole, T = 25-30°C, applied potential = 4.3 V (vs. Ag/AgCl), conductivity = 10 mS/cm, flow rate = 580 mL/min, reaction time = 30 min for rate constant, degree of synergy, energy consumption calculation and 60 min for TOC removal efficiency calculation.*

SCl ratio Na_2SO_4:NaCl	Chemical kinetic constant k (min^{-1})	Degree of synergy S (%)	TOC removal efficiency η_{TOC} (%)(±SD)	Energy consumption EC (kWh/g benzotriazole) (±SD)
1:0	0.034	-	56 (3)	0.82 (0.3)
10:1	0.34	90	83 (1)	0.40 (0.1)
2:1	0.074	54	62 (0)	0.51 (0.1)
2:3	0.038	11	57 (5)	0.88 (0.2)
0:1	0.02	-70	38 (3)	0.93 (0.6)

4.3.4 Effect of Na_2SO_4:NaCl (SCl) ratios on chlorine by-product distribution during benzotriazole degradation

Chlorinated by-products formation, as free chlorine (Cl_2, ClO^-/HClO), chlorate (ClO_3^-), perchlorate (ClO_4^-), and COTPs as AOX, were monitored during benzotriazole degradation in different Na_2SO_4:NaCl (SCl) ratios. As shown in Fig. 4-5 (a), the free chlorine concentration in the 10:1 ratio becomes almost constant, while in 2:1, 2:3, and 0:1 ratios, the concentration continues to increase with time. The constant free chlorine concentration can be explained by the reaction of fresh free chlorine with $HO^\bullet$ to form ClO_3^-. When the Cl^- concentration rises, the free chlorine generation increases [223]. According to Fig. 4-5 (a and b), the free chlorine (ClO^-) concentration increases with initial chlorine ratios. BDD anode is conducive to free chlorine generation [251]. Cl^- is primarily oxidized directly and via $HO^\bullet$ on the BDD surface to active chlorine species (Cl_2, ClO^-/HClO). Free chlorine generation was also faster with BDD anode when compared with Ti_4O_7 anode in electrochemical degradation of PFOS in a chloride-rich electrolyte [251]. Free chlorine is considered one of the precursors of AOX formation. Thus, the AOX concentration also increases with the free chlorine concentration in different ratios (Fig. 4-5b).

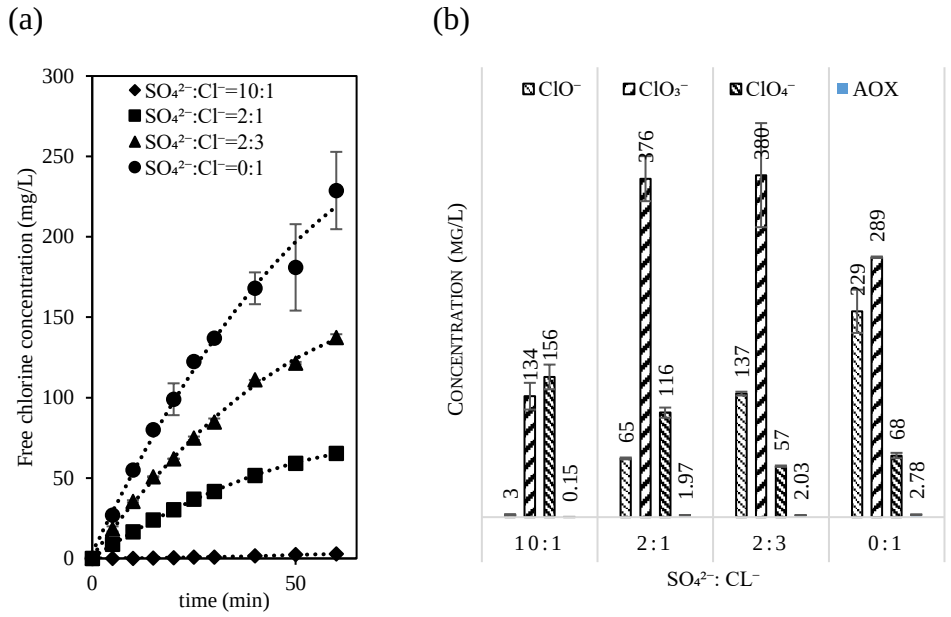

Fig. 4-5. *(a) Free chlorine concentration changing with reaction time (min); (b) Free chlorine, chlorate, perchlorate and AOX concentration in different Na_2SO_4:NaCl (SCl) ratios after 60 min of treatment. Experimental conditions: 10 mg/L benzotriazole, , T = 25-30 ℃, applied potential = 4.3 V (vs. Ag/AgCl), conductivity = 10 mS/cm, flow rate = 580 mL/min, reaction time = 60 min.*

Fig. 4-5b also shows that the ClO_3^- (134 mg/L) and ClO_4^- (156 mg/L) concentration was relatively higher in ratio 10:1 concerning initial Cl^- concentration (210 mg/L) (Fig. S4-6). According to the dominant pathway mentioned in section 3.1, more $HO^\bullet$ generation in SCl ratio 10:1, leading to complete free chlorine conversion to ClO_3^-, which subsequently transformed to ClO_4^-. The ClO_3^- concentration jumped three times with increasing Cl^- ratio from 10:1 to 2:1 and decreased from 380 mg/L to 289 mg/L with further increasing Cl^- ratio from 2:1 to 0:1. Whereas ClO_4^- concentration decreased from 156 mg/L to 68 mg/L with an increasing Cl^- ratio from 10:1 to 0:1. The ClO_3^- and ClO_4^- formation mechanisms can explain their irregular concentration trend. Free chlorine converted to ClO_3^- both non-radically and radically (Eqs. (4.13)-(4.14)) [223]. By contrast, ClO_4^- is mainly generated radically from $^\bullet ClO_3$ and $HO^\bullet$. ClO_3^- is first chemisorbed on the BDD anode as $^\bullet ClO_3$ by directly one-electron transfer and then reacted with $HO^\bullet$ to produce ClO_4^- (Eqs. (4.15)-(4.16)) [87, 161, 184, 223, 251, 253]. Due to both non-radically and radically free chlorine conversion, ClO_3^- formation jumped in the 2:1

SCl ratio solution, but because of less $HO^{\bullet}$ in this with a 2:3 to 0:1 SCl ratio, in which ClO_3^- formation decreased. Besides, there was less available $HO^{\bullet}$ to participate in ClO_3^- to ClO_4^- conversion in 2:1, 2:3, and 0:1 ratios. Thus, a large amount of ClO_3^- was accumulated, and less ClO_4^- was generated in these ratios. ClO_3^- and ClO_4^- are harmful to the ecosystem, which is always a drawback of EO. Therefore, further research is necessary to minimize the toxic ClO_3^- and ClO_4^- formation.

$$6OCl^- + 3H_2O \rightarrow 2ClO_3^- + 4Cl^- + 6H^+ + 1.5O_2 + 6e^- \quad (4.13)$$

$$ClO^- \xrightarrow{HO^{\bullet}} ClO_2^- \xrightarrow{HO^{\bullet}} ClO_3 \quad (4.14)$$

$$ClO_3^- \rightarrow ClO_3^{\bullet} + e^- \quad (4.15)$$

$$ClO_3^{\bullet} + HO^{\bullet} \rightarrow ClO_4^- + H^+ \quad (4.16)$$

4.3.5 Effect of Na_2SO_4:NaCl (SCl) ratios on transformation products distribution during benzotriazole degradation

Seven chlorinated organic transformation products (COTPs), COTP-1 ($C_6H_4ClN_3$), COTP-2 ($C_6H_3Cl_2N_3$), COTP-3 (C_4H_6ClNO), COTP-4 ($C_2H_2Cl_2O_2$), COTP-5($C_2HCl_2N_3$), COTP-6 ($C_5HCl_3O_3$), and COTP-7 ($C_3H_2Cl_2N_2$), were detected during the EO of benzotriazole (Table 4-4). COTP-1 represents the chlorination on the benzene ring. Active chlorine species are capable of electrophilic substitution in C4 and C7 positions on the benzene ring [254]. Thus, two chromatographic peaks corresponding to 153.00966 m/z at 8.445- and 8.807-min retention time represent two possible isomers of COTP-1 (Table 4-4 and Fig. S4-7). The active chlorine species could further chlorinate COTP-1 to produce COTP-2. In 0:1 ratio, COTP-1 and COTP-2 were found. In the 0:1 ratio, more active chlorine species were formed (Fig. 4-5), and the benzotriazole degradation rate was low (0.02 min^{-1}). Thus, benzotriazole was exposed more to active chlorine species for a longer time, enhancing these two COTPs. Two similar COTPs are detached during the chlorination of benzotriazole [254], xylyltriazole (XTRi), and 2-amino-benzothiazole [255]. In the 2:3 ratio, only COTP-1 was detected.

Table 4-4. *List of chlorinated organic transformation products (COTPs) and non-chlorinated transformation products (TPs) detected during benzotriazole degradation in different Na_2SO_4:NaCl (SCl).*

COTPs	Propose Formula	Propose structure	Molecular weight (m/z)	Accuracy (ppm)	Retention Time (min)	Mode (positive/ negative)	Na_2SO_4:NaCl (SCl) ratios				
							1:0	10:1	2:1	2:3	0:1
COTP-1	$C_6H_4ClN_3$	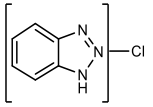	153.00966	1.89	8.445 8.807	+	ND	ND	ND	√	√
COTP-2	$C_6H_3Cl_2N_3$	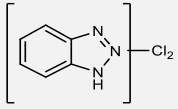	186.97071	1.63	9.485 9.694	+	ND	ND	ND	ND	√
COTP-3	C_4H_6ClNO	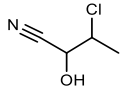	119.01407	2.31	6.177	+	ND	ND	√	√	√
COTP-4	$C_2H_2Cl_2O_2$	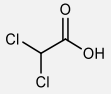	127.94306	-0.94	8.694	−	ND	ND	√	√	√
COTP-5	$C_2HCl_2N_3$		136.9546	-1.15	9.256	−	ND	ND	√	√	√
COTP-6	$C_5HCl_3O_3$	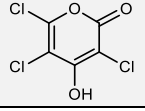	213.89919	0.22	15.14	−	ND	ND	√	√	√

COTP-7	$C_3H_2Cl_2N_2$	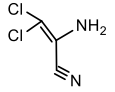	135.95981	2.25	8.134	+	ND	ND	√	ND	√
non-chlorinated transformation products (TPs)											
TP-1	$C_4H_3N_3O_4$	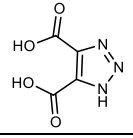	157.01269	-3.02	9.153	−	ND	√	√	√	√

This can be explained by the steric effect and the extent of exposure to active chlorine species. When one chlorine atom is added to the benzene ring, it will be difficult for another chlorine atom to be added on [97]. During EO of 4-ethylphenol in chloride electrolyte, 2-chloro-4-ethylphenol (2C4EP) was detected earlier than 2,6-dichloro-4-ethylphenol (26DC4EP). Besides, 2C4EP and 26DC4EP formation were faster at high than at low Cl^- concentrations [108]. Thus, this reduces the possibilities for COTP-2 formation in 2:3 and lower SCl ratios. In the 2:1 ratio, most of the benzotriazole was oxidized quickly (rate constant = 0.074 min^{-1}) and was not exposed to active chlorine species; therefore, none of these two COTPs were observed under these conditions. Oxidation of organic compounds produces carbonaceous and nitrogenous intermediates before being mineralized to carbon dioxides. These intermediates react with active chlorine species to form COTPs [254]. Initially, oxidation and radicles attack the C6 position on the benzene ring to open up the ring to produce carbonaceous intermediates like TP-1. TP-1 further goes through hydroxylation, bond cleaving, and chlorination to make COPT-4 and COPT-5. On the other hand, Nitrogenous intermediates were produced through the opening of the triazole ring. Which further oxidize, break down, and are chlorinated to form COTP-3 and COTP-7. These COTPs were detected in 2:1, 2:3, and 0:1 SCl ratios. However, none of the chlorinated intermediate compounds were seen in the solution with a 10:1 SCl ratio. Apparently, free chlorine concentrations were too low and were quickly converted to chlorate and perchlorate in the 10:1 SCl ratio. Also, faster simultaneous $HO^\bullet$ and $SO_4^{\bullet-}$ formation in 10:1 SCl ratio facilitated more rapid degradation of benzotriazole and its intermediates. Moreover, $HO^\bullet$ radicals, indeed, manly react to initiate substitution, cleavage of C=C bond, and oxidation of the benzene ring. These $SO_4^{\bullet-}$ radicals are, on the other hand, more inclined to attack the conjugation bond in the molecules [256]. However, a small amount of AOX was still detected in the 10:1 SCl ratio solution (Fig. 4-5). Some small amounts of COTPs formed, which could not be identified in the used LC-MS analysis. In a nutshell, sulfate-rich electrolytes could significantly minimize the formation of chlorinated organic transformation products (COTPs).

4.3.6 Environmental Implications

In practice, many industrial wastewater effluents, landfill leachates, and municipal wastewater contain dissolved salts and POPs [235, 257, 258]. Food

industries like olive oil mills and fish processing industries generate wastewater rich in salts and organic matter [259]. Cooling tower blowdown in industrial and energy sectors also contains a high level of salts (1043 mg/L SO_4^{2-} and 458 mg/L Cl^-) and organic pollutants (40-54 mg/L TOC) [34, 260]. Leather industry effluents were reported to contain 80 g/L NaCl [259]. For high salinity municipal wastewater, the high salinity may be attributed to the influx of saltwater in sewers or by human activities and toilet flushing with seawater [258]. Due to seawater intrusion, the municipal wastewaters can reach 135 mg/L SO_4^{2-} and 334 mg/L Cl^- salts [261]. High salinity content is also found in landfill leachate wastewater during stormy days (539 mg/L SO_4^{2-} and 1.9 g/L Cl^-), usually in coastal areas [235, 257]. Hence, our study shows that the dissolved salts in wastewater effluents can be beneficial as well as detrimental for EO removal of organic bio recalcitrant organic pollutants. Therefore, the control and regulation of the concentration of these dissolved salts in the effluents to be treated with EO are essential for successful and environmentally safe applications. The electrolyte composition plays an important role in organic compounds' degradation, mineralization, energy consumption, and chlorinated byproduct formation. Nanofiltration is an attractive accompanying technology for controlling and regulating the SN and SCl ratios effluents to be treated with EO. It is able to separate divalent species (SO_4^{2-}) from monovalent species (NO_3^- and Cl^-) and adjust the ratio compositions [262]. Thus, SCl electrolyte ratio between 10:1 and 2:1 can be achieved by applying NF. In these ratios, electrochemical oxidation has a high degradation rate, high mineralization efficiency, and low energy consumption due to effective $HO^\bullet$ and reactive sulfate species ($SO_4^{\bullet-}$ and $S_2O_8^{2-}$) formation discussed in sections 4.3.1-4.3.3. Low Cl^- concentration will also decrease the COTPs formation addressed in sections 4.3.3 and 4.3.4. Therefore, electrochemical oxidation combined with nanofiltration is a promising combination and worthy of further investigation.

4.4 CONCLUSIONS

The influence of electrolyte composition on the active sulfate formation and chlorinated by-product distribution in electrochemical degradation of benzotriazole with boron-doped diamond (BDD) anode has been investigated in this research. First, the study shows that $SO_4^{\bullet-}$ has been formed dominantly via $HO^\bullet$ on the electrode surface, and active sulfate species formation was faster in sulfate-rich

Na_2SO_4:$NaNO_3$ (SN) ratios at constant electrolyte conductivity. In contrast, only in SO_4^{2-} electrolyte (1:0) excess SO_4^{2-}, chemisorbs on the BDD anode and hampers the active sulfate species formation. Thereby, the 10:1 Na_2SO_4:$NaNO_3$ (SN) and Na_2SO_4:NaCl (SCl) ratio have the highest benzotriazole degradation rate, mineralization efficiency, synergistic degree, and lowest energy consumption. Decreasing concentrations of Cl^- in Na_2SO_4:NaCl solutions with ratios lower than 10:1 leads to a lower amount of toxic chlorinated organic transformation products and free chlorine formation. LC-MS has analyzed none of the chlorinated organic transformation products in the SCl 10:1 ratio, which -in contrast- were found in all other chloride enriched ratios above this value. However, chlorate and perchlorate concentrations were comparatively higher in the 10:1 ratio due to $HO^\bullet$ generation. Nanofiltration could lead to a sulfate-rich concentrate suitable for electrochemical oxidation in an actual application. Although it is promising to combine electrochemical oxidation with nanofiltration, the economic and environmental feasibility of the combination still needs further research.

Chapter 5.

Heat-activated peroxydisulfate and peroxymonosulfate mediated degradation of benzotriazole: Effects of chloride and pH on kinetics, pathways and product toxicity.

Modified version of this chapter will be published as:
Saha, Pradip, Chenyu Zhou, Mahsa Moradi, Marco Blokland, Huub HM Rijnaarts, Harry Bruning, " Heat-activated peroxydisulfate and peroxymonosulfate mediated degradation of benzotriazole: Effects of chloride and pH on kinetics, pathways and product toxicity." (in preparation,).

Abstract

The impact of chloride (Cl^-) in heat-activated peroxydisulfate (PS) and peroxymonosulfate (PMS) process for benzotriazole (BTA) degradation was investigated. Results showed that 0.42 mM BTA could be degraded by PS and PMS under 70°C in presence and absence of Cl^-. The PMS mediated BTA degradation rate increased with increasing Cl^- concentrations up to 1000 mg/L and declined to increase the Cl^- concentration further. In contrast, Cl^- inhibited PS-mediated BTA degradation at Cl^- concentrations tested between 100 to 10,000 mg/L. Radical scavenging experiments indicated that the BTA degradation was mainly driven by hydroxyl and sulfate radicals in both PS and PMS systems without Cl^-. However, reactive chlorine species significantly boosted the PMS BTA degradation in presence of Cl^-. Variation in pH substantially influenced the PMS system, but not PS in both presence and absence of Cl^-. LC-MS/MS analysis identified forty-two transformation products (TPs) resulting from BTA degradation. Based on the TPs, polymerization, hydroxylation, benzene ring-opening, and carboxylic acid formation were hypothesized to be the main degradation mechanisms in the absence of Cl^-, whereas chlorination, triazole ring-opening, and nitration were the additional degradation steps in presence of Cl^-. These findings help understand the influence of Cl^- on the BTA removal rate and degradation pathway in saline wastewater. Moreover, more chlorinated TPs were found in PMS/Cl^- system than in PS/Cl^- combination, which was also reflected in AOX and end-product toxicity analyses. The PMS/Cl^- process also produced other undesirable by-products such as chlorates, while these were not detected in the PS/Cl^- process. This shows that toxic by-product formation needs to be critically evaluated before applying PS and PMS-based advanced oxidation processes for organic pollutant degradation under saline conditions.

Keywords:

Benzotriazole; Heat-activated peroxydisulfate/peroxymonosulfate; Chloride; Chlorinated by-products; Toxicity.

5.1 INTRODUCTION

Benzotriazole (BTA) is mentioned in the NORMAN network list of emerging pollutants [263] and the Dutch River Water Companies Association (RIWA) list of potential pollutants (Dutch watchlist) [264], as a contaminant of emission to water sources should be reduced BTA is a widely occurring constituent of many chemical products used as corrosion inhibitors, anti-icing fluids, pharmaceuticals, textile dyes, plastics and rubbers, and dishwashing formulas [265, 266]. BTA is frequently found in water bodies because of its high water solubility, low partition coefficient (K_{ow}), poor biodegradability, and incomplete removal in conventional wastewater treatment plants [267-269]. A literature study showed that 7 to 100 μg/L BTA was detected in the European surface waters, and its concentration reached up to mg/L level in the vicinity of the airports [270]. In cooling tower operation, around 3 to 6 mg/L BTA is usually added to the makeup water [17]. BTA can accumulate in the environment and is a carcinogenic and mutagenic compound [271, 272]. Therefore, the development of an effective BTA removal method is essential.

Since its poor biodegradability, advanced oxidation methods are an interesting candidate for treatment. Different advanced oxidation processes (AOPs) have been studied for BTA degradation, such as photoelectrochemical and photocatalytic processes, Fenton-processes, photolysis, vacuum UV, ozonation, and sulfate radical ($SO_4^{\bullet-}$)-based processes (SR-AOPs) [254, 256, 273-281]. SR-AOPs become more interesting for the degradation of recalcitrant organic compounds, like BTA, since $SO_4^{\bullet-}$ has a high oxidation potential, a longer lifetime, and higher stability at a wide pH range as compared to $HO^{\bullet}$ [282-284]. $SO_4^{\bullet-}$ can be formed from peroxydisulfate (PDS) and peroxymonosulfate (PMS) activation, facilitated by heat, light (sunlight or UV), high pH, ultrasound, H_2O_2, activated carbon catalyst, electrochemical process, and different transition metals/metal oxides. Several studies show that SR-AOPs effectively remove BTA from aqueous environments [90, 266, 275, 278, 285, 286]. However, transformation products (TPs) and the fate of chloride ions (Cl^-), often present in the water matrix, still need to be examined critically in BTA degradation in SR-AOPs, for the reason that toxic reaction products can be formed

Chloride (Cl^-) is present in aquatic environments with a concentration range of 0.001 M to 1 M [287]. Several studies have reported that Cl^- might react with $HO^{\bullet}$

and $SO_4^{\bullet-}$ forming less effective chlorine radicals ($Cl^{\bullet}$), which may further be converted to $Cl_2^{\bullet-}$ [288, 289]. Besides, Cl^- may directly react with PMS and PDS to produce free chlorine (Cl_2/HOCl/ClO^-). Thus, Cl^- introduces reactive chlorine species (RCS) ($Cl^{\bullet}$, $Cl_2^{\bullet-}$, and Cl_2/HOCl/ClO^-) in the system, influencing the BTA degradation kinetics, pathways, and TPs distribution.

One study showed that BTA degradation efficiency by heat-activated PDS was enhanced when low concentrations of Cl^- (<10 mM) were added, while higher levels hindered the degradation [278]. However, in the (Cobalt)Co-activated PMS system, phenol and dye degradation efficiencies decreased when the Cl^- concentration was below 5 mM and increased above 50 mM [290-292]. The rate of 4- chlorophenol degradation increased by 47 times during the UV-activated PMS process in presence of high Cl^- concentration [293]. Apart from RCS reactivity with the reactive oxygen species, its reactivity with the organic compounds is also critical in determining the effect of Cl^- in such systems. When the reaction of the organic compound with RCS is fast enough, Cl^- enhances the degradation efficiency; however, when the organic compounds react slowly with RCS, Cl^- hinders the degradation efficiency. In either way, the reaction between organic compounds and RCS may form chlorinated TPs in the form of absorbable organic halides (AOX). Potentially, AOX is more toxic and/or refractory than the parent organic compounds. Based on the previous studies, chlorinated TPs are formed during the degradation of monochlorophenols, bezafibrate, and carbamazepine in UV-activated PS in presence of Cl^- [289, 294]. Similarly, a substantial amount of chlorinated TPs was reported during the degradation of steroid estrogens, methylene blue, 4-chlorophenol, phthalic acid, 2,4,6-trichlorophenol, and phenol in SR-AOPs in presence of Cl^-. Even though several TPs were reported during BTA degradation by SR-AOPs, the evaluation of chlorinated TPs formation and the corresponding degradation pathway still need to be elucidated [256, 279, 295, 296].

Moreover, research shows that chlorate (ClO_3^-) is produced during the SR-AOPs in presence of Cl^- [297]. A study reported that all Cl^- was converted to ClO_3^- before the degradation of perfluorooctanoic acid in the UV-activated PDS system [298]. Another research shows that ClO_3^- has been formed in the UV-activated PDS and Co-activated PMS systems, and the formation rate depended on the Cl^- concentration [299]. The acidic pH was more favorable for ClO_3^- formation in a UV-

activated PS process [295]. Due to the toxicity, the world health organization [300] advises keeping the ClO_3^- concentration less than 0.7 mg/L in the drinking water [300]. The US-EPA and Switzerland authorities also recommend keeping the ClO_3^- level below 200-210 µg/L in drinking water during UV-activated PS treatment [299]. Thus, the formation of ClO_3^- during the BTA degradation in SR-AOPs is essential to monitor.

Therefore, the primary focus of this study is to deeply assess the influence of Cl^- in the BTA degradation using heat-activated PDS and PMS systems. The heat was selected as both PDS and PMS activator due to its simplicity, moderate reaction conditions, no addition of chemicals/catalyst [301], and beneficial use potential of waste heat. Indeed, waste heat from industries, for instance, cooling towers or the textile industry, can be used for PDS and PMS activation [17, 91, 302]. The roles and dominance of important radicals in BTA degradation were investigated with scavenging experiments. TPs were identified by using LC-MS/MS to see their distribution and speciation in presence and absence of Cl^-. Last but not least, AOX, ClO^-, and ClO_3^- accumulation, acute toxicity, and BTA mineralization were explored under the different experimental conditions mentioned. Recommendations are given for PDS and PMS process selection to avoid toxic products forming.

5.2 MATERIALS AND METHODS

5.2.1 Chemicals

1-H benzotriazole (BTA, $C_6H_5N_3$, 99%) and ammonium formate (HCO_2NH_4, HPLC grade) were purchased from Sigma Aldrich Chemie B·V (the Netherlands). Sodium peroxydisulfate (PDS, $Na_2S_2O_8$, 99%), potassium peroxymonosulfate (PMS, $2KHSO_5 \cdot KHSO_4 \cdot K_2SO_4$, 99%), sodium chloride (NaCl, 99%), sodium dihydrogen phosphate (NaH_2PO_4, 99%), sodium hydrogen phosphate (Na_2HPO_4, 99%), Sulfuric acid (H_2SO_4, 95-98%), tert-butyl alcohol (TBA, C_4H_9OH, 99%), sodium hydroxide (NaOH, 99%) ethanol (EtOH, 99%), N,N-diethyl-p-phenylenediamine (DPD, 99%), L-Histidine ($C_6H_9N_3O_2$, ≥99%), and sodium azide (NaN_3, 99.5%) were obtained from Merck Chemicals B.V. (the Netherlands). Methanol ultra (MA, CH_3OH) was obtained from LPS b.v. (the Netherlands) and Formic acid (CH_2O_2, ULC/MS) was purchased from Biosolve BV, the Netherlands.

All the experiments were conducted using Millipore Milli-Q® water purification (electrical resistance 18.6 MΩ; Millipore Corporation, U.S.A.).

5.2.2 Experimental procedures

The experiments were conducted in 150 mL glass bottles equipped with an online pH meter (Prosense, Oosterhout, the Netherlands). The bottles were filled with 0.42 mM BTA, different concentrations of Cl^- (0, 100, 1000, and 10000 mg/L), and 15 mM phosphate buffers unless otherwise mentioned. The bottles were preheated for 30 min in a shaking water bath oscillating at 150 rpm (SW23, JULABO GmbH, Germany), and 15 mM PDS or PMS was added. Pre-tests showed that when PDS or PMS was added to the bottles, the pH decreased quickly even in presence of buffer. Thus, the pH was adjusted by 6 M NaOH to the desired value during the experiment. At specific time intervals, samples were collected and put in an ice bath to quench the reaction immediately. BTA, free chlorine, and PDS or PMS concentration were measured on the same day to rule out storage influence. For TOC, AOX, and ClO_3^- analyses, samples were stored at -20°C and measured on the next day after the experiment. To TPs identification, experiments were carried out in the absence of phosphate buffer to avoid buffers' effects in the TPs formation. A certain amount of EtOH or TBA was added to the bottles as a scavenger for $HO^•$ and $SO_4^{•-}$, respectively [55, 231]. L-Histidine and sodium azide was added to the bottles as singlet oxygen ($^1O_2$) scavengers. Control experiments with BTA without PDS or PMS at 70°C show that BTA was hydrolysis-resistant and thermally stable. Control experiments of BTA degradation with PDS or PMS at 25°C were carried out (Fig. S5-1).

5.2.3 Analytical methods

A Thermo Scientific HPLC quantified the BTA concentration with a fluorescence detector at 278 nm. The separation was performed by a Phenyl-Hexyl column (ACQUITY UPLC, 1.7μm, 2.1×150mm). The mobile phases were (A): water/formic acid 0.01% (v/v) and (B): acetonitrile/formic acid 0.01% (v/v) with a 0.2 mL/min flow rate. The injection volume was 10 μL, and the column temperature was 35°C. TOC was determined by a total organic carbon analyzer TOC-L CPH/CPN system integrated with ASI-L autosampler (Shimadzu, Benelux) using a

Non-Purgeable Organic Carbon (NPOC) method. The PDS/PMS concentration was determined by a spectrophotometric method combined with 0.1 mL of 2.5 mM N, N-diethyl-p-phenylenediamine (DPD) at 510 and 551 nm [303]. The ion chromatograph model, ICS 2100 with Dionex (IonPac AG17 Guard 4x50mm and IonPac AS17 analytical 4x250mm column), was used for measuring the concentration of ClO_3^-. AOX was determined by LCK 930 Hach Dr. Lange cuvette test kits using a Hach DR/3900 spectrophotometer (Hach Lange GmbH, Germany). Marine luminescent *Vibrio Fischeri* bacteria were used to assess the acute toxicity of BTA and its TPs [304]. The inhibition effect of untreated samples was also measured as a control. The free chlorine (FC) concentration was measured with the DPD–FAS standard method [305]. Both PDS and PMS were interfering with the free chlorine measurement; thus, a modification was introduced according to [306] to the standard method. Phosphate buffer and DPD solution were prepared according to the standard DPD–FAS method. 5 ml buffer was mixed with 5 ml of DPD solution; after that, 20 mL of 5% EDTA was added to the mixture. Finally, a 50 mL sample was mixed and titrated with ferrous ammonium sulfate (FAS). 1 mL of FAS is equivalent to 0.1 mg Cl_2.

5.2.4 High-resolution LC-MS/MS analysis for TPs identification

The TPs were analyzed by Ultimate 3000 liquid chromatography coupled with a QExactive Orbitrap MS- a high-resolution accurate-mass mass spectrometer (Thermo Scientific, San Jose, CA, USA). 50 µL injected sample was separated in an Atlantis T3 column (100 mm × 3 mm, 3 µm) with 0.3 mL/min eluant flow for 20 min. Eluant consisted of solution (A): water/2mM ammonium formate/0.016% (v/v) formic acid and (B): methanol/2 mM ammonium formate /0.016% (v/v) formic acid. The elution gradient was 0% B initially, which linearly increased to 45% in 2 min, subsequently increased to 100% in 8 min, and was kept constant up to 14.5 min. In the next 0.5 min, B decreased to 0%, and this condition was maintained until 20 min. The column oven temperature was 40°C, and TPs were detected in full-scan mode (60-700) in both positive and negative ionization modes. During the measurement, MS were at 3.5 kV spray voltage; 48 sheaths and 2 (a.u.) sweep gas flow; 256°C capillary temperature; 413°C aux gas heater temperature and 70000 resolution power. According to the manufacturer protocol, MS was calibrated for each series

using a Pierce™ LTQ Velos ESI positive and negative ion calibration solution (Thermo Scientific).

5.2.5 Data analysis:

5.2.5.1 Data processing for TPs identification

LC-MS raw data files obtained from duplicate measurement were processed by commercially available small molecule structure identification software "Compound Discoverer (CD) v. 3.1" (Thermo Scientific, USA). The environmental workflow template "Environmental w Stats Unknown ID w Online and Local Database Searches" was used. The workflow consists of five general steps: 1) raw files are inputted in the CD and named as sample or blank; 2) spectra of peaks are picked based on minimum peak intensity counts (100,000 a.u), mass tolerance (5 ppm), and retention time shift (0.2 min); 3) the compounds are detected based on mass tolerance, intensity threshold, isotopes integration and ions adducts from extracted ion chromatogram (XIC) traces in the full scans (MS1). Compounds with the same molecular weight and retention time were grouped together; 4) in the predict compositions step, the molecular formula is assigned according to the accurate mass, maximum element counts "$C_{90}H_{190}Cl_{10}N_{10}O_{15}S_5$"; 5) best-fit compounds are selected based on composition and mass from ChemSpider and mass lists database search. The matching results are further filtered and checked based on peak shape, peak area, and relevance to the parent compound to make the results more reliable.

5.2.5.2 Scavengers effect calculation

The percentage decrease in reaction rate constant k_{obs} (PDS/PMS) due to scavengers were calculated by the following formula (Eq. 5.1):

$$\% \text{ decrease of } k_{obs} \text{ (D\%)} = [1- k_{obs(scavenger)}/k_{obs\ (without\ scavengers)}] \times 100\% \quad (5.1)$$

5.2.5.3 Toxicity calculation

The increase of luminescent intensity inhibition was used to evaluate the toxicity and calculated as follows (Eq. 5.2):

$$\text{Increase of inhibition (\%)} = \frac{L_0 - L}{L} \times 100\% \quad (5.2)$$

L_0 is the luminescent intensity of the control sample (before reaction), and L is the luminescent intensity of a sample.

5.3 RESULTS AND DISCUSSION

5.3.1 BTA degradation kinetics in the absence and presence of Cl^-

The effect of 0, 100, 1000, and 10000 mg/L Cl^- on BTA degradation in heat-activated PDS and PMS was investigated and shown in Fig. 5-1.

The Cl^- concentration significantly influenced the BTA degradation in both PDS and PMS systems but in different ways (Fig. 5-1). Fig.5-1a shows that BTA degradation was retarded in the PDS/Cl^- process. In the absence of Cl^-, the pseudo-first-order rate constant (k_{obs}) for BTA degradation was 0.07 min^{-1}. This value was lowered to 0.05 min^{-1} when the Cl^- concentration was increased to100 mg/L. Further increasing the Cl^- concentration to 10000 mg/L led to a continued decrease of the k_{obs} to 0.03 min^{-1}. The BTA removal efficiency was also reduced to 96% in 10000 mg/L Cl^- after 120 minutes of reaction time. Cl^- can react with $SO_4^{\bullet-}$ to produce $Cl^\bullet$ with a rate constant of 3.2×10^8 min^{-1}, pushing back to $SO_4^{\bullet-}$ with a rate constant of the reversed reaction of 2.1×10^8 min^{-1} (eq. 5.3).

$$SO_4^{\bullet-} + Cl^- \leftrightarrow SO_4^{2-} + Cl^\bullet \quad (5.3)$$

$SO_4^{\bullet-}$ has supposedly been produced again, compensating the $SO_4^{\bullet-}$ scavenging at low Cl^- concentration [307-309]. Thus, the low Cl^- concentration lowers the BTA degradation rate slightly. However, when the Cl^- was at an elevated concentration (10000 mg/L), the forward reaction became dominant, resulting in a higher degree of $SO_4^{\bullet-}$ scavenging. Thus, the overall BTA k_{obs} and efficiency decreased with increasing Cl^- concentration. The BTA degradation was promoted remarkably in the PMS/Cl^- process (Fig. 5-1b). The increasing of Cl^- concentration increased the BTA k_{obs} up to 1000 mg/L Cl^-. In the absence of chloride, the k_{obs} was 0.03 min^{-1}. Adding 100 mg/L and 1000 mg/L Cl^- led to a notable increase of k_{obs} to 0.1 min^{-1} (three times higher) and 0.3 min^{-1} (ten times higher), respectively. However, further rising of the Cl^- concentration decreased the rate.

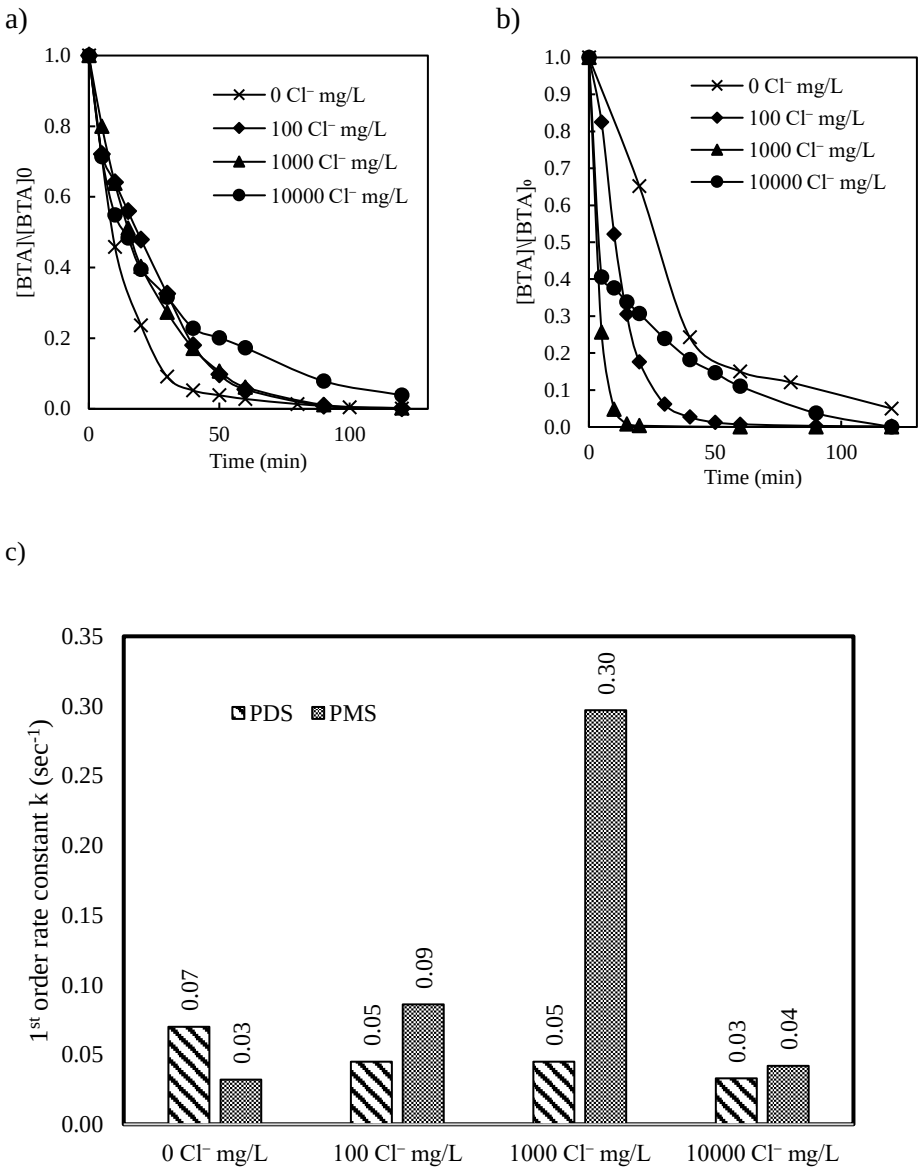

Fig. 5-1. *BTA degradation by (a) PDS and (b) PMS in the presence of 0 mg/L, 100 mg/L, 1000 mg/L and 10000 mg/L Cl^- during 120 min reaction; (c) Pseudo-first-order disappearance of BTA; Experimental conditions: T=70°C, $[BTA]_0$=0.42 mM, $[PDS]_0=[PMS]_0$=15 mM, V=100 mL, all experiments were buffered by 15 mM phosphate and sodium hydroxide was added dropwise to maintain the pH around 6.8-7.3.*

Meanwhile, the BTA removal efficiency after 120 min reaction increased from 95% (without Cl^-) to 100% (100 mg/L, 1000 mg/L and 10000 mg/L Cl^-). Especially when Cl^- was 1000 mg/L, 100% BTA was removed in 20 min. Similar results were obtained in research focused on acid Orange 7 (AO7) degradation by anion activation of PMS, reporting that 10 mM and 100 mM Cl^- could effectively activate the PMS but not the PDS [310]. In a study conducted by Zhang et al. [311], p-aminobenzoic acid degradation efficiency was enhanced with increasing Cl^- dosage by using PMS. An increase of chloride up to 200 mM led to complete removal of p-aminobenzoic acid in 20 min; while in the absence of chloride, p-aminobenzoic acid removal efficiency reached merely 81% in reaction time of as long as 80 min. Direct PMS oxidation was identified as the major contributor to p-aminobenzoic acid degradation, while $HClO/ClO^-$ was identified as the dominant RCS [311]. Another study investigated the role of chloride on ammonia oxidation by cobalt-doped graphitic carbon nitride-activated PMS [312]. It was hypothesized that at pH levels higher than 6, free chlorine species mostly react with water leading to the formation of $HO^\bullet$ thereby boosting the oxidation rate

Due to the unsymmetrical structure of PMS, it is easily attacked by a nucleophile such as Cl^- [313]. Yang et al. also showed that PMS could react with Cl^- producing OCl^- [310, 314]. Thus, active OCl^- together with $HO^\bullet$ and $SO_4^{\bullet-}$ radicles facilitated the degradation of BTA up to 1000 mg/L Cl^-. Further increasing of Cl^- concentration could quench the radicals and hinder the BTA degradation.

5.3.2 pH influence on BTA degradation kinetics in absence and presence of Cl^-

The BTA degradation in PDS and PMS systems at varying pH is shown in Fig. 5-2. Fig. 5-2a indicates that the pH changes barely influenced the BTA k_{obs} in PDS experiments. The 100% BTA removal efficiency was obtained under all set pH conditions after 120 min reaction. The k_{obs} (PS) at pH 7 and 11 was 0.07 min^{-1} both in absence of Cl^-, while in presence of 1000 mg/L Cl^-, k_{obs} (PDS) was 0.05 min^{-1}. Some studies indicated that organics degradation is improved at alkaline conditions compared to acidic conditions [237]. However, the BTA degradation rate was close at pH 7 and 11 [315]. It was interesting to see that the PDS consumptions at pH = 7 and pH = 11 were 33% and 21%, respectively, after 3h (Fig. S5-1). It could be

inferred that $SO_4^{\bullet-}$ radicals were converted to $HO^{\bullet}$ radicals at a high rate [316]. $HO^{\bullet}$ radical has higher redox potential, which is unselective [91]. Thus, the alkaline conditions can reduce the PDS consumption in the absence of Cl^-. However, PDS consumption was similar (around 34%) in both pH levels in presence of Cl^- because Cl^- can be a scavenger for $SO_4^{\bullet-}$ and $HO^{\bullet}$ to produce RCS [317, 318].

Fig. 5-2b indicates that the pH significantly affects BTA degradation in the PMS system. At pH = 11, only 70% of BTA was decomposed after 120 min with a k_{obs} of 0.02 min^{-1} in the absence of chloride, whereas at pH = 7 in identical conditions, 95% BTA removal efficiency was obtained with a k_{obs} of 0.03 min^{-1}. At pH 11, the BTA degradation rate was high in the first 20 min, and then it became extremely low (Fig. 5-2b). From 20 min to 120 min, only 12% of BTA was degraded, whereas 58% of BTA was degraded in the first 20 min. It was reported that SO_5^{2-} , which can be generated at alkaline conditions (Eq. 5.4), is more accessible to activate than HSO_5^-, thus more radicals were produced [319]. This explains the high BTA degradation rate in the first 20 min. However, some PMS were decomposed at pH 11 rather than converting into radicals (Eqs. (5.5)-(5.6)) [320].

$$HSO_5^- + H_2O \rightleftarrows SO_5^{2-} + H_3O^+ \ (pK_{a2}=9.4) \quad (5.4)$$

$$HSO_5^- + SO_5^- \rightarrow \text{the activated complex} \rightarrow HSO_6^- + SO_4^- \quad (5.5)$$

$$HSO_6^- + OH^- \rightarrow SO_4^{-2} + H_2O + O_2 \quad (5.6)$$

Yang et al. [321] found that at pH 11, about 75% of PMS was decomposed after 20 min, and 100% of PMS was decomposed after 120 min in the wet scrubbing process. 2 g/L Na_2SiO_3 was used to make the PMS more stable in their experiments [321]. There was no PMS left at pH 11 and 70°C in 120 min in the current study, but the BTA removal efficiency was only 70%. At 30 min, 82% PMS was consumed (Fig. S5-1). The residual PMS was only 9% with 12% BTA removal efficiency in pH 11 at 25 °C after 120 min (Fig. S5-1). The high PMS consumption rate and low BTA removal efficiency at pH 11 reflected that a large part of PMS was decomposed instead of forming $SO_4^{\bullet-}$ or $HO^{\bullet}$ radicals. Lou et al. [322] reported that the increase of pH resulted in a PMS decay. In a study on the base-activated PMS process, Yang et al. [323] reported that excess NaOH inhibited the degradation of methylene blue. Here, lower BTA degradation was attributed to the PMS self-decomposition.

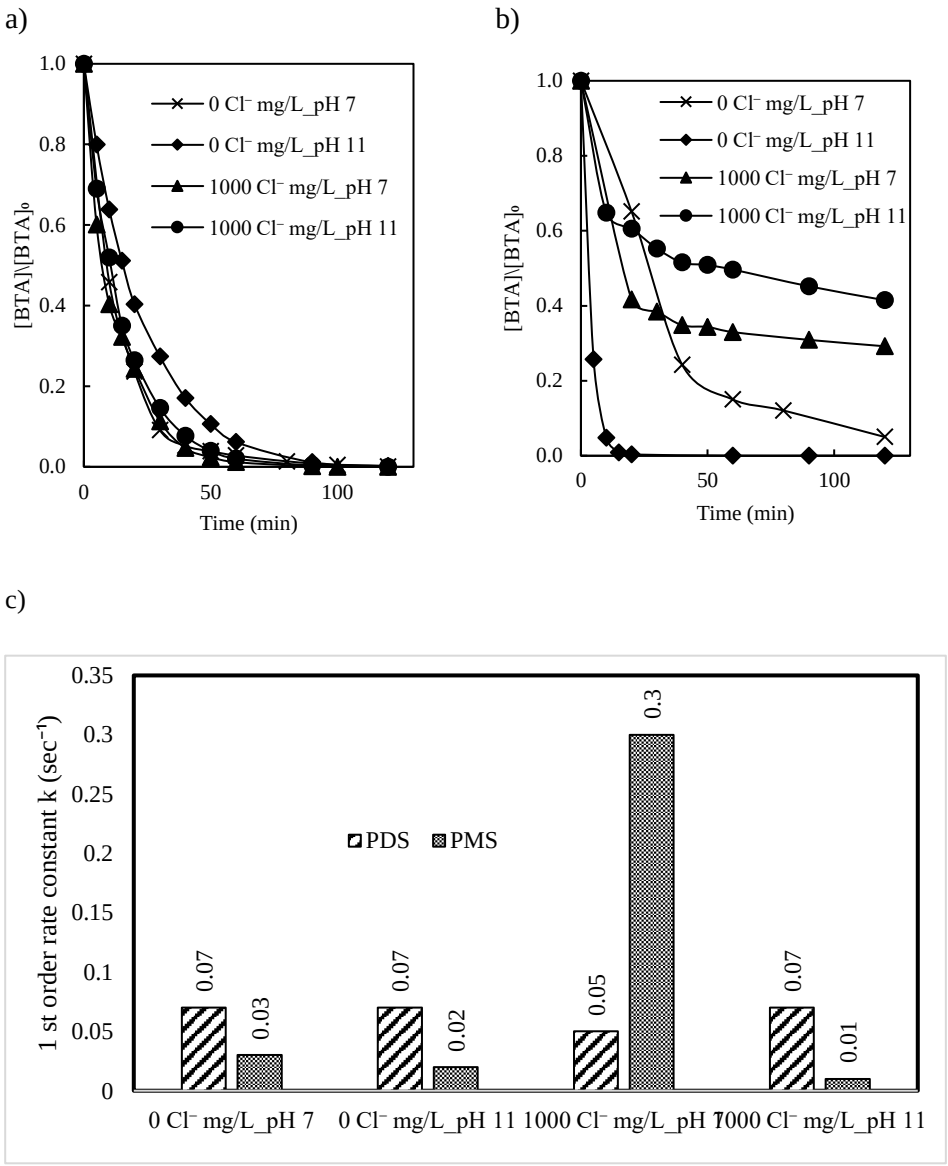

Fig. 5-2. *BTA degradation by (a) PDS and (b) PMS in the presence of 0 mg/L, 100 mg/L, 1000 mg/L and 10000 mg/L Cl^- during 120 min reaction; (c) Pseudo-first-order disappearance of BTA; Experimental conditions: T=70°C, $[BTA]_0$=0.42 mM, $[PDS]_0$=$[PMS]_0$=15 mM, V=100 mL, all experiments were buffered by 15 mM phosphate and sodium hydroxide was added dropwise to maintain the pH around 6.8-7.3.*

Moreover, the presence of Cl^- significantly hampered the BTA degradation at basic conditions. The BTA removal efficiency decreased from 70% (without Cl^- and pH 11) to 58%. The decomposition of PMS and the dissociation of HOCl under pH 11 could explain the significant hindering of BTA removal. HOCl is a weak acid (pK_a=7.49). When the pH rose to 11, more OCl^- with weak oxidation ability (E_0 =0.94V) was produced. Then a series of chain reactions generate other chlorine species leading to the lower BTA removal efficiency [324].

5.3.3 Quenching experiment

To distinguish the predominant species in BTA degradation in PDS and PMS systems, 50 mM EtOH and TBA were selected as both $SO_4^{\bullet-}$ and $HO^\bullet$ radicals scavenger and $HO^\bullet$ radical scavenger, respectively. Anipsitakis and Dionisiou [325] indicated that the reaction rate of TBA with $SO_4^{\bullet-}$ was 4×10^5 to 9.1×10^5 M^{-1} $s^{-1,}$ which was much lower than the rate with $HO^\bullet$ (3.8×10^8 to 7.6×10^8 M^{-1} s^{-1}). Besides, it was reported that the reaction of α hydrogen-containing alcohols (e.g., EtOH) with $HO^\bullet$ occurs with rates around 1.2×10^9 to 2.8×10^9 M^{-1} s^{-1}. In contrast, the reaction rate of EtOH with $SO_4^{\bullet-}$ is 1.6×10^7 to 7.7×10^7 M^{-1} s^{-1} [325].

Fig. 5-3 indicates that the addition of TBA and EtOH showed an inhibition effect on the BTA degradation and removal rate in both PS and PMS experiments. The k_{obs} (PS) decreased from 0.07 to 0.02 min^{-1} when the TBA was added, and k_{obs} (PS) fell to 0.009 min^{-1} when EtOH was added. As for PMS, the k_{obs} (PMS) decreased from 0.03 to 0.013 min^{-1} when the TBA was added, and k_{obs} (PS) fell to 0.008 min^{-1} when EtOH was added. Based on the calculation, the D% (PS) was 87% in presence of EtOH, which represented the contribution of $SO_4^{\bullet-}$ and $HO^\bullet$ to BTA degradation. The D% (PS) was 71% in presence of TBA, which meant the role of $SO_4^{\bullet-}$ to BTA degradation. As for PMS, The D% (PMS) was 73% and 57% in presence of EtOH and TBA, respectively. The results show that both $HO^\bullet$ and $SO_4^{\bullet-}$ were the dominant oxidizing species of BTA degradation in both PS and PMS experiments.

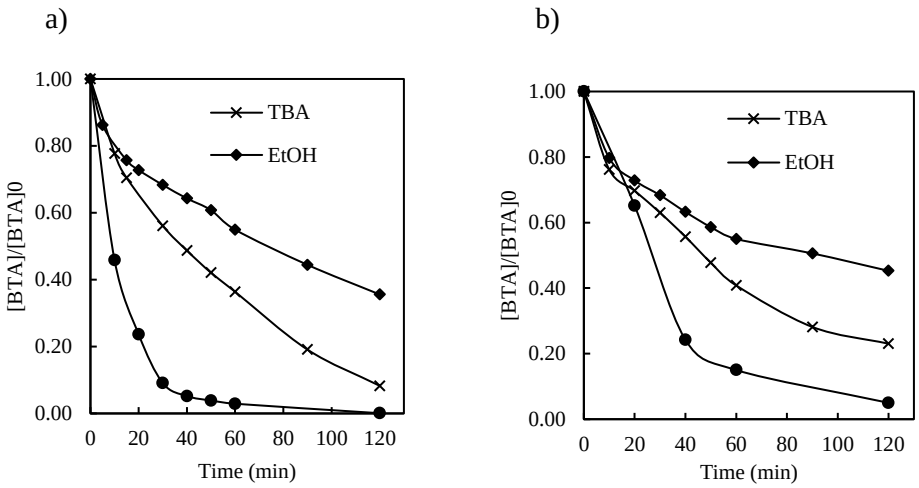

Fig. 5-3. *BTA degradation by (a) PDS and (b) PMS in the presence of radicals scavengers (TBA and EtOH) during 120 min reaction. Experimental conditions: T=70°C, [BTA]0=0.42 mM, TBA=50 mM, EtOH=50 mM, V=100 mL, all experiments were buffered by 15 mM phosphate, and sodium hydroxide was added dropwise to maintain the pH around 6.9-7.4.*

These results were a little bit different from other studies about PDS. Norman et al. [326] reported no ·OH domination when the pH was < 8 in the PDS system. Ji et al. [327] found that 30 mM TBA slightly inhibited ATZ degradation by PDS and; $SO_4^{\bullet-}$ was the dominant radical species when pH was 7. Both $HO^{\bullet}$ and $SO_4^{\bullet-}$ contributed to the degradation of organic pollutants when the pH was 9 [328]. The possible explanation of the high contribution of $HO^{\bullet}$ to BTA degradation in our study could be the extra NaOH which was added to maintain the neutral pH because $SO_4^{\bullet-}$ reacted with OH^-, producing $HO^{\bullet}$.

To further investigate the domination of ROS, L-histidine and sodium azide were added as $^1O_2$ scavengers. In this way, L-histidine substantially suppressed the oxidative degradation of BTA in as much as no degradation efficiency was observed in both PDS and PMS-based processes, either in presence or absence of chloride. In PMS-based processes, $^1O_2$ can be produced by PMS self-decomposition. Nonetheless, due to the rapid depletion of PMS as exposed to L-histidine, domination of $^1O_2$ cannot be confirmed in the studied PMS-based processes. This finding was similar to the results obtained in the study conducted by Gao et al. [326], in which L-histidine suppressed the bisphenol A degradation in the NCN-900/PMS

process. The following equations show the possible generation of $^1O_2$ in PMS-based processes (Eqs. (5.7)-(5.8)) [329].

$$HSO_5^- \rightarrow SO_5^{\bullet -} + H^+ + e^- \quad (5.7)$$

$$2SO_5^{\bullet -} + H_2O \rightarrow 2HSO_4^- + 1.5\,{}^1O_2 \quad (5.8)$$

Likewise, the addition of sodium azide remarkably inhibited the BTA degradation efficiency. However, L-histidine and sodium azide are not supposedly indicative for determining the dominant ROS in PMS-based processes due to their direct reaction with PMS. Also, in the PS-based process, L-histidine and sodium azide inhibited the BTA degradation substantially, representing the possible domination of $^1O_2$. One hypothesis is that the C=O group can be the intermediate precursor for the formation of $^1O_2$ [329]. This structure was also identified amongst the BTA degradation intermediates.

Table 5-1. *Influence of scavengers on BTA degradation rate; Experimental conditions: T=70°C, $[BTA]_0$=0.42 mM, [TBA]=[EtOH]=[L-Histidine]=[sodium azide] =50 mM, V=100 mL, all experiments were buffered by 15 mM phosphate and sodium hydroxide was added dropwise to maintain the pH around 6.9-7.4.*

	k_{obs} (min^{-1})	k_{obs} (D%) with TBA	k_{obs} (D%) with EtOH	k_{obs} (D%) with L-Histidine	k_{obs} (D%) with sodium azide	dominant oxidizing species
PDS	0.07	0.02 (71%)	0.009 (87%)	~0 (99%)	~0 (99%)	$HO^\bullet$ /$SO_4^{\bullet -}$
PDS/1000 mg/L Cl^-	0.05	-	-	~0 (99%)	~0 (99%)	
PMS	0.03	0.013 (57%)	0.008 (73%)	~0 (99%)	~0 (99%)	$HO^\bullet$ /$SO_4^{\bullet -}$
PMS/1000 mg/L Cl^-	0.3	-	-	~0 (99%)	~0 (99%)	

5.3.4 Mineralization, degradation products, and their evolution pathways

According to the results obtained in LC-MS/MS analysis in both positive and negative modes, 42 TPs were detected (Table 5-2). BTA degradation pathways were

proposed in PDS and PMS-based processes (Fig.5-4). This survey was carried out in presence and absence of Cl^- to track the TPs and seek possible changes in the BTA degradation pathway. In absence of chloride, four different pathways were hypothesized, as in Fig. 5-4a. The major degradation mechanisms for BTA were found to be hydroxylation, benzene ring-opening, bond cleavage, and carboxylic acid formation. Surprisingly, in many of the identified TPs, the triazole ring remained stable due to its higher persistence to degradation. A study conducted by Jorfi et al. [279] stated a different finding. They hypothesized that BTA degradation was initiated by triazole ring-opening or destruction of the double-bonded nitrogen in the triazole ring [279]. In another study on the degradation of 4- and 5-methyl-1H-benzotriazole, the triazole ring remained intact [330]. Regarding the identified TPs in Table S5-3, it can be seen that nitric acid (TP27) was identified in PDS and PMS-based processes, both in presence and absence of chloride. Of note, in absence of chloride, nitric acid was merely identified at reaction times of as long as 120 and 180 min. While in presence of chloride, it was observed that nitric acid was also detected at much shorter reaction times; at 10, 30, and 60 min Table S5-3. Considering the identified TPs, triazole ring-opening occurred when chloride was there within the solution, and the triazole ring was the only nitrogen source in the studied matrix. In other words, detection of nitric acid indicated triazole ring-opening; and the rate of this ring-opening reaction appears to be boosted in presence of chloride, especially in PMS/Cl^- process. It has been found that presence of chloride at high concentrations (> 100 mM) can enhance the AOP degradation rate of nitrogen-containing rings and bonds as they occur in azo dyes [291, 331]. Occurrence of polymerization was detected by identifying TP1 and TP2 representing $C_{12}H_8N_6$ and $C_{18}H_{11}N_9$ with m/z of Ca. 236 and 353, respectively. Regarding Table S5-3, the TPs mentioned earlier were identified from the beginning of the degradation reactions in 10 min staying in the solution until over 120 min. Anyway, polymerization is a common mechanism at the beginning of the degradation pathway [276]. BTA also underwent hydroxylation followed by benzene ring-opening and bond cleavage as reflected by the identification of TP4-TP10, especially in absence of chloride. These intermediates were shown up in 10-180 min reaction time as in Table S5-3. Afterward, the intermediates were further oxidized into carboxylic acids. It is worth noting that the solo triazole ring was merely detectable in 180 min within both PDS and PMS-based processes in the absence of Cl^-.

In the case of chloride-laden samples, 28 TPs were detected; many of them were chlorinated. As in Fig. 5-4b, BTA degradation was hypothesized to follow a multilateral pathway, including the previously mentioned mechanisms as well as chlorination of BTA, TPs, and carboxylic acids. In PMS/Cl^-, more chlorinated TPs were detected in comparison with PDS/Cl^-. This finding was in agreement with the results obtained in the mineralization study. As Table 5-3 indicated, PDS-based processes brought about higher mineralization. Using PDS, 90% and 76% TOC removals were obtained in absence and presence of chloride, respectively. Based on LC-MS/MS analysis results, many TPs, particularly TP28-TP35, demonstrated the addition of a chlorine atom to the aromatic structures, making the compound more persistent to oxidative degradation. On the contrary, chloride exhibited a positive effect on TOC removal in a PMS-based process similar to the results obtained and discussed for BTA removal. However, the application of PMS led to far less mineralization (%) as compared to that of PDS (Table 5-3). As depicted in Fig 5-4b, many chlorinated TPs such as TP22, TP23, TP29, TP31, TP32, TP33, and TP34 were formed in the PMS-based process and were mostly persistent until 180 min reaction time. Although the BTA removal rate was significantly high in PMS/Cl^- than PMS (as discussed in the kinetic study), it was initially transformed into chlorinated BTA species through the third and fourth pathways (Fig. 5-4b) with no significant mineralization. Nevertheless, the second pathway mainly consisted of hydroxylation, bond cleavage, benzene, and triazole ring-opening leading to some degrees of mineralization. To sum up, in presence of chloride, heat/PDS revealed better results than the heat/PMS from the aspect of TPs formation and mineralization.

Table 5-2. *Transformation products (TPs) identified during BTA degradation. Experimental conditions: T=70℃, [BTA]0=0.42 mM, [PDS]0 = [PMS]0 =15 mM, [Cl⁻]= 0 or 1000 mg/L, V=100 mL, sodium hydroxide was added dropwise to maintain the pH around 6.9-7.4*

Transformation products (TPs)	Proposed formula	Proposed structure	Observed Molecular weight (m/z)	accuracy (ppm)	Retention time (min)	Mode (positive/ negative)	PDS	PMS	PDS/Cl^-	PMS/Cl^-
TP1	$C_{12}H_8N_6$	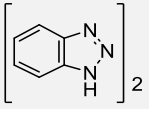	236.08099	-1.19	10.573	Negative	√	√		√
TP2	$C_{18}H_{11}N_9$	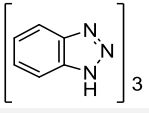	353.11347	-0.66	12.834 12.187 10.809	Positive	√	√		
TP3	$C_{12}H_8N_2$	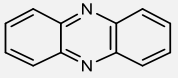	180.06825	-2.74	10.587	Positive	√	√		
TP4	$C_6H_3N_3O_2$	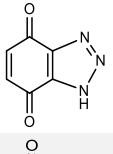	149.02270	1.19	7.711	Negative	√			√
TP5	$C_6H_7N_3O_2$	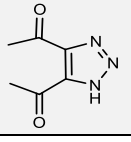	153.05353	2.47	1.967	Positive	√	√		

Transformation products (TPs)	Proposed formula	Proposed structure	Observed Molecular weight (m/z)	accuracy (ppm)	Retention time (min)	Mode (positive/ negative)	PDS	PMS	PDS/Cl^-	PMS/Cl^-
TP6	$C_6H_7N_3O_3$	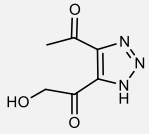	169.04880	0.32	6.181	Negative	√	√		
TP7	$C_6H_9N_3O_4$	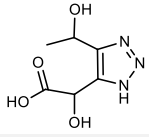	187.05896	-1.84	1.424	Positive	√			
TP8	$C_3H_3N_3O_2$	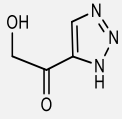	113.02287	2.8	9.121	Negative	√	√		
TP9	$C_4H_3N_3O_3$	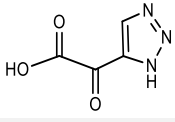	141.01765	1.5	6.208	Negative	√	√		
TP10	$C_4H_3N_3O_4$	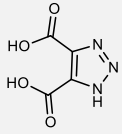	157.01269	-3.02	9.153	Negative	√	√	√	√
TP11	$C_4H_8O_5$	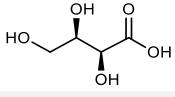	136.03746	2.07	1.425	Negative	√	√		
TP12	$C_4H_4O_4$	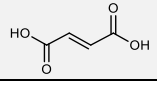	116.01131	-3.05	8.65	Negative	√	√	√	√

TP13	$C_4H_7NO_2$	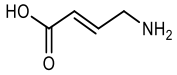	101.04727	-3.05	2.101	Positive	√	√		
TP14	$C_4H_3NO_2$	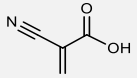	97.016380	-1.96	6.171	Negative	√	√	√	√
TP15	$C_4H_7NO_4$	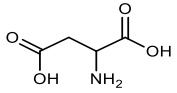	133.03729	-1.60	1.645	Positive	√	√		
TP16	$C_3H_6O_4$	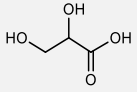	106.02675	1.27	2.032	Negative	√	√	√	√
TP17	$C_3H_4O_3$	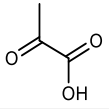	88.01570	-4.02	1.399	Negative	√	√		
TP18	$C_3H_6O_3$	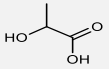	90.03140	-3.26	2.409	Negative	√	√		
TP19	$C_2H_4O_3$	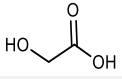	76.01536	-8.74	1.933	Negative	√	√		
TP20	$C_2H_3N_3$		69.0327	-12.88	9.116	Negative	√	√		
TP21	$C_6H_7N_3O_4$	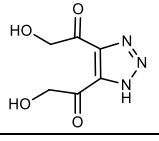	185.04378	0.65	1.742	Negative			√	

Transformation products (TPs)	Proposed formula	Proposed structure	Observed Molecular weight (m/z)	accuracy (ppm)	Retention time (min)	Mode (positive/ negative)	PDS	PMS	PDS/Cl^-	PMS/Cl^-
TP22	$C_6H_4N_4O_2$	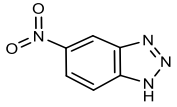	164.033432	1.25	9.150	Negative				√
TP23	$C_6H_4N_4O_3$	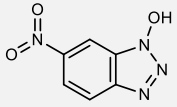	180.028336	0.71	17.287	Negative				√
TP24	$C_6H_5N_3O_5$	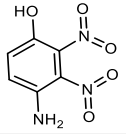	199.02310	0.57	10.906	Negative			√	√
TP25	$C_4H_6O_4$	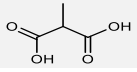	118.02695	2.85	3.357	Negative			√	
TP26	CHN_3O_3	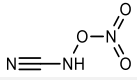	103.00183	0.36	10.076	Negative			√	√
TP27	HNO_3		62.99466	-15.58	6.595	Negative	√	√	√	√
TP28	$C_6H_4ClN_3$	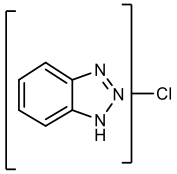	153.00909	1.1	9.683 9.295	Positive and negative			√	√

TP29	$C_6H_3Cl_2N_3$	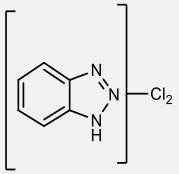	186.97040	-0.59	10.833 10.929	Positive and negative		√
TP30	$C_6H_2Cl_3N_3$	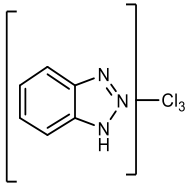	220.931427	-0.54	12.379	Negative	√	√
TP31	$C_6HCl_4N_3$	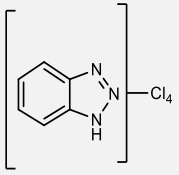	254.892456	0.46	13.949	Negative		√
TP32	$C_6H_4ClN_3O$	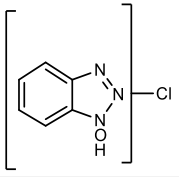	169.00442	0.79	19.285	Negative		√
TP33	$C_6H_3Cl_2N_3O$	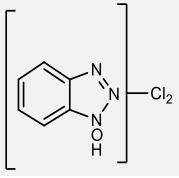	202.965317	0.29	13.672	Negative		√

Transformation products (TPs)	Proposed formula	Proposed structure	Observed Molecular weight (m/z)	accuracy (ppm)	Retention time (min)	Mode (positive/ negative)	PDS	PMS	PDS/Cl^-	PMS/Cl^-
TP34	$C_6H_2Cl_3N_3O$	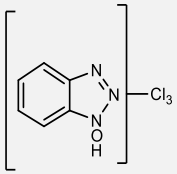	236.92645	0.45	18.332	Negative				√
TP35	$C_6H_7Cl_2N_3O_2$	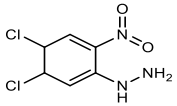	222.99089	-0.47	6.738 7.432	Positive and negative			√	√
TP36	$C_4H_3ClO_4$	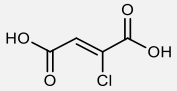	149.971985	1.35	10.993	Negative			√	√
TP37	$C_4H_6ClNO_2$	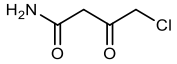	135.00840	-2.3	3.540	Positive			√	√
TP38	$C_3H_3ClO_2$	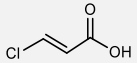	105.982155	0.52	10.989	Negative				√
TP39	$C_2H_2Cl_2O_2$	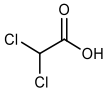	127.94351	2.4	9.729	Negative			√	√
TP40	$C_2H_3ClO_2$	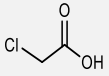	93.982155	-2.07	5.943	Negative				√
TP41	$C_2HCl_2N_3$		136.9546	1.57	10.128	Negative			√	√

TP42	C_2HClN_2O	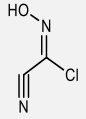	103.97786	1.13	10.478	Negative	√

(a)

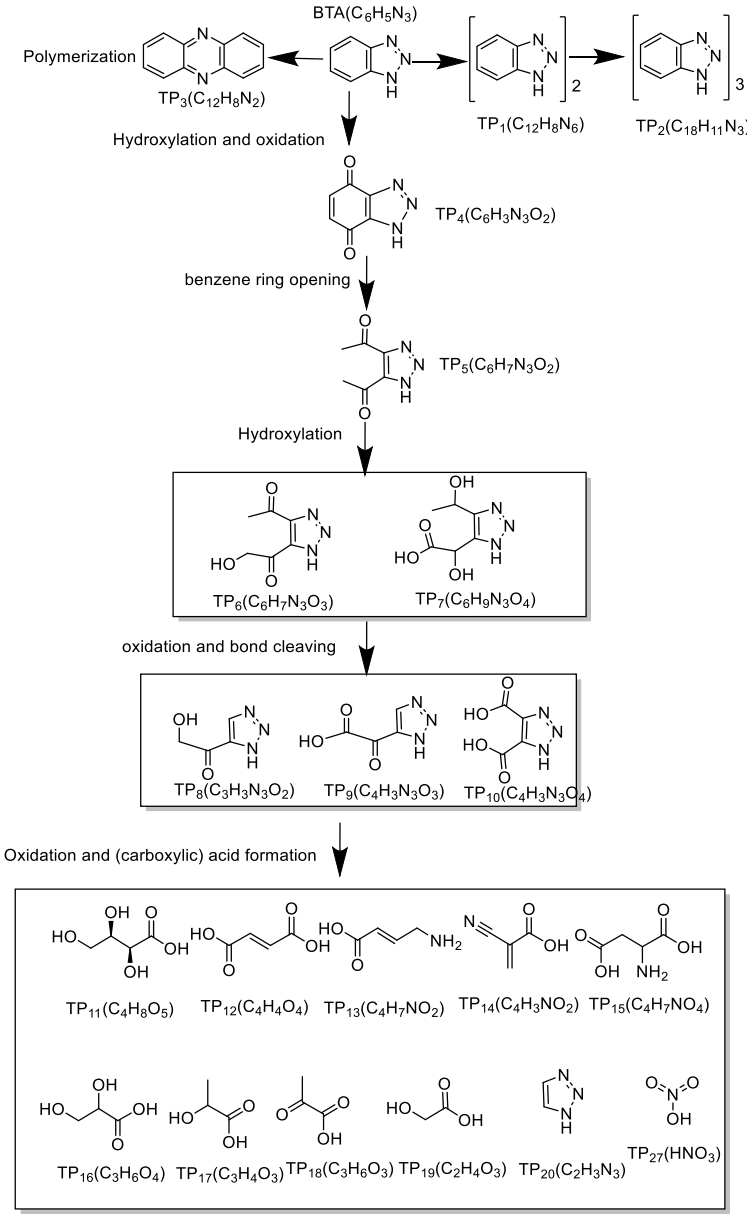

Fig. 5-4a. *Proposed BTA degradation pathways during heat-activated PS/PMS oxidation in absence presence of Cl^-, Experimental conditions: T=70°C, $[BTA]_0$=0.42 mM, $[PDS]_0$ or $[PMS]_0$ =15 mM, $[Cl^-]$= 0 or 1000 mg/L, V=100 mL, sodium hydroxide was added dropwise to maintain the pH around 6.9-7.4*

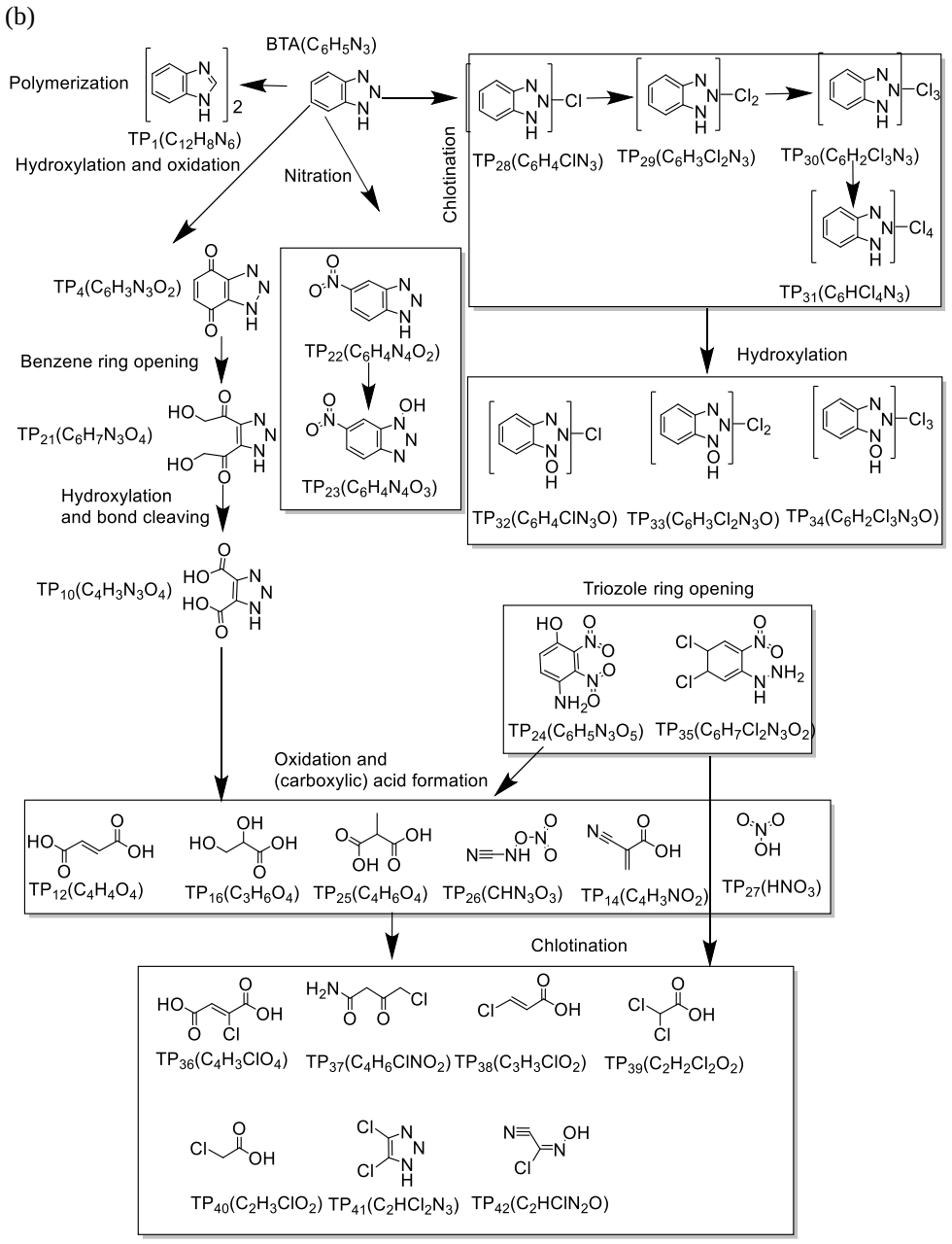

Fig. 5-5b. *Proposed BTA degradation pathways during heat-activated PS/PMS oxidation in presence of Cl^-, Experimental conditions: T=70°C, $[BTA]_0$=0.42 mM, $[PDS]_0$ or $[PMS]_0$ =15 mM, $[Cl^-]$= 0 or 1000 mg/L, V=100 mL, sodium hydroxide was added dropwise to maintain the pH around 6.9-7.4*

Table 5-3. *BTA mineralization in presence and absence of Cl^- after 180 min reaction; Experimental conditions: T=70°C, $[BTA]_0$=0.42 mM, $[PDS]_0$ = $[PMS]_0$ =15 mM, V=100 mL, all experiments were buffered by 15 mM phosphate, and sodium hydroxide was added dropwise to maintain the pH around 6.9-7.4*

	Cl^- (mg/L)	Mineralization (%)
PDS	0	90
	1000	76
PMS	0	14
	1000	43

5.3.5 AOX formation

LC-MS/MS analysis shows that chlorinated transformation products (TPs) are formed and accumulated during BTA oxidation in presence of Cl^-. The AOX concentration was measured to assess the total chlorinated TPs after the treatment (Table 5-4). The AOX concentration of both PDS and PMS experiments increased gradually with the increase of Cl^- concentration. Cl^- concentration from 100 to 10000 mg/L increased the AOX concentration from 2.5 to 9.1 mg/L in PDS and from 6.5 to 19.5 mg/L in the PMS system. Meanwhile, at the same concentration of Cl^-, the PMS system formed more AOX compared with PDS. Applying 100 and 10000 mg/L Cl^- in the PMS system, the AOX level was almost 2 to 3 times that in the PDS system. More free chlorine was formed due to PMS and Cl^- reaction, and free chlorine could chlorine the BTA directly to produce AOX. The AOX level was proportional to the Cl^- level in the Acid Orange 7 degradation in UV/TiO_2 [332]. AOX is always harmful to humans and the ecosystem, and the increase of AOX means the addition of toxicity. The industrial wastewater treatment effluent's AOX should be lower than 0.5 mg/L [333]. The AOX level of our experiments was much higher than 0.5 mg/L crying out for minimization. Applying PDS to treat chloride-containing matrix, chlorine radicals dominantly attack the aromatic ring or double bond, leading to AOX formation. While in the case of PMS-based processes, both chlorine radical and free chlorine predominate, inducing aromatic ring or double bond cleavage and direct chlorination, respectively.

Fang et al. [334] evaluated the effect of chloride on degradation kinetic using AOPs, focusing on AOX evolution. The studied Co/PMS process was more reactive under acidic conditions leading to high levels of AOX. They stated that high chloride levels resulted in AOX accumulation within the Co/PMS process [334]. Thus, it was

found that initial pH highly affected AOX formation during PMS-based AOPs. It was concluded that PMS-based advanced oxidation processes are not recommended to treat highly saline wastewater, regardless of their efficiency in high rate degradation of target organic pollutants [334].

Table 5-4. *AOX, free chlorine chlorate formation, and toxicity in terms of % luminescent inhabitation during BTA degradation at various Cl^- concentrations after 3h: Experimental conditions: T=70℃, $[BTA]_0$=0.42 mM, $[PDS]_0$ or $[PMS]_0$ =15 mM, V=100 mL, sodium hydroxide was added dropwise to maintain the pH around 6.9-7.4*

	Cl^- (mg/L)	AOX (mg/L as Cl_2)	Free chlorine (mg/L Cl_2)	ClO_3^- (mg/L)	Increase of inhibition (%)
PDS	100	2.5	1.4	ND	9
	1000	7.5	2.5	ND	14
	1000 (25^{O}C)	-	-	ND	-
	10000	9.1	2.4	ND	36
PMS	100	6.5	4.6	9.6	17
	1000	9.4	65	14.0	21
	1000 (25^{O}C)	-	98	16.7	-
	10000	19.5	223	32.3	42

5.3.6 Free chlorine and chlorates formation

In the present study, the formation of free chlorine and ClO_3^- after 180 min reaction in the PDS and PMS process in presence of Cl^- was investigated and shown in Table 5-4. Only a small concentration of free chlorine and no ClO_3^- was observed in the PDS process at any concentration of Cl^-. PMS produced a certain amount of free chlorine and ClO_3^- at any concentration of Cl^-. Additionally, with the increase of Cl^- concentration, the amount of free chlorine and ClO_3^- increased. The formation of ClO_3^- was raised by a factor of 3.5 when the concentration of Cl^- was 100 mg/L and 10000 mg/L. Free chlorine is the precursor for ClO_3^- formation. In the PDS system, $SO_4^{\bullet-}$ rather than PDS, reacts with Cl^- generating free chlorine, while in the PMS-based process, apart from the radical pathway, PMS directly reacts with chloride leading to the generation of free chlorine. Thus 98 mg/L free chlorine and 17 mg/L ClO_3^- was formed in the 1000 mg/L Cl^-/ PMS process at 25 ^{O}C (Table. 5-4). At 25^{O}C, radical formation is limited, and ClOx formation is mainly mediated by

direct PMS and Cl^- reaction. Hou et al. [299] comprehensively investigated chlorate formation in the co-exposure of SO_4^{2-}, Cl^- and organics in PDS and PMS-based processes. They also reported a higher generation of ClO_3^- in the PMS-based process than the PDS process. It was mentioned that the application of sulfate radical-based AOPs needs more attention in acidic pH.

5.3.7 Toxicity of degradation products

Luminescent bacteria were used to analyze the toxicity in both PDS and PMS systems. The raising of luminescence inhibition represents the increase of toxicity in samples. Table 5-4. summarizes the toxicity of each sample. Bacteria are sensitive to environmental changes, so the micro-toxicity experiments are not quantitative. After the reaction in 100 mg/L Cl^-, the luminescence inhibition was increased by 9% and 17% in PDS and PMS experiments, respectively. The luminescence inhibition was increased by 14% and 21%, at 1000 mg/L Cl^-, and to 35.67% (PDS) and 42.00% (PMS), at 10000 mg/L Cl^-. Overall, the higher the Cl^- concentration, the higher value of inhibition was obtained. These results also reflect two effects: i) the PMS system produced more AOX than the PDS system at any Cl^- concentration, and ii) the accumulation of AOX increased the toxicity [335].

5.4 CONCLUSIONS

This study shows that heat-activated PDS/PMS is capable of degrading BTA. PDS outcompeted the PMS process in the absence of Cl^-; however, PMS outcompeted the PDS process in presence of Cl^-. Both $HO^\bullet$ and $SO_4^{\bullet-}$ radicals contributed to BTA degradation in PDS and PMS systems. The BTA degradation in PDS was barely affected by pH. In contrast, pH 7 was the best condition for PMS. Although a higher degradation rate at pH 11 was initially seen in PMS, after 20 min, less BTA degradation was observed since the PMS was easy to decompose at basic conditions. In the PDS experiment, low concentrations (100 mg/L) of Cl^- slightly reduced the BTA degradation rate, but higher concentrations (1000 mg/L or 10000 mg/L) inhibited the reaction significantly because of radical scavenging. In PMS, increasing Cl^- concentration significantly increased the reaction rate, at optimum at a Cl^- concentration of 1000 mg/L due to active chlorine formation. At any concentration of Cl^-, both PDS and PMS produced a significant amount of AOX.

PMS produced more AOX than PDS. Transformation products (TPs) analysis showed that degradation pathways were significantly altered in presence of Cl^-. Polymerization, hydroxylation, benzene ring-opening, and carboxylic acid formation were the common degradation steps with and without Cl^-. However, the Triazole ring was broken quickly in presence of Cl^-, which was more stable in the absence of it. In addition, chlorination reaction dominated, producing several chlorinated TPs, including chlorinated BTA and chlorinated carboxylic acids. The micro-toxicity test indicated that the toxicity increased in the treated samples in presence of Cl^- due to chlorinated TPs. These by-products were more toxic than the parent compound in both PDS and PMS. No chlorate was formed in PDS at any Cl^- concentration but, ClO_3^- was found in PMS. This finding may help better understand the influence of Cl^- in the BTA degradation rate and pathway in PDS and PMS base oxidation. To avoid AOX formation, as little as possible Cl^- is recommended.

Chapter 6.

Advanced oxidation processes for removal of organics from cooling tower blowdown: Efficiencies and evaluation of chlorinated species.

This chapter has been published as:
Saha, Pradip, Yicheng Wang, Mahsa Moradi, Robert Brüninghoff, Gholamreza Moussavi, Bastian Mei, Guido Mul, Huub H.M. Rijnaarts, and Harry Bruning. "Advanced oxidation processes for removal of organics from cooling tower blowdown: Efficiencies and evaluation of chlorinated species." Separation and Purification Technology 278 (2022): 119537.

Abstract

One of the major challenges in reusing cooling tower blowdown water (CTBD) utilizing membrane processes is its remaining organic compounds, e.g., humic substances leading to biofouling. Besides, the possible abundance of chloride in CTBD imposes the concern of the formation of chlorinated by-products. To choose a pre-treatment process for the studied CTBD composition, various advanced oxidation processes (AOPs), including electrooxidation (EO), photocatalytic degradation (PCD), heat-activated persulfate (peroxydisulfate) oxidation (PS), UVC/vacuum UV (UVC/VUV), and UVC processes, were evaluated and compared based on two main targets: i) highest removal and mineralization of the organics, especially humic substances; and ii) lowest formation of chlorinated by-products including adsorbable organic halides (AOX) and oxychlorides. All the processes were conducted in the natural conditions of the real CTBD, while solution pH was monitored. Based on results of chemical oxygen demand, total organic carbon, dissolved organic carbon, UV_{254} absorbance, liquid-chromatography–organic carbon detection (LC-OCD), and fluorescence excitation-emission matrices (FEEM), it is concluded that PS leads to complete removal of organic compounds along with the lowest formation of low molecular weight organic acids and organic neutrals. FEEM and LC-OCD data also indicated that EO, PCD, PS, and UVC/VUV processes brought about substantial removal of organic compounds and broke down the humic substances into low molecular weight building blocks and organics. Besides, EO exhibited the highest AOX and oxychlorides formation, while these were limited when using the other AOPs. To summarize, PS, PCD, and UVC/VUV were efficient processes for the degradation and mineralization of organics without generating significant amounts of chlorinated by-products.

Keywords:

Dissolved organic carbon; Humic substances; Saline water; Chlorinated by-products; Advanced oxidation processes.

6.1 INTRODUCTION

Water reuse, especially in industrial applications, is highlighted in the sustainable development goals as one of the promising strategies to avoid freshwater scarcity [336]. In many industries, water plays a vital role in energy transportation through a cooling tower [32]. The water is usually supplied from freshwater resources, and several chemicals, e.g., acids, antiscalants and corrosion, and microbial inhibitors, are added as conditioning chemicals. The water becomes concentrated due to evaporation due to the conversion of heat to latent heat. It is discharged as a cooling tower blowdown water (CTBD) to maintain the overall water quality. Thus, the cooling tower blowdown (CTBD) is expected to have high salinity and contains humic substances (HS) and other organic compounds (OCs) in variable concentrations [32]. Löwenberg et al. [11] reported that CTBD from *Dow Benelux B.V.* (the Netherlands) contained 70 to 75% of OCs as HS. There are various treatment approaches for CTBD, and recently, membrane technologies have been studied and applied for the desalination of CTBD streams. However, membrane fouling is still the most concerning and inevitable challenge for reliable membrane performance. Thus, CTBD requires effective pre-treatment before membrane desalination [337]. HS is associated with bio-fouling [40]. G. Amy [40] summarized that different fractions of dissolved organic matter (DOM) exhibited organic fouling to both low and high-pressure membranes. Low-pressure processes such as microfiltration [338] or ultrafiltration are commonly used as pre-treatment technologies before the application of high-pressure processes, like Nano-filtration or reverse osmosis. However, the microfiltration and ultrafiltration show limited removal efficiency for the dissolved organic fraction, especially the HS, which governs foulant for high-pressure membrane [339]. The application of advanced oxidation processes (AOPs) as a pre-treatment step of membrane processes is a promising approach [340, 341]. In AOPs, highly reactive oxidative species (ROS), e.g., hydroxyl radicals ($HO^{\bullet}$)and sulfate radicals ($SO_4^{\bullet-}$), are generated. These ROS attack OCs, including HS from source water, organic additives, microorganisms, etc. [341]. Within the last decade, ozone, H_2O_2, UV, Cl_2, Persulfate [342], and electrochemical (EO)-based AOPs were studied for mitigating membrane fouling. These studies showed a significant reduction of fouling by HS [340, 343-346]. However, the generation of chlorinated organics has been reported as intermediates

or by-products of AOPs due to the simultaneous presence of organics, ROS, and reactive chlorine species, e.g., $Cl^{\bullet}$, $Cl_2^{\bullet-}$, Cl_2, or HOCl [178, 347, 348]. Furthermore, unfavorable toxic oxychlorides such as ClO^-, ClO_3^- and ClO_4^- have been reported in AOPs due to Cl^- reaction with ROS and reactive chlorine species [299]. In this way, various AOPs exhibit different performances towards producing the above-mentioned chlorinated by-products [349]. For example, photocatalytic degradation (PCD) has been shown to generate significantly fewer chlorinated by-products as compared to electrochemical oxidation (EO) [108]. The ultraviolet light C and vacuum-ultraviolet light (UVC/VUV) study by Moradi et al. [350] for sulfamethoxazole showed that Cl^- reacts with $HO^{\bullet}$ to form $ClOH^{\bullet-}$, which is a transient intermediate and dissociates back to $HO^{\bullet}$. Likewise, oxidation of Cl^- to $ClO_2^{\bullet-}$ by $HO^{\bullet}$ is less probable at a pH of 7 while it is viable at acidic conditions. Other studies also showed that UVC/VUV and UVC processes could reduce AOX formation during the oxidation of HS [351]. Hou et al. [299] studied the chlorate formation during the persulfate-based AOPs in the presence of DOC. The study showed that chlorate formation was in the forms of $HOCl/OCl^-$ and $SO_4^{\bullet-}$ mediated compounds, which were significantly scavenged by the DOC, eventually inhibiting chlorate formation [299].

Hence, this study focused on organic compounds (OCs) removal and chlorinated by-product formation during cooling tower blowdown (CTBD) treatment with different types of AOPs, namely: electrooxidation (EO), photocatalytic degradation (PCD), heat-activated persulfate process (PS), UVC, and UVC/VUV (UVC/VUV) process. Due to the complexity of the water matrix, the performance of the various processes was evaluated by following the chemical oxygen demand (COD), total organic carbon (TOC), dissolved organic carbon (DOC), UV_{254} absorbance, OCs molecular weight distribution by liquid-chromatography–organic carbon detection (LC-OCD) and fluorescence excitation-emission matrices (FEEM) analyses. Organic and inorganic chlorinated by-product formation was monitored by considering adsorbable organic halides (AOX) and oxychloride species (ClO^-, ClO_3^-, and ClO_4^-). The influence of pH on COD, TOC removal, and by-product formation was also studied.

6.2 MATERIALS AND METHODS

6.2.1 Chemicals

Sodium peroxydisulfate ($Na_2S_2O_8$, ≥99%), sulfuric acid (H_2SO_4, 95%), sodium hydroxide (NaOH, ≥99%), N,N-diethyl-p-phenylenediamine (DPD, 99%), sodium chloride (NaCl, ≥99%), sodium chlorate ($NaClO_3$, 99%), perchlorate standard for ion chromatography (ClO_4^-, 996±6mg/L), ethylenediaminetetraacetic acid disodium salt (EDTA, ≥99%), monosodium phosphate (NaH_2PO_4, ≥99%), disodium hydrogen phosphate (Na_2HPO_4, ≥99%), hydrogen peroxide (H_2O_2, 30%), potassium iodide (KI, ≥99%), and uridine ($C_9H_{12}N_2O_6$, ≥99%) were obtained from Merck Chemicals B.V. (the Netherlands).

6.2.2 Experimental procedure and Experimental setup

CTBD used in all the experiments was collected from *Dow* premises in Terneuzen (the Netherlands) and stored at 4°C to limit microbial growth. The characteristics of the CTBD are given in Table 6-1 and Table S6-1. CTBD was filtered through a 110 mm membrane (Whatman, GE Healthcare) before each experiment. pH adjustment was achieved by the addition of concentrated H_2SO_4 (pH 3) or NaOH (pH 10). All experiments were conducted in duplicate, and blank control tests were carried out. All the experiments were conducted for five hours, and the samples were collected at 0 h, 1 h, 2 h, 3.5 h, and 5 h. Free chlorine was measured immediately after the experiment. Samples were kept in a refrigerator at -20°C for further analysis.

Table 6-1. *Important parameters of cooling tower blowdown. Detail characteristics are tabulated in Table S6-1*

Parameter	Unit	Avg. (±SD)
Cl^-	mg/L	467 (3)
TOC	mg/L	47(1)
COD	mg/L	105 (4)

6.2.2.1 EO experimental setup:

The EO experimental setup is described in [198]. In short, experiments were carried out in an undivided flow cell with a 775 mL/min flow and a reactor volume of 33.6 mL. A boron-doped diamond (BDD) electrode as anode and platinum-coated titanium electrode as a cathode with an effective surface area of 22.4 cm^2 were used (Magneto Special Anodes, the Netherlands). A current density of 8.5 mA/cm^2 was applied for all the EO's experiments using an IviumStat.h potentiostat controlled by Iviumstat software (Ivium Technologies B.V., the Netherlands).

6.2.2.2 PCD experimental setup:

PCD experiments were carried out in a glass beaker. 80 mL CTBD was pre-saturated with air for 20 min before the degradation experiments, and 40 mg (±1) TiO_2 photocatalyst (Hombikat UV100) was added. Pre-treatment of TiO_2 photocatalyst, via annealing at 600°C for 4 h, was performed to achieve improved photocatalytic performance (optimum between adsorbed surface OH groups and available holes at the surface), as reported in earlier work by our group [108, 352]. The catalysts themselves are stable, and additional treatments are generally not required. The beaker was covered with a quartz lid and stirred at 350 rpm in dark conditions for 30 min. UV-irradiation at 375 nm was achieved using a closed box reactor equipped with eight 18W TL-D UV lamps (Philips). The intensity of the lamp at 375 nm was ≈ 0.32 mW/cm^2 [108]. Samples were centrifuged for 10 min at 8000 rpm to separate the TiO_2 before analysis.

6.2.2.3 PS experimental setup:

The PS experiments were conducted in glass bottles equipped with a pH meter. The temperature was kept at 70°C, and the bottles were thoroughly mixed using a shaking water bath (SW23, JULABO GmbH, Germany), oscillating at 150 rpm. CTBD was preheated in the water bath for 30 min, and a freshly prepared 10 mM PS (peroxydisulfate) solution was added to the bottles. During PS activation, H^+ ions are generated, leading to a pH drop [278]. Therefore, a concentrated NaOH solution was added to maintain constant pH during the experiment. Initially, PS was conducted for 5 hours. Since the TOC removal changed little after 3 hours, all data up to 3 hours' reaction was analyzed for PS and compared with other AOPs. Samples were taken and immediately put in an ice bath (< 4°C) to quench the reaction.

6.2.2.4 UVC and UVC/VUV experimental setup:

The UVC process and UVC/VUV experiments were conducted in stainless steel 0.3 L annular reactor (400 mm length × 25 inner and 40 mm outer diameters) shown in Fig. 6-S1. A low-pressure mercury UV_{254} lamp for UVC or a $UV_{185/254}$ lamp for UVC/VUV was fixed at the center of the reactor encompassed in a quartz sleeve with 25 mm outer diameter (25 W, Van Remmen UV Technology, the Netherlands). According to H_2O_2 actinometry [353] and uridine actinometry [354], it was estimated that the $UV_{185/254}$ - lamp emitted 8.2 mW/cm^2 intensity at 185 nm and UV_{254} lamp emitted 20.9 mW/cm^2 intensity at 254 nm. Further details of the actinometric methods are given in the supporting information (SI) (text S6-2, Fig. S6-2, and Fig. S6-3). CTBD was recirculated using a peristaltic pump through the reactor at 2 L/min from a circulation bottle. The temperature was constant to avoid the influence of elevated temperature on the reaction rate. The CTBD temperature was kept at 25 (± 2)^{o}C with cold water recirculation through a cooling coil submersed in the circulation bottle (Fig. S6-1). Cold water was coming from a water bath (F25-HE, Julabo GmbH, Germany). The lamp and nitrogen stream was turned on 30 min before the experiment to reach the photons' stable output and eliminate the oxygen inside the lamp and quartz sleeve's interspace to prevent ozone formation [124].

6.2.3 Analytical methods

TOC of the samples was measured by a TOC analyzer (TOC-L CPH/CPN, Shimadzu, Benelux) using the Non-Purgeable Organic Carbon method (text S6-1.a) [355]. A Hach DR 3900 spectrophotometer (Hach Lange GmbH, Germany) with Hach test kits LCK1414/LCK314 and LCK 390 was used to analyze the COD and AOX, respectively. Dionex ICS-2100 (Thermo, USA) ion chromatography and Perkin Elmer ICP-OES AVIO 500 plasma atomic emission spectroscopy were used for quantification of anions and cations, respectively (text S6-1.b). PS, H_2O_2, free chlorine, and uridine determination methods are described in the SI (text S6-1.c) and text S6-1.d). UV_{254} was measured with an M200 Infinite Pro Microplate Reader (Tecan, Switzerland). The Fluorescence excitation-emission matrix (FEEM) was measured using a Perkin Elmer LS50B fluorimeter (text S6-1.e). The molecular size distribution of hydrophilic fraction and quantification of hydrophobic fraction of the CTBD's OCs were determined with size-exclusion liquid chromatography (LC-

OCD) (Model 8, DOC-Labor, Germany). According to the molecular weight, hydrophilic organics are fractionated into biopolymers (>20000 g/mol), humic substances (~1000 g/mol), low molecular weight (LMW) acid, and LMW neutral (<350 g/mol) (text S6-1.f) [26].

6.2.4 Energy consumption calculation

Energy consumption per order can be expressed as $E_{E/O}$ (kWh/m^3), which means the energy required to remove 90% of the TOC. The following equation can be used to calculate the $E_{E/O}$ (Eq. 6.1) [356]

$$E_{EO} = \frac{P \cdot t}{V \cdot \log\left(\frac{c_i}{c_f}\right)} \quad (6.1)$$

P is the t energy input in KW, t is the time in h, V is the liquid volume in L, Ci is the initial TOC, and C_f is the final TOC concentration in mg/L.

Detailed of power consumption calculation is given in SI text S6-3.

6.3 RESULTS AND DISCUSSION

6.3.1 Evaluation of AOPs for COD and TOC removals

The selected AOPs were applied to remove COD and TOC from the CTBD at pH = 7.4 (± 0.3). As shown in Fig. 6-1, the highest COD removal was obtained by EO, and complete COD removal was observed in 3.5 h. Due to the use of BDD as anode and presence of chloride in the CTBD, both direct/anodic and indirect/mediated electrooxidation have supposedly occurred with synergistic action of ROS and reactive chlorine species for oxidation and mineralization of OCs [108, 198, 357]. While the highest COD removal was obtained for EO, the EO's efficiency for TOC removal was similar to that of PCD and UVC/VUV processes. Around 50%-55% TOC removal was obtained. Our previous study on CTBD oxidation with BDD showed that due to partial oxidation and chlorination of the OCs, the oxidation state of the organic carbon was increased, and oxygen demand was reduced [198]. A detailed description of this oxidation state phenomenon was reported in [198]. Thus, the TOC removal was lower than COD removal, as shown in Fig. 6-1.

The highest exponential TOC removal (around 95%) was obtained using PS-AOP. COD removal was not determined for PS due to the interference of PS in COD measurement. In case of PS, O–O bond in PS was homolyzed by heat at 70ºC, leading to ROS generation, especially $SO_4^{\bullet -}$ and $HO^{\bullet}$ [358]. Those two radicals have supposedly attacked the OCs of CTBD, leading to a high degree of mineralization. A sufficient amount of persulfate guaranteed abundant formation of ROS to react with organic carbon in the reactor. When lowering the persulfate dose from 10 mM to 5 mM, the TOC removal after 3 hours reduced from 83% to 57% (Table S6-2), agreeing with the results obtained in other similar studies [327, 359].

During the PCD, COD and TOC removal were up to 55% and 50%, respectively, linearly correlated with time. In PCD, the generation of photo-induced holes (h^+) and electrons (e^-) leads to the occurrence of redox reactions on the heterogeneous solid surface of photocatalyst [360]. Also, various oxidative species, especially the ROS, mainly including $^{\bullet}O_2^-$, H_2O_2, $^1O_2$, and $HO^{\bullet}$ are generated within the solution attacking the OCs [108, 360].

UVC/VUV showed around 58% removal for COD and 54% for TOC, like PCD. In UVC/VUV, organics are attacked/influenced through the following ways: i) homolysis of water molecules when exposed to 185 nm UV and generation of $H^{\bullet}$ and $HO^{\bullet}$; ii) water ionization and generation of free electrons, which are superior for reductive degradation reactions; iii) generation of ozone and H_2O_2; and iv) direct photolysis [350]. Fig. 6-1 shows that using the UVC process, merely 25% COD and 20% TOC were removed through direct photolysis after 5 hours. An experiment in identical conditions with Milli-Q showed that about 9.0 µM H_2O_2 was accumulated in UVC/VUV. Still, no H_2O_2 was detected for the UVC process, indicating $HO^{\bullet}$ generation during UVC/VUV (Fig. S6-2) [126]. With a high oxidation potential of 2.80 V/SHE, $HO^{\bullet}$ enhanced the removal efficiency of OCs in UVC/VUV [350]. On the contrary, UV photolysis is efficient only in compounds with a high molar absorption coefficient at the used light source [361]. Compared to the other AOPs, in the UVC process, the OCs removal mainly occurred within the first 1 hour, while after that, fluctuations around the average value were observed. A possible explanation could be the limited photolysis ability of UVC light towards the OCs, which reached its maximum value within 1 hour. In similar cases of applying UVC, removal capacity has also reached its maximum within one hour [362-365].

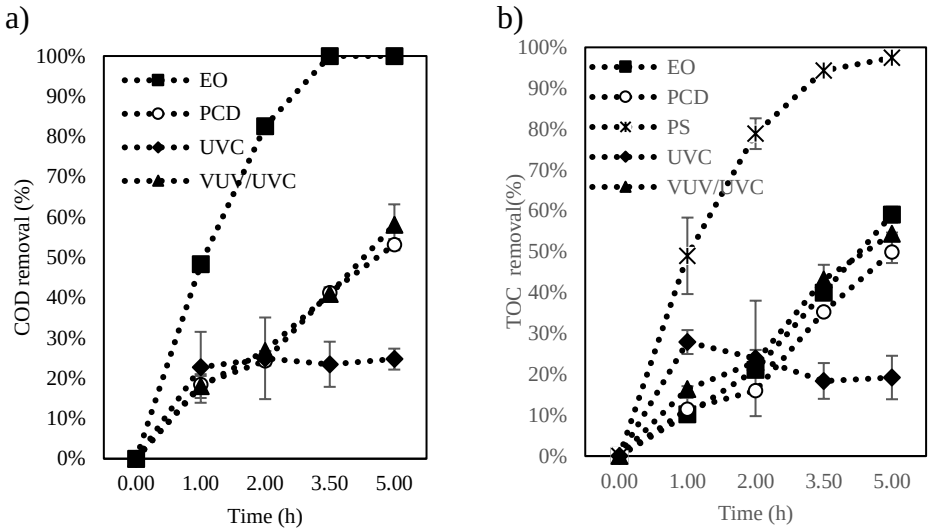

Fig. 6-1. *Removal of (a) COD and (b) TOC from CTBD during different AOPs:(■) EO with BDD anode at 8.5 mA/cm^2, (○) PCD with TiO_2 catalyst at 375 nm UV light, (×) PS with 10 mM PS, 70°C, (♦) UVC/VUV with 185/254 nm UV light, and (▲) UVC with 254 nm UV light, initial pH = 7.4.*

6.3.2 Degradation of the humic substances

6.3.2.1 Influence of AOPs on UV_{254} removal

UV absorbance at 254 nm (UV_{254}) was determined before and after the treatment, and the results are depicted in Fig. 6-2. As seen, UVC/VUV brought about the highest UV_{254} removal (85%), although it did not result in the maximum TOC removal. Similarly, the UVC process alone removed 19% of TOC while a 67% UV_{254} reduction was achieved. Unlike TOC, UV_{254} decrease indicates a decline of HS's aromatic and conjugated double bond [366]. These reactions are reported to coincide with a partial breakdown of HS's complex and large molecules to smaller molecules with lower molar absorption coefficients [367]. Research from García et al. [368] also concluded that decreasing specific UV absorption (reduction of aromaticity) was not strictly correlated with HS's complete depletion. In EO, PCD, and PS, the UV_{254} removal efficiencies were ca. 75%. In these processes, the generation of ROS led to the destruction of HS's aromatic content [369].

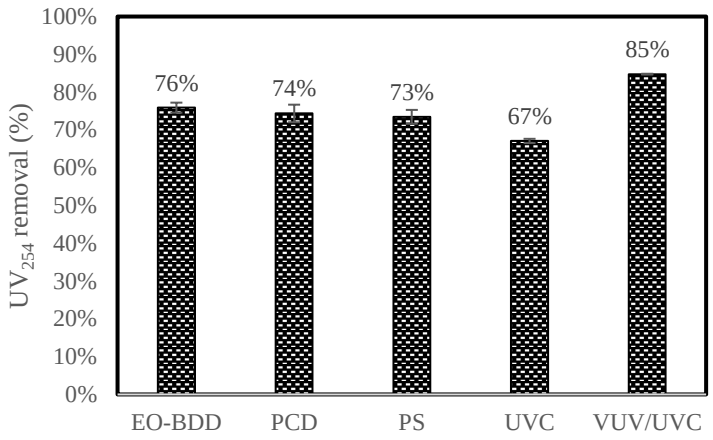

Fig. 6-2. *UV_{254} absorbance removal of the CTBD in various AOPs: (1) EO with BDD anode at 8.5 mA/cm^2 (5 h), (2) PCD with TiO_2 catalyst at 375 nm UV light (5 h), (3) PS with 10 mM PS, 70^{o}C (3 h), (4) UVC/VUV with 185/254 nm UV light (5 h), and (5) UVC with 254 nm UV light (5 h), initial pH = 7.4.*

6.3.2.2 Change of molecular weight distribution

To follow the DOC molecular weight distribution, LC-OCD analysis was carried out for all AOPs, and corresponding results are shown in Fig. 6-3 and Fig. S6-4. The highest DOC removal was observed in PS, by which 35.7 mg/L DOC was removed (80% DOC removal) in 3 h. Indeed, HS was substantially removed, which is desired for the membrane desalination feed water preparation. By EO, a DOC removal of 23.6 mg/L was obtained. Using EO, 19.8 mg/L HS and 1.0 mg/L hydrophobic organic carbon were removed, while 0.5 mg/L LMW acids and 1.4 mg/L LMW organic neutrals were generated as reflected in LC-OCD results. In PCD, 24.0 mg/L DOC involving 25.4 mg/L HS was eliminated, while 3.2 mg/L LMW acids were formed. Applying UVC/VUV, 19.35 mg/L DOC was removed. Although this process exhibited high removal of HS (23.9 mg/L), generations of LMW acids (4.0 mg/L) and organic neutrals (2.6 mg/L) lowered the overall DOC removal. Similarly, in the UVC process, DOC removal was only 10.1 mg/L, whereas HS removal was 13.9 mg/L. Thus, LMW acids and neutrals were formed, lowering the overall DOC removal. Also, the LC-OCD chromatogram (Fig. S6-4) indicated a shoulder peak corresponding to HS's building blocks becoming prominent after the treatment by PCD, EO, UVC/VUC, and UVC process. This building block formation confirms

the structural change of the HS and higher UV_{254} removal. Accordingly, LC-OCD analysis showed that even though hydrophobic organic carbon as HS decreased, the concentration of building blocks, LMW acids, and neutrals increased for EO, PCD, UVC/VUV, and UVC processes. Such an increase will potentially lead to enhanced biofouling in membrane processes [370]. The PS exhibited efficient DOC removal with no notable LMW acids and neutrals formation. It is hypothesized that in PS, generation of ROS was sufficient due to the excessive amounts of PS, showing up as the remaining PS after the process (Table S6-2), resulting in efficient degradation and mineralization of organics.

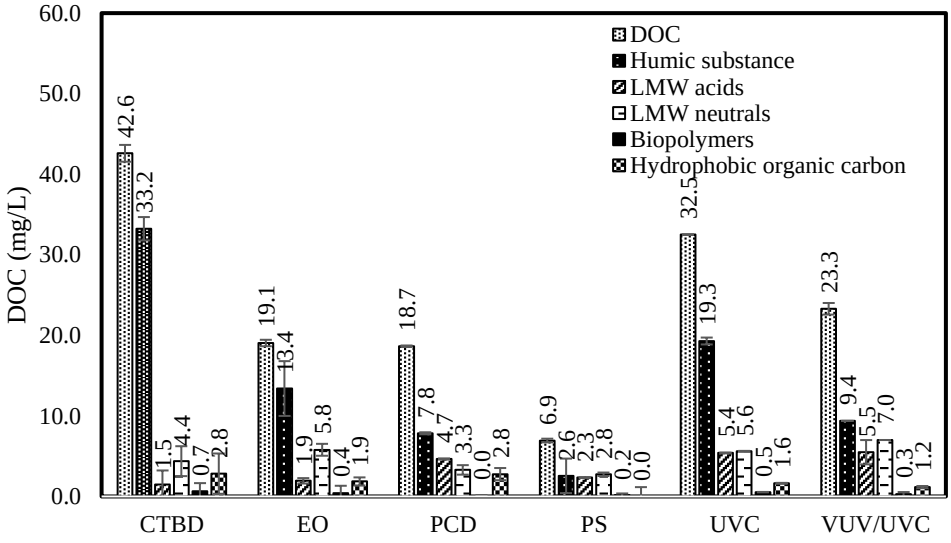

Fig. 6-3. *Speciation of dissolved organic carbon (DOC) of untreated CTBD and after treating CTBD when applying (1) EO with BDD anode at 8.5 mA/cm^2 (5 h), (2) PCD with TiO_2 catalyst at 375 nm UV light (5 h),(3) PS (10 mM), 70^{o}C (3 h), (4) UVC/VUV with 185/254 nm UV light (5 h), and (5) UVC with 254 nm UV light (5 h), initial pH = 7.4.*

6.3.2.3 DOC characterization using FEEM

FEEM, along with LC-OCD and $UV_{254,}$ provides valuable insights into the DOC spectral changes for the studied AOPs. Fluorescence measurements reveal that humic acid (HA)-like, fulvic acid-like, and protein-like HS compounds are present [371, 372].

a)

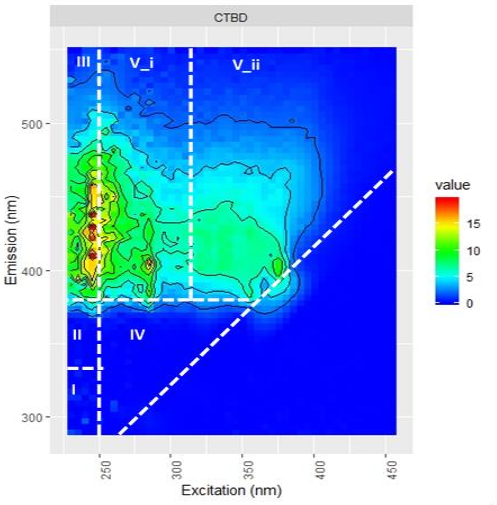

b)

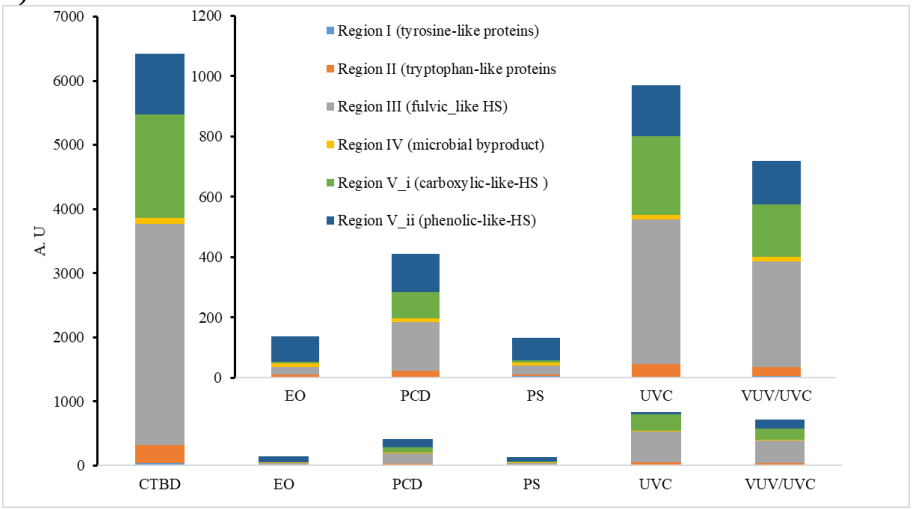

Fig. 6-4. *DOC FEEM profile (a), and (b) FRI intensity of CTBD before and after different AOPs treatments: (1) EO with BDD anode at 8.5 mA/cm^2 (5 h), (2) PCD with TiO_2 catalyst at 375 nm UV light (5 h), (3) PS with 10 mM PS, 70^{o}C (3 h), (4) UVC/VUV with 185/254 nm UV light (5 h), and (5) UVC with 254 nm UV light (5 h), initial pH = 7.4.*

These categories are attributed to DOC's origin, while the variability of these categories represents the degradation status and formation of new fluorophores [373]. The FEEM and fluorescence regional integration (FRI) of FEEM intensity for

CTBD before AOPs treatments are presented in Fig. 6-4a and Fig. 6-4b. As can be seen, CTBD is mainly comprised of HA and fulvic acid-like HS. Thus, the FEEM analysis was consistent with LC-OCD analysis, giving about 33 mg/L HS in initial water samples. The FRI analysis shows that CTBD contains 58% fulvic acid (region III), 27% carboxylic-like HA (region V-i), and 16% phenolic-like HA (region V-ii). All these HS are capable of causing internal membrane fouling [374]. These HS factions are hardly removed with coagulation/flocculation and powdered activated carbon treatment [11, 40].

As shown in Fig 6-4b and Table S6-5, PS exhibited 98% overall FRI intensity removal, which is a valuable output in feed preparation for membrane processes. In the EO, DOC removal was 57%, whereas the overall FRI intensity removal was 97%. This decrease in FRI can be attributed to partial oxidation of the DOC's carbon double bonds and chlorination. Several authors have reported that chlorination of DOC reduces the fluorescence intensity [375, 376]. Similarly, PCD, UVC/VUV, and UVC processes exhibited 93%, 89%, and 85% overall FRI intensity removal, whereas the DOC removals were 50%, 54%, and 19%, respectively (Table S6-5).

For all the processes, the overall region's FRI intensity removal was similar to individual region removal for the corresponding AOP (Table S6-5). Thus, FEEM and UV_{254} results mainly indicate that DOC organic molecular structure changes are reductions in the aromaticity and double-bond fractions. So, from the FEEM analyses, it can be concluded that PCD, EO, and VUV/UVC substantially degraded the HS structure to LMW substance, which may cause less internal fouling to the membranes. However, TOC/DOC removal was only around 50 to 55%.

6.3.3 pH influence on COD and TOC removals in different AOPs

As a parameter that controls oxidation mechanisms, the solution pH effect on the process efficiency was investigated, and the results are presented in Fig. 6-5. The initial and the final pH after treatment was tabulated in Table S6-3. Variations of the pH may influence the process through: i) chemical speciation of organic and inorganic constituents of the CTBD; ii) speciation of the generated ROS; iii) influencing catalyst's surface reactions in PCD regarding the point of zero charges (pH_{zpc}) and; iv) affecting current efficiency and diffusion rate of substances from the solution to the electrode [377, 378]. As can be observed, EO exhibited complete

COD removal and around 60% TOC removal independent of solution pH after 5 h reaction time. The pH influence was limited because the reaction was mass transfer limited [198]. Nevertheless, the other AOPs depended on solution pH, especially the UVC/VUV and UVC processes. The UVC/VUV brought about almost complete COD removal and 89% TOC at pH 3, 53, and 45%, respectively, at pH 7 and pH 10 in 5 h. The higher light absorbance of HS caused this high removal efficiency at acidic pH due to the structural change of molecules resulting from protonation [379]. This phenomenon was also confirmed by a 25% increase in COD and TOC removal in the UVC process performed at pH 3 compared to pH 7. In the UVC process, HS undergoes molecular destruction mainly due to photolysis, while the ROS generation is negligible [380]. The pH value affects HS's speciation and affinity towards photons' absorbance and thereby influences the degradation rate [381]. Using PS, TOC removal efficiencies of ca. 71%, 76%, and 83% were obtained after 3 h, at pH levels of 10, 3, and 7, respectively. The pH plays a complex role in heat-activated PS [382, 383]. In acidic pH, $SO_4^{\bullet-}$ is the predominant radical, while at pH 9, both $SO_4^{\bullet-}$ and $HO^{\bullet}$ are generated and coexist. When pH exceeds 12, $HO^{\bullet}$ becomes the predominant radical due to the reaction of $SO_4^{\bullet-}$ with hydroxyl ion [91, 382, 384]. The $SO_4^{\bullet-}$ and $HO^{\bullet}$ reaction mechanisms with OCs are different. For instance, $SO_4^{\bullet-}$ is mainly involved in electron transfer with OCs, while for $HO^{\bullet}$, the reaction mechanism dominantly includes an addition to C=C as well as H abstraction from N-H, C-H, or O-H [382, 383]. This difference in the ROS composition and reaction mechanisms is responsible for different TOC removals in the PS at various pH levels. In PCD, COD and TOC removals were increased from 34% to 50% and 55%, respectively, changing the CTBD pH from acidic to alkaline. The effective degradation in the alkaline environment can be attributed to less inhibition of the TiO_2 catalyst surface due to less effective interaction of the anion species with the negatively charged catalyst surface, and the point of zero charges of TiO_2 is at ~pH 6 [385-387].

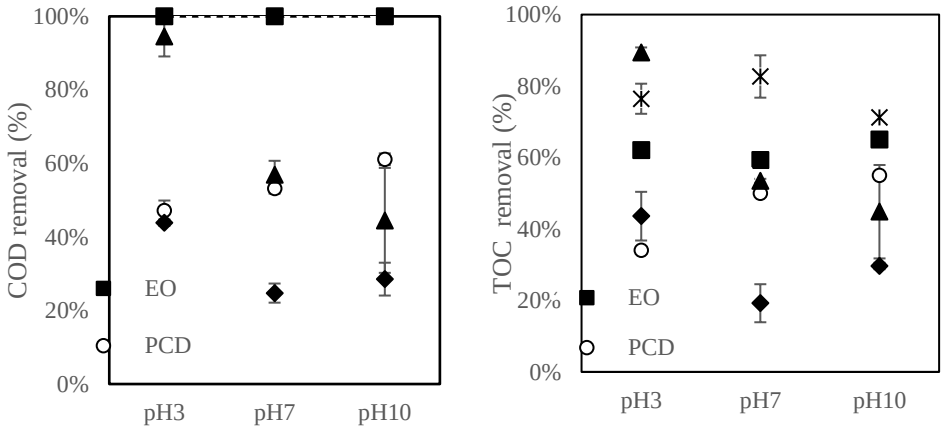

Fig. 6-5. *The influence of pH on (a) COD and (b) TOC removal from CTBD during different AOPs: (■)EO with BDD anode at 8.5 mA/cm2 (5 h), (○)PCD with TiO_2 catalyst at 375 nm UV light (5 h), (×)PS with 10 mM PS, 70°C (3 h), (♦)UVC/VUV with 185/254 nm UV light (5 h) (▲)UVC with 254 nm UV light (5 h)*

6.3.4 pH influence on AOX and oxychloride species formation in different AOPs

The influence of initial solution pH on chlorinated organic and inorganic by-products was evaluated. In UVC/VUV, PCD, and UVC processes, the formation of i) AOX and ii) oxychlorides was negligible (Table 6-2). Chlorine species (ClO^-/HClO) and chloride radical species are the main precursors of AOX formation.

Thus, when the generation of chlorine species is eliminated, the AOX generation is also suppressed [299]. Besides, HS and chloride are both radical sinks, while HS's reaction rate with the radical species is higher than that of the chloride, leading to a lower AOX formation. Also, as indicated in Table 6-2, zero or negligible amounts of chlorine species were detected after these processes. Thus, AOX formation was suppressed by the absence of one of its major precursors.

However, the EO exhibited significant AOX and chlorine oxyanions formation amongst the studied AOPs independent of pH. AOX formation in EO can be attributed to the simultaneous presence of HS and the high concentration of chlorine

species [388]. Generally, chlorine evolution is unavoidable at the higher cell potential, leading to reactive chlorine formation. These electro-generated chlorine species react with HS to produce AOX [389].

Table 6-2. *Effect of initial solution pH on AOX and inorganic chlorine species during different AOPs of CTBD: (1) EO with BDD anode at 8.5 mA/cm2 (5 h), (2) PCD with TiO_2 catalyst at 375 nm UV light (5 h), (3) PS with 10 mM PS, 70°C (3 h), (4) UVC/VUV with 185/254 nm UV light (5 h), and (5) UVC with 254 nm UV light (5 h)*

AOPs	pH	ΔCl^- (mg/L)	ΔAOX (mg Cl^-/L)	ΔClO^- (mg/L)	ΔClO_3^- (mg/L)	ΔClO_4^- (mg/L)
EO	3	-314 (16)	11.8	160	437(9)	133 (15)
	7	-294 (1)	9.2 (1.0)	210 (10)	459 (2)	149 (2)
	10	-259 (5)	9.5	160	489 (7)	128 (15)
PCD	3	-5 (1)	0.2 (0.1)	ND	ND	ND
	7	-2 (1)	0.2 (0.1)	ND	ND	ND
	10	1 (0.1)	0.1 (0.0)	ND	ND	ND
PS	3	-27 (2)	2.6 (0.1)	0.3 (0.03)	0.7 (0.2)	ND
	7	-16 (0.3)	-0.2 (0.2)	0.2 (0.02)	0.2 (0.2)	ND
	10	-13 (2.5)	-0.1 (0.1)	0.3 (0.05)	0.2 (0.3)	ND
UVC	3	-7	-0.5 (0.1)	ND	ND	ND
	7	-2	-0.2 (0.1)	ND	ND	ND
	10	-9	-0.6 (0.1)	ND	ND	ND
VUV/UVC	3	-2	-0.6 (0.2)	ND	ND	ND
	7	-5	-0.5 (0.1)	ND	ND	ND
	10	-6	-0.7 (0.1)	ND	ND	ND

Notes: ND stands for not detected (below detection limit).

However, the EO exhibited significant AOX and chlorine oxyanions formation amongst the studied AOPs independent of pH. AOX formation in EO can be attributed to the simultaneous presence of HS and the high concentration of chlorine species [388]. Generally, chlorine evolution is unavoidable at the higher cell potential, leading to reactive chlorine formation. These electro-generated chlorine species react with HS to produce AOX [389]. The generated AOX, such as polychlorinated organic compounds, are likely persistent to oxidation; thus, they are not detected by the COD analysis; however, they are measured by TOC/DOC analysis (Fig. 6-1, Fig. 6-3, and Fig. 6-5) [390]. Besides, notable amounts of oxychlorides were observed at all pH levels after 5 h EO treatment. The electro-

generated chlorine species was accumulated in bulk solution and further oxidized through chain reactions to produce ClO_3^- and ClO_4^-. Using EO, the highest concentrations of AOX were observed at acidic pH of 3, similar to the other studies [390, 391]. Another research stated that in alkaline conditions, ClO_3^- concentration increased [69], which was also seen in the study reported here. To sum up, considering complete COD removal at all pH levels but 60% TOC removal along with the high concentration of chlorine oxoanions and AOX in EO; the following subsequent processes mechanism can be assumed to occur in EO: i) direct and ROS mediated oxidation of organics on the high oxygen over-potential BDD anode resulted in degradation of organics; ii) chlorine species accumulated in the system showing up as chlorine oxoanions; iii) formation of persistent AOX as a consequence of chain reactions of OCs and chlorine oxoanions.

As shown in Table 6-2, in PS, 2.6 mg/L AOX was detected in acidic pH of 3, and a small amount of ClO^- and ClO_3^- were detached at all pH conditions. Yang and co-authors [392] investigated the overestimated adverse effect of halides in the performance of the heat/persulfate process for the degradation of wastewater contaminants. Similarly, they observed a few AOX formations and concluded that the heat-activated PS process did not lead to a significant accumulation of AOX in the presence of halides [392]. They stated that in the heat/PS process, $Cl_2^{\bullet-}$ was the primary active chlorinated species when the matrix contained chloride [392].

6.3.5 Implications for real application

When considering treatment to remove recalcitrant organics from CTBD or similar water, several issues are recommended to be considered from the application, namely: i) initial characteristics of the matrix and required preparation of the sample (e.g., pH adjustment, OCs removal, etc.); ii) factors associated with the setup and process (reactor design and optimization, energy supply, ease of operation, etc.); iii) intermediates and by-products; and iv) energy consumption. In Table 6-3, TOC removal efficiency, energy consumption in terms of $E_{E/0,}$ chlorinated intermediates in terms of AOX, and oxychlorides are indicated for each of the studied processes.

As shown in Table 6-3, in the natural conditions of the studied CTBD, the highest TOC removal and the detection of no (insignificant) AOX and oxychlorides were accomplished using PS. To elaborate further, neither pH adjustment nor

consideration for PS activation was required. PS has an excellent potential to treat CTBD since it can take advantage of the cooling tower's waste heat to activate the persulfate. At the same time, its post-treatment should be carefully designed to remove the extra chemicals added during PS.

Table 6-3. *Performance of the applied AOPs for the treatment of the studied CTBD. Conditions: (1) EO with BDD anode at 8.5 mA/cm^2 (5 h), (2) PCD with TiO_2 catalyst at 375 nm UV light (5 h), (3) PS with 10 mM PS, 70^{o}C, (4) UVC/VUV with 185/254 nm UV light (5 h), and (5) UVC with 254 nm UV light (5 h), initial pH = 7.4*

AOPs	TOC removal (%)	oxychlorides	AOX	$E_{E/O}$ (kWh/m^3)
EO	59	High	High	52.6
PCD	50	ND	ND	13.1 */**
PS	83 (3h) >95 (5h)	~0	ND	42(5h) ***
UVC	19	ND	ND	322 *
UVC/VUV	53	ND	ND	116 *

Notes: ND stands for not detected (below detection limit).
* If the light efficiency is 100% (all the electrical energy converted to corresponding photon energy)
** equivalent energy for TiO_2 production is not included
***equivalent energy for PS production is not included

UVC/VUV process also fulfilled high TOC removal (89%) merely in acidic pH of 3. This operation at acidic pH necessitates a final polishing step, especially for reuse. Besides, in applying light-induced systems, especially for the treatment of real wastewaters, photon transfer limitations should be overcome [143]. This issue is also controversial for process feasibility in UVC and PCD processes. Using PCD, 50% TOC removal was obtained in the natural pH of the CTBD, although its highest efficiency was marginally higher and was observed at alkaline pH. In this process, AOX and oxychlorides were not detected. However, separation of the catalyst is a notable issue in applying PCD on a full scale, although this can be overcome by developing immobilized heterogeneous catalysts [143, 393]. Among the studied processes, EO was the worst in the generation of oxychlorides and AOX, the reasons for which were discussed comprehensively in previous sections. In the presence of chlorine species and HS, EO is not assumed to be a suitable option, leading to the generation of oxoanions of chlorine and AOX in notable concentrations.

For energy consumption, values are calculated for each process as in Table 6-3. Here it should be noted that processes were not optimized for comparison and only considered to evaluate different AOPs for the treatment of a real CTBD under natural conditions concerning OCs removal and the generation of chlorinated intermediates. Overall, amongst the studied AOPs, PS appears to be a promising option for treating matrixes containing OCs and chlorinated species without generating AOX and oxychlorides. It requires 42 kWh/m^3 energy per order of TOC removal. The energy requirement for persulfate activation can be solved using the waste heat from the cooling tower. Obviously, persulfate needs to be supplied continuously, adding cost to the process. EO and PCD also show excellent potential from an energy perspective. They require 52.6 kWh/m^3 and 13.5 kWh/m^3 energy input, respectively. However, BDD anode for EO and TiO_2 catalyst for PCD process would increase the cost.

6.4 CONCLUSIONS

The removal of organic compounds (OCs) from CTBD was carried with electrooxidation (EO), photocatalytic degradation (PCD), heat-activated persulfate oxidation (PS), UVC/vacuum UV (UVC/VUV-AOP), and the UVC process. Several parameters were measured to assess and compare the treatment efficiency of different AOPs: removal of TOC and COD, the concentration of oxoanions of chlorine and AOX, UV_{254}, liquid-chromatography organic carbon detection (LC-OCD), and fluorescence excitation-emission matrices (FEEM).

The following conclusions can be drawn based on the experiments:

- EO, PCD, PS, and UVC/VUV, all removed organic compounds (OCs), while PS provided the highest removal under the experimental conditions chosen.
- UV_{254} and FEEM results showed that the fraction of humic substance (HS) of the OCs was converted to building blocks and LMW substances, leading to a strongly reduced membrane fouling potential.
- Acidic conditions strongly favor UVC/VUV treatment performance, explained by an increase of light absorbance, whereas basic conditions

favor PCD treatment performance. The pH hardly influences other treatments.

- AOX and oxychlorides formations were mainly dependent on the formation of reactive chlorine species, which were present, if any, below the detection level of the applied analytical procedure in the UVC, PCD, UVC/VUV, and in insignificant levels in PS.
- PS could be a suitable method in OCs removal and energy perspective when cooling tower waste heat can be used

Overall, while EO generated chlorinated by-products and chlorinated species-laden solutions, PCD, PS, and UVC/VUVOP demonstrated suitable pre-treatment technologies for the removal of HS/OCs from CTBD and similar waters. Thus PCD, PS, and UVC/VUVOP AOPs before membrane desalination enable reducing membrane fouling effects without significantly forming unwanted chlorinated by-products.

Chapter 7.

Lowering the industrial freshwater footprint by treating cooling tower water with a technology train: Constructed wetlands, nanofiltration, electrochemical oxidation, and reverse osmosis.

Modified version of this chapter will be published as:
Thomas V. Wagner, Pradip Saha, Harry Bruning, and Huub H. M. Rijnaarts. " Lowering the industrial freshwater footprint by treating cooling tower water with a technology train: Constructed wetlands, nanofiltration, electrochemical oxidation, and reverse osmosis." (in preparation)

Abstract

Reusing cooling tower water blowdown (CTBD) in the industry would significantly lower the industrial freshwater footprint. Due to its elevated salinity, phosphate, and organic carbon concentrations, cooling tower water blowdown cannot be reused for industrial processes. This study tested a treatment train to remove these components, consisting of various technologies developed within the Water Nexus research program framework. This program focused on using and reusing saltwater streams within the industry to lower the pressure on valuable freshwater sources. In that context, constructed wetlands, nanofiltration, and electrochemical oxidation were studied for the treatment of CTBD and integrated into a treatment train together with reverse osmosis. The treatment train was tested with real CTBD, focusing on the produced water quality, the fate of industrial chemical benzotriazole, membrane performance, and potential production of unwanted by-products. The treatment train was capable of reaching the desired water quality. Benzotriazole was removed by the constructed wetlands that acted as pre-treatment before nanofiltration as a result of biodegradation. The production of inorganic carbon species in the constructed wetlands resulted in increased fouling of the subsequent nanofiltration membranes. These membranes mainly retained divalent ions and did not retain monovalent ions, which resulted in a permeate stream whose electrical conductivity was too high for reuse applications and therefore required further treatment by reverse osmosis. The concentrate that was produced as a result of nanofiltration was treated by electrochemical oxidation. Electrochemical oxidation of the concentrate was more efficient in terms of degradation of recalcitrant humic acids. It produced fewer unwanted chlorinated organic by-products than direct oxidation of CTBD due to different ion ratios which retention by the nanofiltration membranes. Before the full-scale application of the treatment train for CTBD treatment, consider ways to improve the water recovery, include innovative new nanofiltration membranes that can make the use of reverse osmosis redundant, and adopt new methods insights in preventing unwanted by-product formation during electrochemical oxidation.

Keywords

Cooling tower water blowdown; treatment train; constructed wetlands; electrochemical oxidation; Nanofiltration; Benzotriazole.

7.1 INTRODUCTION

The reuse of industrial wastewater within the industry itself significantly lowers the industrial freshwater footprint, thereby mitigating future freshwater provision problems. Large parts of the world suffer from freshwater stress as a result of climate change and over-extraction [394, 395]. The industrial freshwater withdrawal accounts for up to 55 % of the total freshwater withdrawal in industrialized countries [396]. A substantial part of this freshwater is used for the cooling of process streams in cooling towers [397]. After the cooling process, the cooling tower water is generally discharged as cooling tower blowdown (CTBD) because the salinity increases as a result of evaporation, resulting in an increased probability of scaling and corrosion of the system [398]. The reuse of this currently discharged brackish CTBD through treatment towards make-up water quality and use in the cooling tower itself would significantly lower the freshwater footprint of cooling towers.

The reuse of CTBD in the cooling tower requires desalination. CTBD generally has an electrical conductivity (EC) of 1.5 – 5 mS/cm [18, 399], while typically an EC of < 1 mS/cm is required for its reuse in the cooling tower [17]. Besides, Groot et al. (2015) established concentration limits for use in the cooling tower for chloride (<150 mg/L), phosphate (<1 mg/L), suspended solids (<1 mg/L) and total organic carbon (TOC) (<15 mg/L)[17]. Various desalination technologies for CTBD have been studied, such as reverse osmosis [13, 19, 22], electrodialysis [17], capacitive ionization [17, 135] and membrane distillation [17, 32, 34]. A common phenomenon that was observed in these studies is fouling of the desalination membranes as a result of: i) compounds present in the CTBD due to the use of surface water as cooling tower water, such as phosphate and dissolved organic carbon; ii) chemicals that are added to the CTBD to protect the cooling system, such as biocides, antiscalants and corrosion inhibitors [18, 399]. Hence, pre-treatment of the CTBD is needed before desalination, and various pre-treatment methods have been assessed, such as activated carbon adsorption [11], coagulation [11, 132], and ultrafiltration [11, 22]. However, an optimal combination of pre-treatment and desalination technologies for CTBD has not been established yet.

Within the Dutch research program Water Nexus, several technologies have been studied for the (pre)treatment of CTBD. The aim of Water Nexus is to lower the pressure on freshwater resources in fresh water-stressed delta areas by reusing

saline industrial wastewater, such as CTBD, this way lowering the industrial freshwater footprint [9]. Water Nexus combines the development of digital tools for mapping, management, and control of freshwater resources with the development of innovative water treatment technology for saline industrial wastewater. A substantial part of Water Nexus is dedicated to developing technologies that facilitate the reuse of CTBD, such as constructed wetlands (CWs) [18, 140, 187, 191, 400], advanced oxidation processes [108, 198, 401], and nanofiltration (NF) with novel layer-by-layer membranes [402, 403], with the aim of integrating these technologies in a treatment-train for CTBD. A first technology integration step of earlier mentioned technologies was executed in **Chapter 3**, in which a combination of CWs and electrochemical oxidation (EO) was used to treat CTBD [260]. CW-treatment followed by EO resulted in more efficient removal of organic compounds from CTBD than EO followed by a CW [260]. In addition, when applying a CW after EO, the CW suffered from the production of toxic by-products by EO [260]. In addition, **Chapter 4** highlighted that sulfate-enriched electrolytes facilitated faster and effective oxidation of the organic compound together with less chlorinated organic by-product formation. NF could yield sulfate-enriched electrolytes [402]. In the present study, we build upon the insights obtained in **(chapters 3 and 4)** [260] and [402] and novel process insights to answer newly arising questions when developing a treatment train for CTBD treatment. This study will assess a technology train consisting of CWs, NF, EO, and reverse osmosis (RO), with specific emphasis on:

- The use of hybrid-CWs as pre-treatment of CTBD before NF-treatment to prevent fouling of the NF membranes.
- The use of commercially available NF membranes for treatment of CW pre-treated and untreated CTBD to retain monovalent and divalent ions prior to reverse osmosis.
- The use of EO to treat the NF concentrate and degrade the concentrated organics.
- The reverse osmosis to treat the nanofiltration permeates and produces water with an electrical conductivity of < 1 mS/cm that can be reused for various industrial purposes, such as in the cooling tower itself.

7.2 MATERIALS & METHODS

7.2.1 Cooling tower blowdown

Real CTBD was obtained from the cooling towers of the ELSTA power facilities of Dow Benelux BV (Terneuzen, The Netherlands) on November 19th, 2020. Sand-filtered surface water is used as a freshwater source for these cooling towers [17]. Various chemicals are added to this sand-filtered surface water to maintain optimal functioning of the cooling system: NaClO, H_2SO_4 (96%), two corrosion inhibitors (Nalco 3DT187 and Nalco 3DT199 (sodium benzotriazole, 3.2-6.3 mg/L)) and a bio dispersant (Nalsperse 7348, 4.3 mg/L) [17]. The composition of the CTBD was measured (Table 7-1) and is comparable to the earlier measured composition of the same CTBD in [11, 17, 34, 198, 260, 404].

Table 7-1. *Composition of cooling tower blowdown*

Component	Concentration	Component	Concentration
Electrical conductivity	4.4(±0,3) mS/cm	Na^+	390 mg/L
pH	7.6 (±0,5)	K^+	70 mg/L
TC	53.3 mg/L	Ca^{2+}	399 mg/L
TOC	43.9 mg/L	Mg^{2+}	67 mg/L
TIC	9.4 mg/L	Cl^-	584 mg/L
TN	15.8 mg/L	NO_3^-	53 mg/L
Benzotriazole	82.9 µg/L	NO_2^-	<1 mg/L
ortho-PO_4^{3-}	2.2 mg/L	SO_4^{2-}	1310 mg/L

7.2.2 Technology train

Treatment of the CTBD was performed with two different treatment trains (Fig. 7-1). Treatment-train 1 consisted of a hybrid-CW followed by NF. The concentrate of the NF was treated by EO, while RO treated the permeate. Treatment-train 2 was

similar to treatment-train 1, except that pre-treatment by the hybrid-CW was excluded. This allowed determining the impact of CW pre-treatment on the fouling behavior and separation efficiency of the NF-membranes.

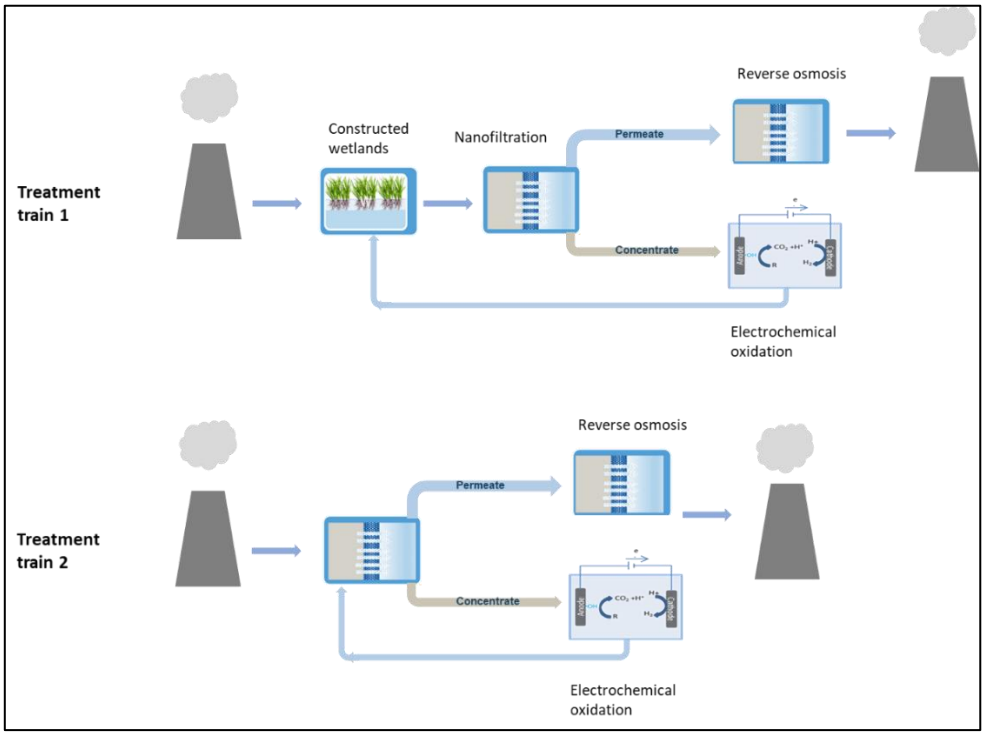

Fig. 7-1. *Two different treatment trains were assessed in the present study*

7.2.2.1 Constructed wetlands set-up

A pilot-scale hybrid-CW similar to the hybrid-CWs in [187] was used to pre-treat CTBD before NF. The hybrid-CW consisted of a vertical subsurface-flow CW (96 x 143 x 97 cm) followed by a surface-flow CW (145 x 145 x 30 cm) and a horizontal subsurface-flow CW (145 x 145 x 39 cm) (see picture in supplementary info (SI), Fig. S7-1). The CWs were connected by tricoflex tubing connected to pond pumps that were controlled by LOGO! automation software (Siemens, Amersfoort, The Netherlands) controlled the total hydraulic retention time of the hybrid-CW of ± 120 h. The substrate of the subsurface-flow CWs consisted of gravel with a diameter of 16-32 mm and sand with a diameter of >250 µm, and the subsurface-flow CWs were planted with *Phragmites australis*. Because the hybrid-CW was located aboveground, the sides were insulated with insulation foam to prevent

extreme heating or cooling (not yet installed in Fig. S7-1). Further details about the set-up of the hybrid-CWs are described in [187].

The hybrid-CW was built on June 6th, 2018, and the plants and microbial community were allowed to grow, fed by tap water and rainwater, until November 18th, 2019. From that day onwards, the hybrid-CW was fed with CTBD from an influent tank refilled with fresh CTBD weekly. Samples were taken weekly from July 16th, 2020, until November 25th, 2020, from the CTBD and the effluent of all three different CW flow types to determine the removal efficiency for target compounds during summer and winter conditions. On November 19th, 2020, 90 L of hybrid-CW effluent and 90 L of not pre-treated CTBD were obtained for further treatment by NF.

Temperature data for the hybrid-CWs was obtained from the official Royal Netherlands Meteorological Institute (KNMI) weather station in Wilhelminadorp, located 37 km from the hybrid-CW location.

7.2.2.2 Nanofiltration set-up

Nanofiltration was performed on a Mexplorer lab-scale nanofiltration set-up (NXFiltration, Enschede, The Netherlands) containing a rotary vane pump (Fluid-o-Tech PO211, Milan, Italy) that allowed a flowrate of 73-292 L/h at 0 bar and operating pressure of 0-10 bar at 20°C. A dNF40 membrane (NXFiltration, Enschede, The Netherlands) was used, which is a hollow-fiber negatively charged polyelectrolyte multilayer membrane unit containing 120 fibers with an inner diameter of 0.7 mm, a length of 30 cm, a nominal membrane area of 0.065 $m^{2,}$ and a molecular weight cutoff of 400 Da. Before use, the membrane was cleaned from its storage solution with 150 L of tap water according to the manufacturer's instructions. The pure-water permeance *PWP* (L/m^2.h.bar) of the membrane was determined with demineralized water according to Eq. 7.1.

$$\mathrm{PWP} = \frac{\mathrm{V_{permeate}}}{\mathrm{At\Delta P}} \tag{7.1}$$

where $V_{permeate}$ (L) corresponds to the collected permeate volume, A (m^2) corresponds to the membrane area, t (h) corresponds to the time of permeate collection, and ΔP corresponds to the transmembrane pressure. The *PWP* of the membrane was 7.0 L/m^2.h.bar, which is similar to the pure-water permeance of the

same type of membrane observed by [405]. During NF of CW-treated and untreated CTBD, a 100-micron filter (Amiad Water Systems Europe, Bochum, Germany) was used to prevent solids entering the system.

The performance of the membrane and impact of CW-pretreatment was assessed in various ways:

- By assessing the impact of varying transmembrane pressures on the retention of target solutes and required time for the production of 30 mL of permeate from both pre-treated and untreated CTBD by the NF membrane. Transmembrane pressures of 1, 2, and 3 bar were assessed at a fixed crossflow-velocity of 0.5 m/s. Tests were performed in duplicate
- By assessing the impact of varying crossflow velocity on the retention of target solutes and required time for the production of 30 mL of permeate from both pre-treated and untreated CTBD by the NF membrane. Crossflow velocities of 0.5, 0.75, and 1.0 m/s were assessed at a fixed transmembrane pressure of 1 bar. Tests were performed in duplicate

By assessing the impact of pre-treatment on target solutes by the membrane during four consecutive concentration runs with a permeate recovery of 80%, at a crossflow-velocity of 0.5 m/s and a transmembrane pressure of 2 bar. 10 L batches of both pre-treated and untreated CTBD were recirculated until 80% permeate was recovered, regularly taking samples for target solute measurement and monitoring the transmembrane pressure and feed flow rate.

7.2.2.3 Electrochemical oxidation set-up

EO experiments were performed as described previously [198, 260, 404] in an electrochemical cell in batch recirculation mode using 350 mL NF concentrate of either CW pre-treated or untreated CTBD that was concentrated four times. The electrochemical cell contained a single-flow chambered flat plate reactor assembly with an active electrode surface area of 22.4 cm^2 and an inter-electrode distance of 1.5 cm and sensors for the online measurement of pH, electrical conductivity and temperature. The CTBD was pumped through the electrochemical cell with a peristaltic pump, while the system was maintained at a temperature of 21-23°C. A boron-doped diamond (BDD) electrode (Magneto Special Anodes, Schiedam, The Netherlands) was used as the working anode, while a platinum-coated titanium

electrode was used as the cathode. A silver/silver chloride (Ag/AgCl) electrode (QM711X/Gel, Prosense, The Netherlands) was used as a reference electrode, ionically plugged into the EO cell using Haber-Lugging capillaries filled up with a 1M potassium nitrate solution. EO experiments were conducted galvanostatically using an IviumStat.h potentiostat (Ivium Technologies B.V. The Netherlands) attached in a three-electrode conformation (anode, cathode, and reference electrode). Iviumstat software was used to record and analyze the experimental electrochemical data. To evaluate the EO performance, the instantaneous current efficiency (%ICE) was determined according to equation Eq. (7.2) [198].

$$\%\mathrm{ICE} = \mathrm{FV_S}\left(\frac{\mathrm{COD_0} - \mathrm{COD_t}}{8\mathrm{I}\Delta\mathrm{t}}\right)\mathrm{x}100 \qquad (7.2)$$

Where: $COD_0$and COD_t is the COD concentration at the beginning and time interval t, respectively, in g_{O_2}/L, Faraday's constant F (96485 C/mol), Electrolyte volume V_S (L), applied current I (A), the electrolysis time interval Δt (S). 8= oxygen equivalent mass (g_{O_2}eq/mol).

7.2.2.4 Reverse osmosis set-up

Reverse osmosis (RO) was performed with a lab-scale RO-system dedicated to developing and testing new types of membranes (Alfa Laval Test Unit M20, Nijmegen, The Netherlands). This setup allows a maximum inlet pressure of 60 bar and a 5–24 L/min cross-flow range. The system was equipped with a spiral membrane of polypropylene (Alfa Laval RO98pHt, Nijmegen, The Netherlands), with NaCl retention of >98 % at 16 bar and 25°C, according to the supplier. RO occurred with an operating pressure of 40 bar at 20°C. The NaCl retention at these conditions was tested with a 2 mS/cm NaCl solution prior to RO of the CTBD, resulting in a NaCl retention of >98.5 %. The RO experiments were performed with ± 32 L of either the CW-pre-treated or untreated NF-concentrate.

7.2.3 Analytical methods

The Total Inorganic Carbon (TIC) fraction was determined by converting carbonate/bicarbonate in acidic conditions to CO_2, which was sparged from the solution and quantified in a non-dispersive-infra-red (NDIR) gas analyzer

(Shimadzu, TOC-L CPH/CPN, Kyoto, Japan). The Total Carbon (TC) (organic and inorganic) was analyzed by complete oxidation at 680°C to CO_2, quantified via the same NDIR gas analyzer. The Total Organic Carbon (TOC) content was determined by subtracting the TIC from TC. The equipment's lower limit of detection (LLD) was 1 mg/L (DOW Reference method: NEN-EN 1484).

The Total Nitrogen (TN) content was determined on the Shimadzu TOC-L instrument, together with the TOC content. Sample nitrogen introduced into the combustion tube converts to nitrogen monoxide. Nitrogen gas in the carrier gas (air) did not interfere. The carrier gas containing the nitrogen monoxide (NO) was directed to the TNM-L total nitrogen unit, a chemiluminescence-based detector. In the detector, ozone was added, which reacts with NO to a combination of NO_2 and excited NO_2*. When NO_2* returns to NO_2, radiation is emitted, which is measured photometrically. This analysis determines the sum of N-NH_3, N-NO_3, N-NO_2, and Organic-N (DOW Reference method: NEN-EN 12260).

Orthophosphate (O-PO_4) was determined via spectrophotometry using a HACH DR3900 VIS spectrophotometer and HACH cuvette tests (LCK-349 (0.05–1.50 mg/L PO_4—P, 0.15–4.50 mg/L PO_4^{3-}, or 0.15–3.50 mg/L P_2O_5).

Chloride (Cl^-), Nitrite (NO_2^-), Nitrate (NO_3^-), and Sulphate (SO_4^{2-}) were determined via a Thermo Scientific Dionex™ ICS-2100 Ion Chromatography System using an IonPac AS15 analytical column with an IonPac AG15 analytical column. Chloride and Sulphate were quantified using the suppressed conductivity detection system. Nitrite and Nitrate were quantified using a UV-spectrophotometric detector (DOW Reference method: NEN-EN-ISO 10304-1).

1-H-Benzotriazole (BT) and 4- and 5-Methyl-benzotriazole (MBT) were analyzed using high-pressure liquid chromatography together with quadrupole time-of-flight high-resolution mass spectrometry (UHPLC/QTOF-HRMS). The analytical system consists of an Agilent 1290 Infinity II high-speed pump, Agilent 1290 Infinity II Multi sampler with a built-in cooler, and an Agilent 1290 Infinity II column compartment. A C18 ZORBAX ECLIPSE PLUS C18 RRHD 1.8 µm 2.1 x 50mm is used for chromatographic separation. The identification and quantification were made on an Agilent 6545 QTOF tandem mass spectrometer. Samples were filtered over a 0.45 µm filter before analyses.

The Ca^{2+}, K^{+}, Mg^{2+}, and Na^{+} content was determined using ICP-OES (inductively coupled plasma optical emission spectrometry) on an Agilent 5100 instrument. The samples were filtered over a 0.45 µm filter, diluted using Milli-Q water depending on the expected concentrations, acidified, and measured. Quantification was done using matrix-matched external standards. The measured wavelengths were 396.8 and 422.7 nm for Ca, 766.5 nm for K, 279.6, 280.3, and 285.2 nm for Mg, and 589.0 and 589.6 for Na.

After EO-treatment, Hach DPD powder pillows were used for free chlorine determination, Hach LCK-314/LCK-1414 kits were used for COD determination, and Hach LCK-390 cuvette tests were used for AOX determination ((Hach Lange GmbH, Germany). Dionex ICS-2100 ionic chromatography (IC) determined chloride, chlorate, and perchlorate. The detail of all these analytical methods is described in [198, 404].

7.3 RESULTS AND DISCUSSION

7.3.1 Hybrid constructed wetland pretreatment

Pretreatment of the CTBD by a hybrid-CW before NF removes phosphate, nitrate, and benzotriazole, but an increase in the total carbon content and EC (Table 7-2).

Table 7-2. *Average effluent concentrations and removal efficiency of hybrid constructed wetland for cooling tower water, 16 samples from July-November 2020. (vertical subsurface flow (VSSF); surface flow (SF); horizontal subsurface flow (HSSF)*

Parameter	Average influent concentration	Average VSSF-CW effluent concentration	Average SF-CW effluent concentration	Average HSSF-effluent concentration	Average hybrid-CW removal efficiency
Electrical conductivity (mS/cm)	4.3 (±0.4)	4.6 (±0.6)	4.7 (±0.7)	5.2 (±1.2)	-
pH	7.5 (±0.2)	7.0 (±0.4)	7.8 (±0.6)	7.4 (±0.5)	-
Total nitrogen (mg/L)	20.8 (±6.4)	15.4 (±4.1)	12.3 (±3.2)	6.8 (±3.9)	67.4%
Nitrate (mg/L)	73.8 (±26.4)	56.3 (±18.4)	34.3 (±18.3)	16.5 (±16.5)	77.7%
Ortho-phosphate (mg/L)	5.6 (±0.4)	1.8 (±1.0)	1.0 (±1.1)	b.d.l[a]	>95%
Total carbon (mg/L)	65.6 (±8.4)	74.3 (±14.2)	81.4 (±16.7)	94.6 (±25.4)	-44.2%
Total organic carbon (mg/L)	55.5 (±6.9)	54.6 (±9.9)	57.5 (±13.6)	60.4 (±17.1)	-8.9%
Total inorganic carbon (mg/L)	10.0 (±2.7)	19.6 (±5.2)	22.4 (±7.9)	33.1 (±10.9)	-230.6%
COD (mg/L)	140.1 (±26.5)	130.3 (±27.1)	145.6 (±31.5)	149.5 (±42.4)	-6.7%
Benzotriazole (µg/L)	120.8 (±17.2)	24.5 (±10.2)	17.4 (±5.2)	11.4 (±2.3)	90.6%

[a]b.d.l = below detection limit of 0.3 mg/L

Hybrid-CW treatment results in an average increase of the EC of the CTBD over the various hybrid-CW compartments during the experimental period and does not result in the EC reuse quality target of 1 mS/cm (Table 7-2; Fig. S7-2). Hence, desalination is still required after hybrid-CW treatment before the CTBD can be reused in the cooling tower. The EC of the hybrid-CW effluent shows seasonal variation with substantially higher values during periods with higher temperatures (Fig. S7-3; Fig. S7-4) due to evapotranspiration. Increased EC values were most apparent in the HSSF-CW (Fig. S7-2) due to its shallow depth. In contrast, hybrid-CW effluent EC values lower than the influent were observed with lower temperatures and rainfall due to lower evapotranspiration and dilution by rainfall (Fig. S7-2). Varying EC values over the year provide a good proxy for the amount of evapotranspiration/dilution of the CTBD within the hybrid-CW. Still, they will likely influence the efficiency of subsequent membrane-based desalination technologies with specific ion retention capacity.

Phosphate is completely removed from the CTBD by the hybrid-CW (Table 7-2, Fig. S7-5; Fig. S7-6), producing a concentration below the 1 mg/L threshold for reuse in the cooling tower [17]. However, the phosphate removal decreases with lower temperatures in the VSSF-CW starting compartment. A similar tendency was observed in the hybrid-CWs fed with synthetic CTBD of [187]. Phosphate is removed by both biological and physical/chemical removal processes in CWs [189, 406]. The decreasing removal efficiency with decreasing temperature indicates that biological removal processes play an important role in phosphate-removal in the VSSF-compartment of the hybrid-CW. However, in the future, a decreasing phosphate removal efficiency as a result of saturation of the CW substrate might be observed, which could result in membrane fouling of the subsequent membrane desalination technologies [407].

The hybrid-CW's nitrate and benzotriazole removal efficiency from real CTBD (Table 7-2) is comparable to the removal efficiency from synthetic CTBD observed in earlier experiments [187]. Nitrate is mainly removed in the anaerobic horizontal subsurface flow (HSSF) compartment (Fig. S7-7) due to denitrification [406]. With decreasing temperatures, the nitrate removal efficiency decreases as a result of decreasing microbial activity (Fig. S7-8), resulting in a flux of nitrate-containing CTBD towards subsequent desalination technologies, where it could act as a nutrient

for membrane-fouling microorganisms [408]. This flux likely doesn't contain significant amounts of benzotriazole since benzotriazole is removed in the vertical subsurface flow (VSSF) compartment (Fig. S7-9) during the whole experimental period (Fig. S7-10), mainly as a result of aerobic biodegradation [140, 187].

The hybrid-CW has a negative TOC removal efficiency (Table 7-2; Fig. S7-11; Fig. S7-12), which is in contrast with >80% TOC removal efficiencies observed for synthetic CTBD [187]. The TOC of the synthetic and real CTBD consisted mainly of humic acids [11, 198, 404]. The difference in removal efficiency is likely caused by not being able to completely dissolve humic acid for the synthetic CTBD, resulting in its physical filtration in the hybrid CW's substrate [187]. In contrast, the completely dissolved humic acids in the real CTBD were not filtered out. In addition, these humic acids are not removed by other removal processes in the hybrid-CW, such as biodegradation, because humic acids are generally not readily biodegradable [200]. This results in an effluent concentration behavior similar to the EC (Fig. S7-2; Fig. S7-12), indicating the influence of evapotranspiration and dilution on the final concentration. As a result of not removing humic acids, there is also no net removal of total carbon from the CTBD by the hybrid CW (Table 7-2; Fig. S7-13; S7-14). However, the net increase of the effluent concentration compared to the influent concentration of total carbon is higher than expected when only influenced by climatic circumstances, such as evapotranspiration and dilution (Fig. S7-2). This results from a substantial increase in the inorganic carbon concentration, especially in the horizontal subsurface flow -CW effluent (Fig. S15; Fig. S16). The formation of inorganic carbon in CWs was observed before in Wieβner et al. (2005) when treating synthetic domestic wastewater in lab-scale circulating vertical subsurface flow-CWs with alternating redox conditions [409]. In this study, inorganic carbon production was attributed to converting organic carbon into inorganic carbon species, CO_2, and methane [409]. However, there is no evidence for the conversion of organic carbon into inorganic carbon in the present study. A potential source of inorganic carbon could be the sandy substrate, which might have contained calcium carbonate ($CaCO_3$), that dissolved into the passing CTBD. Increased inorganic carbon species might have a negative effect on subsequent membrane desalination processes, where it can result in membrane scaling [410, 411].

7.3.2 Nanofiltration membrane performance

After CW treatment, the CTBD was treated by NF. The impact of CW pre-treatment was assessed in two different ways: on the retention of the membrane under the influence of different trans-membrane pressures and crossflow velocities and the influence of the retention of the membranes and stability of the system during 4 subsequent 80% recovery runs of 10 L of either untreated or CW pre-treated CTBD.

7.3.2.1 Membrane performance: The influence of varying trans-membrane pressure and crossflow velocities on the production time and composition of the permeate

An increasing transmembrane pressure impacts the permeate production speed and composition more than an increasing crossflow velocity (Table 7-3).

The EC of the CTBD is reduced by ± 40 % as a result of NF at a transmembrane pressure of 1 bar and cross-flow velocity of 0.5 m/s (Table 7-3). Increasing the transmembrane pressure from 1 to 3 bar reduced by a factor of three the required time for the production of 30 mL permeate by both the untreated and CW-pretreated CTBD (Table 7-3). For the CW pre-treated CTBD, this quicker permeate production is accompanied by a decrease in the EC of the permeate, while for the untreated CTBD, an increase in the EC is observed (Table 7-3). This different behavior of the EC with increasing transmembrane pressures is due to differences in the retention of specific ions from the untreated and CW-pretreated CTBD (Table 7-3). Divalent ions are retained for >50%, and increasing transmembrane pressures result in increased retention of divalent ions, such as SO_4^{2-} and Mg^{2+} (Table 7-3). Monovalent ions were less well retained, an increase in Cl^- observation is observed in the permeate, which increases as a result of increasing transmembrane pressures (Table 7-3).

Table 7-3. *The influence of varying trans-membrane pressure and crossflow velocities on the production time and composition of the permeate. Grey column = non-pre-treated cooling tower water; Green column = constructed wetland pre-treated cooling tower water. TMP = transmembrane pressure; CFV = crossflow velocity.*

			Influence of varying TMP (CFV: 0.5 m/s)						Influence of varying CFV (TMP: 1 bar)					
	Influent		TMP 1 bar		TMP: 2 bars		TMP: 3 bars		CFV 0.5 m/s		CFV: 0.75 m/s		CFV: 1.0 m/s	
30 mL permeate production time	-		474	395	196	167	130	101	474	395	460	406	382	354
EC (mS/cm)	3.95	3.76	2.28	2.29	2.25	2.16	2.42	2.06	2.28	2.29	2.42	2.30	2.46	2.32
pH	7.4	6.7	7.5	6.9	7.4	6.8	7.3	6.7	7.5	6.9	7.5	6.9	7.5	6.8
TC (mg/L)	53.31	54.4	11.2	15.9	11.7	16.9	9.1	15.4	11.2	15.9	10.7	18.1	12.2	15.4
TOC (mg/L)	43.9	35.8	4.8	3.1	5.2	3.5	3.7	3.1	4.8	3.1	3.8	5.2	5.3	4.1
TIC (mg/L)	9.4	18.6	6.4	12.8	6.5	13.4	5.4	12.3	6.4	12.8	6.9	12.9	6.9	11.3
Benzotriazole (µ/L)	83.0	0	0	0	0	0	0	0	0	0	0	0	0	0
TN (mg/L)	15.8	2.6	13.2	2.5	15.6	2.4	14.2	2.4	13.2	2.5	14.9	2.4	15.6	2.4
SO_4^{2-} (mg/L)	1310	1240	64	82	39	40	24	27	64	82	73	76	76	83
NO_3^- (mg/L)	53	7.5	59	8.7	57	8.6	61	8.7	59	8.7	61	8.7	60	8.8
Cl^- (mg/L)	577	535	593	621	629	621	599	584	593	621	673	632	669	636
Ca^{2+} (mg/L)	399	233	110	131	108	102	97	108	110	131	132	130	134	124
Mg^{2+} (mg/L)	67	63	18	19	12	13	10	13	18	19	19	19	19	19
K^+ (mg/L)	70	73	43	51	44	41	42	47	43	51	46	49	46	51
Na^+ (mg/L)	390	347	260	248	278	207	269	233	260	248	283	244	283	241

The retention of organic carbon-containing compounds is >90 % for both the CW pre-treated as untreated CTBD. This high retention is because the organic fraction in the studied CTBD mainly consists of humic acids [11, 34], whose size is large enough to retain the membranes. The relatively small organic corrosion inhibitor benzotriazole also seems to be retained by the NF-membrane since it is not observed in the permeate during the short-term membrane retention tests (Table 7-3). This is unexpected since the size of benzotriazole (119.20 da) is smaller than the molecular weight cut-off of the membrane of 400 Da. Generally, the retention of micropollutants by membranes is the result of solute-membrane interactions, such as electrostatic repulsion, size exclusion, and hydrophobic interactions. The retention is likely not the result of electrostatic repulsion, considering that benzotriazole is neutral at the experimental pH. Similar high retention was not observed in other studies where the retention of benzotriazole by NF-membranes was studied, such as in Huang et al. (2021), where retention of benzotriazole up to 40% from a synthetic solution for differently coated NF-membranes was observed [412]. However, longer nanofiltration runs showed that there was a delay in the breakthrough of benzotriazole through the membrane and its appearance in the permeate (section 7.3.2.2).

An increasing crossflow velocity increases the EC for both streams but does not influence permeate production rate as much as the transmembrane pressure (Table 7-3). This increase in EC is likely the result of slightly lower retention of divalent ions with increasing cross-flow velocities (Table 7-3). A change in the retention of inorganic and organic carbon and different nitrogen species was not observed with increasing cross-flow velocities (Table 7-3).

7.3.2.2 The impact of pre-treatment on 80% nanofiltration permeate recovery and its composition

Four sequential runs in which 10 L of either untreated CTBD or CW pre-treated CTBD was filtered took 48 h for the untreated CTBD and 35 h for CW pre-treated CTBD (Table 7-4). The shorter time required for the treatment of the CW pre-treated CTBD results from an increasing transmembrane during membrane treatment (Table 7-4; Fig. S7-17), which has been shown to decrease the time for permeate collection (Table 7-3).

Table 7-4. *Experimental conditions and composition of permeate and concentrate after 4 subsequent 80 % permeate recovery runs with an initial volume of 10 L, initial trans-membrane pressure of 1.0, and initial crossflow velocity of 0.5 m/s. The influent value represents the composition of 1st 10 L batch. Permeate value represents the value of the combined permeate of 4 runs.*

	Direct cooling tower water			Constructed wetland pre-treated		
Total run-time	48 h			35 h		
TMP after 80% concentration runs	1.0			1.7		
	Influent	Permeate	Concentrate	Influent	Permeate	Concentrate
EC	3.81	2.59	6.37	3.76	2.37	6.67
pH	6.98	7.42	7.54	7.43	7.04	7.79
TC (mg/L)	48	12	120	60	24	140
TOC (mg/L)	37	2	112	36	1	123
Benzotriazole (µg/L)	64	57	35	0	0	0
TIC (mg/L)	11	10	8	24	22	17
TN (mg/L)	15	14	15	4	3	9
NO_3^- (mg/L)	49	57	32	6	10	5
SO_4^{2-} (mg/L)	1321	263	2397	1240	157	2479
Cl^- (mg/L)	559	616	382	522	605	353
Ca^{2+} (mg/L)	414	163	-	406	145	-
Mg^{2+} (mg/L)	69	27	-	61	22	-
K^+ (mg/L)	62	45	-	70	51	-
Na^+ (mg/L)	391	283	-	336	253	-

The increased transmembrane pressure could be an indication for membrane fouling [11, 345]. NF-membranes fouling by, for instance, humic acids is a commonly observed phenomenon [411-413] and result from either adsorption in or pore blocking of the membrane pores or cake layer formation or gel layer formation on the membrane surface [413, 414]. However, considering the similar concentrations of TOC, which mainly consists of humic acids, in the CW pre-treated and untreated CTBD, fouling by humic acids was most likely not the cause for the

increased transmembrane pressure during NF of the CW pre-treated CTBD. A potential cause for the increased transmembrane pressure could be elevated inorganic carbon concentrations in the CW effluent (section 7.3.1). Carbonates have been shown to result in pore blocking of NF-membranes [415, 416], which would result in increased transmembrane pressure. No further membrane analyses were performed to analyze this potential fouling mechanism.

The increased transmembrane pressure results in slight differences in the untreated and CW pre-treated NF-permeate composition. A slightly lower concentration of divalent ions is observed in the permeate of the CW pre-treated permeate (Table 7-4) as a result of increasing retention with increasing membrane pressure (section 7.3.2.1). This results in a lower EC of the permeate after 80% recovery for the CW pre-treated permeate compared to the untreated permeate (Table 7.4). The EC of both streams is not low enough to meet the threshold value of 1 mS/cm for a broad range of industrial reuse options [17]. Next to differences in composition resulting from an increasing transmembrane pressure, differences in composition can be observed due to pre-treatment by CWs: The CW pre-treated permeate contains less nitrogen and benzotriazole as a result of their removal in the CWs (Table 7-4; Table 7-2). Interestingly, benzotriazole does appear in the bulk permeate after longer NF operation (Table 7-4), whereas during short-term membrane characterization experiments, benzotriazole was not observed in the permeate (section 7.3.2.1). Detailed sampling over time showed that it took 6 h before benzotriazole was first observed in the permeate (Fig. S19). Apparently, benzotriazole is temporarily retained by NF-membranes, which could be due to adsorption to the membrane surface. Adsorption of micropollutants, such as benzotriazole, to NF-membrane surfaces has previously been shown to result in an overestimated retention of the micropollutants [417, 418], which was especially the case for electrostatically neutral compounds, such as benzotriazole [419]. A breakthrough is observed after the initial adsorption, and benzotriazole accumulates in the permeate (Fig. S7-19; Table 7-4). However, as discussed earlier, CW pre-treatment could prevent the accumulation of small organic micropollutants that NF-membranes do not retain in the permeate.

7.3.3 Electrochemical oxidation of the nanofiltration concentrate

7.3.3.1 COD and TOC removal

Three kinds of CTBD were electrochemically oxidized with a BDD anode:

a) Untreated CTBD (EO-CTBD)

b) NF-concentrate of untreated CTBD, as a result of 80% NF-permeate recovery (EO-NF-CTBD)

c) NF-concentrate of CW-pretreated CTBD, as a result of 80% NF-permeate recovery (EO-CW-NF-CTBD)

Pre-treatment by NF resulted in substantially higher removal of organic compounds at different current densities than untreated CTBD due to differing ions-ratios of the starting solutions (Fig. 7-2).

At a current density of 8.5 mA/cm^2, a similar trend in COD removal for the EO-NF-CTBD and EO-CW-NF-CTBD was observed, with the COD removal reaching 100% within 6 h (Fig. 7-3a). Corrosion inhibitor benzotriazole, which was still present in the EO-CTBD and EO-NF-CTBD feed, was also completely removed as a result of EO-treatment at the two different applied current densities of 8.5 and 14.3 mA/cm^2 (Table S7-1). This finding is in line with observations from earlier experiments focussed on benzotriazole removal [198]. The COD removal rate was higher for the EO-CTBD compared to the EO-NF-CTBD and EO-CW-NF-CTBD at a current density of 8.5 mA/cm^2, reaching a removal of 80% after 2 h (Fig. 7-3a). However, due to the 3.7 times lower initial COD concentration, the reaction rate decreased drastically after 2 h because of diffusive mass transfer limitation on the BDD anode [173, 198]. With an increasing current density from 8.5 mA/cm^2 to 14.3 mA/cm^2, the COD removal rate for the EO-NF-CTBD and EO-CW-NF-CTBD increased (Fig. 7-3a). This increasing removal rate is likely due to the generation of more reactive oxidative species, such as $HO^{\bullet}$, due to higher energy input and electrode potential, leading to more $SO_4^{\bullet -}$ formation, which facilitated a faster removal of COD [162].

The TOC removal rate at a current density of 8.5 mA/cm^2 for EO-CTBD was 0.09 h^{-1}, with a final removal efficiency of 75% after 8 h of electrochemical oxidation (Fig. 7-2b).

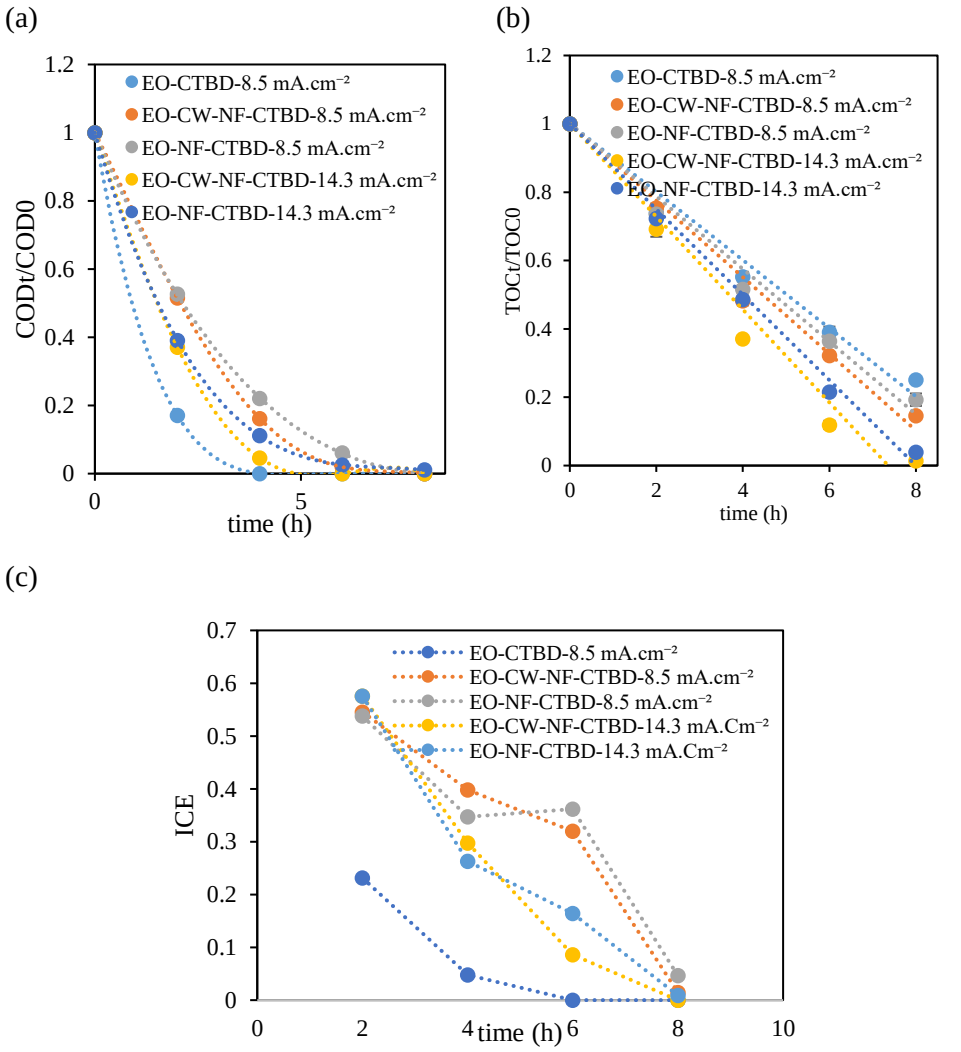

Fig. 7-2. *(a) COD_t/COD_0, (b) TOC_t/TOC_0 and (c) Instantaneous current efficiency (ICE) changing with reaction time (h). Experimental conditions: 350 mL sample, T = 25-30°C, current density = 8.5 or 14.3 mA/cm², conductivity = 3.63 (EO-CTBD) and 6.36 (NF-CTBD/CW-NF-CTBD) mS/cm, flow rate = 580 mL/min, reaction time = 8 h.*

In contrast, the removal rate for the concentrated CTBD samples increased from 0.11 h^{-1} to 0.14 h^{-1} and the removal efficiency from 80% to >98% with an increasing current density from 8.5 mA/cm² to 14.3 mA/cm² for the EO-NF-CTBD (Fig. 7-2b). The concentration of the TOC by the NF-membranes seemed to have improved the EO performance. This is also reflected by the instantaneous current efficiency (ICE),

which was approximately 34 % for the EO-NF-CTBD after 4 h of treatment, while this was 5 % for the EO-CTBD (Fig. 7-2c). The increased EO performance as a result of prior concentration by NF membranes could be a result of a change in electrolyte ratio. The electrolyte ratio for SO_4^{2-}:Cl^- in the EO-NF-CTBD was approximately 2.5:1, while this is 0.9:1 for the non-concentrated EO-CTBD, as a result of SO_4^{2-} retention by the NF membrane (Table 7-4). A previous study has shown that SO_4^{2-}:Cl^- electrolyte ratios between 10:1 and 2:1 can substantially enhance the radical formation and thereby result in a better removal performance (**chapter 4**). A relatively higher SO_4^{2-} content results in an increased formation of $HO^{\bullet}$, which facilitates the formation of $SO_4^{\bullet-}$, leading to efficient pollutant degradation and mineralization (**chapter 4**). Hence, concentrating the CTBD before EO treatment increases the removal efficiency, removal rate and ICE. Treatment of the CTBD by CWs before concentration by NF does not seem to have an apparent effect on the EO performance.

7.3.3.2 Chlorinated byproduct monitoring

The concentrations of chloride and chlorinated by-products in terms of halogenated organic compounds (AOX), free chlorine, chlorate, and perchlorate were monitored during EO treatment to assess the formation of potentially toxic by-products. The EO-CTBD sample contained approximately 463 mg/L chlorides, while this was approximately 375 mg/L for the concentrated EO-NF-CTBD and EO-CW-NF-CTBD (Fig. 7-3a). The starting concentration of AOX is 0.9 mg/L, whereas the initial concentration of the other chlorinated products is zero.

After 6 h of EO-treatment at 8.7 mA/cm^2, 70-75 % of the chloride was converted into other chlorine species, and this increased to a 90 % conversion after 8h (Fig. 7-3a). At 14.3 mA/cm^2, more than 95 % of the chloride was converted to other chlorine species (Fig. 7-3a). During treatment of the EO-CTBD, 60 mg/L of free chlorine was formed after 6 h, which decreased to a concentration of 30 mg/L after 8 h (Fig. 7-3b). Substantially less free chlorine was formed during EO-treatment of the concentrated CTBD for both current densities after 6 and 8 h. (Fig. 7-3b). A higher free chlorine production in the original CTBD was the result of higher chloride concentrations and less active radicle formation. In addition to free chlorine, AOX was formed, with the highest concentrations observed for the EO-CW-NF-CTBD treatment at 8.5 mA/cm^2 after 6 h (Fig. 7-3c).

(a) Chloride

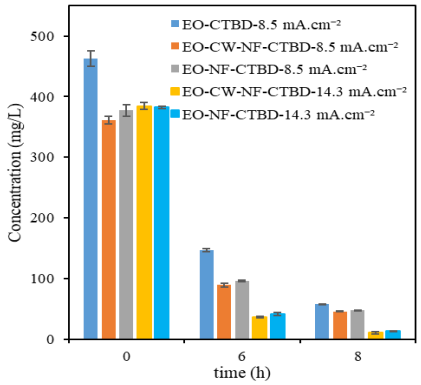

(b) Free chlorine

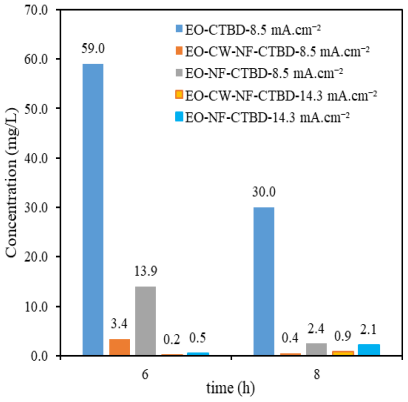

(c) AOX

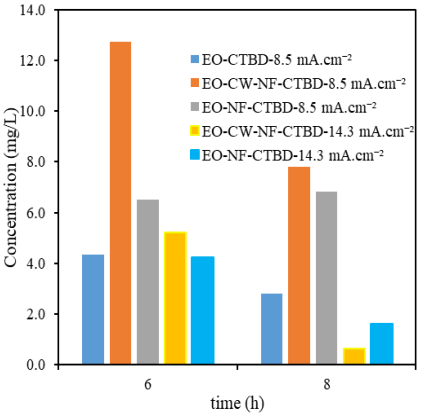

(d) Chlorate

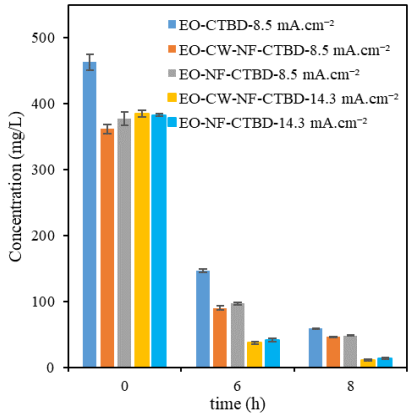

(e) Perchlorate

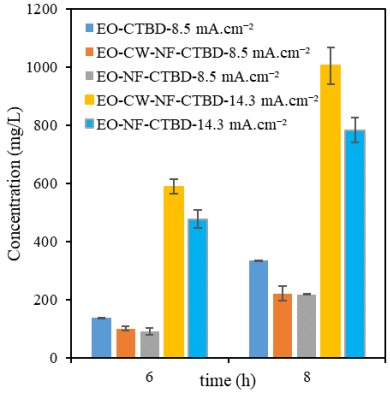

Fig. 7-3. *(a) Chloride, (b) free chlorine, (c) AOX (d) Chlorate and (e) perchlorate . Experimental conditions: 350 mL sample T = 25-30°C, current density = 8.5 or 14.3 mA/cm², conductivity = 3.63 (EO-CTBD) and 6.36 (NF-CTBD/CW-NF-CTBD) mS/cm, flow rate = 580 mL/min, reaction time = 8 h.*

Increasing current densities and treatment times resulted in decreasing AOX concentrations (Fig. 7-3c). The concentrations of AOX and free chlorine in this study were lower than observed in a previous CTBD EO study of our group, of which 17 mg Cl^-/L of AOX and 152 mg/L of free chlorine were produced at comparable experimental conditions (an EC of 3.7 mS/cm and applied current density of 8.7 mA/cm^2) [198, 260]. A higher current density and extended oxidation period most likely facilitated the degradation of AOX, but also converted free chlorine to chlorate and perchlorate for all pre-treatments after 6 h (Fig. 7-3d, 7-3e). A substantially higher amount of perchlorate was produced during 6h EO-treatment of the concentrated samples EO-NF-CTBD and EO-CW-NF-CTBD compared to the non-concentrated EO-CTBD (Fig. 7-3e). Increasing the treatment time to 8 h led to a decrease in the chlorate concentration (Fig. 7-3d) and further perchlorate production (Fig. 7-3e). The chlorate and perchlorate concentrations produced for the EO-CTBD (Fig. 7-3d; 7-3e) are higher than observed in previous studies at comparable experimental conditions (EC of 3.7 mS/cm and an applied current density of 8.7 mA/cm2) were 302 mg/L chlorates and 82 mg/L perchlorates were produced [198, 260]. This is likely the result of an extended oxidation duration, leading to the generation of more $HO^{\bullet}$ that facilitates the conversion of chlorate to perchlorate. An increasing applied current density similarly results in an increased generation of $HO^{\bullet}$. It can be concluded that prior concentration of CTBD by NF or before EO-treatment does not have a unilateral effect on the formation of toxic by-products: On the one hand, concentrating the CTBD results in a lower formation of free chlorine, while on the other hand, the production of AOX, chlorate and perchlorate increases. An increasing oxidation time results in a decreased concentration of free chlorine, AOX, and chlorate, while more perchlorate is produced, which becomes more apparent at higher applied current densities. Constructed wetland pre-treatment before NF-concentration seems to result in a slightly increased formation of, especially, perchlorate.

7.3.4 Reverse osmosis of the nanofiltration permeate

RO of the NF permeate resulted in a permeate that met a set of generic water quality requirements for broad reuse application in the industry for both treatment trains, as defined by Groot et al. (2015): an EC of < 1 mS/cm, chloride concentration of < 150 mg/L, TOC concentration of < 15 mg/L, phosphate concentration of < 1

mg/L (Table 7-5) [17]. Consequently, a concentrate was produced that contained high concentrations of mono- and divalent ions (Table 7-5). In the case of non-CW pre-treated CTBD, this concentrate also contains substantially higher concentrations of NO_3^- and benzotriazole than the initial CTBD, which could result in problems with further treatment or disposal.

Table 7-5. *Composition of reverse osmosis permeates and concentrates.*

	NF-permeate of direct cooling tower water			NF-permeate of constructed wetland pre-treated cooling tower water		
	Influent	Permeate	Concentrate	Influent	Permeate	Concentrate
EC (mS/cm)	2.59	0.05	12.6	2.37	0.04	11.9
pH	7.42	6.22	7.7	7.04	6.12	7.78
TC (mg/L)	12	2.95	61.41	24	2.9	128
TOC (mg/L)	1.7	1.9	11	1	1.2	3.7
Benzotriazole (µg/L)	57	<2.5	667	<2.5	<2.5	<2.5
TIC (mg/L)	10	1	50	22	1.7	124
TN (mg/L)	14	0	77	3	0	12
NO_3^- (mg/L)	57	1.8	319	10	0.4	47
SO_4^{2-} (mg/L)	263	2	1581	157	1.1	904
Cl^- (mg/L)	616	10	3534	605	10	3523
Ca^{2+} (mg/L)	163	1.5	977	145	1.2	850
Mg^{2+} (mg/L)	27	0.3	160	22	0.2	133
K^+ (mg/L)	45	0.8	257	51	1	310
Na^+ (mg/L)	283	5.6	1650	253	5	1494

7.3.5 Considerations for full-scale application of the integrated technology-train

Using an integrated treatment train of CWs, NF, EO, and RO, it is possible to produce a water stream from CTBD that can be applied for many purposes within the industrial sector. However, various factors should be taken into consideration before the full-scale application of this treatment train for the treatment of CTBD, such as the water recovery, the production and disposal of concentrated streams, the reuse of water quality requirements and application, the maturity of the technological and green compartments of the treatment train and the related CAPEX and OPEX [17, 420-422]. The water recovery of the currently studied treatment train is < 70% and varies over the year as the result of climatic influences on the CWs, such as increased evapotranspiration in summer resulting in an increased water loss (Fig.

S7-2). This water recovery is lower than earlier studied options for recovery of the same water stream, such as electrodialysis reversal (81%), capacitive deionization (71%), and membrane distillation (76%) [17]. However, various potential show stoppers that were identified with these technologies, such as too high residual concentrations of TOC and phosphate [17], were overcome by combining the technologies in the studied treatment train. The water recovery of the studied treatment train can be increased. 80% of the total water volume from the CW effluent was recovered after NF. A higher recovery could be obtained by a higher concentration of the CTBD, which could, however, lead to increased fouling of the NF membranes [423]. In addition, the concentrate could be brought back into the treatment train, for instance, after EO-treatment. EO-treatment results in the degradation of organic substances but in the production of unwanted by-products (section 7.3.2.2). However, CWs can remove these by-products, albeit at the expense of the viability of the plants [260]. Nevertheless, a sacrificial CW without plants could be used in sequence or parallel with the CWs to directly treat CTBD to remove these by-products from the concentrate. In addition, by-product formation from EO-treatment of CTBD can be prevented as a result of new insights into the effects of ion ratios on the by-product formation **(Chapter 4)**. A further step to increase the water recovery would be to leave out RO of the treatment train since RO results in a final product of which the main product quality requirement EC of 50 µS/cm is far below the required product quality of 1000 µS/cm for generic reuse of water for industrial applications [17]. This would mean that NF only would be responsible for the desalination of the CTBD. The NF membrane currently does not retain enough monovalent ions to reach the desired product quality. However, ongoing developments in the field of membrane fabrication resulted in the development of layer-by-layer membranes with alternating charge densities that increase the retention of monovalent ions [400, 401], which can eventually reach the desired product quality with only NF. The application of only one filtration technology would also lead to only one concentrated stream to treat or dispose of, instead of the NF-concentrate and RO-concentrate in the currently studied treatment-train. However, the technology readiness level (TRL) of these innovative membranes is currently not sufficient yet for full-scale application, although the developments follow rapidly as a result of their potential broad application. The same applies for EO-treatment with the anodes that were applied in this study. In contrast, the CWs, NF-membranes used in this study and RO are of a sufficient TRL for full-scale

application at this moment. A detailed CAPEX and OPEX analysis of the treatment-train as studied was outside the scope of this study.

7.4 CONCLUSION

The integration of CWs, NF, EO, and RO in a treatment train allows the production of a water stream from CTBD that meets commonly applied industrial reuse threshold concentrations for EC, chloride, phosphate and total organic carbon. The use of CWs as a first treatment step prevents the accumulation of commonly applied corrosion inhibitor benzotriazole and nitrogen species in later concentrate streams as a result of complete biodegradation in the CW. Pre-treatment by CWs does seem to result in increased fouling of NF-membranes as a result of inorganic carbon species. The applied NF-membranes had a limited capability in retaining monovalent ions, and therefore, subsequent desalination by RO was still needed. The retention of divalent ions by the NF-membranes led to more efficient EO-treatment of the NF-concentrate compared to direct CTBD in terms of degradation of recalcitrant humic acids and less chlorinated by-product (AOX, and chlorate) formation as a result of different SO_4^{2-}:Cl^- ratios. But perchlorate formation was increased. Full-scale application of the treatment train would benefit from the demonstrated improvement in water recovery, the application of innovative new NF-membranes (that may make RO-treatment redundant), and the adoption of new anode material in preventing unwanted by-products formation during EO-treatment.

Chapter 8. *General discussion*

Advanced oxidation processes in saline water for organic compound removal.

8.1 INTRODUCTION

"Freshwater is the most essential natural resource on the planet" [424]. Only 1.8% of total global water is freshwater, of which only 3% is considered to be easily accessible for ecosystem and human activity [425, 426]. Human activities, such as irrigation, industrial process, and energy generation, heavily depend on a significant amount of freshwater available. It is also seen that human activity is responsible for the redistribution of the global water cycle. IPCC's sixth climate change assessment report emphasizes that "Continued global warming is projected to intensify further the global water cycle, including its variability, global monsoon precipitation, and the severity of wet and dry events" [424]. Thus, ensuring the freshwater demand and supply concerning time and place is essential for a safe and sustainable ecosystem, human life, and economic activity. Cooling systems in the energy generation and process industry use a huge amount of freshwater [14, 427]. The reuse of the discharge of these systems could reduce the freshwater footprint and contribute to preserving the water cycle.

The cooling system discharges, called cooling tower blowdown (CTBD), contain organic compounds (OCs) and salts. Removing the organic compounds and the salts is essential to enable the CTBD to be reusable. In addition, many of the organic compounds are non-biodegradable and challenging to remove with conventional wastewater processes. In the last couple of decades, advanced oxidation processes (AOPs) have become an attractive technology to eliminate those OCs. In the AOPs, highly reactive oxidating species are produced, which are potent to degrade non-biodegradable OCs. In this thesis, four AOPs were studied for better understanding and improvement for application in real saline conditions. Electrochemical oxidation, photocatalytic degradation, heat-activated persulfate oxidation, UVC/vacuum UV process were studied. Special attention was given to the electrochemical oxidation process. All AOPs were evaluated and compared with respect to OCs removal efficiency and toxic by-products formation potential. In this general discussion chapter, three issues are elaborated: 1) significance of AOPs for CTBD treatment, 2) application of AOPs, 3) a survey is carried out on the fate of chlorine ions in state-of-the-art AOPs. This has been done by studying the differences in the working principle, radical sources, and activation mechanisms in the different AOPs based on this thesis and literature. This chapter will provide

essential knowledge to select suitable AOPs for removing organics in saline conditions. A graphical presentation of this chapter to visualize the content is shown in Fig. 8-1.

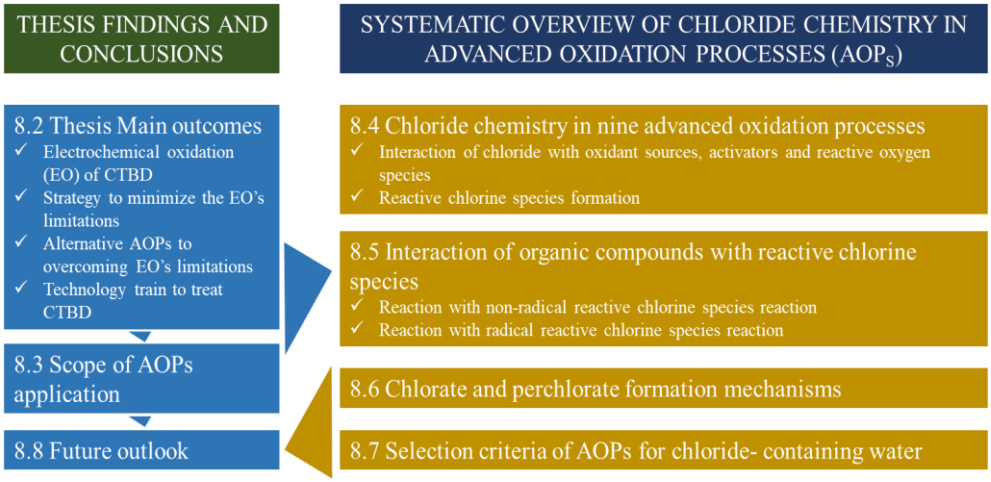

Fig. 8-1. *Outline of this chapter*

8.2 MAIN OUTCOMES OF THIS THESIS

8.2.1 Feasibility and the limitation of electrochemical oxidation

Cooling tower blowdown water (CTBD) contains OCs and salts. In order to reuse the CTBD in the cooling tower itself, both salts and the OCs need to be removed. Membrane desalination techniques have been used for years to remove salts. However, OCs, especially humic substances, present in the CTBD cause membrane fouling and need to be removed in a pre-treatment. In **chapter 2,** the potential and limitations of the electrochemical oxidation process were studied with respect to OCs removal from CTBD. Experiments indicate that EO could mineralize half of the OCs with boron-doped diamond (BDD) at an applied current density of 8.3 mA/cm^2 after three hours of treatment. In contrast, the rest of the OCs were partially oxidized to low molecular OCs. Interestingly it was also found that COD removal was almost 100%. This difference in COD and TOC removal indicates that most organic carbons were oxidized and chlorinated to a higher oxidation state. This type of removal implies that EO could be an interesting technique to remove the

OCs from CTBD and reduce the membrane fouling during desalination. The mixed metal oxide (MMO) anode showed limited OCs removal efficiency. In addition, process parameters including pH, hydrodynamic conditions, and the addition of supporting electrolytes had little effect on the process performance. Unfortunately, a substantial amount of chlorinated compounds, including AOX, chlorate, and perchlorate, were formed during the EO process, especially with the BDD anode and at a higher applied current. This unwanted chlorinated by-product formation limits the application of the EO under the real conditions that exist in practice.

8.2.2 Minimizing the limitations of the electrochemical oxidation process

From Chapter 2, it was found that still half of the TOC remains in the CBTD after EO treatment. In addition, chlorinated by-products were formed. In order to minimize those limitations, EO was combined with vertical-flow constructed wetlands (VFCWs). **Chapter 3** shows that integrated VFCW followed by the EO (CFCW-EO) system could remove more organic compounds than the standalone EO systems with BDD or MMO anode. Thus, VFCW help to improve the OCs removal. However, the subsequent EO process produces a significant amount of chlorinated compounds toxic to *Vibrio fischeri*. In a system with EO followed by VFCW, OCs removal was less effective. However, the VFCW was able to remove a substantial amount of chlorinated compounds. Unfortunately, the toxic chlorinated compound negatively affected the VFCW performance and even caused plants death. Thus, further research is required to understand the toxicity mechanism in the VFCW and find out mitigation strategies. Furthermore, evapotranspiration in the VFCW caused a significant water loss during the lab experiment. Maybe under real outdoor conditions, water loss would be compensated with precipitation.

In the electrochemical oxidation process, hydroxyl radicals and active chlorine species are formed, which facilitates the oxidation of the OCs. The active chlorine species are responsible for the chlorinated by-product formation. Previous research shows that reactive sulfate species (sulfate radicals and peroxydisulfate) could be generated during the EO of sulfate-containing water. These reactive sulfate species also could facilitate the oxidation of the OCs. In **chapter 4**, the effect of electrolyte composition on active sulfate formation, benzotriazole degradation, and chlorinated

by-products distribution during EO was studied. Results show that hydroxyl radicals mediate the active sulfate species (sulfate radicals and peroxydisulfate) formation at the BDD anode. In addition, active sulfate species formation was higher at a high sulfate to nitrate ratio. Interestingly, active sulfate species formation was low at electrolytes containing only sulfate due to the chemisorption of sulfate on the BDD anode. Benzotriazole degradation and mineralization were faster in high sulfate to nitrate or chloride ratios. Higher sulfate to chloride ratio also helps to suppress the chlorinated organic by-products formation. Furthermore, energy consumption becomes less in sulfate-rich conditions. This finding indicates that combining the EO with a desalination technique to yield sulfate-rich conditions will be interesting. However, chlorate and perchlorate formation was unavoidable, even becoming more dominating at sulfate-enrich conditions. Thus, an alternative process is required to minimize the unwanted chlorate and perchlorate formation.

8.2.3 Application of persulfate, photocatalytic, and ultraviolet-based (VUV/UVC) as alternative treatment techniques

Chapters 2, 3, and 4 show that reactive oxygenated species (hydroxyl radicals, active sulfate species, and reactive chlorine species) could oxidize the OCs. However, chlorinated by-product formation was unavoidable during electrochemical oxidation. It is well established that direct oxidation of the chloride ion on the electrode surface produces the reactive chlorine species. Those chloride species are responsible for the chlorinated by-product formation. In **chapter 5,** a persulfate-based oxidation process was studied to evaluate its performance in the presence of chloride. The study used heat-activated- peroxydisulfate (PS) and peroxymonosulfate (PMS) processes for radical formation. Benzotriazole (BTA) was used as a model organic compound, a concerning micropollutant that is found in CTBD. Chloride ion negatively affects the BTA degradation in PS at all concentrations. On the other hand, chloride ion positively affects the BTA degradation in PMS up to certain concentrations. PMS directly reacts with the chloride to produce free chlorine, which boosts the BTA oxidation and formation of chlorinated compounds, and 14 chlorinated organic transformation products were found after the PMS-based oxidation. In addition, 10 to 30 mg/L chlorate was formed in this PMS process. In the case of the PS-based oxidation, chlorate was not

detected, but eight chlorinated organic transformation products were found. A very small amount of free chlorine was found after the PS process. Sulfate radicals formed in the PS process could react with chloride ions and yield chlorine radical, further converted to free chlorine. Those free chlorine and chlorine radicals could initiate the chlorinated organic transformation products in PS. This study shows that free chlorine was the main precursor of chlorinated by-produce formation. Thus, free chlorine formation should be avoided or minimized to subside chlorinated by-product formation.

The outcome of **chapter 5** was tested in real CTBD conditions, and experiment results have been reported in **chapter 6**. This chapter evaluated and compared electrochemical oxidation, photocatalytic degradation, heat-activated persulfate oxidation, UVC/vacuum UV process based on OCs removal efficiency, and chlorinated by-products formation tendency. After five hours of treatment, heat-activated peroxydisulfate (PS) AOP reached almost complete mineralization of OCs presence in the CTBD. On the other hand, electrochemical oxidation, photocatalytic degradation, and VC/vacuum could get 50-60% mineralization. Detail analysis of the humic substance analysis shows that electrochemical oxidation, photocatalytic degradation, and UVC/vacuum break down the humic substances to low molecules substance. However, the PS process could break down the humic substances completely. As mentioned in chapter 5, free chlorine is the key to chlorinated by-product formation. Chlorinated by-products, AOX and chlorate, were not detected during photocatalytic degradation, heat-activated peroxydisulfate oxidation, and UVC/vacuum UV AOPs. These AOPs would be promising techniques for the (pre)treatment of saline water, like CTBD, containing organic compounds, including humic substances.

8.2.4 Technology train to treat cooling tower blowdown

Chapter 3 shows that constructed wetland (CW) could remove the organic compound, including benzotriazole. In addition, a fellow PhD researcher of the Water Nexus program shows that constructed wetland could remove humic substances and benzotriazole [18, 140, 187, 191, 400]. Moreover, **chapter 4** shows that electrochemical oxidation of the organic compound in sulfate-enriched electrolytes was more effective concerning removal rate, energy efficiency, and

chlorinated organic by-product formation. Based on the outcomes mentioned above, a technology train was proposed for CTBD treatment in **Chapter 7**. Technology train included CW, nanofiltration (NF), EO of NF concentrate, and reverse osmosis (RO) of NF permeate. CW has effectively removed benzotriazole and nitrogen species, increasing inorganic carbon concentration in the effluent. CW pre-treatment negatively affected subsequent NF flux. Direct NF of CTBD effectively separated OCs and divalent ions, but benzotriazole passed through it. The polishing RO step could remove the nonvolant salts and the remaining OCs from the NF permeate. Due to sulfate-enriched electrolytes conditions, EO of NF concentrated was more effective and energy-efficient than direct EO of CTBD. However, perchlorates formation was significantly high during the EO of NF concentrate. The EO experiment outcome was in agreement with the outcome of **chapter 4.** Overall, it was concluded that further improvement of the NF membrane and the EO process is required before full-scale application.

8.3 SCOPE OF APPLICATION OF AOPS

On one hand, freshwater demand is increasing; on other hand, freshwater supply is shrinking. Water suppliers and companies thus, start looking for wastewater reuse potential. For instance, municipalities are interested in using treated municipal wastewater as a source of drinking water; industries are looking for the opportunity to reuse treated industrial wastewater themself or use it in other applications. Because of increasing anthropogenic activities, wastewater becomes more contaminated with persistent organic pollutants (POPs), such as pesticides, pharmaceuticals, personal care products, and industrial chemicals. It is documented that 2 million tons of domestic, agricultural, and industrial waste are discharged into the water body each day globally [428]. AOPs are capable of eliminating these POPs. Therefore, AOPs are becoming an integral part of water reuse treatment, drinking water production, and municipal and industrial wastewater treatment technology trains.

In many places, drinking water is produced from surface water sources, including lakes, ponds, and rivers [97]. Intentionally or unintentionally, treated and untreated municipal and industrial wastewater ends up in the surface water source after discharge. AOPs work as barriers for POPs and pathogens to protect these

water sources. For instance, many potable water reuse plants use the UV/H_2O_2 AOP as the tertiary treatment step [97]. In 2016, the terminal island water treatment plant, Los Angeles, CA, USA, started using UV/Cl_2 AOP to remove pathogens and trace POPs [97]. Andijk WTP, built by PWN Water Supply Company, North-Holland, shows that a technology train including coagulation → sedimentation→ rapid sand filtration → medium pressure UV/H_2O_2 → biologically active carbon filtration → dune infiltration is able to produce safe drinking water. In this plant, Lake Ijssel is used as the raw water source. In this treatment train, UV/H_2O_2 AOP serves as a barrier for micropollutants [97]. Ozone-based AOPs (alone or combined with UV/H_2O_2) also get extensive attention for potable water reuse treatment plants. However, bromate formation hinders the application of ozone-based AOPs for drinking water production [429, 430]. Day by day, groundwater also gets contaminated with the POPs, creating concern for water companies [431]. AOPs, mostly UV/H_2O_2, is applied to eliminate POPs [97].

In general, municipal wastewater treatment consists of primary treatment (screening and primary clarification), secondary treatment (secondary clarification normally with the activated sludge process), and polishing treatment with (membrane) filtration. In this technology train, AOPs can be used as a pre-treatment step before secondary treatment to degrade POPs to small molecules, which could be removed in subsequent activated sludge processes. AOPs can also be used as post-treatment of secondary clarification effluent to remove emerging micropollutants. In addition, AOPs can also be applied as a disinfection step after polishing. Research also shows that AOPs can help with sludge conditioning and reverse osmosis concentrate treatment. So AOPs have the potential to become an integral part of the municipal wastewater treatment system [56, 60, 97, 432].

Like municipal wastewater treatment, AOPs can serve as a pre-treatment step to increase the bio-degradability of POPs and as a post-treatment step to remove the remaining OCs from industrial wastewater. Numerous studies have reported the application of AOPs for pharmaceutical, textile, pesticide, paper mills, petrochemical, food, tannery industries, and landfill leachate wastewater treatment. It is noteworthy to mention that industrial wastewater properties vary from industry to industry and within the industry [97, 283, 433]. Therefore, the selection of AOPs is crucial for effective performance.

Water from all the sources contains chloride ions. As discussed before, AOPs have high potentials to remove OCs from wastewater; however, they face challenges due to toxic chlorinated by-products formation. Research in this thesis shows that the effects of chloride ions varied a lot in different AOPs. Also, the chlorinated by-product formation mechanism depends on the reactive chlorine species and their distribution. For instance, free chlorine/ hypochlorite ions are the precursor of both organic and inorganic chlorinated compound formation. This precursor is dominant in electrochemical oxidation and some other processes (**chapters 4 and 5**). Thus, it is crucial to understand the chloride chemistry in each AOPs, which could guide stakeholders to select a suitable technique to remove organic compounds in saline conditions without toxic by-products formation.

8.4 CHLORIDE CHEMISTRY IN DIFFERENT AOPS

Generally, AOPs produce reactive oxygen species to degrade the OCs. Reactive oxygen species are generated as a result of the interaction of the source and the activator. The presence of chloride in the water introduces additional dynamics in the treatment system. Chloride chemistry and its dynamics vary a lot in different AOPs studies in this thesis. For instance, it was reported in this thesis; chloride could interact with the reactive oxygen species, sources, and activators involved in the AOPs. All the interactions are different and need proper understanding to minimize their negative influence. In this following section, chloride interaction in all state-of-the-art AOPs is elaborated based on this thesis and literature.

8.4.1 Electrochemical oxidation

In electrochemical oxidation (anodic oxidation), electrical energy is applied to oxidize the water to yield hydroxyl radicals **(chapter 2)**. In addition, active sulfate species (sulfate radical and peroxydisulfate) are also produced **(chapter 4)**. In general, more than 2.6V/SHE has to be maintained in the anode to facilitate radical formation [69, 231]. In presence of chloride, direct electrolysis of chloride takes place at this potential. Chloride oxidation on the anode surface yields Cl_2 **(chapters 2, 3, 4, and 6)**[69]. In general, either active anodes (RuO_2-, Sb_2O_4, IrO_2, TiO_2, or mixed metal oxide of these materials) or nonactive anodes (SnO_2, PbO_2, BDD, and Ti_4O_7) are used [434]. Active anodes are suitable for chlorine evaluation reactions

[435]. Nonactive anodes also catalyze the chlorine evaluation reaction to form chlorine only at higher operation potential [221, 251, 436]. **Chapter 2** shows that both MMO and BDD anode produce active chlorine species. Three different chlorine evolution pathways have been proposed in the literature [437]. Among those, the Volmer–Heyrovsky mechanism is considered as the most probable pathway on RuO_2- anode. In this path, chloride ions are initially directly adsorbed to the active sites of the anode surface and recombine with another adsorbed chloride ion to yield chlorine (Eq. 8.1) [437]. This chlorine Cl_2 reacts with water to form HClO and ClO^- by pH-controlled equilibrium reactions Eqs. (8.2-8.3) [438]. This unavoidable chlorine evolution reaction in the electrochemical oxidation process makes this process most vulnerable for chlorinated by-product formation.

$$2Cl^- \rightarrow Cl_2 + 2e^- \quad (8.1)$$

$$Cl_2 + H_2O \rightleftarrows HClO + Cl^- + H^+ \quad (8.2)$$

$$HClO \rightleftarrows ClO^- + H^+ \quad (8.3)$$

In addition, hydroxyl radical and active sulfate species are the dominating oxidant involved in the anodic oxidation process **(chapter 4)**. Interaction of chloride with active sulfate species has been discussed in detail in the context of sulfate-based AOPs (section 8.4.2). The hydroxyl radical directly reacts with chloride ions to form ClOH• (Eq. 8.4). This reaction has a very low reaction rate. ClOH• undergoes a series of equilibrium reactions to form $Cl^•$ and $Cl_2^{•-}$ (Eqs. 8.5-8.6). Details of the reaction mechanism are found elsewhere [439]. The overall rate constant of the final reactions is $k = 1.4\times10^5$ $M^{-1}s^{-1}$. $Cl_2^{•-}$ is the dominant radical species in natural conditions. All those reactions are very pH sensitive and become significant at acidic pH (<3). Recombination of two $Cl_2^{•-}$ or interaction between $Cl^•$ and $Cl_2^{•-}$ could yield chlorine (Eq. 8.7) [439] that further hydrolyzes to hypochlorite, as discussed earlier (Eqs 8.2-8.3).

$$HO^• + Cl^- \rightarrow ClOH^{•-} \qquad k = 0.7 \pm 0.13\ M^{-1}s^{-1} \quad (8.4)$$

$$ClOH^{•-} + H^+ \rightarrow Cl^• + H_2O \qquad k = 7.2 \pm 1.6 \times 10^6\ M^{-1}s^{-1} \quad (8.5)$$

$$Cl^• + Cl^- \rightarrow Cl_2^{•-} \qquad k = 1.4 \pm 0.2 \times 10^5\ M^{-1}s^{-1} \quad (8.6)$$

$$Cl^•(Cl_2^{•-}) + Cl_2^{•-} \rightarrow (2)Cl^- + Cl_2 \quad (8.7)$$

8.4.2 Sulfate radical based AOPs

In sulfate radical-based AOPs, sulfate radicals are produced by activating peroxymonosulfate (PMS) or peroxydisulfate (PDS) **(Chapters 5 and 6)**. Numerous activation processes have been studied until now. In general, heat (30-70^{o}C), UV light (248-351 nm), transition metal and metals and oxides [(Fe^0, Fe (III)), Co(II), $CuCo_2O_4$, $LnMnO_3$, Fe/Co, Co_3O_4/C_3N_4], alkaline conditions, gamma-ray, ultrasound, activated carbon, graphene, biochar, H_2O_2, ozone, electrochemistry and organics (Phenol/quinones) are used to activate PDS and PMS [90, 440]. The interaction of chlorine with electrochemistry, UV, H_2O_2, ozone, gamma-ray, and ultrasound, is the same as described in the relevant sections 8.4.1, 8.4.4, 8.4.5, 8.4.7, and 8.4.9. Heat, alkaline conditions, activated carbon, graphene, and biochar have less direct interaction with chloride. After activation, sulfate radicals, hydroxyl radicals, and $HO_2^{\bullet}/O_2^{\bullet-}$ are the dominating reactive radical species formed in this AOP [55, 284, 329]. The reaction of chloride with hydroxyl radicals is broadly discussed in the electrochemical oxidation AOP (section 8.4.1). Chloride ion reacts with sulfate radicals by an electron transfer mechanism to form chlorine radicals (Eq. 8.8) (3.2×10^8 M^{-1} s^{-1}) which rapidly convert to $Cl_2^{\bullet-}$ [299]. $HO_2^{\bullet}$ /$O_2^{\bullet-}$ show limited reactivity with chloride [441]. In addition, several other non-radical mechanisms have been reported for organic compound degradation. The non-radical mechanism includes $^1O_2$ (surface-mediated) electron transfer; surface bounded active complex formation, high valent metal oxidation, and inorganic oxidants (ClO^-/HOCl) [329, 440]. $^1O_2$ is moderately electrophilic. Chloride ions react very slowly with $^1O_2$ (10^3 $M^{-1}s^{-1}$ in D_2O), whereas $^1O_2$ can be quenched by water at the rate of 2.5×10^5 s^{-1} [441]. Thus, a reaction between $^1O_2$ and chloride would be less obvious. Several authors believe that the non-radical mechanism, including surface-mediated electron transfer, surface bounded active complexes, and high valent metal is less influenced by the chloride ion. Since these non-radical mechanisms do not involve radicals, it is hypothesized that active chlorine species formation will be avoided [329, 440]. Therefore, AOX and chlorate, and perchlorate formation could be prevented. However, the direct interaction of PMS with chloride ions occurs regardless of the radical or non-radical pathway [442]. PMS and chloride ions react to form free chlorine, which is enough to initiate AOX and chlorate formation **(chapter 5)**. It is considered that ClO^-/HOCl is the dominating precursor of starting

the formation of the chlorinated by-product. Fortunately, PDS has very limited direct interaction with the chloride ion. Thus, PDS-mediated non-radical oxidation of OCs will be less vulnerable to toxic chlorinated formation than PMS-mediated **(chapter 5)**.

$$SO_4^{\bullet-} + Cl^- \rightleftarrows Cl^{\cdot} + SO_4^{2-} \qquad k_f = 3.2 \times 10^8\ M^{-1}s^{-1};\ k_b = 2.5 \times 10^8\ M^{-1}s^{-1} \qquad (8.8)$$

Sulfate radical-based oxidation is more sensitive to chloride ions compared to hydroxyl radical-based oxidation. The reaction between sulfate radicals and chloride ions yields chlorine radicals, which are similar to hydroxyl radicals' reaction with chloride ions to form chlorine radicals. However, the former reaction is less influenced by the solution pH, whereas the reaction between sulfate radical and chloride ion interaction is very pH-dependent and mainly occurs in acidic conditions [97]. So, in sulfate radical-based oxidation, the introduction of $Cl^{\bullet}$ and $Cl_2^{\bullet-}$ is more evident. Therefore, monitoring the AOX, chlorate, and perchlorate formation are equally important with monitoring the OCs removal efficiency.

8.4.3 (Electro-)Photocatalytic AOPs

As discussed in **Chapters 1 and 6**, the photocatalytic process involves semiconducting materials like TiO_2 with UV photons to generate holes and excited electrons, which further interact with O_2 and water at the catalytic surface yielding hydroxyl radicals, $^1O_2$ and $O_2^{\bullet-}$. In the photocatalytic process, metal oxides (TiO_2, ZnO), metal or graphene composites, doped and organics-modified TiO_2 materials, and ternary metal oxides ($BiVO_4$, $AgNbO_3$) are used as the catalysts [443, 444]. TiO_2 is the most studied photocatalyst for water treatment. Generally, UV light at higher than the UVB wavelength is used to activate the catalyst [97, 443]. At this wavelength, chloride does not have any direct interaction with photons. Catalysts also do not show any direct interaction alone with chloride rather than passivation of the catalyst surface by blocking the active side or forming salt layers at high chloride concentration [108]. Also, several studies and also **chapter 6** show that active chlorine (free chlorine) was not found during the photocatalytic process [445-447]. At pH >6.2, the TiO_2 surface becomes negatively charged, repulsing the chloride ion from the surface and reducing chloride's direct oxidation. However, a substantial amount of free chlorine was formed in the photo-electrocatalytic process at a slightly positive potential (0.1 V/SHE). Interestingly, the applied potential is too

low to facilitate direct oxidation of the chloride. In addition, at this potential, it is impossible to enable hydroxyl radical formation and water oxidation. Thus, the combined effect of photon and the positive bias allows the TiO_2 catalyst to facilitate reactive chlorine formation [108]. It was also found that in the TiO_2 based photo-electrocatalytic process under an anode potential of 1.2 V/SHE, free chlorine was the main active chlorine species, and $ClO^{\bullet}$ was absent, but high chlorate levels were found. WO_3 also showed higher chlorate formation; however, substantial $ClO^{\bullet}$ was found at similar conditions. Interestingly, a photo-electrocatalytic process using $BiVO_4$ as a photoanode did not produce free chlorine, and only a small amount of chlorate was formed in the same condition [446, 447]. Thus, the chloride oxidation pathway and corresponding active chlorine, chlorate, and AOX formation vary largely in the different semiconducting materials used in the electro-photocatalytic process.

8.4.4 Ultraviolet-based (UV) based

In these AOPs, sunlight, visible, and UV light have been extensively studied to remove organic pollutants from the different water streams [441]. The chloride ion does not directly absorb sunlight, visible light, and UV light higher than 260nm wavelength; thus, it does not influence the process [441]. However, a light at a wavelength higher than 254 nm has a minimal capacity to degrade the targeted pollutants directly. Thus, organic (sensitizers) and inorganic (photocatalyst) catalysts are applied to indirectly generate reactive oxygen species to oxidize the organic compound [448-451]. The interaction of chloride with photocatalysts is described in the previous section (section 8.4.3). Organic compounds, mainly methylene blue, rose bengal, porphyrins, and phthalocyanines, have been applied as photosensitizers [448]. Photosensitizers absorb the photon energy, go to an excited state, which further goes to a triplet excited state. This (triplet) excited state electron can be directly transferred to organic molecules or oxygen to form free radicals and superoxide ions. In addition, the energy of the excited state can be transferred to oxygen to produce singlet oxygen [449, 450]. Some studies show that dissolved organic matter (DOM) present in the water can be sensitized by photon energy to an excited triplet state (^{3}DOM*) [452]. It is speculated that the aromatic ketones and carbonyl-containing sites of the DOM facilitate this photosensitization. This photosensitized (^{3}DOM*) is capable of oxidizing chloride to $Cl^{\bullet}$ by a one-electron

transfer mechanism [441, 452]. It reacts further to $Cl_2^{\bullet-}$ (Eq. 8.9) [441]. The interaction of photosensitizer with chloride ions is rarely documented in the literature and needs further attention to avoid toxic chlorinated by-products formation. Since photosensitizers contain aromatic ketones and carbonyl groups, they may show similar interaction as DOM.

$$3_{DOM^*} + 2Cl^- \rightarrow Cl_2^{\bullet-} + DOM^{\bullet-} (< 10^6 m^{-1} s^{-1}) (E^0\, Cl^{\bullet}/Cl^- 2.59\, V/SHE) \qquad (8.9)$$

To intensify the hydroxyl radical formation in the UV-based AOPs, oxidants like hydrogen peroxide, ozone, persulfate (peroxydisulfate and peroxymonosulfate), and free chlorine have been used as the source of radicals.

In UV/H_2O_2 AOPs, UV wavelengths between 215 and 280 nm have been applied to photolyze H_2O_2 to hydroxyl radicals. At this wavelength(>200nm), chloride can absorb some photon energy but not efficiently initiate reactive chlorine species formation reactions [97, 441]. Also, in **chapter 6,** it is shown that UVC light did not influence chloride ions. In addition, the direct reaction of H_2O_2 and chloride ions are rarely reported in UV/H_2O_2 AOPs. In addition, the reactions between chloride and hydroxyl radical are the same as other AOPs (Section 8.4.1).

In UV/ozone AOP, UVC light is used to photolyze ozone to hydroxyl radical. Ozone has a maximum absorption coefficient at 260 nm [97]. Again, the direct interaction of chloride with this wavelength is less prominent. During the photolysis of ozone, initially, oxygen atoms and oxygen molecules at both ground state and excited states are formed. Later, oxygen atoms (O) and molecules undergo complex reactions to form hydroxyl radicals, ozone, and hydrogen peroxide. The detailed mechanism is discussed elsewhere [97]. Excited oxygen atoms ($O(^1D)$) are very reactive and strongly electrophilic. In an electrophilic addition reaction with chloride ion, it forms free chlorine. Ground state oxygen atoms ($O(^3P)$) are less energetic and electrophilic than excited oxygen atoms; however, they still can interact with chloride to yield free chlorine.

This reaction is similar to the reaction seen in the electrical discharge plasma process (section 8.4.8). Thus, the introduction of free chlorine in the system will then initiate AOX and chlorate formation. Studies show that ozone's introduction in a UV/chlorine process can facilitate chlorite and chlorate formation [453]. The interaction of chloride with ozone is discussed in the ozonation section (section

8.4.5). Thus, the UV/ozone process in the presence of chloride ions should monitor the AOX and oxychloride distribution.

In the UV/persulfate process, the peroxymonosulfate and peroxydisulfate are activated to generate sulfate radicals and hydroxyl radicals. UV irritation at 254nm is generally used to activate the persulfate. The interaction of chloride with this UV wavelength is limited. The interaction of persulfate with chlorides is discussed in the persulfate-based AOPs (section 8.4.2).

In the UV/chlorine process, free chlorine absorbs the UV photon energy at a wavelength between 200 to 375nm. The maximum absorption coefficient for HOCl is 101 $M^{-1}cm^{-1}$ at 236 nm, and for ClO^- is 365 $M^{-1}cm^{-1}$ at 292 nm. At 254 nm, absorbance is around 60-66 $M^{-1}cm^{-1}$ for both species [97]. At neutral pH, HOCl is the dominating form. Photolysis of HOCl primarily produces $HO^\bullet$, $Cl^\bullet$, and oxygen atoms (O). Together with the free chlorine, these species undergo a series of complex reactions to produce several oxidants, including $ClO^\bullet$, Cl_2O_2, Cl_2O, ClO_2, O_3, and H_2O_2, and perchlorate as a by-product [97]. The distribution of the chlorine species depends on UV wavelength, pH, and O_2 concentration in the aqueous environment. Thus, in the UV/chlorine process, all the reactive chlorine species are presents which cause substantial AOX, chlorate, and perchlorate formation.

In VUV AOPs, the light at a vacuum wavelength less than 200 nm is used (**chapter 6)**. Usually, low-pressure mercury lamps are used to emit light in this wavelength. This kind of lamp generally produces 90% light at 254 nm and around 10% at 184 nm wavelength [454]. Photolysis of water at 184 nm forms $H^\bullet$ and $HO^\bullet$, and e_{aq}^- is also expected together with $H^\bullet$ and $HO^\bullet$ when VUV wavelength is close to 200nm. e_{aq}^- and $H^\bullet$ are strong reducing agents[97] and thus, less favor interaction with chloride. Instead, these active species facilitate the reduction of chlorinated compounds, chlorate, and perchlorate. For instance, a chlorinated compound undergoes a reductive dechlorination reaction with e_{aq}^- at a diffusion control rate. The chloride ion directly absorbed the 185nm light. The molar absorption coefficient of chloride is around 3800 M^{-1} cm^{-1}. Photodissociation at this condition produces $Cl^\bullet$ and aqueous electrons [454-456]. When the water matrix contains 15 to 20 mg/l chloride, half of the photon intensity at 185nm is adsorbed by chloride. Thus, a higher chloride concentration solution would produce more chloride radicals than hydroxyl radicals [456]. Therefore, VUV treatment of chloride-containing

water would introduce $Cl^{\bullet}$ and $Cl_2^{\bullet-}$ and needs proper monitoring to minimize AOX formation.

8.4.5 Ozone based AOPs

During ozonation, organic compounds can be directly degraded by the electrophilic attack by the ozone molecules and indirectly by attack by the reactive oxygen species formed from the ozone [429]. Ozone can be activated or combined with other processes, including hydrogen peroxide, UV, catalyst (Fe^{2+}, metal oxide. activated carbon), photocatalysis, sonolysis, and the Fenton process. The interaction of chloride with the listed activators is discussed in the corresponding sections in this chapter.

$$O_3 + Cl^- + H_2O \rightarrow ClOH + O_2 + HO^- \qquad (k < 3x10^{-3}\ M^{-1}s^{-1}) \qquad (8.10)$$

The interaction of ozone with chloride in an aqueous solution leads to the generation of active chlorine species and chlorate (ClO_3^-) [430]. The ClOH formation reaction is comparatively slow [457]. Levanov et al. (2019) demonstrate the generation of chlorinated oxyanions due to chloride reaction with ozone and the generated hydroxyl radicals. According to this study, the chlorate formation rate depends on concentrations of the initial substances, ozone and chloride ion, solution pH, ionic strength, and temperature. For instance, the primary by-product at acidic pH is molecular chlorine (Cl_2); in alkaline and neutral conditions, ClO_3^- predominates. In acidic pH, the yield of ClO_3^- is 50-100 times lower. Recently the same groups showed that during ozonation, perchlorate also is formed [458]. Studies show that chlorate and perchlorate formation largely depends on the state of the chlorine present in the aqueous system. In chloride-dominated solution, perchlorate formatting potential was lower than in the solution containing ClO_2^- or free chlorine Fig. 8.2 [459].

Perchlorate was detected in the ozonation process because a reaction between ozone and chlorate can generate chlorate ion radicals, which leads to perchlorate formation [459-461]. These chlorate ion radicals react with the hydroxyl radical and form perchlorate [461]. In other hydroxyl radical-based processes, like UV or Fenton, hydrogen peroxide process, conversion of chlorate to chlorate ion radical is limited.

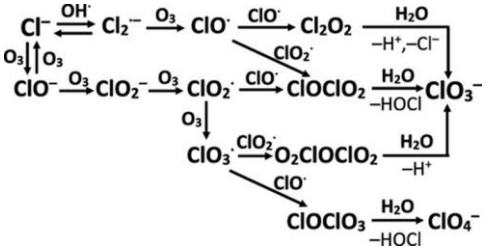

Fig. 8.2. *Proposed reaction mechanism of ozone with chloride (figure taken from Levanov et al. (2020)) [459]*

In the O_3/H_2O_2 process, the reaction between HO_2^- and O_3 at elevated pH yields hydroxyl radicals [97]. This reaction is slow at neutral conditions since the pKa of H_2O_2 is 11.8 [97]. The radical formation involves several elementary steps. It was summarized that each mole of ozone could generate one mole of hydroxyl radicals. In the elementary steps, $HO_2^{\bullet-}$, $HO_3^{\bullet}$, $O_2^{\bullet-}$, and $O_3^{\bullet-}$ are formed. Chloride does not react with $HO_2^{\bullet-}$ and $O_2^{\bullet-}$ [97]. But the reaction possibility of $HO_3^{\bullet}$ and $O_3^{\bullet-}$ with chloride is hardly studied. In addition, it is already discussed that reaction between ozone and chloride could produce free chlorine, AOX, chlorate, and perchlorate. Thus, the O_3/H_2O_2 AOP in the presence of chloride needs critical evaluation.

8.4.6 (Photo-) (Electro-) Fenton process

In the classical Fenton process, Fe^{2+} reacts with H_2O_2 and generates hydroxyl radicals and Fe^{3+}. The Fenton process generally takes place at pH 3 or lower [462, 463]. In order to intensify and (re)generate Fenton reagents, the Fenton process has been modified and combined with other processes. In the photo-Fenton process, UV and visible light irritation increase the process effectiveness by regenerating the Fe^{3+} to Fe^{2+} and forming additional hydroxyl radicals [464]. In presence of chloride and pH < 2.5, $FeCl^{2+}$ and $FeCl_2^+$ are the dominating species rather than the Fe^{3+}due to the interaction of chloride and Fe^{3+}. $FeCl^{2+}$ absorbs UV photons and is photolyzed to $Cl^{\bullet}$ [97]. As said before, $Cl^{\bullet}$ further reacts with chloride ions to form $Cl_2^{\bullet-}$. Thus, the photo-Fenton process shows higher possibilities to introduce reactive chlorine species in the system than the classical Fenton process.

In the electro-Fenton process, both Fe^{2+} and H_2O_2 can be (re)generated in situ. Fe^{3+} produced due to the classical Fenton reaction can be cathodically reduced to $Fe^{2+,}$ and cathodic reduction of oxygen can generate hydrogen peroxide. In addition,

anodic oxidation can also introduce an additional hydroxyl radical when the proper electrode and applied current are applied. In the case of anodic hydroxyl radical formation, chlorine chemistry is similar to electrochemical oxidation, which is discussed in the electrochemical oxidation (section 8.4.1.). In the electro-Fenton process, moderate oxidation conditions (applied potential is lower than the hydroxyl radical formation potential) are capable of producing chlorate, volatile chlorine, and free chlorine, but no perchlorate is formed, even when a BDD anode is used [465, 466]. Free chlorine introduction and consumption increases the AOX and chlorate formation in electro-Fenton. In the sono-Fenton process, ultrasound is introduced to accelerate the hydroxyl radical formation [467]. Furthermore, different Fenton-like reagents (Mn^{2+}, Cu^{2+}, $Co^{2+,}$ Ti^{3+}) and nanoparticles are also used to intensify the Fenton process [463, 468]. The influence of ultrasound, Fenton-like reagents, or nanoparticles on chloride species is limitedly emphasized in the literature.

8.4.7 Gamma-ray and electron beam-based AOPs

In the radiation-based (gamma-ray and electron beam) AOPs, water is radiolyzed to hydrated electrons (e_{aq}–), hydroxyl radicals, and hydrogen atoms ($H^{\bullet}$) [469]. e_{aq}– are nucleophilic; thus, it does not show affinity to react with chloride ions directly. In addition, e_{aq}– and the $H^{\bullet}$ are strongly reactive to oxygen to form $O_2^{\bullet-}/HO_2^{\bullet}$. So in oxygenated conditions, the contribution of e_{aq}– and the H• to degrade organic compounds can be neglected due to the low concentration of the organic compounds (10^{-4} mol/L) with respect to dissolved oxygen and high rate constant with the reaction with oxygen [97]. Thus, in ionizing radiation-based AOPs, hydroxyl radical is the dominating reactive species. $H^{\bullet}$ has an electrophilic character like $HO^{\bullet}$, but 3-4 order of magnitude less reactive with organic compounds. An experiment by Om P. Mishra (2016) shows that gamma-irradiated hydroxyl radicals interact with a chloride ion present in a physiological liquid and generate free chlorine [470]. The role of the gamma-irradiation in the free chlorine formation was clear, and they detected $Cl^{\bullet}$ and $Cl_2^{\bullet-}$ [470]. Thus, the direct interaction of chloride with ionization irradiation needs further study.

8.4.8 Electrical discharge plasma-based AOPs

The electrical discharge plasma AOPs involved both physical and chemical effects, which facilitate the degradation of the organic compounds. Physical effects include UV light emission, shockwave generation, electrohydraulic cavitation, and high-temperature pyrolysis. Whereas chemical effects include reactive species formation ($H^{\bullet}$, O, $HO^{\bullet}$, H_2O_2, and O_3) based on background molecules present within the discharge area [471]. Primarily, water and oxygen are the common background species that interact with plasma energy and generate reactive species. The distribution of the reactive species and the physical effect largely depend on the intercity of the discharge plasma[471]. Most of the studies focus on the formation of the physical and chemical impact and the degradation mechanism of the targeted compound. It is still unclear how the physical and chemical effects influence the chloride chemistry in the electrical discharge plasma AOPs.

High energy applied in the discharge plasma process may directly ionize chloride salts to the chlorine atom (Cl). In addition, oxygen atoms (O) could be formed due to the dissociation of oxygen molecules in the plasma process [471]. Wende et al. (2015) hypothesize that the interaction of the oxygen atom and the chloride ion could facilitate the free chlorine formation; however, it was not observed experimentally [472]. One study recently showed that a substantial amount of free chlorine was formed during an experiment involving an atmospheric pressure plasma jet, chloride-containing solution, and oxygen [473]. Haghihat et al. (2017) reported that the methylene blue degradation in saline condition was accelerated by the reactive chlorine species ($Cl_2^{\bullet-}$, HOCl) during single electrode streamer corona discharge [474]. More recently, Vít Jirásek et al. 2019 show plasma-induced free chlorine, chlorate, and chlorite formation (Fig. 8.3) [475]. In addition, Nikolenko et al. showed that a substantial amount of chlorite, chlorate, and perchlorate was from an aqueous NaCl solution in a glow-discharge plasma system [476, 477].

Aqueous oxygen atom initiates the hypochlorite ion formation, further oxidizing to chlorite and chlorate in the plasma-induced system [476, 477]. The reaction between the hypochlorite ion and the hydrogen peroxide triggers the chlorite ion, which further oxidizes to chlorate and perchlorate [475, 478]. However, the exact perchlorate formation mechanism needs further illustration. Dissolved oxygen can initiate ozone formation in the discharge plasma process, facilitating the chlorate to

perchlorate formation, the explanation of which is in the ozonation AOPs (section 8.4.5). In addition, plasma energy could start the chlorate to $ClO_3^{\bullet}$ conversion, which transferred to perchlorate via the reaction with $HO^{\bullet}$ described in the electrochemical oxidation of chlorinated solution with BDD anode.

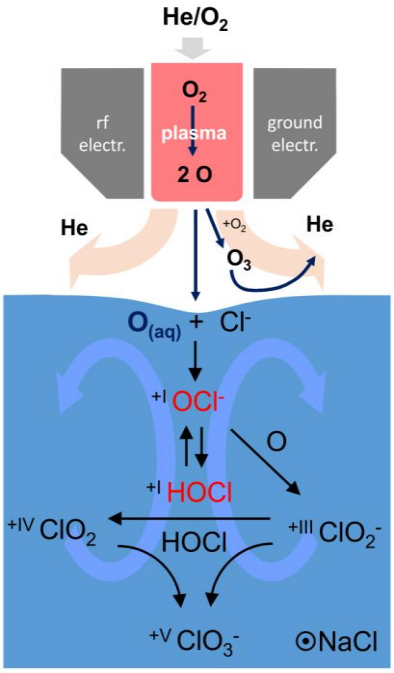

Fig. 8.3. *Oxychloride species formation pathways in the plasma discharge process (figure taken from Vít Jirásek et al. (2019) [478]*

In contrast, V. Lakhian (2020) demonstrated that aqueous phase corona discharge reduced the chlorite to chloride ion by the $H^{\bullet}$ generated during the discharge plasma [479]. Thus, both oxidation and reduction of oxychlorination compounds are expected during discharge plasma-based AOPs. So proper understanding of chloride chemistry in the discharge plasma-based AOPs is not very well explored and is essential to minimize the toxic by-product formation.

8.4.9 Ultrasound based AOPs

During the ultrasound process, cavitation bubbles are generated. During collapsing, the bubble reaches extreme conditions (4000k temperatures and 1000 atm pressure) in which radicals are produced. [97]. Dissociation of the O-H-bond in

the water molecules introduces $H^{\bullet}$, $OH^{\bullet}$, and $HO_2^{\bullet}$ radicals in the system, first within the bubble. After that, these radicals can move towards the bubble liquid interface [480]. In this way, organic compounds can cause either pyrolysis inside the bubble or/and at the bubble-liquid interface by the reactive oxygen species. During the degradation of halogenated organic compounds, like carbon tetrachloride, reactive chlorine species ($Cl^{\bullet}$, $^{\bullet}CCl_3$, $:CCl_2$, Cl_2, and HOCl) are generated [480]. In addition, the bond energy for Na-Cl is 406 KJ/ mol, which is lower than the bond energy of the O-H (460 KJ/mol) in the water molecules. Therefore, direct interaction of ultrasounds and chloride ions can be foreseen. However, it is also said that the energy is concentrated in the bubble that only contains water vapor and volatile compounds. Thus, direct chloride ion interaction is less likely to happen. However, if the water contains volatile chlorinated compound, active chlorine species are formed. The fate of chloride ions was less reported in literature on the ultrasound-based advanced oxidation process and needs more research.

8.5 REACTIVITY OF ORGANIC COMPOUNDS WITH ACS

$Cl^{\bullet}$, and $Cl_2^{\bullet-}$ are the main radical reactive chlorine species, and Cl_2, HOCl, and ClO^- are the non-radical reactive chlorine species found in the AOPs. The reactivity of the active chlorine species is described below.

8.5.1 non-radical reactive chlorine species reaction with organic compounds

Of all non-radical reactive chlorine species, HOCl is the dominant reactive chlorine species at neutral pH [97]. In the aqueous phase, the HOCl bond becomes polarized and forms $Cl^{\delta+}$ and $OH^{\delta-}$ [481]. Due to this polarization, HOCl shows three different reactions: electrophilic substitution, addition, and oxidation. In addition to reactions, a chloride ion is added to electron-rich sites of the organic compound. In a substitution reaction, an atom is substituted from the nucleophilic sites of the compounds [481]. Addition and substation reactions are mainly responsible for toxic chlorinated organic compound formation. M. Deborde and U. von Gunten (2008) comprehensively review the reactions of organic compounds

with free chlorine during water treatment [481]. The addition reaction mainly occurs in unsaturated bonds; however, the reaction rate is very low and generally neglected in water treatment conditions [482]. However, the reaction could happen at a considerable rate where the unsaturated bond is attached to electron-donating groups (amine, hydroxyl, or carbonyl) [482-484]. An organic compound containing methylene group between oxygenated moieties is able to undergo a haloform reaction to produce trihalomethanes like chloroform. Aldehydes or ketones are formed during the oxidation of alcohols containing moiety. Those aldehydes or ketones further participate in the haloform reaction [481]. Overall, chlorination reactions of the carbonyl and sulfate-containing organic compounds could reach around 10^5-10^8 $M^{-1}s^{-1}$ [481]. The aliphatic amines are chlorinated rapidly at a second-order reaction rate of 10^3-10^8 $M^{-1}s^{-1}$. Primary and secondary amines have a higher reaction rate than tertiary amines. In addition, the chlorination tendency and mechanism of amino acids and peptides are similar to the amines.

HOCl shows selective reaction tendency with compounds that have electron-rich moieties. So, in addition to the reaction with the functional groups attached to the aromatic ring, chlorination could occur to the aromatic ring via electrophilic substitution reaction. The chlorination reaction takes place in the ortho and the para position of the ring. The nature of the groups attached to the ring also affects the reaction rate. For instance, electron-donating groups attached to the ring increase the charge density, which leads to a quicker reaction rate. However, electron density varies due to intermolecular interaction and resonance in polycyclic aromatic and heterocyclic structures. Thus, it is difficult to predict the possible chlorination reaction sites. However, in general, chlorine reactivity could be arranged according to decreasing order as follows reduced sulfur moieties < primary and secondary amines < tertiary amines, phenols, < double bonds, other aromatics, carbonyls [481].

Micropollutants like atenolol, metoprolol, nadolol, propranolol, sulfamethoxazole, ciprofloxacin, and enrofloxacin contain amine function groups [481]. This amine is the primary site of attack during chlorination. For instance, b-blockers and ciprofloxacin include primary and secondary amines, and they have a second-order rate constant of 10^8 $M^{-1}s^{-1}$. Another antibacterial, enrofloxacin, contains tertiary amine and a chlorination rate of 10^3 M^{-1} s^{-1}, similar to the plane tertiary amine. Like enrofloxacin, flumequine contains tertiary amine; however, this

one was less reactive to chlorine. The nitrogen atom in the flumequine was more acidic than the nitrogen in the enrofloxacin [481].

The ortho and para position of the phenol ring is the primary electrophilic chlorination side of the micropollutants like nonylphenol, bisphenol A, steroid hormones, and acetaminophen. They show a rate constant of about 10^3 $M^{-1}s^{-1}$. Phenol may present as an undissociated and dissociated form. Dissociated phenol has a higher electron density, therefore, shows a higher chlorination reaction rate. In gemfibrozil and naproxen, ortho and para positions corresponding to the alkoxy functional group are the possible chlorination site. However, the reaction is very low, 10^{-1}- 10^{-2} $M^{-1}s^{-1}$. Sulfonamide antibacterial contains aniline group suitable to chlorination at a rate of 10^2 - 10^3 M^{-1} s^{-1} [481]. Thus, all in one, it can be concluded that organic compounds containing amine, reduced sulfur, or activated benzene rings are prone to electrophilic substation reaction with chlorine at a meaningful rate. It is interesting to mention that ozone and chloride show similar electrophilic reaction tendencies to the benzene ring. However, chlorination reaction with HOCl is four orders of magnitude slower than the reaction with ozone [97, 481].

Table 8-1. *Comparison of chlorination tendency of Fulvic fraction and Humic fraction [485]*

	Fulvic fraction	Humic fraction
Average C %	54.3	54.8
Average N %	1.17	1.9
Average aromatic %	17	32
Average aliphatic %	83	68
Average carboxyl groups	5.7	4
Phenolic groups	1.5	2.6
Chlorine consumption mg/mg of TOC	1.4	2.14
TOX ug/mg of TOC	191	256
Dichloroacetonitrile	0.64	1.48
Activated aromatic content mM/g of C	1.7	3.2

The complete structure of the humic substrate is still elusive [486]. However, analysis of humic substances shows that primary, secondary and tertiary amines, pyridine, and aniline are the major N containing functional groups in the humic substance. 65 to 90 of the N-containing functional groups are from peptide bonds that are prone to chlorination reactions [481]. Analysis shows that active aromatic sites undergo chlorination reactions. In addition, the nitrogen content is generally less in fulvic acids [486, 487], so it has less AOX formation tendency. In an experiment, David A. Reckhow (1990) estimated that 7 to 8 moles of active chlorine were consumed for each mole of the active aromatic ring. In addition, more dichloroacetonitrile was found during humic fraction chlorination (Table 8.1) [485]. The higher dichloroacetonitrile may correlate with the faster chlorination of the amine groups since the humic fraction contain more N (Table 8. 1).

Thus, the formation of HOCl needs to be avoided during AOPs to minimize the chlorinated by-production formation during the oxidation of organic compounds (micropollutants and humic substances) containing functional groups which favor the electrophilic substitution and addition reactions.

8.5.2 Radical reactive chlorine species reaction with organic compounds

$Cl^{\bullet}$ and $Cl_2^{\bullet-}$ are the main radical reactive chlorine species during AOPs. The oxidation potential of $Cl^{\bullet}$ is 2.43V, and 2.13V/SHE is for $Cl_2^{\bullet-}$ [488]. Radical reactive chlorine species show three different reactions pathway with organic compounds, including H-atom abstraction, one-electron transfer reactions, and addition reactions in unsaturated sites or electron-rich sites like benzene rings [97]. Reaction rate constants of radical reactive chlorine species with organic compounds are rarely available. The reaction rate between $Cl^{\bullet}$ and aliphatic hydrocarbon is 10^7-10^{10} M^{-1} s^{-1}, almost the same order of magnitude as with $HO^{\bullet}$. Aromatic hydrocarbons react with $Cl^{\bullet}$ at diffusion control level ($>10^{10}$ $M^{-1}s^{-1}$) [97]. Compounds with oxygenated moieties (alcohols, aldehydes, ketones, and acids) undergo H-abstraction from the C-H bond [481]. Also, H-abstraction from the O-H site can take place by a one-electron reaction. Like the chlorination reaction (section 8.5.1), H-atom abstraction and one-electron transfer reactions are also influenced by the properties of adjacent atoms (functional groups) present next to the CH and OH

groups. H-abstraction occurs more readily in a tertiary carbon than a primary carbon because an adjacent -CH_3 group to the C-H bond stabilizes the carbon-centered radicals formed due to reaction with chloride atom (Eq. 8.11). So, electron-donating groups (-CH_3, -OR, NR_2) attached to a C-H bond favor the H-abstraction reaction [441]. During the addition reaction, $Cl^{\bullet}$ attracts to the unsaturated bond and produces a corresponding chlorinated radical (Eq. 8.13), which subsequently is converted to a chloroacetic acid in the presence of oxygen. $Cl^{\bullet}$ can also be added to the benzene ring of aromatic compounds like benzene, benzoic acid, and toluene, producing chlorinated products like chlorobenzene, dichlorobenzene, or di- or trichloro phenol [441].

The lifetime of $Cl^{\bullet}$ is picosecond, whereas $Cl_2^{\bullet-}$ has a longer lifetime [97]. So, $Cl_2^{\bullet-}$ accumulates in the system, and its reaction cannot be neglected. The reaction tendency of $Cl_2^{\bullet-}$is similar to $Cl^{\bullet}$. However, the reaction rate constants are lower by 2 to 5 orders of magnitude. The reaction rate constant of $Cl_2^{\bullet-}$ with oxygenated moieties are 10^3-10^5 $M^{-1}s^{-1}$, with amino acids 10^3-10^5 $M^{-1}s^{-1}$and with unsaturated aliphatic compounds 10^6-10^8 $M^{-1}s^{-1}$ [97, 441]. With aromatic compounds, the reaction rate constant is 10^6-10^9 $M^{-1}s^{-1}$ for acids, phenol, and aniline derivatives. Both $Cl^{\bullet}$ and $Cl_2^{\bullet-}$ dominantly show H-abstraction reactions with aliphatic and aromatic compounds with NH_2 groups. One electron transfer reaction dominates with the organic compounds with electron-rich substituents, such as OH, NH_2, and OCH_3. On the positive side, this H- abstraction and one electron transfer reaction do not initiate chlorinated by-product formation.

$$RH + Cl^{\bullet}(Cl_2^{\bullet-}) \rightarrow (2)\, Cl^{-} + H^{+} + R^{\bullet} \qquad \text{H-abstraction} \qquad (8.11)$$

$$R_n(N,O,S) + Cl^{\bullet}(Cl_2^{\bullet-}) \rightarrow (2)\, Cl^{-} + R_n(N.O,S)^{\bullet} \qquad \text{Electron transfer} \qquad (8.12)$$

$$C = C + Cl^{\bullet}(Cl_2^{\bullet-}) \rightarrow Cl - C - C - Cl^{\bullet}(Cl^{-}) \qquad \text{Addition reaction} \qquad (8.13)$$

It can be seen that the addition reaction is the dominating pathway for the chlorinated by-product formation. The addition reaction is more dominating with a compound containing unsaturated bonds. The addition reaction produces chlorohydrins, chloroketons, and chloroaldehydes. Aromatic compounds containing alkyl, -Cl, and NO_2, etc. substitution in the benzene ring can undergo an addition reaction, whereas having OH, NH_2, or OCH_3 undergo a one-electron transfer

reaction [97, 441]. Thus, AOPs, in which $Cl^{\bullet}/Cl_2^{\bullet-}$ dominate, would be less favorable for treating wastewater that contains unsaturated organic compounds.

8.6 CHLORATE AND PERCHLORATE FORMATION MECHANISMS:

$ClOH^{\bullet}$, $Cl^{\bullet}$, and $Cl_2^{\bullet-}$ are the main reactive chlorine radicals, and Cl_2, HOCl, and ClO^- are the non-radical reactive species found in the AOPs. These reactive chlorine species facilitated chlorate and perchlorate formation in the oxidative condition of the AOPs.

8.6.1 Chlorate formation:

Both radical and non-radical pathways are responsible for chlorate formation. In the non-radical pathway, HOCl/ ClO^- undergoes oxidation reactions to chlorate (Eqs. 8.14-8.17). This direct oxidation is comparatively slow; however, it dominates at higher HOCl/ClO^- concentrations [489]. Higher HOCl/ClO^- was found in the anodic oxidation process and peroxymonosulfate based oxidation process **(Chapters 2, 4, and 5)**. Thus, these processes yielded a high concentration of chlorate (**chapters 2, 4, and 5**).

$$6\,ClO^- \rightarrow 2ClO_3^- + 6H^+ + 4Cl^- + \frac{3}{2}O_2 + 6e^- \quad (8.12)$$

$$2\,HClO + ClO^- \rightarrow ClO_3^- + 2H^+ + 2Cl^- \quad (8.13)$$

$$2\,HClO \rightarrow ClO_2^- + 2H^+ + Cl^- \quad (8.14)$$

$$HClO + ClO_2^- \rightarrow ClO_3^- + H^+ + Cl^- \quad (8.15)$$

In addition, an exciting state oxygen atom is also capable of oxidizing ClO^- to chlorate [475]. The excited state oxygen atom is found in electrical discharge plasma, UV/O_3, and UV/free chlorine AOPs [457, 471, 475, 490, 491]. Thus, chlorate formation is expected in the AOPs in which free chlorine and the excited state oxygen atom coexists.

$$O(^1D) + ClO^- \rightarrow ClO_2^- \quad (8.16)$$

$$O(^1D) + ClO_2^- \rightarrow ClO_3^- \quad (8.17)$$

Moreover, ozone can non-radically oxidize the ClO^- to form chlorate according to the pathway described in (Fig 8.4)[458, 492]. It is important to consider that the second-order rate constant of the 1st reaction (eq. 20) is only 30 $M^{-1}s^{-1}$[493].

$$O_3 + ClO^- \rightarrow ClO_2^- + O_2 \quad (8.20)$$

$$O_3 + ClO_2^- \rightarrow ClO_3^- + O_2 \quad (8.21)$$

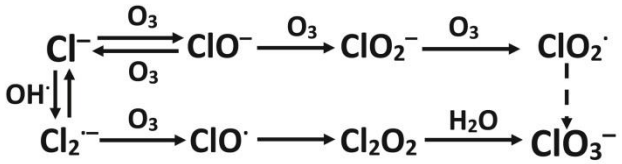

Fig. 8.4. *The reaction of ozone with chlorinated species (taken from Levanov et al. (2019)[458].*

In the radical-mediated pathway, the hydroxyl radical initiates a series of complex reactions. HOCl/ClO^- quickly reacts with hydroxyl radical to form $ClO^•$ radicals (Eq. 8.22-8.23) [97]. In addition, $Cl^•/Cl_2^{•-}$ can undergo an oxidation reaction with ozone to $ClO^•$ radicals (Eqs. 8.24-8.25) [458]. Moreover, $Cl^•$ also oxidizes ClO^- to $ClO^•$ radicals (Eq. 8.27)[97]. HClO also directly undergoes an electron transfer reaction on the electrode surface in the electrochemical oxidation process to form $ClO^•$ (Eq. 8.28) [494]. $ClO^•$ radicals are further converted to chlorite via disproportionation of Cl_2O_2 (Eq. 8.29 or 8.31) [97, 493]. In addition, on the electrode surface, $ClO^•$ radicals and hydroxyl radicals can directly react to yield chlorite (Eq. 8.30) [97, 495].

$$HClO + HO^• \rightarrow ClO^• + H_2O \quad (8.22)$$

$$ClO^- + HO^• \rightarrow ClO^• + HO^- \quad (8.23)$$

$$Cl^• + O_3 \rightarrow ClO^• + O_2 \quad (8.24)$$

$$Cl_2^{•-} + O_3 \rightarrow ClO^• + Cl^- + O_2 \quad (8.25)$$

$$HClO \rightarrow [HClO]^+ + e^- \rightarrow ClO^• + e^- + H^+ \quad (8.26)$$

$$ClO^- + Cl^• \rightarrow ClO^• + Cl^- \quad (8.27)$$

$$2ClO^{\bullet} \rightarrow Cl_2O_2 \quad (8.28)$$

$$Cl_2O_2 + H_2O \rightarrow 2ClO_2^- + ClO^- + 2H^+ \quad (8.29)$$

$$ClO^{\bullet} + HO^{\bullet} \rightarrow HClO_2 (ClO_2^- + 2H^+) \quad (8.30)$$

$$Cl_2O_2 + H_2O \rightarrow 2ClO_3^- + Cl^- + 2H^+ \quad (8.31)$$

Similarly, $HClO_2/ClO_2^-$ reacts with hydroxyl radicals or ozone to form $ClO_2^{\bullet}$ radicals (Eqs. 8.32-8.33) [494]. $HClO_2$ can directly undergo electron transfer reaction on the electrode surface to form $ClO_2^{\bullet}$ (Eq. 8.35). $ClO_2^{\bullet}$ and hydroxyl radical or ozone can now react to yield chlorate (8.34-8.36) [97]. In electrochemical oxidation, electrodes play a vital role in the reactions Eqs. 8.30 and 8.36. Hubler et al. (2014) show that ≡C-O$^{\bullet}$ and =C$^{\bullet}$-HO sites could form on the BDD surface. These active sites react with $ClO^{\bullet}$ and $ClO_2^{\bullet}$ to yield chemical absorbed intermediates [495]. These chemisorbed intermediates further react with hydroxyl radicals to yield corresponding oxychloride ions [495]. Because of chemisorption, $ClO^{\bullet}$ and $ClO_2^{\bullet}$ have more time to react with hydroxyl radicles and produce more chlorite and chlorate.

$$HClO_2 + HO^{\bullet} \rightarrow ClO_2^{\bullet} + H_2O \quad (8.32)$$

$$ClO_2^- + HO^{\bullet} \rightarrow ClO_2^{\bullet} + HO^- \quad (8.33)$$

$$ClO_2^- + O_3 \rightarrow ClO_2^{\bullet} + O_2 \quad (8.34)$$

$$HClO_2 \rightarrow [HClO_2]^+ + e^- \rightarrow ClO_2^{\bullet} + e^- + H^+ \quad (8.35)$$

$$ClO_2^{\bullet} + HO^{\bullet} \rightarrow HClO_3 (ClO_3^- + 2H^+) \quad (8.36)$$

Thus, hydroxyl radicals, ozone, and electrode play an important role in facilitating chlorate formation in the radical pathway.

8.6.2 Perchlorate formation:

It is noteworthy to remember that hydroxyl radicals cannot directly oxidize chlorate to perchlorate [97]. Initially, chlorate is oxidized by $Cl^{\bullet}$ or direct electron transfer on the electrode to form chlorate ion radical ($ClO_3^{\bullet -}$) Eqs. 8.37 and 8.43. In addition, $ClO_2^{\bullet}$ may interact with ozone to yield $ClO_3^{\bullet -}$(Eq. 8.38). It is important to note that ozone did not directly react with chlorate to chlorate ion radicals. The $ClO_3^{\bullet -}$ further could dimerize to Cl_2O_6 and then decomposed to chlorate and

perchlorate (Eq. 8.42) [97, 459, 460, 478, 496]. The chemisorption of hydroxyl radical on the anode is the rate-limiting step for perchlorate formation in electrochemical oxidation [497]. This step requires substantial activation energy [495]. In addition, similar to $ClO^{\bullet}$ and $ClO_2^{\bullet}$, chemisorption of chlorate ion or chlorite radical ion might take place on ≡C-O$^{\bullet}$ and =C$^{\bullet}$-HO sites of the BDD surface and form chemisorbed intermediates (Eq. 8.43). Which further oxidized to perchlorate with chemically absorbed hydroxyl radical or aqueous hydroxyl radical (Eq. 8.44). Chemically absorbed chlorate radicals and hydroxyl radicals are more stable and have a longer lifetime to react [495, 498]. Therefore, a higher perchlorate concentration was observed in electrochemical oxidation. More hydroxyl radical was produced with the BDD anode compared with the MMO; therefore, more chlorate was found with the BDD anode (**chapter 2**). In magneli phase Ti_4O_7 anode, less perchlorate was formed compared with BDD anode [251]. This could be explained by the lack of chlorate ion or chlorite radical chemisorption on the magneli phase Ti_4O_7 surface. In addition, $ClO_3^{\bullet-}$ can be directly oxidized by hydroxyl radical to perchlorate [461]. Moreover, the chemisorption of hydroxyl radicals can also lead to a one-electron transfer reaction to an adsorbed oxygen atom. This adsorbed oxygen atom can convert chlorate to perchlorate (Eq. 8.45) [438, 461].

$$ClO_3^- + Cl^{\bullet} \rightarrow ClO_3^{\bullet} + Cl^- \quad (8.37)$$

$$ClO_2^{\bullet} + O_3 \rightarrow ClO_3^{\bullet} + O_2 \quad (8.38)$$

$$ClO_3^{\bullet} + ClO^{\bullet} \rightarrow Cl_2O_4 \quad (8.39)$$

$$Cl_2O_4 + H_2O \rightarrow ClO_4^- + HClO + 2H^+ \quad (8.40)$$

$$ClO_3^{\bullet} + ClO_3^{\bullet} \rightarrow Cl_2O_6 \quad (8.41)$$

$$Cl_2O_6 + H_2O \rightarrow ClO_4^- + ClO_3^- + 2H^+ \quad (8.42)$$

$$ClO_3^- \rightarrow (ClO_3^{\bullet})_{ad} + e^- \quad (8.43)$$

$$(ClO_3^{\bullet})_{ad} + (HO^{\bullet})_{ad} \rightarrow ClO_4^- + e^- + H^+ \quad (8.44)$$

$$ClO_3^- + (O)_{ad} \rightarrow ClO_4^{-} \quad (8.45)$$

The formation of $ClO_3^{\bullet-}$ is the critical step to perchlorate formation. The $ClO_3^{\bullet-}$ formation is only initiated in AOPs which involve, $Cl^{\bullet}$, a BDD anode, adsorbed oxygen atoms, or ozone.

8.7 SELECTION CRITERIA OF AOPS IN THE PRESENCE OF CHLORIDE IONS

According to WHO, chlorate and perchlorate concentrations should be less than 0.7 mg/l and 0.07mg/L in drinking water, respectively [499, 500]. Because of their toxicity, AOX, representing chlorinated organic compounds, is unwanted in drinking water and treated wastewater. Thus, together with effective removal of OCs, chlorinated by-products formation should be taken into account to select AOPs in saline conditions. Chloride ions are ubiquitous in the aqueous environment. Chloride ions' interaction with reactive oxygen species, sources, and activations/initiators should be critically evaluated to select the effective and safe AOPs. In section 8.4, chloride interaction in different AOPs has been discussed. In section 8.5, the reactivity of the reactive chlorine species with organic compounds has been illustrated. In section 8.6, chlorate and perchlorate formation mechanisms are elaborated. Based on these sections and the experimental chapters of this thesis, chlorinated by-product patterns in different AOPs are summarized in Table 8-2.

Table 8-2 shows that the possibility of AOX and chlorate formation is high in the AOPs involving free chlorine (ClO^-/HClO). The free chlorine formation dominates in electrochemical oxidation, sulfate radical based AOPs involving peroxymonosulfate, electro-photocatalytic AOPs, UV/chlorine (free chlorine), and electro-Fenton process. In addition, O_3 based AOPs, electrical discharge plasma, and gamma-ray/electron beam-based AOPs show a noticeable amount of free chlorination formation tendency. As discussed in section 8.5, free chlorine undergoes substitution and addition reactions with organic compounds and yield higher AOX concentrations. Also discussed in section 8.6, a higher free chlorine concentration promotes non-radical chlorite formation. Thus, AOX and chlorate formation would be higher in these AOPs.

As discussed in section 8.6, perchlorate formation required specific circumstances to convert chlorate to the chlorate ion radical. BDD anode at high

potential can facilitate this conversion reaction. In addition, $Cl^{\bullet}$ and (adsorbed)O atoms have enough potential for this reaction. Thus, perchlorate formation is more elevated in electrochemical oxidation with a BDD anode, electro-Fenton process with BDD anode at higher potential, UV/free chlorine process, ozone-based AOPs, especially with UV process, and electrical discharge plasma AOPs.

$Cl^{\bullet}/Cl_2^{\bullet}$ can be directly produced due to the interaction of radicals with chloride. The interaction of hydroxyl radicals is less prominent at neutral pH. Thus, H_2O_2 and UV-based AOPs are less influenced by chloride. Sulfate radicals, however, react with chloride ions to yield $Cl^{\bullet}/Cl_2^{\bullet}$. This reaction heavily depends on the chloride concentration. This reaction is less prominent at low chloride concentrations, but it becomes dominant at higher concentrations and produces a significant amount of $Cl^{\bullet}/Cl_2^{\bullet}$. Free chlorine can be formed radically at higher $Cl^{\bullet}/Cl_2^{\bullet}$ and chloride concentrations, further initiating AOX and chlorate formation. Thus, sulfate radical-based AOPs is recommended only at low chloride concentrations. Vacuum UV, UV/Photosensitizer, photo-Fenton, and electrical discharge plasma AOPs could also directly produce $Cl^{\bullet}/Cl_2^{\bullet}$. This $Cl^{\bullet}/Cl_2^{\bullet}$ formation reaction is a side reaction and becomes dominant at higher chloride concentration and acidic conditions. Thus, water pH and chloride concentration need to be considered before applying these AOPs.

Based on this discussion, it could be summarized that UV, UV/H_2O_2, classical Fenton, photo-Fenton, photocatalysis, and ultrasound-based AOPs are the safest processes with low chlorinated by-products formation tendency. After that, peroxydisulfate based, VUV, ozone-based, Gamma-ray, and electron beam-based AOPs could be considered safe AOPs under controlled conditions, such as specific pH, chloride concentration, and applied energy. Chlorinated by-product formation would be unavoidable in electrochemical oxidation, electro-Fenton, electro-photocatalysis, peroxymonosulfate based, UV/free chlorine, UV/(H_2O_2)O_3, and electrical discharge plasma AOPs.

Table 8-2. *Summary of the dominating reactive species, AOX, chlorate, and perchlorate formation in different AOPs*

AOPs	Sources/ activators/ conditions	Dominating reactive oxygen species	Dominating reactive chlorine species	AOX formation	Chlorate formation	perchlorate	comments	reference
Electrochemical oxidation	Active anodes (MMO)	$HO^{\bullet}$	$Cl^{\bullet}$, $Cl_2^{\bullet-}$, Cl_2, ClO^-/HClO	Very high	Very high	Very low/ND		Chapters 2 and 3
	Non- active anodes (BDD)	$HO^{\bullet}$, $SO_4^{\bullet-}$	$Cl^{\bullet}$, $Cl_2^{\bullet-}$, Cl_2, ClO^-/HClO	Very high	Very high	Very high		Chapters 2-4 and 6
Sulfate radical based	PDS	$HO^{\bullet}$, $SO_4^{\bullet-}$	$Cl^{\bullet}$, $Cl_2^{\bullet-}$	ND/very low	ND/very low	ND		Chapters 5 and 6
	PMS	$HO^{\bullet}$, $SO_4^{\bullet-}$, $HO_2^{\bullet}/O_2^{\bullet-}$, $^1O_2$	$Cl^{\bullet}$, $Cl_2^{\bullet-}$, Cl_2, ClO^-/HClO	Very high	Very high	ND		Chapter 5
Photocatalysis	TiO_2/UVA/ UVB (pH>7)	$HO^{\bullet}$, $O_2^{\bullet-}$, $^1O_2$, e^-, h_{VB}	Limited	Very low	ND	ND		Chapter 6

AOPs	Sources/ activators/ conditions	Dominating reactive oxygen species	Dominating reactive chlorine species	AOX formation	Chlorate formation	perchlorate	comments	reference
Photocatalysis *(continued)*	TiO_2/WO_3/potential (even at <1.2 V)	$HO^{\bullet}$, $O_2^{\bullet-}$, $^1O_2$, e^-, h_{VB}	$ClO^{\bullet}$, $Cl^{\bullet}$, $Cl_2^{\bullet}$, ClO^-/HClO	High	High	ND		[446]
	$BiVO_4$/potential (even at <1.2 V)	$HO^{\bullet}$, $O_2^{\bullet-}$, $^1O_2$, e^-, h_{VB}	Limited	Very low	Very low	ND		[446, 447]
Ultraviolet-based (UV)	UV > 254 nm	Photolysis of the organic compounds	ND	ND	ND	ND		Chapter 6
	UV> 260 nm +Photosensitizers	Excited-state triplet organic matter (^{3}OM), $^1O_2$, $HO^{\bullet}$(NO_2/NO_3+hv), $O_2^{\bullet-}$, e_{eq}^-, H_2O_2	$Cl^{\bullet}$, $Cl_2^{\bullet-}$ (very low)	very low	ND	ND		[441, 501]

Ultraviolet-based (UV) *(continued)*	UV < 200 nm (VUV)	$HO^{\bullet}$, $H^{\bullet}$, e_{eq}^{-}, $O_2^{\bullet-}$/ $HO_2^{\bullet}$	$Cl^{\bullet}$, $Cl_2^{\bullet-}$	ND	ND	ND	Chapter 6
	UV/ H_2O_2 > 200 nm	$HO^{\bullet}$, H_2O_2, $HO_2^{\bullet}$/ $O_2^{\bullet-}$	ND	ND	ND	ND	[502-504]
	UV/ chlorine (Cl_2/HOCl)	$HO^{\bullet}$, $O_2^{\bullet-}$/$HO_2^{\bullet}$ $O(^1D)$	$Cl^{\bullet}$, $Cl_2^{\bullet-}$, ClO_2, Cl_2, HOCl	Very high	Very high	high	[490, 505-507]
Ozone based	O_3 (pH>10)	O_3, $HO^{\bullet}/O^{\bullet-}$	Very little (ClO^-/HClO)	Very low	Very low	Very low	[97, 457-459]
	UV/ O_3	O_3, $HO^{\bullet}$, $O(^1D)$, $O(^3P)$, $^1O_2$, H_2O_2	ClO^-/HClO/ $Cl^{\bullet}$, $Cl_2^{\bullet-}$,	High	Low	Very low	
	H_2O_2/O_3	$HO_2^{\bullet}$, $O_2^{\bullet-}$, O_3, $O^{\bullet-}$, $HO^{\bullet}$, H_2O_2	Very little (ClO^- /HClO)	Very low	Very low	Very low	

AOPs	Sources/ activators/ conditions	Dominating reactive oxygen species	Dominating reactive chlorine species	AOX formation	Chlorate formation	perchlorate	comments	reference
Ozone based *(continued)*	$UV/H_2O_2/O_3$	$HO_2^{\bullet}$, $O_2^{\bullet-}$, O_3, $O^{\bullet-}$, $HO^{\bullet}$, H_2O_2, $O(^1D)$, $O(^3P)$, $^1O_2$,	$ClO^-/HClO/$ $Cl^{\bullet}$, $Cl_2^{\bullet-}$	High	Low	low		[97, 457-459]
	Ultrasound/ O_3	O_3, $HO^{\bullet}$, $O(^1D)$, $^1O_2$, H_2O_2	Not know (Very little) ($ClO^-/HClO$)	Not reported (Very little)	Not reported (Very little)	Not reported (Very little)	Based on literature	
Fenton process	Fe^{2+}/H_2O_2/ pH <3	$HO^{\bullet}$, H_2O_2,	($FeCl^{2+}$ and $FeCl_2^+$)	ND	ND	ND		[97, 462, 464, 465]
	Fe^{2+}/H_2O_2/UV/pH <3	$HO^{\bullet}$, H_2O_2,	$Cl^{\bullet}$, $Cl_2^{\bullet-}$	Low	ND	ND		
	Fe^{2+} $/H_2O_2$/potential <1.6V/ pH <3	$HO^{\bullet}$, H_2O_2,	$ClO^-/HClO$	High	High	ND		

Fenton process *(continued)*	Fe^{2+} /H_2O_2/potential >1.6V/BDD anode pH <3	$HO^{\bullet}$, H_2O_2,	$Cl^{\bullet}$, $Cl_2^{\bullet-}$, Cl_2, ClO^-/HClO	High	High	high		
	Fe^{2+} /H_2O_2/ultrasound	$HO^{\bullet}$, H_2O_2,	Not reported	Not reputed	Not reported	Not reputed		[95, 460, 462, 463
	Fe^{2+} /H_2O_2/ Mn^{2+}, Cu^{2+}, $Co^{2+,}$ Ti^{3+}/ Nanoparticles	$HO^{\bullet}$, H_2O_2,	Not reported	Not reputed	Not reported	Not reputed		
Gamma-ray and electron beam-based AOPs		$HO^{\bullet}$, $H^{\bullet}$, e_{eq}^-,H_2O_2, $O_2^{\bullet-}$, $HO_2^{\bullet}$	ClO^-/HClO	Not reported (Very little)	Not reported (Very little)	Not reported (ND)	Based on literature	[97, 470, 508, 509]
Electrical discharge plasma		e^-, $O(^1D)$, O_3, $HO^{\bullet}$, $H^{\bullet}$, H_2O_2	$Cl^{\bullet}$, $Cl_2^{\bullet-}$, ClO^-/HClO	Not reported (high)	High	Not reported (high)	Based on literatures	[97, 471, 475, 477, 479]

AOPs	Sources/ activators/ conditions	Dominating reactive oxygen species	Dominating reactive chlorine species	AOX formation	Chlorate formation	perchlorate	comments	Reference
Ultrasound		$HO^{\bullet}$, $H^{\bullet}$, $HO_2^{\bullet}$, H_2O_2	$Cl^{\bullet}$, $Cl_2^{\bullet-}$	Not reported (Very little)	Not reported (ND)	Not reported (ND)	Based on literature	[97, 480]

The species are $O(^1D)$ (oxygen atom in its excited state), $O(^3P)$ (oxygen atom in its ground state), singlet oxygen ($^1O_2$)

8.8 FUTURE OUTLOOK

On top of increasing the removal/mineralization efficiency and decreasing energy consumption, chlorinated compound formation aspects need to be considered for AOPs application in saline conditions.

In general, AOPs consist of two steps: generation of reactive actives species and oxidation of the targeted compounds. Components involved in reactive oxidizing species (ROS) formation are sources of the oxidants and the activators. For the last 30–40 years, most research has mainly focused on finding effective oxidant sources and efficient activation techniques. The limitations of AOPs are the short lifetime and low concentration of ROS. In addition, in many cases, the concentration of the targeted pollutant is very low. Thus, effective ROS formation does not reach the desired performance because of mass transfer limitations. One of the smart ways to overcome this limitation is to study reactor design optimization. Optimal reactor designs for AOPs are hardly found in the literature for all AOPs. There is more literature about the optimization of photo-reactors for UV-based AOPs only.

The activation process to generate ROS is an energy-intensive process. Each year numerous papers are published about the development of new activation methods like catalysts. However, hardly any or very few catalysts are in a real application. From my point of view, it will be more interesting to study the application of those catalysts in real cases and find out the limitations rather than just developing more new catalysts.

As discussed in detail in this thesis, the presence of chloride ions influences different AOPs differently. Thus, in future research, the influence of chloride should be critically monitored. Most of the research focuses on promoting or scavenging the effects of chloride in the process performance. However, the fate of chloride should be included. For a quick assessment, chlorinated organic compounds in terms of AOX as a marker could be analyzed. In addition, chlorate and perchlorate concentrations should be monitored in the AOPs studies involving chloride ions. To analyze the detailed chlorinated organic compounds, chloromethane, chloroethane, chloropropene, chloroacetic acid, chloroethylene, and chlorobenzene could be monitored. If bromine and fluoride are present in the water, brominated and

fluorinated OCs also should be monitored. One of the common perceptions is that all chlorinated compounds are toxic. However, it could be that the chlorinated compounds are less toxic than the parent compound. So at least the overall toxicity of the treated water should be monitored.

Most importantly, more research is required to avoid or minimize the chlorinated by-product formation. For this, there can be two directions mentioned, namely:

1. Strategy to avoid or minimize the free chlorine formation: In the case of electrochemical oxidation, graphite-based electrode shows excellent resistance to chloride oxidation. In the future, more research needs to focus on material development to reduce the direct chlorine oxidation on the electrode surface.

2. Considering the properties of the targeted organic compounds

Studies show that some organic compounds are less reactive to the reactive chlorine species and other groups of organic compounds are very reactive. In future research, the properties of the organic compounds should be considered before applying the AOPs in saline water.

In general, each technology has its limitations. Thus, it is essential to consider the limitations before application to ensure that technology used to solve one problem does not (or has a minimum possibility to) create another problem.

Supplementary information

SUPPLEMENTARY MATERIALS: CHAPTER 2

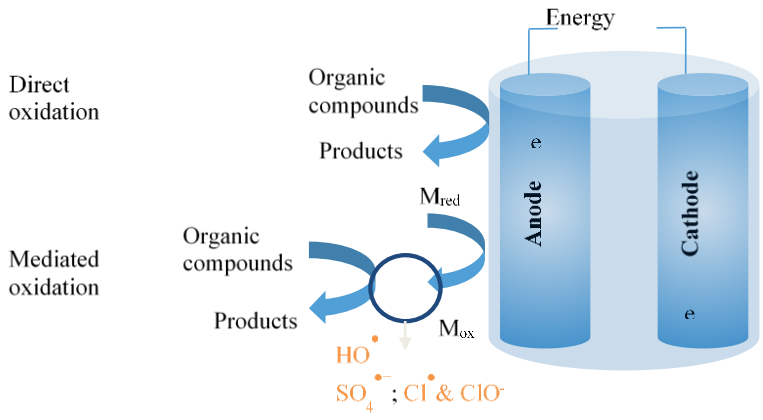

Fig. S2-1. *Principle of electrochemical oxidation*

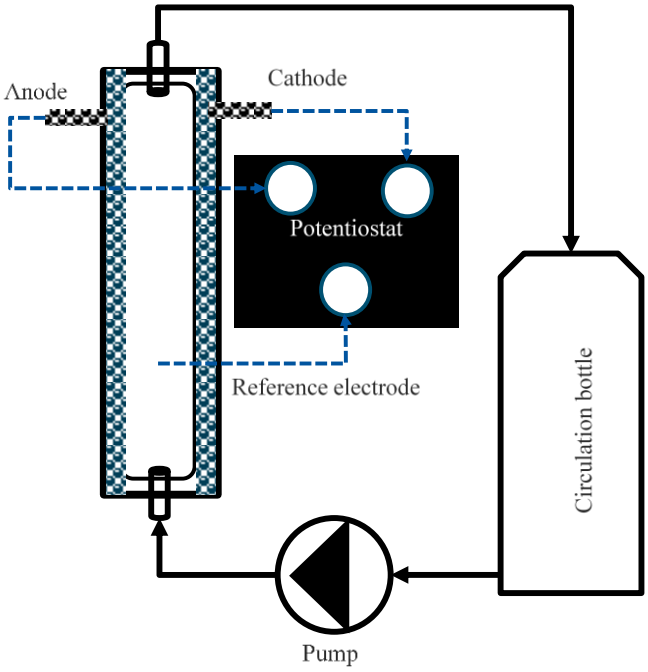

Fig. S2-2. *Schematic of the electrochemical reactor.*

Table S2-1. *Characteristics of cooling tower blowdown used in this study.*

Parameter	Unit	Avg. (±SD)
Conductivity	mS cm^{-1}	3.7 (0.3)
Cl^-	mg L^{-1}	505 (12)
NO_3^-	mg L^{-1}	153 (3)
SO_4^{2-}	mg L^{-1}	1192 (48)
Na^+	mg L^{-1}	325 (6)
Ca^{2+}	mg L^{-1}	417 (4)
Mg^{2+}	mg L^{-1}	63(2)
K^+	mg L^{-1}	89 (9)
TOC	mg L^{-1}	52 (4)
COD	mg L^{-1}	112 (7)
AOX	mg Cl^- L^{-1}	1.78 (0.4)
pH	-	6.9 (0.3)

Table S2-2. *COD and TOC removal at different flowrate with the BDD-anode and MMO-anode. Experimental conditions: T = 21-23°C, Conductivity = 3.7 mS* cm^{-1}*, pH = 6.9.*

Anode	flowrate ($L.h^{-1}$)	%COD removal (±)	%TOC removal (±)
BDD	18	87 (2.5)	53 (1.4)
	30	84 (2.5)	51 (1.4)
	46	94 (1.0)	57 (2.1)
MMO	18	53 (3.3)	16 (1.4)
	30	60 (2.0)	15 (1.5)
	46	63 (1.3)	17 (2.1)

Table S2-3. *Synthetic water for toxicity experiment.*

Constituent (Unit)	Concentration
$NaNO_3$ (mg L^{-1})	100
$CaCl_2$ (mg L^{-1})	800
Na_2SO_4 (mg L^{-1})	1500

LC-OCD profile of CTBD before and after treatment.

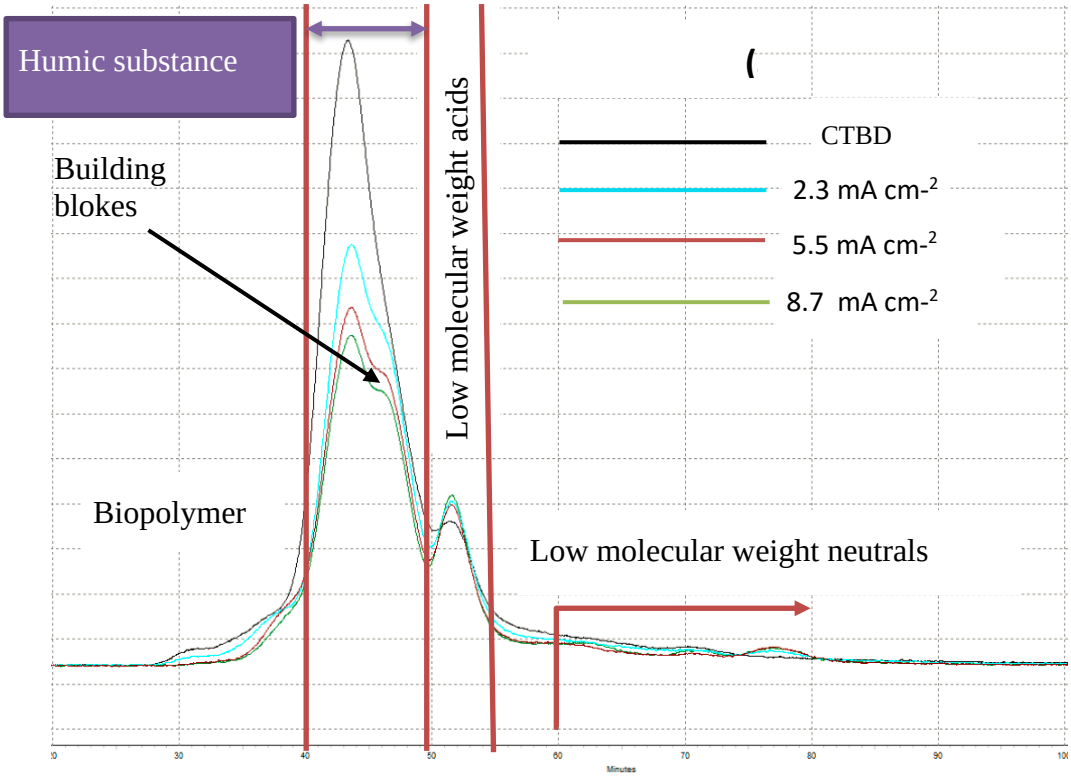

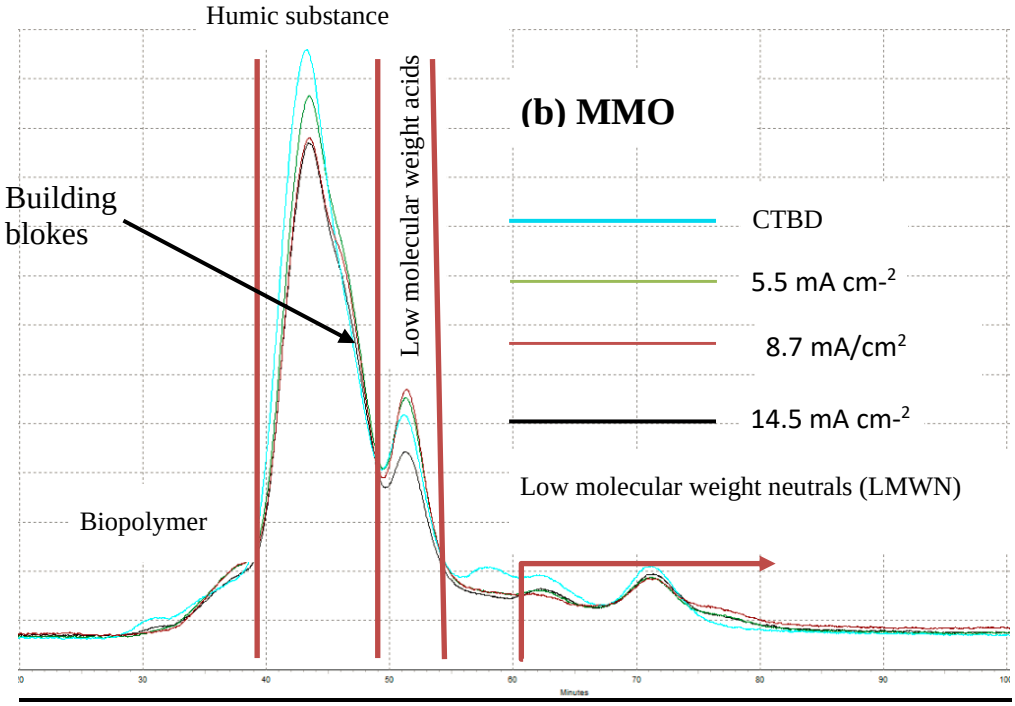

Fig. S2-3. *Influence of applied current density (j) on LC-OCD total ion chromatograms with (a) BDD-anode and (b) MMO- anode. Experimental conditions: T=21-23℃, Conductivity = 3.7 mS cm^{-1}, pH = 6.9, recirculation flow rate = 30 L h^{-1}, treatment time = 3 h.*

SUPPLEMENTARY MATERIALS: CHAPTER 3

Text S3.1. Combine efficiency calculation:

The 1st step removal efficiency ($mbRE_1$), 2nd step removal efficiency ($mbRE_2$) and combine removal efficiency ($mbRE_c$) can be expressed as follows,

$$\mathrm{mbRE_1} = \left(1 - \frac{\mathrm{Y}}{\mathrm{X}}\right) \times 100\% \quad \text{(S3.1)}$$

$$\mathrm{mbRE_2} = \left(1 - \frac{\mathrm{Z}}{\mathrm{Y}}\right) \times 100\% \quad \text{(S3.2)}$$

$$\mathrm{mbRE_C} = \left(1 - \frac{\mathrm{Z}}{\mathrm{X}}\right) \times 100\% \quad \text{(S3.3)}$$

Where: X , Y, and Z are considered as mass base concertation of feed, 1st step outlet, and 2nd step outlet, respectively. Combining the Eq. (S3.1),Eq.(S3.2) and Eq.(S3.3), $mbRE_c$ can be expressed as

$$mbRE_C = mbRE_1 + mbRE_2 - (mbRE_1 \, x \, mbRE_2) \quad \text{(S3.4)}$$

Table S3-1. *Water evapotranspiration during the experimental period*

Day	VFCW-EO	EO/BDD-VFCW	EO/MMO-VFCW
0			
3	28%	32%	30%
6	31%	34%	32%
9	30%	30%	34%
12	33%	33%	34%
15	32%	33%	33%
18	30%	36%	35%
21	34%	28%	38%
24	34%	28%	34%
27	30%	40%	31%
30	34%	39%	38%
33	36%	34%	36%
36	32%	34%	32%
39	36%	35%	29%
42	27%	38%	33%
45	33%		
48	35%		
51	30%		
54	34%		
57	30%		
60	29%		
63	36%		
66	29%		
69	25%		
72	31%		
75	28%		
78	28%		
81	28%		
84	33%		
87	36%		
90	39%		
Average (±SD)	32% (3)	34% (4)	33% (3)

Table S3-2. *Energy consumption (kWh/kg COD) during the EO treatment of original CTBD (EO-VRCW) and VFCW pre- treated CTBD (VFCW-EO)*

Energy consumption during the EO for	VFCW pre- treated CTBD (kWh/kg COD)	Original CTBD (kWh/kg COD)
BDD cell	19	23
MMO cell	64	79

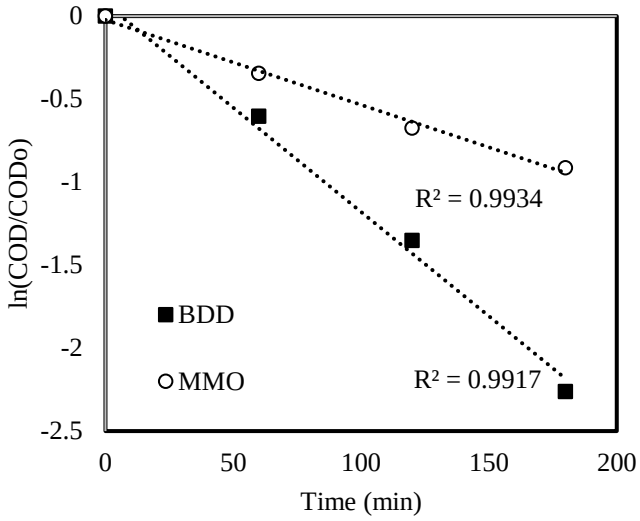

Fig. S3- 1. *first order COD removal kinetics during the EO of Day-3 VFCD effluent. COD: 61 mg/L, Conductivity: 4.8 mS/cm, pH: 7.08, Applied current density: 5.5 mA/cm^2 for BDD anode and 8.7 mA/cm^2 for MMO anode.*

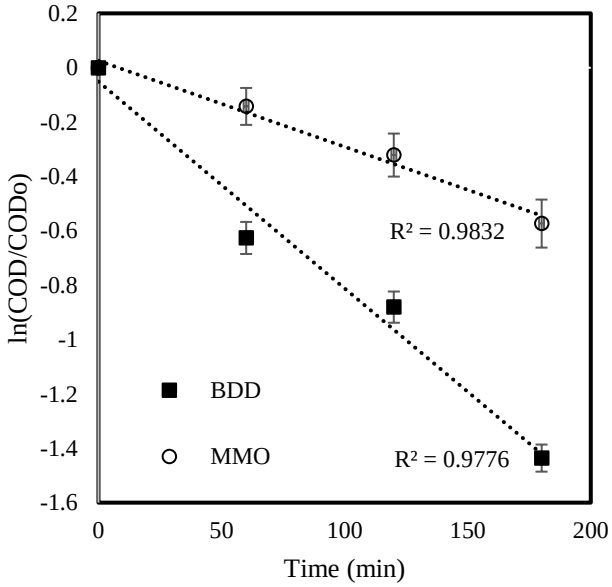

Fig. S3- 2. *first order COD removal kinetics during the EO of original CTBD. Average COD: 107 mg/L, Conductivity: 3.4 mS/cm, pH: 6.8, Applied current density: 5.5 mA/cm^2 for BDD anode and 8.7 mA/cm^2 for MMO anode*

SUPPLEMENTARY MATERIALS: CHAPTER 4

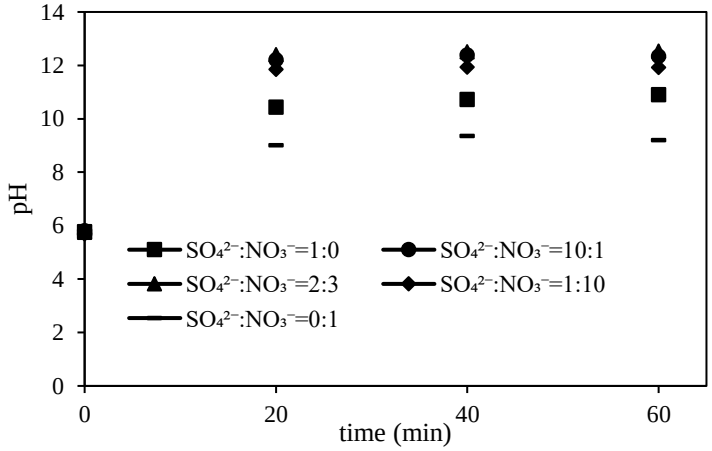

Fig. S4- 1. *pH changing with reaction time (min) in different Na_2SO_4:$NaNO_3$ (SN) ratios. Experimental conditions: different electrolyte ratios, T = 25-30℃, applied potential = 4.3 V (vs. Ag/AgCl), conductivity = 10 mS/cm, flow rate = 580 mL/min.*

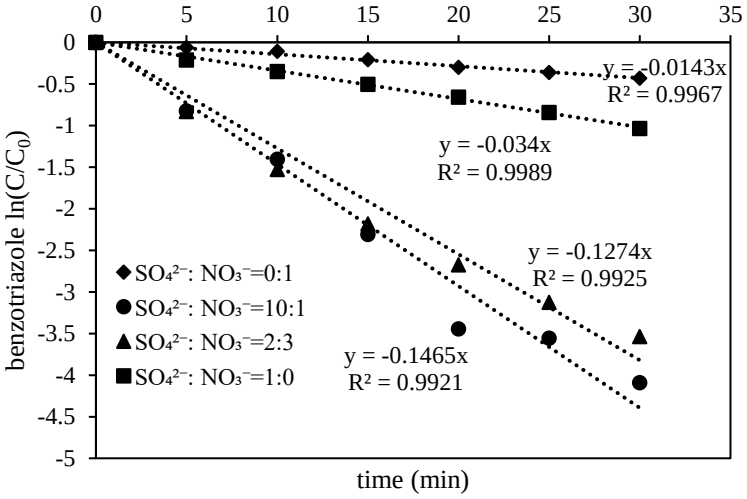

Fig. S4- 2. *Benzotriazole degradation rate (min^{-1}) in different Na_2SO_4:$NaNO_3$ (SN) ratios. Experimental conditions: 10 mg/L benzotriazole, different electrolyte ratios, T = 25-30℃, applied potential = 4.3 V (vs. Ag/AgCl), conductivity = 10 mS/cm, flow rate = 580 mL/min.*

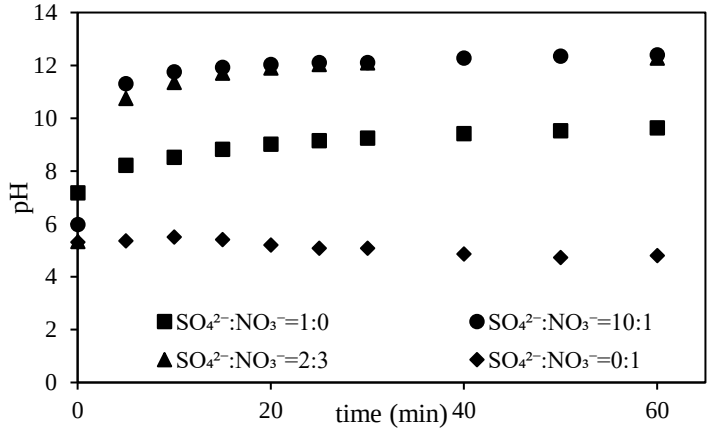

Fig. S4- 3. *pH changing with reaction time (min) in different Na_2SO_4:$NaNO_3$ (SN) ratios. Experimental conditions: 10 mg/L benzotriazole, different electrolyte ratios, T = 25-30℃, applied potential = 4.3 V (vs. Ag/AgCl), conductivity = 10 mS/cm, flow rate = 580 mL/min.*

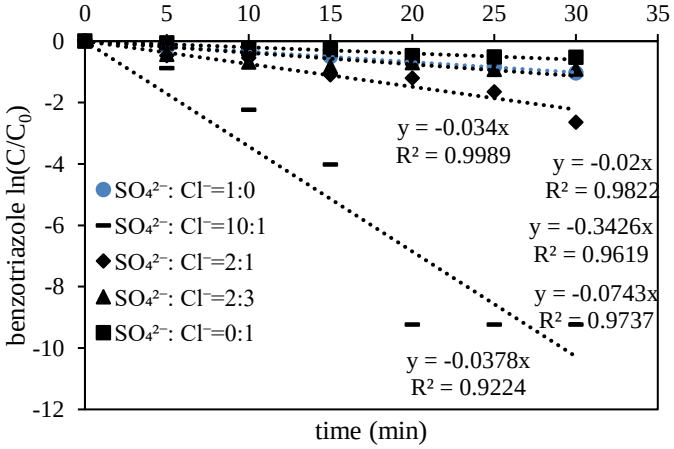

Fig. S4- 4. *Benzotriazole degradation rate (min^{-1}) in different Na_2SO_4:NaCl (SCl) ratios. Experimental conditions: 10 mg/L benzotriazole, different electrolyte ratios, T = 25-30℃, applied potential = 4.3 V (vs. Ag/AgCl), conductivity = 10 mS/cm, flow rate = 580 mL/min.*

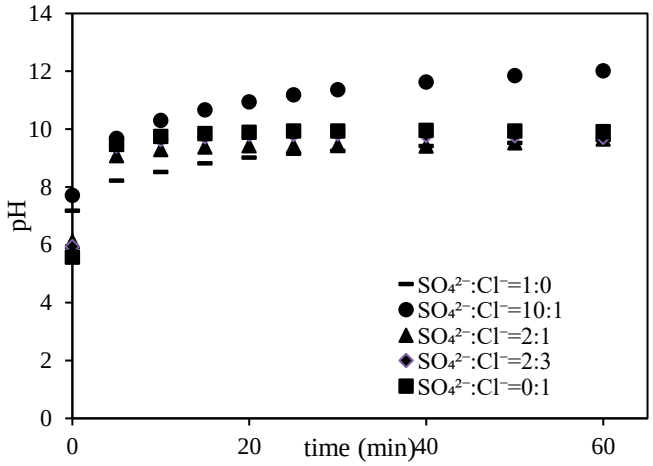

Fig. S4- 5. *pH changing with reaction time (min) in different Na_2SO_4:NaCl (SCl) ratios. Experimental conditions: 10 mg/L benzotriazole, different electrolyte ratios, T = 25-30℃, applied potential = 4.3 V (vs. Ag/AgCl), conductivity = 10 mS/cm, flow rate = 580 mL/min.*

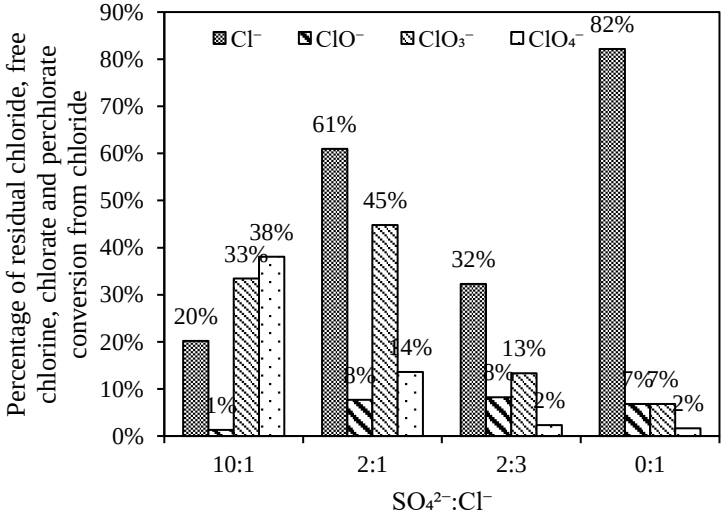

Fig. S4- 6. *Percentage of residual chloride, free chlorine, chlorate and perchlorate conversion from chloride in different Na_2SO_4:NaCl (SCl) ratios. Experimental conditions: 10 mg/L benzotriazole, different electrolyte ratios, T = 25-30℃, applied potential = 4.3 V (vs. Ag/AgCl), conductivity = 10 mS/cm, flow rate = 580 mL/min.*

Table S4-1. *chlorinated organic transformation products (COTPs) and nonchlorinated transformation products (TPs) peak area change with time (min) during benzotriazole degradation in different Na_2SO_4:NaCl (SCl). Experimental conditions: : 10 mg/L benzotriazole, , T = 25-30℃, applied potential = 4.3 V (vs. Ag/AgCl), conductivity = 10 mS/cm, flow rate = 580 mL/min, reaction time = 60 min.*

COTPs	Propose Formula	Propose structure	Molecular weight (m/z)	Retention Time (min)	SCl: 1:0	SCl: 10:1	SCl: 2:1	SCl: 2:3	SCl: 0:1
COTP-1	$C_6H_4ClN_3$	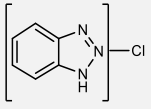	153.00966	8.4388.800	ND	ND	ND	60 min	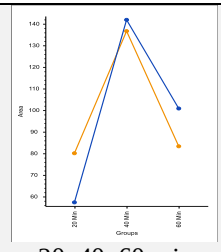 20, 40, 60 min
COTP-2	$C_6H_3Cl_2N_3$	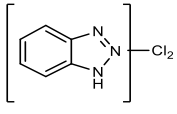	186.97071	9.4859.689	ND	ND	ND	ND	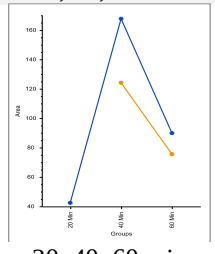 20, 40, 60 min

COTP-3	C_4H_6ClNO	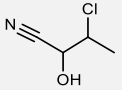	119.01407	6.177	ND	ND	60 min	60 min	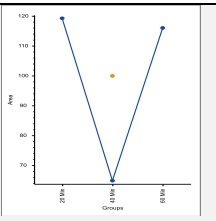 20, 40, 60 min
COTP-4	$C_2H_2Cl_2O_2$	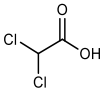	127.94306	8.694	ND	ND	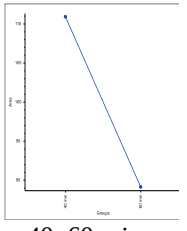 40, 60 min	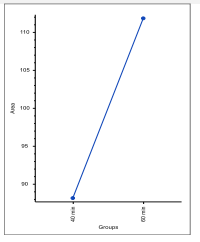 40, 60 min	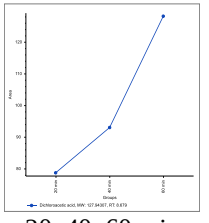 20, 40, 60 min
COTP-5	$C_2HCl_2N_3$		136.9546	9.256	ND	ND	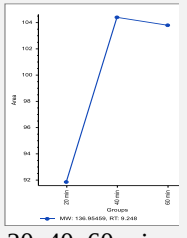 20, 40, 60 min	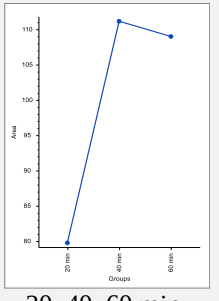 20, 40, 60 min	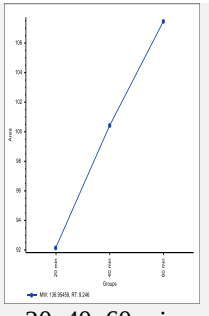 20, 40, 60 min

COTPs	Propose Formula	Propose structure	Molecular weight (m/z)	Retention Time (min)	SCl: 1:0	SCl: 10:1	SCl: 2:1	SCl: 2:3	SCl: 0:1
COTP-6	$C_5HCl_3O_3$	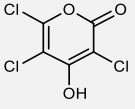	213.89919	15.14	ND	ND	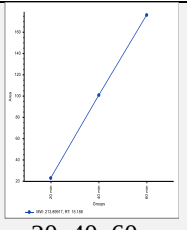 20, 40, 60 min	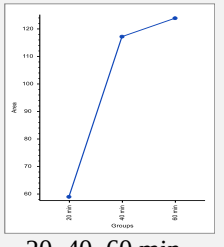 20, 40, 60 min	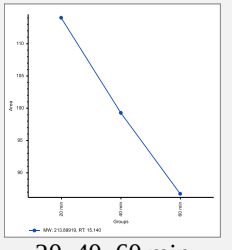 20, 40, 60 min
COTP-7	$C_3H_2Cl_2N_2$	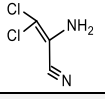	135.95981	8.134	ND	ND	ND	ND	40 min
non-chlorinated transformation products (TPs)									
TP-1	$C_4H_3N_3O_4$	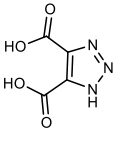	157.01269	9.153	ND	20 min	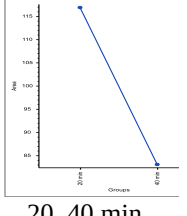 20, 40 min	20 min	20 min

*ND: not detected (time in minutes at which compound found)

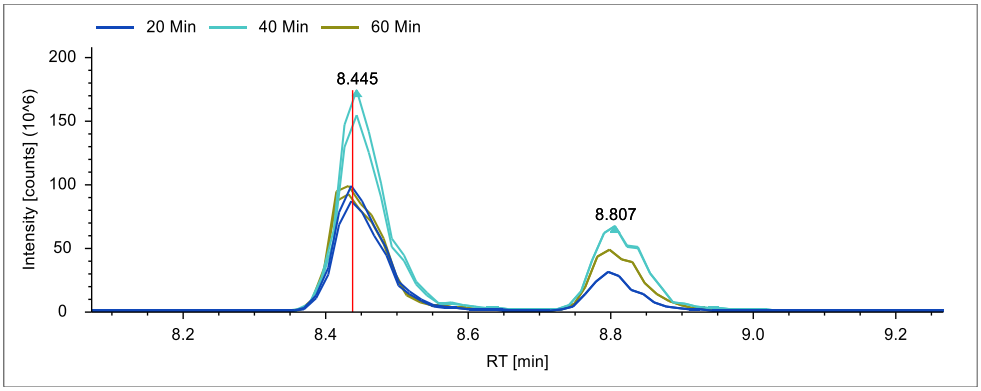

Fig. S4-7. *LC-MS chromatographic Peak cluster of COTP1- $C_6H_4ClN_3$ isomers. Experimental conditions: Na_2SO_4:NaCl ratio =0:1, 10 mg/L benzotriazole, , T = 25-30℃, applied potential = 4.3 V (vs. Ag/AgCl), conductivity = 10 mS/cm, flow rate = 580 mL/min, reaction time = 60 min.*

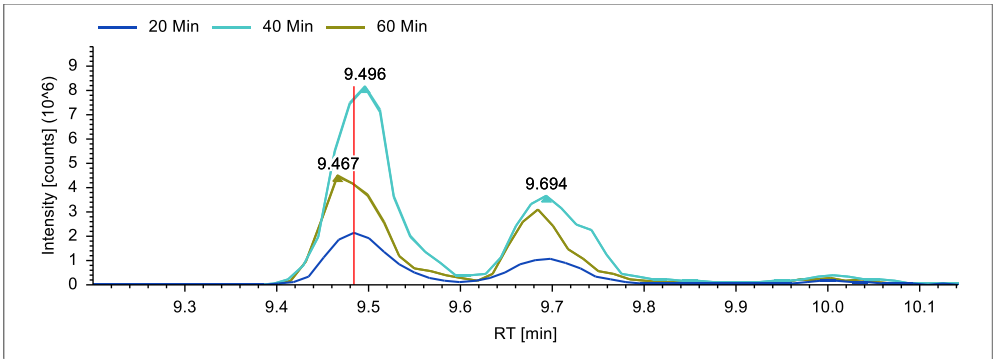

Fig. S4-8*. LC-MS chromatographic Peak cluster of COTP1- $C_6H_3Cl_2N_3$ isomers. Experimental conditions: Na_2SO_4:NaCl ratio =0:1, 10 mg/L benzotriazole, , T = 25-30℃, applied potential = 4.3 V (vs. Ag/AgCl), conductivity = 10 mS/cm, flow rate = 580 mL/min, reaction time = 60 min*

SUPPLEMENTARY MATERIALS: CHAPTER 5

Table S5-1. *Basic properties of 1-H benzotriazole (BTA)*

Properties	1-H benzotriazole
Molecular formula	$C_6H_5N_3$
Structure	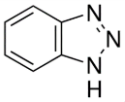
Molecular Weight	119.127 g/mol
CAS number	95-14-7
Solubility	1 to 5 mg/mL at 24°C

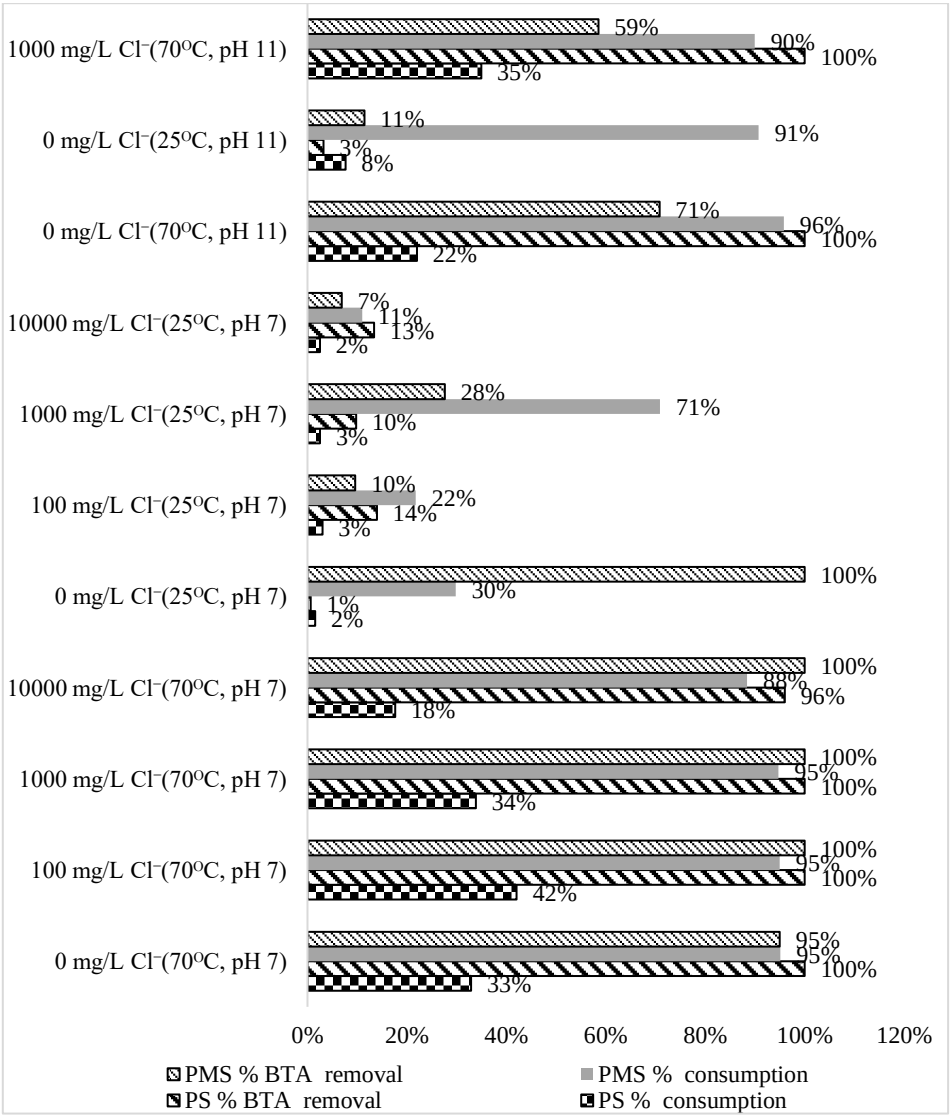

Fig. S5-1. *BTA removal efficiency, PS/ PMS consumption Experimental conditions: $[PS]_0$ =$[PMS]_0$=15 mM, [BTA]0=0.42 mM, V=100 mL, all experiments were buffered by 15 mM phosphate and sodium hydroxide was added dropwise to maintain the desired pH (pH7: 6.5-7.7; pH11: 10.9-11.5).*

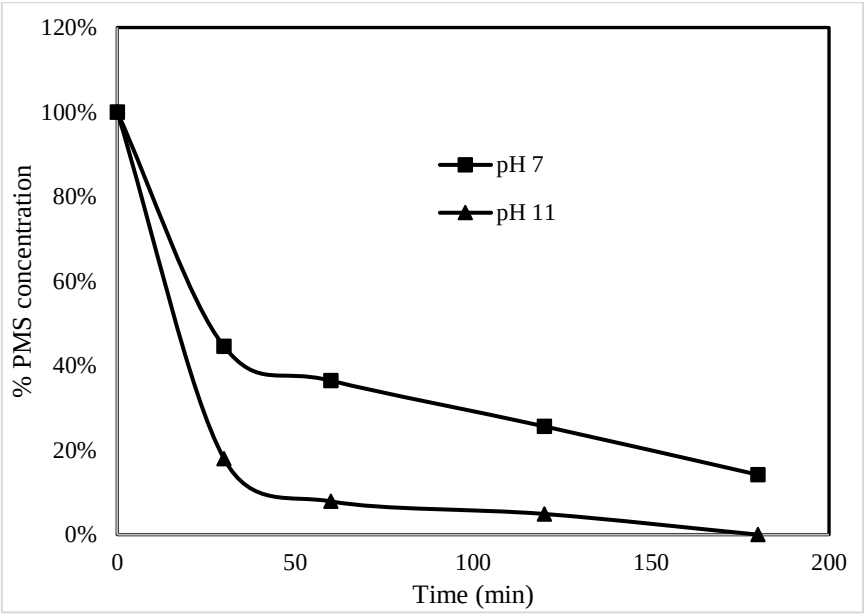

Fig. S5-2. *PMS concentration over time at 70°C; PMS]0=15 mM, [BTA]0=0.42 mM, V=100 mL, all experiments were buffered by 15 mM phosphate, and sodium hydroxide was added dropwise to maintain the desired pH (pH7: 6.5-7.7; pH11: 10.9-11.5).*

Table S5-2. *Transformation products (TPs) peak area change with time (min) during BTA degradation. Experimental conditions: T=70℃, [BTA]$_0$=0.42 mM, [PS]$_0$ = [PMS]$_0$ =15 mM, [Cl$^-$]= 0 or 1000 mg/L, V=100 mL, sodium hydroxide was added dropwise to maintain the pH around 6.9-7.4*

Transformation products (TPs)	Proposed formula	Proposed structure	Observed Molecular weight (m/z)	PS _Peak area change Time (min)	PMS_Peak area change Time (min)	PS/Cl-_Peak area change Time (min)	PMS/Cl_Peak area change Time (min)
TP1	$C_{12}H_8N_6$	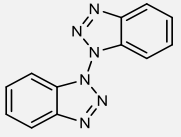	236.08099	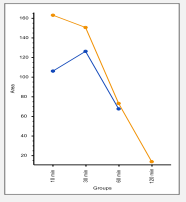 10,30,60,120	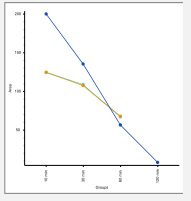 10,30,60,120		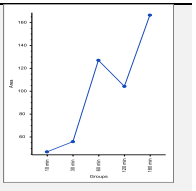 10,30,60,120,180
TP2	$C_{18}H_{11}N_9$	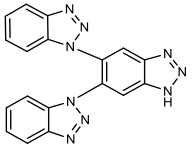	353.11347	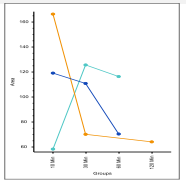 10, 30,60,120	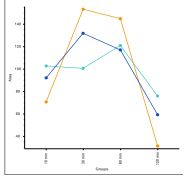 10,30,60,120		

Transformation products (TPs)	Proposed formula	Proposed structure	Observed Molecular weight (m/z)	PS _Peak area change Time (min)	PMS_Peak area change Time (min)	PS/Cl-_Peak area change Time (min)	PMS/Cl_Peak area change Time (min)
TP3	$C_{12}H_8N_2$	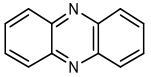	180.06825	30	10		
TP4	$C_6H_3N_3O_2$	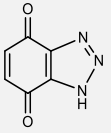	149.02270	60			10
TP5	$C_6H_7N_3O_2$	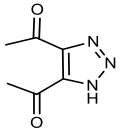	153.05353	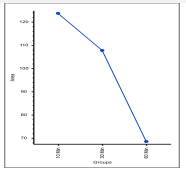 10,30,60	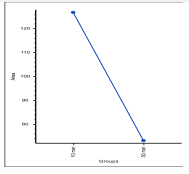 10,30		
TP6	$C_6H_7N_3O_3$	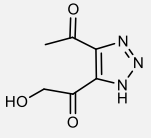	169.04880	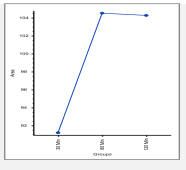 30,60,120	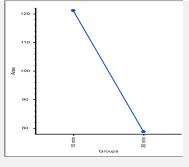 10,30		

TP7	$C_6H_9N_3O_4$	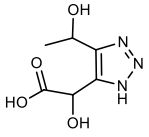	187.05896	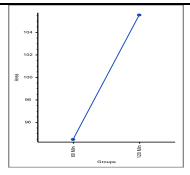			
				60, 120			
TP8	$C_3H_3N_3O_2$	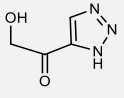	113.02287	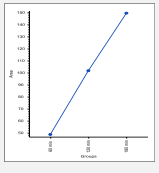	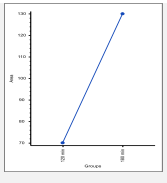		
				60,120,180	120,180		
TP9	$C_4H_3N_3O_3$	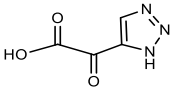	141.01765	120	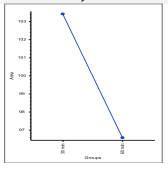		
					30, 60		
TP10	$C_4H_3N_3O_4$	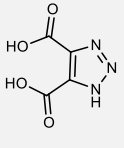	157.01269	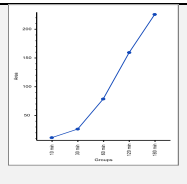	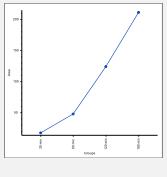	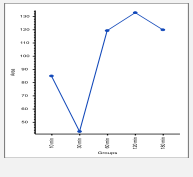	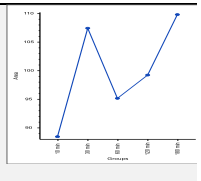
				10,30,60, 120,180	30,60, 120,180	10,30,60,120,180	10, 30,60,120,180

Transformation products (TPs)	Proposed formula	Proposed structure	Observed Molecular weight (m/z)	PS _Peak area change Time (min)	PMS_Peak area change Time (min)	PS/Cl-_Peak area change Time (min)	PMS/Cl_Peak area change Time (min)
TP11	$C_4H_8O_5$	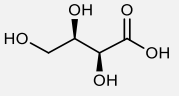	136.03746	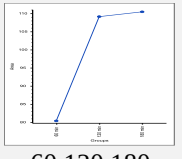 60,120,180	180		
TP12	$C_4H_4O_4$	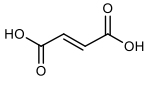	116.01131	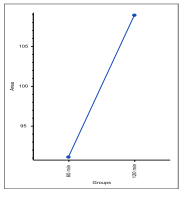 60, 120	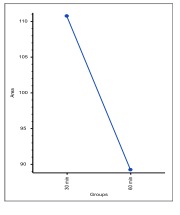 30, 60	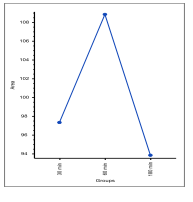 30, 60, 180	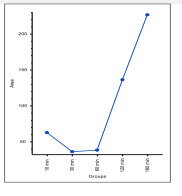 10,30,60,120,180
TP13	$C_4H_7NO_2$	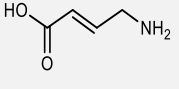	101.04727	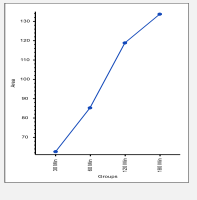 30,60,120,180	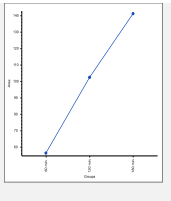 60,120,180		

TP14	$C_4H_3NO_2$	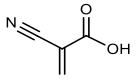	97.016380	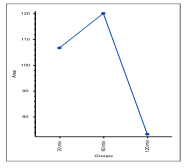 30,60,120	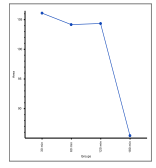 30,60,120,180	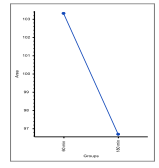 60,180	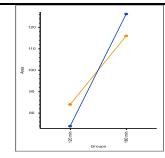 120,180
TP15	$C_4H_7NO_4$	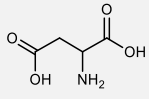	133.03729	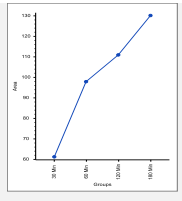 30,60,120,180	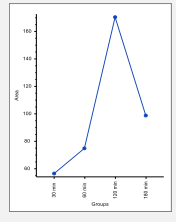 30,60,120,180		
TP16	$C_3H_6O_4$	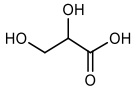	106.02675	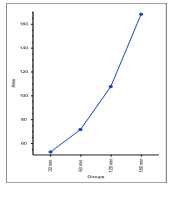 30,60,120,180	180	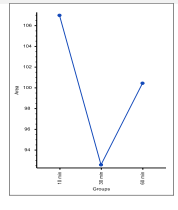 10,30,60	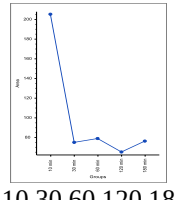 10,30,60,120,180
TP17	$C_3H_4O_3$	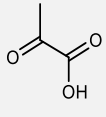	88.01570	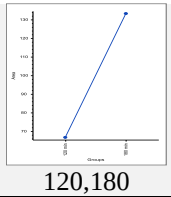 120,180	180		

Transformation products (TPs)	Proposed formula	Proposed structure	Observed Molecular weight (m/z)	PS _Peak area change Time (min)	PMS_Peak area change Time (min)	PS/Cl-_Peak area change Time (min)	PMS/Cl_Peak area change Time (min)
TP18	$C_3H_6O_3$	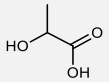	90.03140	180	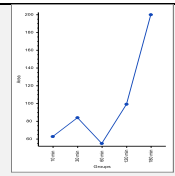 10,30,60,120,180		
TP19	$C_2H_4O_3$	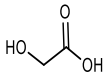	76.01536	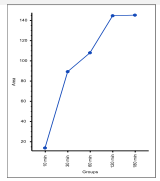 10,30,60,120,180	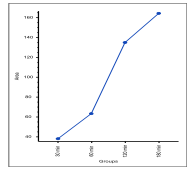 30,60,120,180		
TP20	$C_2H_3N_3$		69.0327	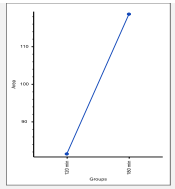 120,180	180		

TP21	$C_6H_7N_3O_4$	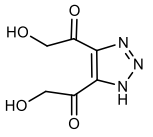	185.04378	60	
TP22	$C_6H_4N_4O_2$	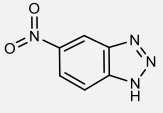	164.033432		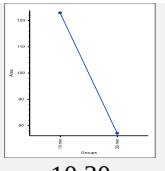 10,30
TP23	$C_6H_4N_4O_3$	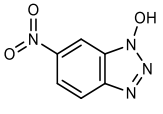	180.028336		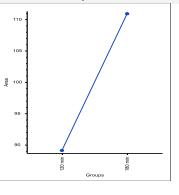 120,180
TP24	$C_6H_5N_3O_5$	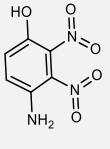	199.02310	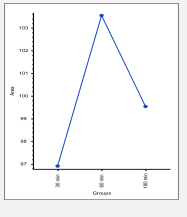 30,60,180	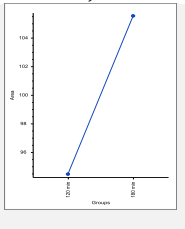 120,180

Transformation products (TPs)	Proposed formula	Proposed structure	Observed Molecular weight (m/z)	PS _Peak area change Time (min)	PMS_Peak area change Time (min)	PS/Cl-_Peak area change Time (min)	PMS/Cl_Peak area change Time (min)
TP25	$C_4H_6O_4$	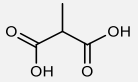	118.02695			30	
TP26	CHN_3O_3	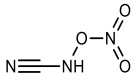	103.00183			30	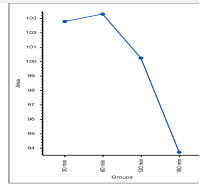 30,60,120,180
TP27	HNO_3		62.99465	180	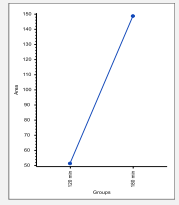 120,180	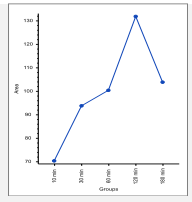 10, 30,60,120, 180	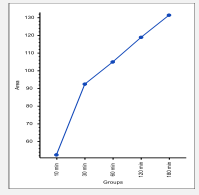 10, 30,60,120, 180
TP28	$C_6H_4ClN_3$	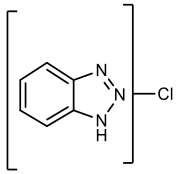	153.00909			10	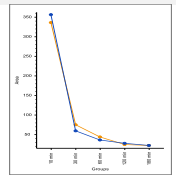 10,30,60,120,180

TP29	$C_6H_3Cl_2N_3$	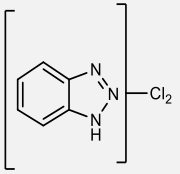	186.97040		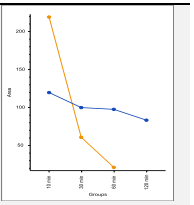 10,30,60,120,180
TP30	$C_6H_2Cl_3N_3$	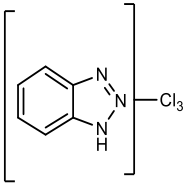	220.931427	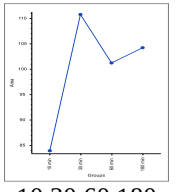 10,30,60,180	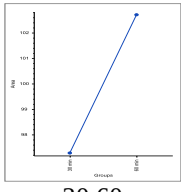 30,60
TP31	$C_6HCl_4N_3$	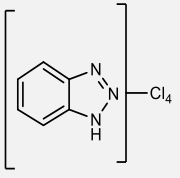	254.892456		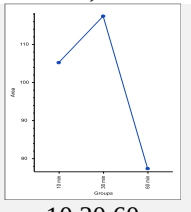 10,30,60
TP32	$C_6H_4ClN_3O$	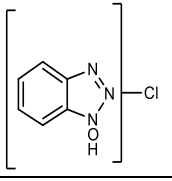	169.00442		180

Transformation products (TPs)	Proposed formula	Proposed structure	Observed Molecular weight (m/z)	PS _Peak area change Time (min)	PMS_Peak area change Time (min)	PS/Cl-_Peak area change Time (min)	PMS/Cl_Peak area change Time (min)
TP33	$C_6H_3Cl_2N_3O$	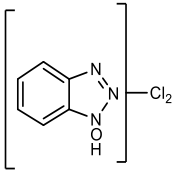	202.965317				180
TP34	$C_6H_2Cl_3N_3O$	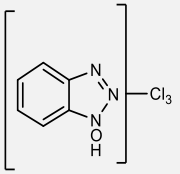	236.92645				180
TP35	$C_6H_7Cl_2N_3O_2$	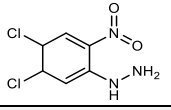	222.99089				10
TP36	$C_4H_3ClO_4$	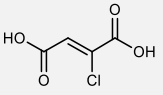	149.971985			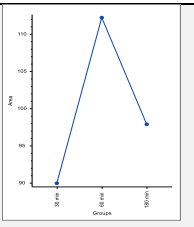 30,60,120	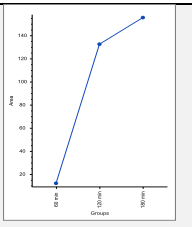 60,120,180

TP37	$C_4H_6ClNO_2$	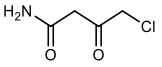	135.00840		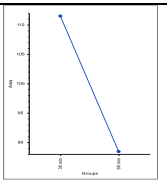 30,60
TP38	$C_3H_3ClO_2$	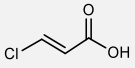	105.982155		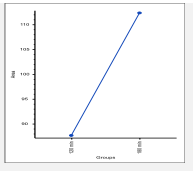 120, 180
TP39	$C_2H_2Cl_2O_2$	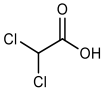	127.94351	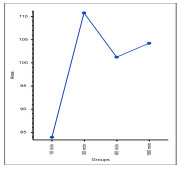 10,30,60,120,180	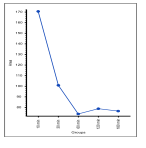 10,30,60,120,180
TP40	$C_2H_3ClO_2$	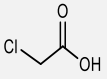	93.982155		10

Transformation products (TPs)	Proposed formula	Proposed structure	Observed Molecular weight (m/z)	PS _Peak area change Time (min)	PMS_Peak area change Time (min)	PS/Cl-_Peak area change Time (min)	PMS/Cl_Peak area change Time (min)
TP41	$C_2HCl_2N_3$		136.9546			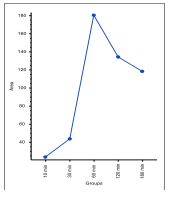 10,30,60,120,180	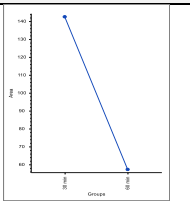 30, 60
TP42	C_2HClN_2O	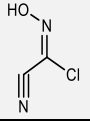	103.97786			180	

SUPPLEMENTARY MATERIALS: CHAPTER 6

Analytical methods:

Text S6-1.a: Total organic carbon (TOC)

Total organic carbon TOC of the samples were analyzed by a TOC-L CPH/CPN analyzer (Shimadzu, Japan) integrated with an ASI-L autosampler (Shimadzu, Benelux). The non-purgeable organic carbon (NPOC) determination method was used for TOC analysis because of the absence of purgeable organic components in CTBD. The sample was introduced into a syringe for acidification with 20% sulphuric acid to convert all the dissolved inorganic carbon to carbon dioxide. Then the syringe was sparged with CO_2-free systemic air for removing carbon dioxide from the injected sample. After that, the inorganic carbon-free sample was introduced into a furnace full of pellets coated with platinum acting as a catalyst for carbon oxidation formation from carbon, at the temperature of 720^{o}C presence of CO_2-free synthetic air. In these conditions, all the organic carbon was converted to carbon dioxide and was analyzed employing a nondispersive IR detector (NDIR) as total organic carbon (TOC) [355].

Text S6-1.b: Anion and cation determination

The anions (Cl^-, ClO_3^-, ClO_4^-, NO_3^-, NO_2^-, and SO_4^{2-}) concentration was measured by Dionex ICS-2100 ion chromatography (IC) (Thermo, USA). The IC was equipped with Dionex, IonPac AS19, and a 4×250 mm ion exchange column. The anions were separated in the column due to the eluent gradient. The eluent was automatically prepared in a KOH cartridge (Dionex P/N 058900) using deionized water as the carrier. The ions were detected in the DS6 heated conductivity cell. Perkin Elmer ICP-OES AVIO 500 plasma atomic emission spectroscopy (ICP) was used to determine the cations (Na^+, Ca^{2+}, Mg^{2+}, and K^+). Flat Plate™ plasma technology was used in the ICP to produce the plasma from 10 L.min^{-1} Argon. The ICP was equipped with the high-energy (f/6.7) echelle-based Polychromator detector utilizing two segmented-array charges-coupled devices (SCD) covering the spectral range from 163-782 nm. Syngistix Software was used to analyze the results

Text S6-1.c: Free chlorine analysis:

ClO^- concentration for EO, UVC, and UVC/VUV experiments were measured using Hach chlorine (free & total chlorine) reagent (Hach Lange GmbH, Germany). For the PCD experiment, the ClO^- concentration was determined using a Hanna Instruments Free Chlorine Photometer (HI 96711) and reagents (HI-93701). Due to residual PS interference in the PS process samples, ClO^- concentration was analyzed using a modified DPD–FAS standard (APHA, 1995) based on the reported method [306]. In this way, 20 mL EDTA (5%) was added to 5 mL buffer and 5 mL DPD and mixed with a 50 mL sample to avoid PS interference. The mixture was titrated with ferrous ammonium sulfate (FAS) (1 mL FAS = 0.1 mg Cl_2). Samples were measured directly after all experiments.

Text S6-1.d: PS and H_2O_2 analysis

The PS and H_2O_2 concentrations were determined by the spectrophotometric method. For PS measurement, 1 mL diluted sample, 3.9 mL Milli-Q, 5 mL phosphate buffer (50 Mm), and 0.1 mL N, N-diethyl-p-phenylenediamine (DPD) solution (0.25 M) were mixed in 12 mL sampling tube. After 10 min, the mixed solution was measured in a cuvette with a spectrophotometer (Hach DR/3900, Lange GmbH, Germany) at 552 nm and 510 nm [243]. H_2O_2 concentration was analyzed based on the method presented in a previous study [510]. 0.5 mL of the sample was mixed with 0.5 mL phosphate buffer (10 mM, pH = 7.0) and 1 mL KI (1 M), and the absorbance of the mixed solution was measured at 352 nm with the same spectrophotometer [510].

Text S6-1.e: Fluorescence excitation-emission matrix (FEEM)

Perkin Elmer Luminescence Spectrometer LS50B (United Kingdom) was used for Fluorescence excitation-emission matrix (FEEM) analysis. FEEM gives a contour plot of excitation wavelength vs. emission wavelength vs. fluorescence intensity. Before FEEM measurement, samples were diluted to maintain the UV_{254} absorbance falling between 0.07-0.09 cm^{-1} [511]. Data processing was done with the StaRdom package in R [512]. Data processing included baseline correction, blank subtraction, RAMAN normalization, scattering removal, dilution correction, and interpolation. According to Chen et al. (2003), FEEM spectra are divided into five regions: Regions I and II (Ex<250 nm, Em<380 nm) for aromatic proteins such as tyrosine-like and tryptophan-like substances; region III (Ex<250 nm, Em>380 nm) for fulvic-like substances; region IV (Ex>250 nm, Em<380 nm) for soluble

microbial byproduct-like substances; and region V (Ex >250 nm, Em >380 nm) for humic-like substances [513]. Also, in region V, Ex/Em: 250-320/380-550 nm (region V-i) and Ex/Em: 320-380/380-480 nm (region V-ii) corresponds to carboxylic-like substances and phenolic-like substances of the HA, respectively [513-515]. Fluorescence regional integration (FRI) of these regions' intensity was calculated according to the method prescribed in previous works [514].

Text S6-1.f: liquid chromatography-organic carbon detector (LC-OCD)

Size-exclusion liquid chromatography-organic carbon detector (LC-OCD) device (Model 8, DOC-Labor, Germany) was used for OCs molecular size distribution analysis. Before analysis, samples were filtered with a 0.45 μm polytetrafluoroethylene filter. The LC-OCD was equipped with a Siemens Ultramat 6^E NDIR detector, together with an Agilent 1260 organic nitrogen detector (UV 220 nm) and UV detector (254 nm). The size exclusion of each sample was performed in "Agilent BioSec 5 5μm 1000 A (7.8 mm × 300 mm) column followed by a Toyopearl HW-50S 30 μm (20 mm × 250 mm) column". On-line purified 28 mmol phosphate buffer at pH = 6.6 was used as mobile phase with a flow rate of 1.1 mL/min [166, 516]

Text S6-2: Determination of total exposure of photon fluence for VUV and UVC (actinometry)

The total exposure of photon fluence (F_p) for VUV and UVC was measured by chemical actinometry according to the method from [517]. For $F_{p,UVC}$, a uridine solution (0.12 mM) was circulated in the UVC system for 10 min. In the uridine experiment, samples were taken every minute and measured at 262 nm with a UV-VIS spectrophotometer (M200 Infinite Pro Microplate Reader, Tecan, Switzerland). Then, the $F_{p,UVC}$ was calculated as:

$$F_{p,UVC} = E_{p,UVC}\, t_{ee} = \frac{k_u}{\mathrm{In}(10) \times 0.1 \times \varepsilon_\lambda \times \Phi_u}\, t_{ee} \quad \text{(S6.1)}$$

$$t_{ee} = \frac{\pi r^2 h}{V} t \quad \text{(S6.2)}$$

Where $E_{p,UVC}$ is the photon fluence rate (Einstein·m^{-2}·S^{-1}), k_u is the slope of ln([uridine]/[uridine]$_0$)-timeline plotting from experimental data (s^{-1}); ε_λ is the dyadic molar absorption coefficient at an exposure wavelength (λ), ε_{254} is 8775 (M^{-1}·cm^{-1}); Φ_u is the quantum yield of uridine 0.020; r and h are the radius and

length of the reactor (m), respectively; V is the total sample volume (m^3); t is the reaction time (s).

For $F_{p,VUV}$, H_2O_2 accumulation in the VUV system was measured and used for calculation [353]. The experimental setup and procedure were the same as UVC/VUV experiment. 1 L Milli-Q water was circulated in the reactor. The samples were collected at one-minute intervals for the first 5 min; after that sample was collected in every five-minute interval. The $F_{p,VUV}$ was calculated as:

$$F_{p,UVC} = \frac{q}{S} \quad \text{(S6.3)}$$

$$q = \frac{r_{H2O2} V}{\emptyset} \quad \text{(S6.4)}$$

Where q is the absorbed VUV photon flux (einstein·s^{-1}), S is the cross-sectional area of the reactor (m^2), r H_2O_2 equals 1.7×10^{-8}, Φ is the total quantum yields of HO· produced from VUV photolysis of water equals to 0.024 [353].

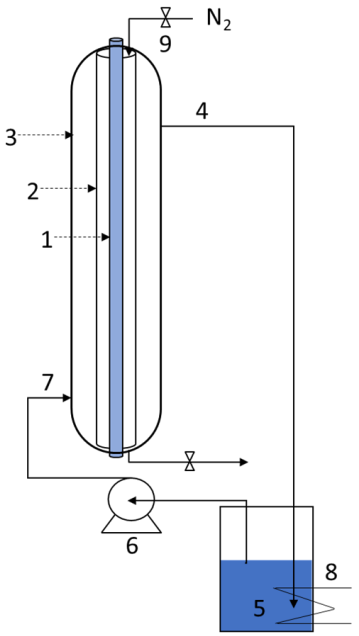

Fig. S6-1. *Schematic of VUV/UVC and UVC experimental setup. 1. UV lamp, 2. quartz sleeve, 3. stainless steel photoreactors, 4. reactor outlet, 5. circulation water tank, 6. peristaltic pump, 7. reactor inlet, 8. cooling water circulation, 9. N2 purging between UV lamp and sleeve.*

Text S6-3: Power consumption calculation:

1. EO:

In the EO process, the power consumption can be expressed by

$$P\ (w) = V_c \times I \quad \text{(S6.5)}$$

Vc is the cell voltage in Volts, and I is the applied current in A. The Applied current was 0.19 A during the experiment, and the average cell voltage was 7.5 V.

PCD:

It was reported that UV light emits 0.32 mW/cm^2 intensity at 375nm [108]. The dimension of the Glass Beaker was 5x7 cm (d x h). So, the power consumption can be expressed by

$$P\ (w) = \text{Photon energy } \left(\frac{w}{cm^2}\right) \times \text{surface area } (cm^2) \quad \text{(S6.6)}$$

PS:

In PS experiments, 150 ml CTBD was heated from 25 to 70^{o}C. The energy requirement for heating the CTBD can be calculated by

$$\text{Energy for heating } (wh) = m \times C_p \times \Delta T \quad \text{(S6.7)}$$

Here m is the mass of the CTBD in g. It was assumed that the density of the CTBD was equal to the water. Cp is the heat capacity of the CTBD in J/g°C. It was assumed that the Cp of the CTBD was 4.184 joules/g °C. 1 joule= 0.000278 wh. ΔT is the temperature difference in ^{o}C.

In addition, during the experiment, the heat was lost. Heat loss can be expressed by Q (w) as

$$Q\ (w) = h \times A \times \Delta T \quad \text{(S6.8)}$$

Here, h is the heat transfer coefficient in W/m^2.K. A is the contact surface area in m^{2,} which was in contact with air. Here the radiation heat transfer is neglected. The radius of the reactor was 0.025 m. ΔT is the temperature difference in K. It is assumed that the convective heat transfer coefficient, h, for air-water is 2.5 W/m^2.K.

So, the total energy requirement for heating was

$$\text{Total heating energy (wh)} = \text{Energy for heating (wh)} + Q\,(w) * t(h) \quad \text{(S6.9)}$$

Here, t is the duration of the experiment in hours.

UVC

It was measured that UVC light emits 20.9 mW/cm^2 intensity at 254 nm. The dimension of the inner surface was 2.5x40 cm (d x h). So, the power consumption can be expressed as

$$P_{UVC}(w) = \text{Photon energy } \left(\frac{w}{cm^2}\right) \times \text{surface area } (cm^2) \quad \text{(S6.10)}$$

Here the surface area (cm^2) can be calculated as 2πrh. R is the r radius of the surface, and h is the height.

UVC/VUV

It was measured that UVC light emits 8.2 mW/cm^2 intensity at 185 nm. The dimension of the inner surface was 2.5x40 cm (d x h). So, the power consumption can be expressed as

$$P_{VVC}(w) = \text{Photon energy } \left(\frac{w}{cm^2}\right) \times \text{surface area } (cm^2) \quad \text{(S6.11)}$$

Here, surface area (cm^2) can be calculated as 2πrh. R is the radius of the surface, and h is the height. Generally, the VUV lamp emitted 90% UVC light and 10% VUV light. In addition, Mengkai Li et al. [518] show that contribution of the UVC light from UVC and VUV lamp was close. Therefore, total photon energy can be expressed as

$$P_{VVC/UVC}(w) = P_{VVC}(w) + (0.9 \times P_{UVC})(w) \quad \text{(S6.12)}$$

Table S6-1. *Characteristics of cooling tower blowdown used in this study*

Parameter	Unit	Avg. (±SD)
Conductivity	mS/cm	3.4 (0.1)
Cl^-	mg/L	467 (3)
NO_3^-	mg/L	31 (1)
SO_4^{2-}	mg/L	1201(50)
Na^+	mg/L	237 (40)
Ca^{2+}	mg/L	300 (7)
Mg^{2+}	mg/L	58 (14)
K^+	mg/L	79 (14)
CO_3^{2-} and HCO_3^- (Total inorganic carbon)	mg/L	10 (1)
DOC	mg/L	42 (1)
TOC	mg/L	47(1)
COD	mg/L	105 (4)
AOX	mg Cl^-/L	1.3 (0.1)
pH	-	7.4 (0.3)

Table S6-2. *TOC removal of CTBD water after treating by PS with differing initial PS dose at pH = 7, 70℃, 3 h.*

PS concentration (mM)	TOC (mg/L)	Removal (%)	PS consumption (mM)
5	16.282	57	4.1
10	5.940	83	5.7
15	2.316	94	5.2

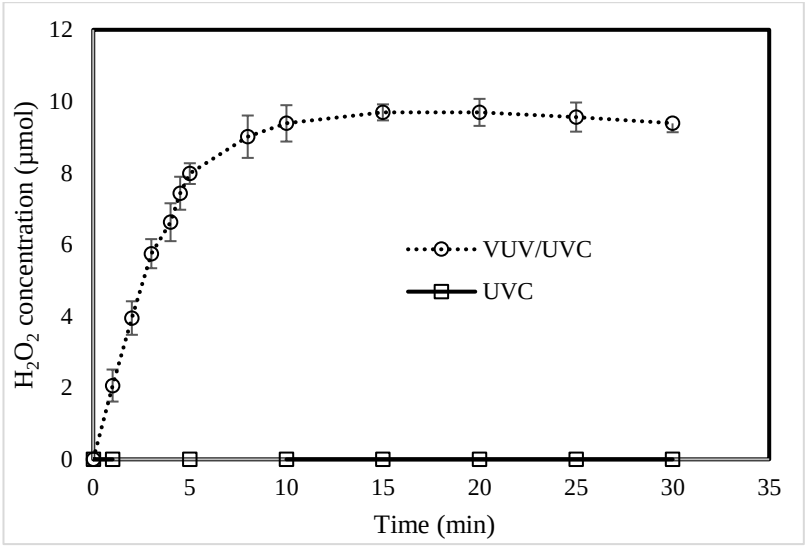

Fig. S6-2. *H_2O_2 accumulation in VUV/UVC and UVC system in Milli-Q*

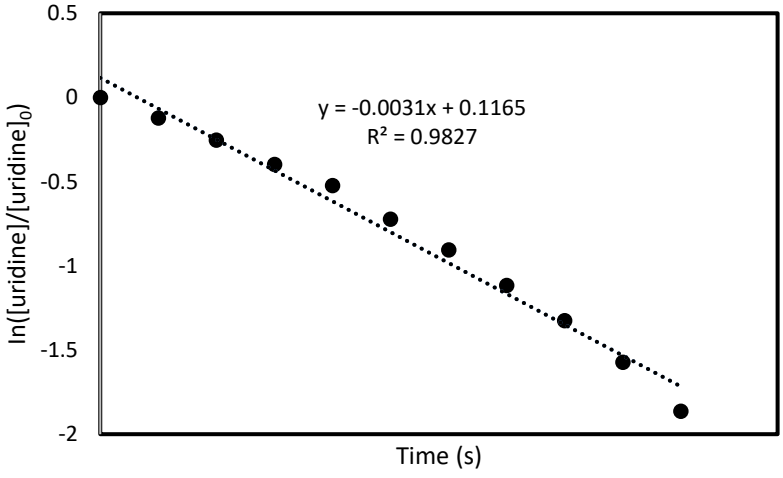

Fig. S6-3. *Change of uridine concentration in operating UVC system*

Table S6-3. *pH change after different AOPs treatment*

AOPs	Initial pH	Final pH
EO	3.0	3.5
	7.3	6.9
	10.0	9.2
PCD	3.0	3.1
	7.7	6.9
	10.0	7.4
PS	3.2	2.7
	7.2	6.7
	9.8	9.9
UVC process	3.0	3.4
	7.5	7.3
	10.0	7.3
UVC/VUV	3.1	3.4
	7.7	7.3
	9.9	7.6

Table S6-4. *COD and TOC removal from CTBD during blank experiments*

	Conditions	% COD removal	% TOC removal
EO	No current	02	-
PCD	UV-375 (No cat.)	01	01
	Catalyst in dark	09	10
PS	70 ºC (no PS)	02	-
	10 mM PS, 25 ºC	-	14
UVC/VUV	In dark	01	-

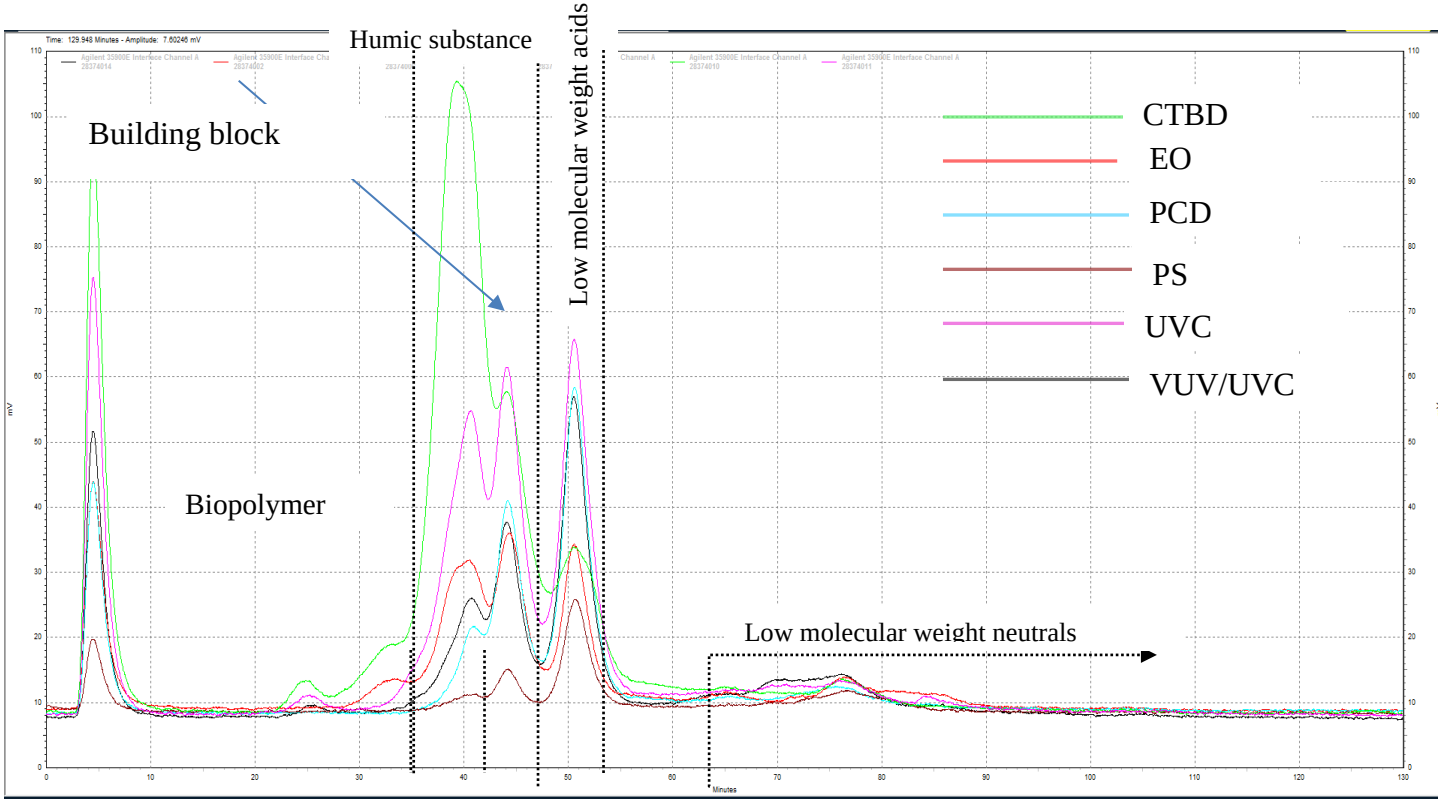

Fig. S6-4. *LC-OCD change of chromatographic peaks of the CTBD before and after treatment*

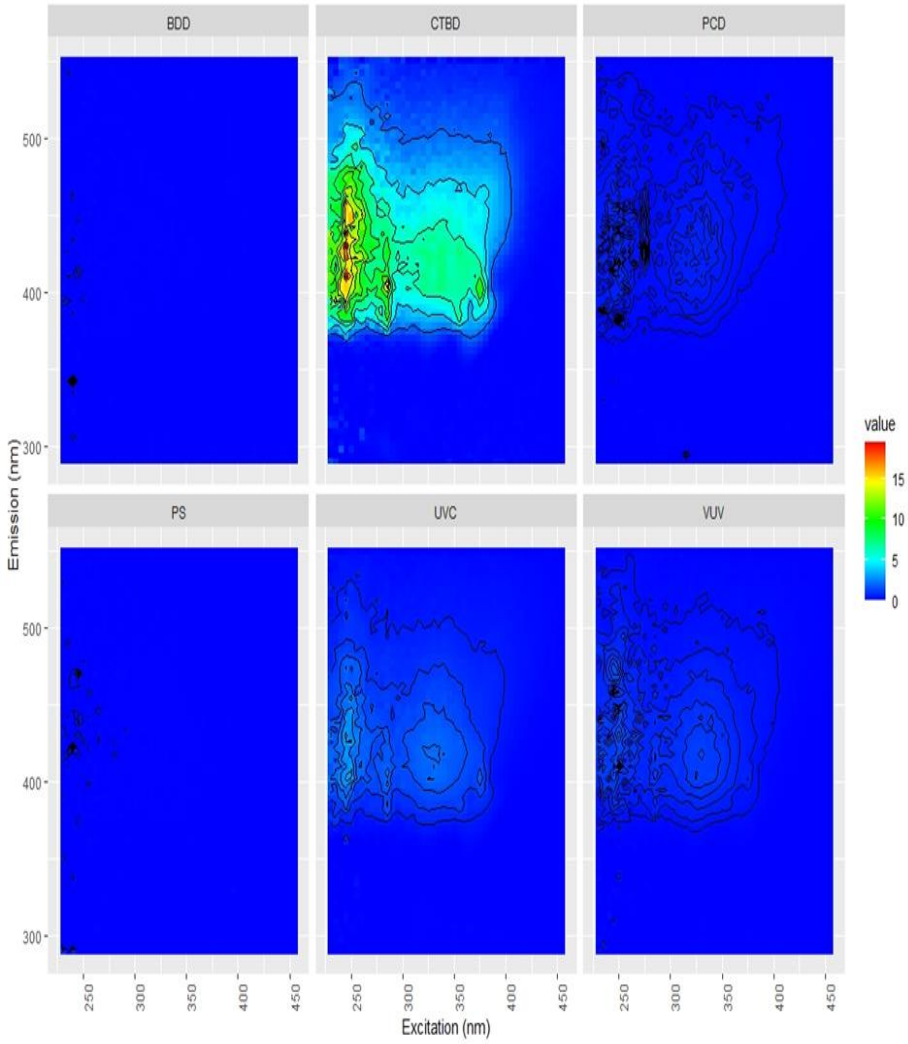

Fig.S6-5. *Change of humic substance FEEM profile during different AOPs: (1) EO with BDD anode at 8.5 mA/cm^2 (5 h), (2) PCD with TiO_2 catalyst at 375 nm UV light (5 h), (3) PS with 10 mM PS, 70°C (3 h), (4) UVC/VUV with 185/254 nm UV light (5 h), and (5) UVC with 254 nm UV light (5 h), pH = 7.4.*

Table S6-5. *Individual regions' and total fluorescence regional integration (FRI) intensity removal after AOPs treatments: : (1) EO with BDD anode at 8.5 mA/cm^2 (5 h), (2) PCD with TiO_2 catalyst at 375 nm UV light (5 h), (3) PS with 10 mM PS, 70℃ (3 h), (4) UVC/VUV with 185/254 nm UV light (5 h), and (5) UVC with 254 nm UV light (5 h), pH = 7.*

% FRI removal for each Region	EO	PCD	PS	UVC	VUV/UVC
Region I (tyrosine-like proteins)	94%	92%	87%	96%	87%
Region II (tryptophan-like proteins	97%	93%	98%	84%	89%
Region III (fulvic like HS)	99%	95%	99%	86%	90%
Region IV (microbial by-product)	89%	86%	90%	84%	84%
Region V (humic acid like-HS)	95%	90%	95%	83%	87%
Region V_i (carboxylic-like-HS)	100%	95%	99%	84%	89%
Region V_ii (phenolic-like-HS)	91%	87%	92%	82%	85%
% FRI removal for overall region	97%	93%	98%	85%	89%

SUPPLEMENTARY MATERIALS: CHAPTER 7

Fig. S7-1. *Pilot-scale hybrid constructed wetlands, located close to the cooling tower (red circle). Cooling tower water flows from right to left vertical subsurface-flow constructed wetland → surface flow constructed wetland → horizontal subsurface flow constructed wetland.*

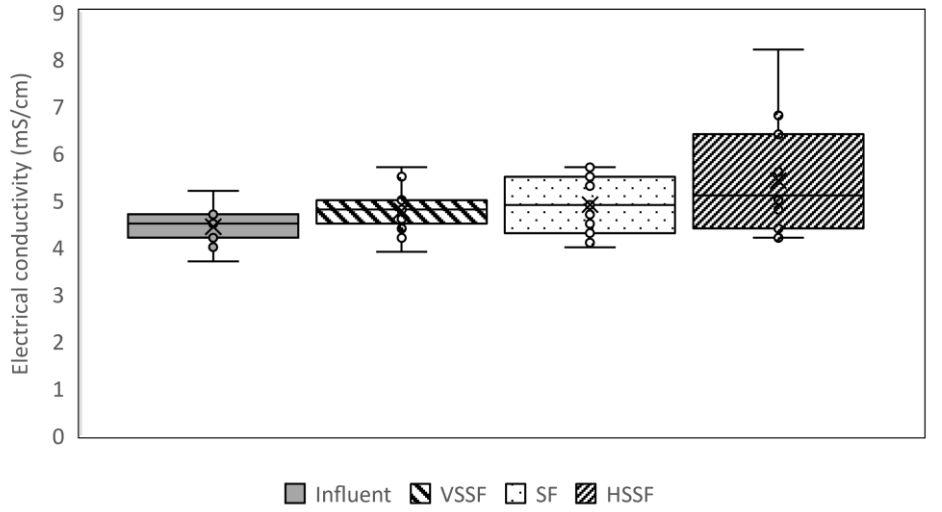

***Fig. S7-2**. Electrical conductivity of the effluent of the different hybrid constructed wetland compartments. The HSSF compartment equals the effluent of the complete hybrid constructed wetland. The horizontal line represents the median value, the X represents the average value, the boxes represent the first and third quartile and the whiskers represent the maximum values.*

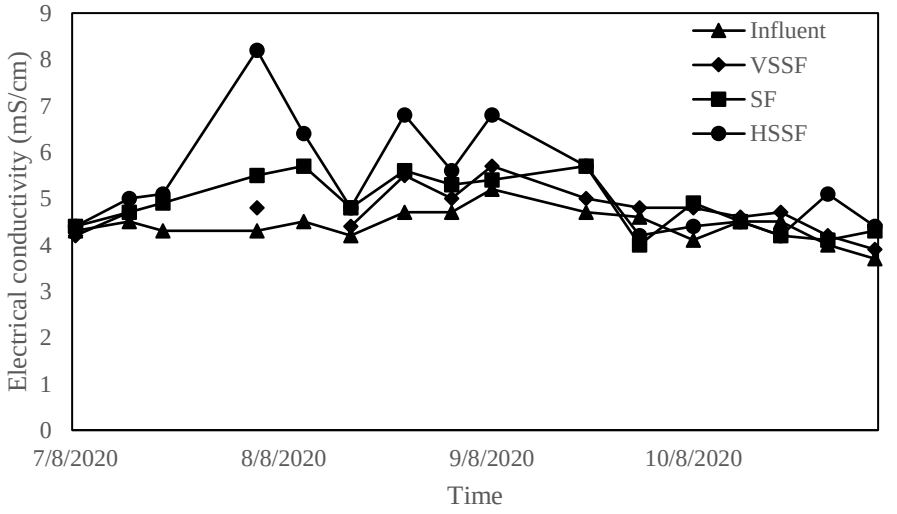

***Fig. S7-3.** Electrical conductivity of the effluent of the different hybrid constructed wetland compartments over the experiment period. The HSSF compartment equals the effluent of the complete hybrid constructed wetland.*

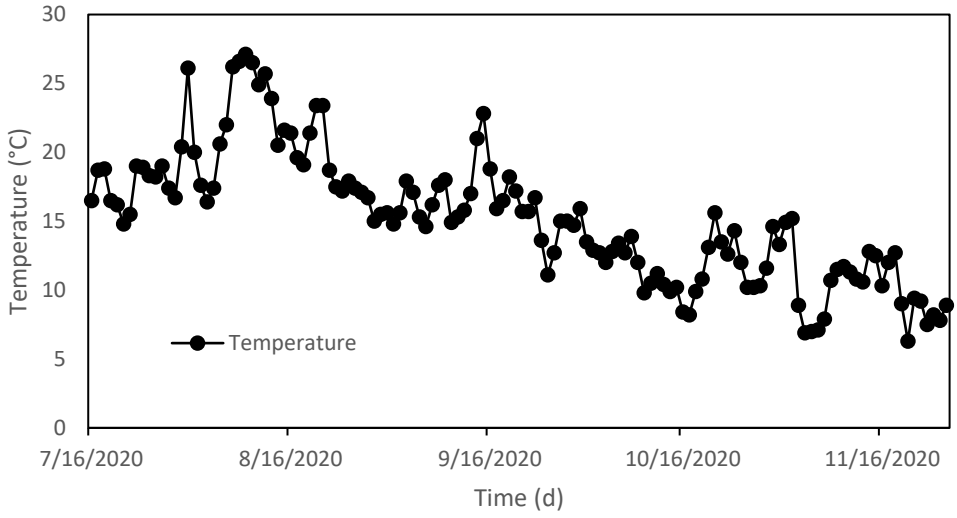

Fig. S7-4. *Average daily temperature (°C) in Wilhelminadorp (37 km from the hybrid constructed wetland location).*

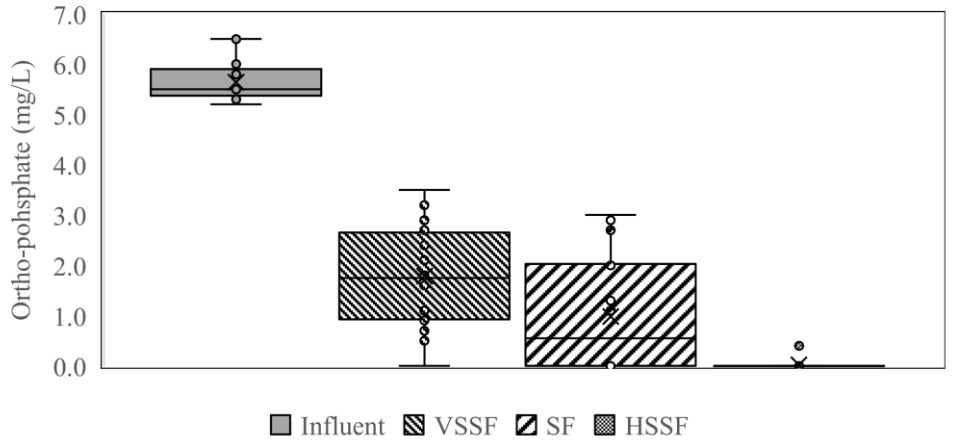

Fig. S7-5. *Phosphate concentration (mg/L) in the effluent of the different hybrid constructed wetland compartments. The HSSF compartment equals the effluent of the complete hybrid constructed wetland. The horizontal line represents the median value, the X represents the average value, the boxes represent the first and third quartile and the whiskers represent the maximum values.*

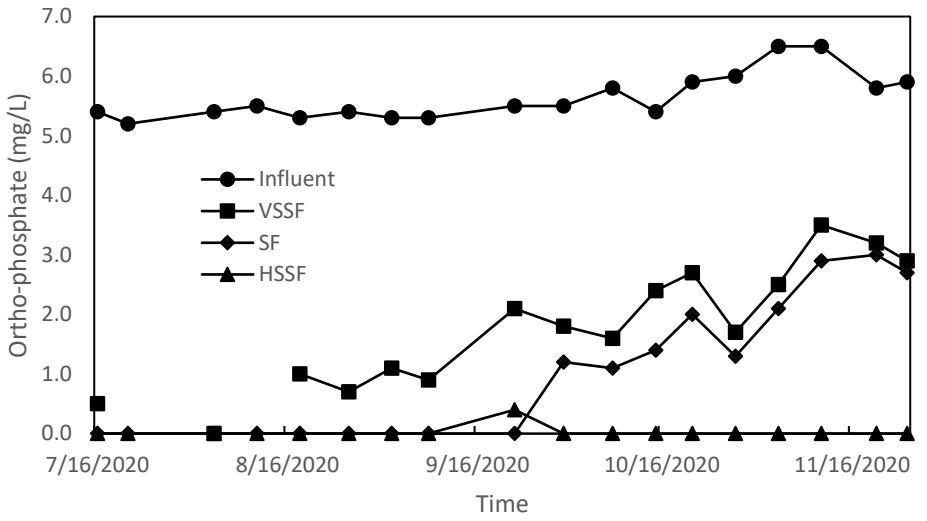

Fig. S7-6. *Phosphate concentration (mg/L) in the effluent of the different hybrid constructed wetland compartments over the experimental period. The HSSF compartment equals the effluent of the complete hybrid constructed wetland.*

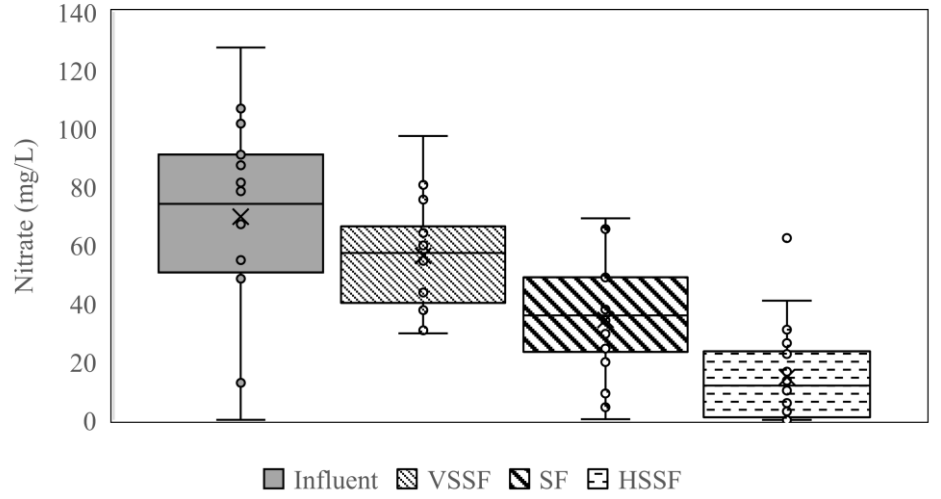

Fig. S7-7. *Nitrate concentration (mg/L) in the effluent of the different hybrid constructed wetland compartments. The HSSF compartment equals the effluent of the complete hybrid constructed wetland. The horizontal line represents the median value, the X represents the average value, the boxes represent the first and third quartile and the whiskers represent the maximum values.*

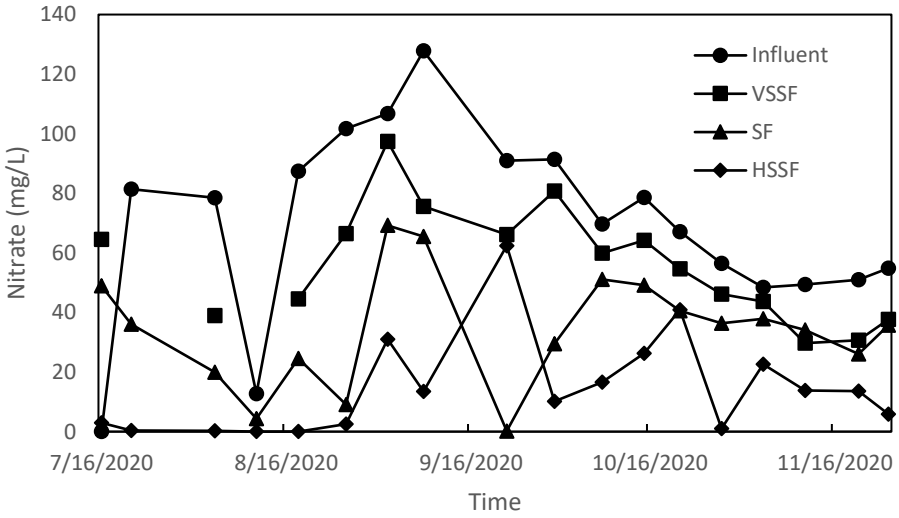

Fig. S7-8. *Nitrate concentration (mg/L) in the effluent of the different hybrid constructed wetland compartments over the experimental period. The HSSF compartment equals the effluent of the complete hybrid constructed wetland.*

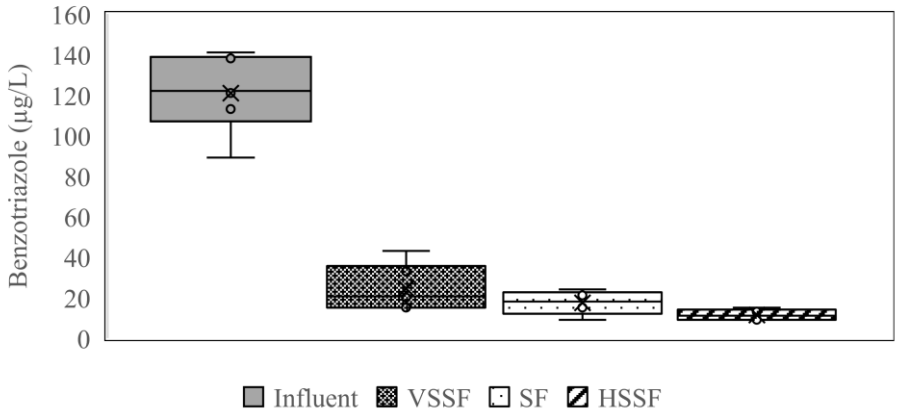

Fig. S7-9. *Benzotriazole concentration (µg/L) in the effluent of the different hybrid constructed wetland compartments. The HSSF compartment equals the effluent of the complete hybrid constructed wetland. The horizontal line represents the median value, the X represents the average value, the boxes represent the first and third quartile and the whiskers represent the maximum values.*

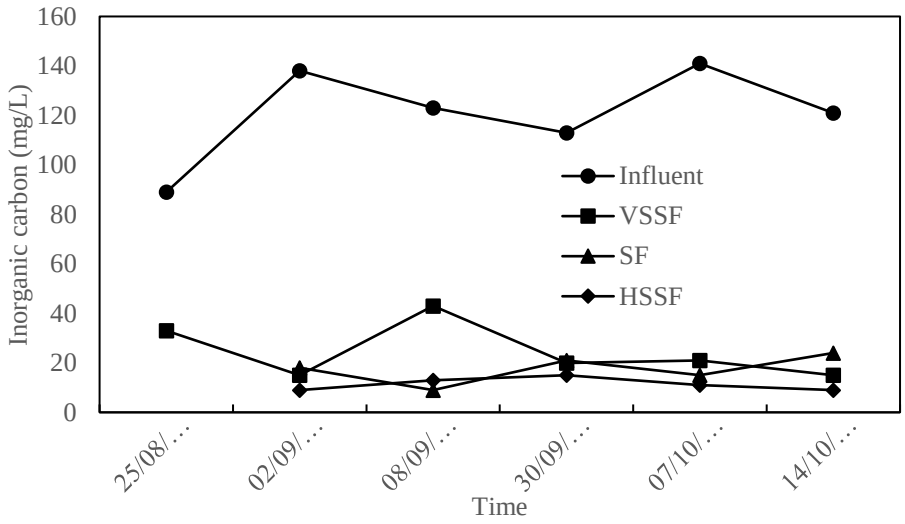

***Fig. S7-10**. Benzotriazole concentration (µg/L) in the effluent of the different hybrid constructed wetland compartments over the experimental period. The HSSF compartment equals the effluent of the complete hybrid constructed wetland.*

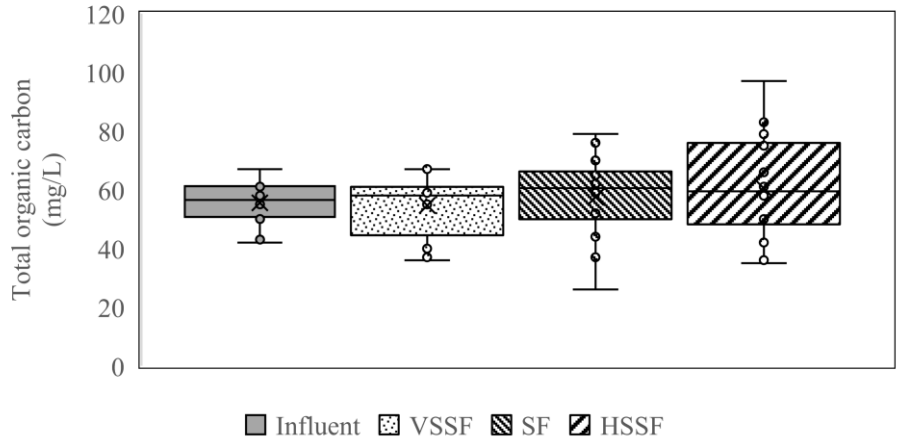

***Fig. S7-11.** Total organic carbon concentration (mg/L) in the effluent of the different hybrid constructed wetland compartments. The HSSF compartment equals the effluent of the complete hybrid constructed wetland. The horizontal line represents the median value, the X represents the average value, the boxes represent the first and third quartile and the whiskers represent the maximum values.*

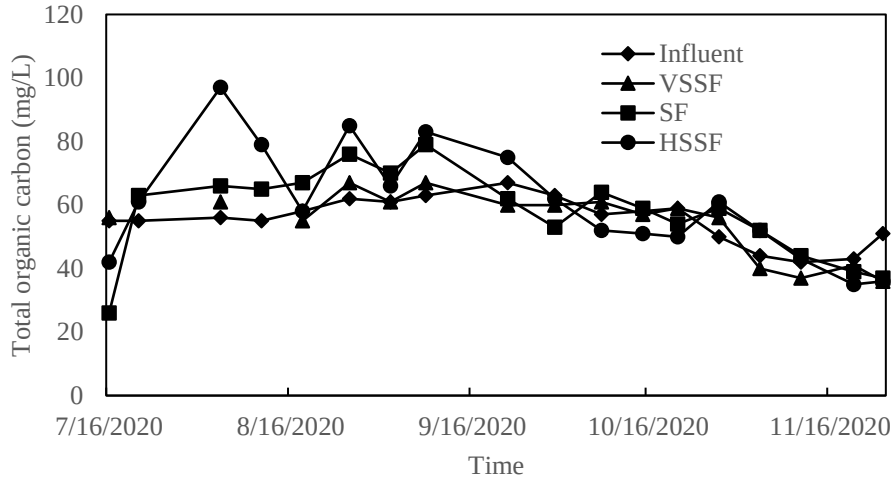

Fig. S7-12. *Total organic carbon concentration (mg/L) in the effluent of the different hybrid constructed wetland compartments over the experimental period. The HSSF compartment equals the effluent of the complete hybrid constructed wetland.*

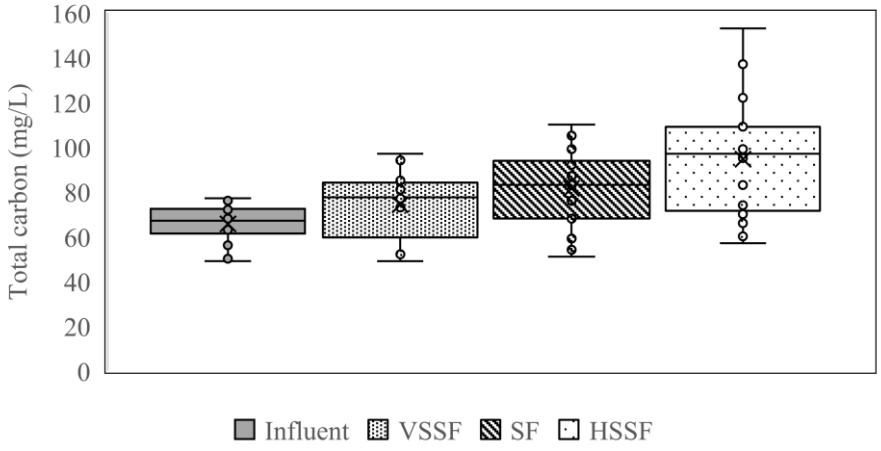

Fig. S7-13. *Total carbon concentration (mg/L) in the effluent of the different hybrid constructed wetland compartments. The HSSF compartment equals the effluent of the complete hybrid constructed wetland. The horizontal line represents the median value, the X represents the average value, the boxes represent the first and third quartile and the whiskers represent the maximum values.*

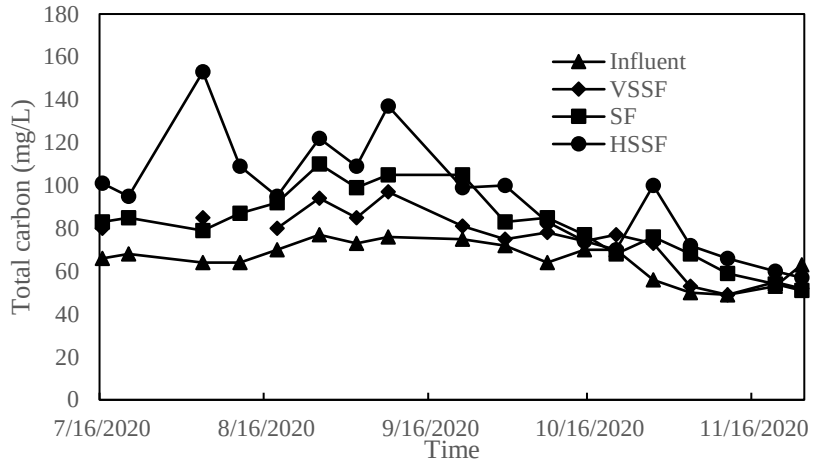

Fig. S7-14. *Total carbon concentration (mg/L) in the effluent of the different hybrid constructed wetland compartments over the experimental period. The HSSF compartment equals the effluent of the complete hybrid constructed wetland.*

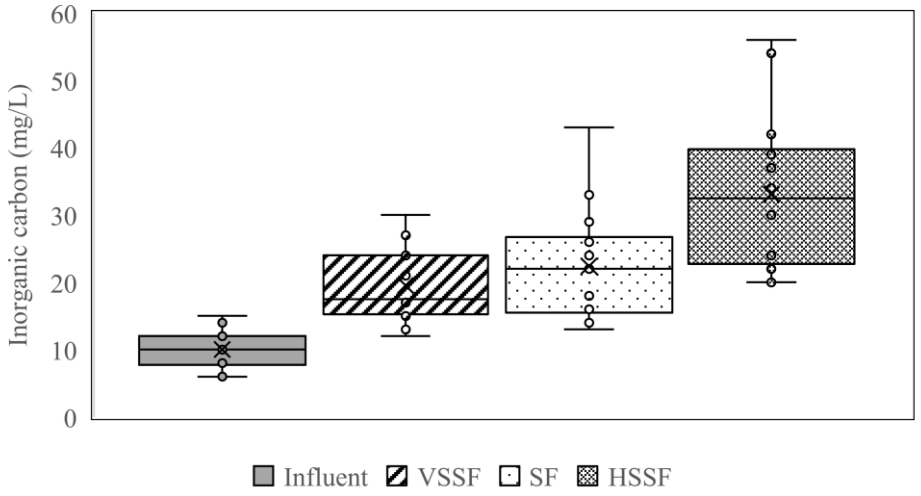

Fig. S7-15. *Total inorganic carbon concentration (mg/L) in the effluent of the different hybrid constructed wetland compartments. The HSSF compartment equals the effluent of the complete hybrid constructed wetland. The horizontal line represents the median value, the X represents the average value, the boxes represent the first and third quartile and the whiskers represent the maximum values.*

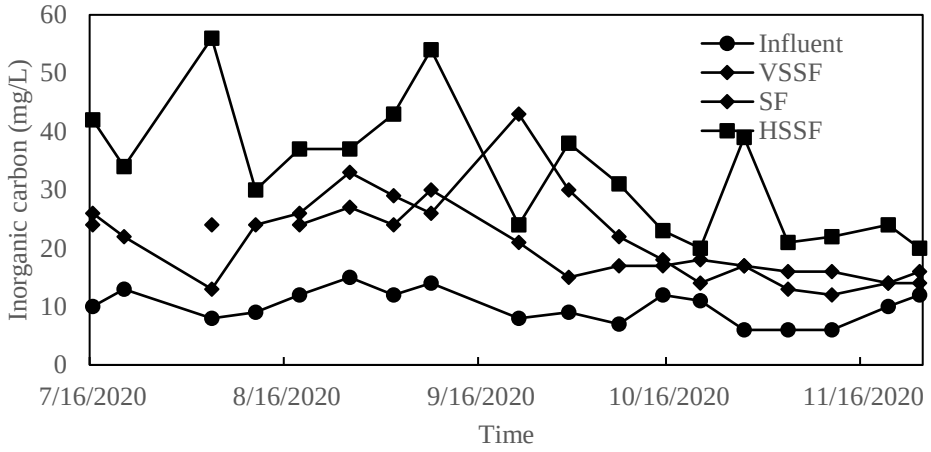

Fig. S7-16. *Total inorganic carbon concentration (mg/L) in the effluent of the different hybrid constructed wetland compartments over the experimental period. The HSSF compartment equals the effluent of the complete hybrid constructed wetland.*

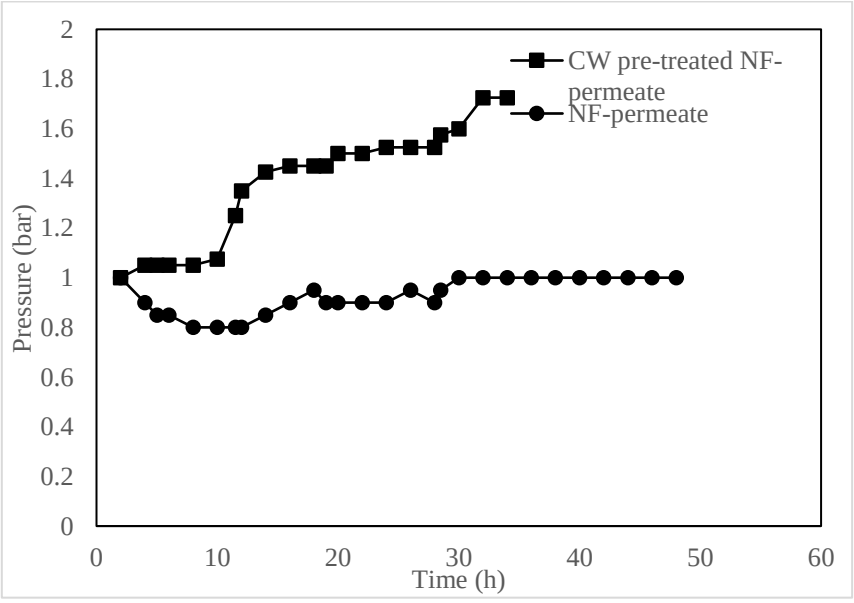

Fig. S7-17. *Transmembrane pressure during 4x10L 80% NF concentration runs*

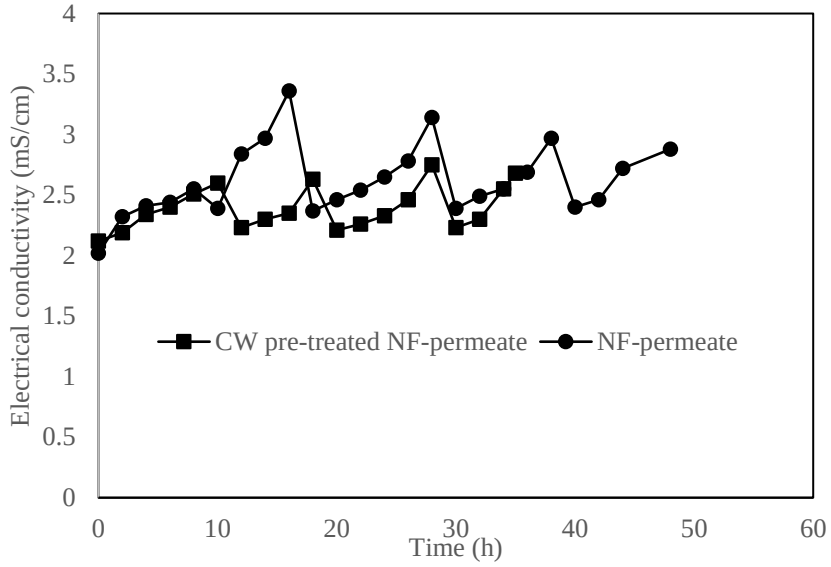

Fig. S7-18. *Electrical conductivity over time for both non-pre-treated and constructed wetland pre-treated permeate*

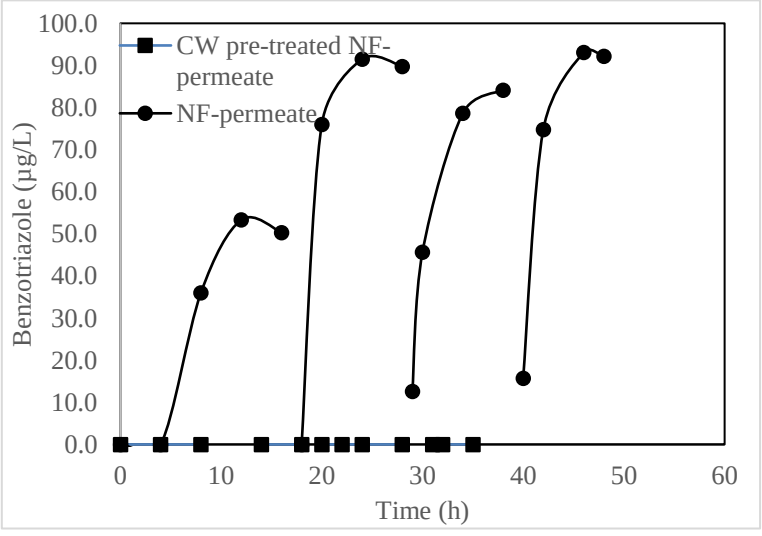

Fig. S7-19. *Benzotriazole concentration of time for constructed wetland pre-treated nanofiltration permeate and non-pre-treated permeate.*

Table S7-1. *Benzotriazole removal from different samples at different applied current densities*

Sample	Benzotriazole concentration (µg/L)
CTBD	82.9
NF concentrate	35
CW pre-treated NF concentrate	8.9
EO-CTBD[1] (8.5 mA/cm^{-2})	<2.5
EO-NF-CTBD[2] (8.5 mA/cm^{-2})	<2.5
EO-CW-NF-CTBD[3] (8.5 mA/cm^{-2})	<2.5
EO-NF-CTBD (14.3 mA/cm^{-2})	<2.5
EO-CW-NF-CTBD (14.3 mA/cm^{-2})	<2.5

[1]Electrochemical oxidation of cooling tower water

[2]Electrochemical oxidation of the nanofiltration concentrate of cooling tower water

[3]Electrochemical oxidation of the nanofiltration concentrate of cooling tower water after constructed wetland pre-treatment

Bibliography

1. UNESCO, U.-W., *United Nations World Water Development Report 2020: Water and Climate Change*. 2020: Paris.
2. Daghrir, R., P. Drogui, and J. Tshibangu, *Efficient treatment of domestic wastewater by electrochemical oxidation process using bored doped diamond anode.* Separation and Purification Technology, 2014. **131**: p. 79-83 https://doi.org/10.1016/j.seppur.2014.04.048.
3. Cities, C. *Restoring the flow*. 2018; Available from: www.c40.org/other/the-future-we-don-t-want-restoring-the-flow.
4. Li, H., et al., *Control of mineral scale deposition in cooling systems using secondary-treated municipal wastewater.* Water Res, 2011. **45**(2): p. 748-60 https://doi.org/10.1016/j.watres.2010.08.052.
5. Ch. COMNINELLIS, A.N., *Anodic oxidation of phenol in the presence of NaCl for wastewater treatment.* Journal of Applied Electrochemistry, 1995. **25**: p. 23-28.
6. *Business Guide to Circular Water Management: Spotlight on Reduce, Reuse and Recycle. Geneva, WBCSD. www.wbcsd.org/ Programs/Food-Land-Water/Water/Resources/spotlight-on-reduce-reuse-and-recycle.* 2017.
7. Green, P.A., et al., *Freshwater ecosystem services supporting humans: Pivoting from water crisis to water solutions.* Global Environmental Change-Human and Policy Dimensions, 2015. **34**: p. 108-118 https://doi.org/10.1016/j.gloenvcha.2015.06.007.
8. Vorosmarty, C.J., et al., *Global water resources: vulnerability from climate change and population growth.* Science, 2000. **289**(5477): p. 284-8 https://doi.org/10.1126/science.289.5477.284.
9. Nexus, W. *www.waternexus.nl*. 2021.
10. Wagner, T.V., *Removal and transformation of conditioning chemicals in constructed wetlands treating cooling tower water*. 2020.
11. Löwenberg, J., et al., *Comparison of pre-treatment technologies towards improving reverse osmosis desalination of cooling tower blow down.* Desalination, 2015. **357**: p. 140-149 https://doi.org/10.1016/j.desal.2014.11.018.
12. Ecofys, *Pilot project on availability, use and sustainability of water for the production of nuclear and fossil energy - geo-localized inventory of water use in cooling processes, assessment of vulnerability and of water use management measures. End Report*. 2014.
13. Wang, Z., et al., *Study of integrated membrane systems for the treatment of wastewater from cooling towers.* Desalination, 2006. **191**(1-3): p. 117-124 https://doi.org/10.1016/j.desal.2005.04.125.
14. Lohrmann, A., et al., *Global scenarios for significant water use reduction in thermal power plants based on cooling water demand estimation using satellite imagery.* Nature Energy, 2019. **4**(12): p. 1040-1048 https://doi.org/10.1038/s41560-019-0501-4.
15. Cañizares, P., et al., *Synthesis of novel oxidants by electrochemical technology*. Journal of Applied Electrochemistry, 2009. **39**(11): p. 2143-2149 https://doi.org/10.1007/s10800-009-9792-7.
16. Hosseini, S.G. and S. Safshekan, *Synthesis, characterization and application of BiVO 4 photoanode for photoelectrochemical oxidation of chlorate.* Chinese Journal of Catalysis, 2017. **38**(4): p. 710-716 https://doi.org/10.1016/s1872-2067(17)62788-8.
17. Groot, C.K., et al., *Mild desalination of various raw water streams.* Water Sci Technol, 2015. **72**(3): p. 371-6 https://doi.org/10.2166/wst.2015.228.
18. Wagner, T.V., et al., *A review on the removal of conditioning chemicals from cooling tower water in constructed wetlands.* Critical Reviews in Environmental Science and Technology, 2019. **48**(19-21): p. 1094-1125 https://doi.org/10.1080/10643389.2018.1512289.
19. Altman, S.J., et al., *Membrane treatment of side-stream cooling tower water for reduction of water usage.* Desalination, 2012. **285**: p. 177-183 https://doi.org/10.1016/j.desal.2011.09.052.
20. Tae Kim, W., Y.I. Cho, and C. Bai, *Effect of electronic anti-fouling treatment on fouling mitigation with circulating cooling-tower water.* International Communications in Heat and Mass Transfer, 2001. **28**(5): p. 671-680 https://doi.org/10.1016/s0735-1933(01)00271-8.
21. Zhang, J.D., et al., *Pilot testing of outside-in MF and UF modules used for cooling tower blowdown pretreatment of power plants.* Desalination, 2007. **214**(1-3): p. 287-298 https://doi.org/10.1016/j.desal.2006.12.004.
22. Zhang, J.D., et al., *Pilot test of UF pretreatment prior to RO for cooling tower blowdown reuse of power plant.* Desalination, 2008. **222**(1-3): p. 9-16 https://doi.org/10.1016/j.desal.2007.01.123.
23. Farahani, M.H.D.A., S.M. Borghei, and V. Vatanpour, *Recovery of cooling tower blowdown water for reuse: The investigation of different types of pretreatment prior nanofiltration and reverse osmosis.* Journal of Water Process Engineering, 2016. **10**: p. 188-199 https://doi.org/10.1016/j.jwpe.2016.01.011.

24. Pinel, I.S.M., et al., *Bacterial community dynamics and disinfection impact in cooling water systems.* Water Res, 2020. **172**: p. 115505 https://doi.org/10.1016/j.watres.2020.115505.
25. Paranjape, K., et al., *Presence of Legionella spp. in cooling towers: the role of microbial diversity, Pseudomonas, and continuous chlorine application.* Water Res, 2020. **169**: p. 115252 https://doi.org/10.1016/j.watres.2019.115252.
26. Abdel-Shafy, H.I., et al., *Electrochemical treatment of industrial cooling tower blowdown water using magnesium-rod electrode.* Water Resources and Industry, 2020. **23** https://doi.org/10.1016/j.wri.2019.100121.
27. Li, X.L., et al., *Treatment of cooling tower blowdown water by using adsorption-electrocatalytic oxidation: Technical performance, toxicity assessment and economic evaluation.* Separation and Purification Technology, 2020. **252** https://doi.org/10.1016/j.seppur.2020.117484.
28. Matson, J.V. and T.G. Harris, *Zero Discharge of Cooling Water by Sidestream Softening.* Journal Water Pollution Control Federation, 1979. **51**(11): p. 2602-2614.
29. EPRI and Palo Alto, *Use of Produced Water in Recirculated Cooling Systems at Power Generating Facilities.* . 2006.
30. Al-Radif, A., *Review of various combinations of a multiple effect desalination plant (MED) and a thermal vapour compression unit.* Desalination, 1993. **93**(1-3): p. 119-125 https://doi.org/10.1016/0011-9164(93)80099-9.
31. Miller, J.E., *Review of Water Resources and Desalination Technologies* 2003: Albuquerque, New Mexico 87185 and Livermore, California 94550.
32. Yu, X.G., et al., *Experimental evaluation on concentrating cooling tower blowdown water by direct contact membrane distillation.* Desalination, 2013. **323**: p. 134-141 https://doi.org/10.1016/j.desal.2013.01.029.
33. Bisselink, R., et al., *Mild desalination demo pilot: New normalization approach to effectively evaluate electrodialysis reversal technology.* Water Resources and Industry, 2016. **14**: p. 18-25 https://doi.org/10.1016/j.wri.2016.03.003.
34. Koeman-Stein, N.E., et al., *Membrane distillation of industrial cooling tower blowdown water.* Water Resources and Industry, 2016. **14**: p. 11-17 https://doi.org/10.1016/j.wri.2016.03.002.
35. Project, E.F.C., *"E4Water" – Economically and ecologically efficient water management in the European chemical industry*. 2016: Theodor-Heuss-Allee 25 60486 Frankfurt am Main Germany.
36. Tijing, L.D., et al., *Fouling and its control in membrane distillation-A review.* Journal of Membrane Science, 2015. **475**: p. 215-244 https://doi.org/10.1016/j.memsci.2014.09.042.
37. Srisurichan, S., R. Jiraratananon, and A.G. Fane, *Humic acid fouling in the membrane distillation process.* Desalination, 2005. **174**(1): p. 63-72 https://doi.org/10.1016/j.desal.2004.09.003.
38. Mikhaylin, S. and L. Bazinet, *Fouling on ion-exchange membranes: Classification, characterization and strategies of prevention and control.* Adv Colloid Interface Sci, 2016. **229**: p. 34-56 https://doi.org/10.1016/j.cis.2015.12.006.
39. Adusei-Gyamfi, J., et al., *Natural organic matter-cations complexation and its impact on water treatment: A critical review.* Water Res, 2019. **160**: p. 130-147 https://doi.org/10.1016/j.watres.2019.05.064.
40. Amy, G., *Fundamental understanding of organic matter fouling of membranes.* Desalination, 2008. **231**(1-3): p. 44-51 https://doi.org/10.1016/j.desal.2007.11.037.
41. Mossad, M. and L. Zou, *Study of fouling and scaling in capacitive deionisation by using dissolved organic and inorganic salts.* J Hazard Mater, 2013. **244-245**: p. 387-93 https://doi.org/10.1016/j.jhazmat.2012.11.062.
42. Yu, W., et al., *Ultrafiltration and nanofiltration membrane fouling by natural organic matter: Mechanisms and mitigation by pre-ozonation and pH.* Water Res, 2018. **139**: p. 353-362 https://doi.org/10.1016/j.watres.2018.04.025.
43. Rijnaarts, T., et al., *Role of anion exchange membrane fouling in reverse electrodialysis using natural feed waters.* Colloids and Surfaces a-Physicochemical and Engineering Aspects, 2019. **560**: p. 198-204 https://doi.org/10.1016/j.colsurfa.2018.10.020.
44. Yadav, S., et al., *Organic Fouling in Forward Osmosis: A Comprehensive Review.* Water, 2020. **12**(5) https://doi.org/10.3390/w12051505.
45. Zhang, H.Z., et al., *Investigations on the fouling characteristic of humic acid and alginate sodium in capacitive deionization.* Water Reuse, 2021. **11**(2): p. 160-176 https://doi.org/10.2166/wrd.2021.104.
46. Kobus, E.J.M. and P.M. Heertjes, *The poisoning of anion-selective membranes by humic substances.* Desalination, 1973. **12**(3): p. 333-342 https://doi.org/10.1016/s0011-9164(00)80098-3.
47. Pinel, I.S.M., *Biofouling in open recirculating cooling systems: Characterization and control of biofilms and Legionella pneumophila.* , in *Thesis*. 2021, TU Delft.

48. Li, J., et al., *Study of using microfiltration and reverse osmosis membrane technologies for reclaiming cooling water in the power industry.* Water Environ Res, 2007. **79**(7): p. 753-8 https://doi.org/10.2175/106143006x95384.
49. Zeng, H.M., J.D. Zhang, and C.S. Ye, *Comparison of an ultrafiltration membrane fed with raw seawater, coagulated seawater and cooling tower blowdown.* Desalination, 2009. **244**(1-3): p. 199-207 https://doi.org/10.1016/j.desal.2008.04.044.
50. *Ceramic ultrafiltration and cooling tower blowdown recovery.* Membrane Technology, 2015. **2015**(10): p. 8-9 https://doi.org/10.1016/s0958-2118(15)30203-2.
51. Liao, Z., et al., *Treatment of cooling tower blowdown water containing silica, calcium and magnesium by electrocoagulation.* Water Sci Technol, 2009. **60**(9): p. 2345-52 https://doi.org/10.2166/wst.2009.675.
52. Matilainen, A., M. Vepsalainen, and M. Sillanpaa, *Natural organic matter removal by coagulation during drinking water treatment: a review.* Adv Colloid Interface Sci, 2010. **159**(2): p. 189-97 https://doi.org/10.1016/j.cis.2010.06.007.
53. Särkkä, H., M. Vepsäläinen, and M. Sillanpää, *Natural organic matter (NOM) removal by electrochemical methods — A review.* Journal of Electroanalytical Chemistry, 2015. **755**: p. 100-108 https://doi.org/10.1016/j.jelechem.2015.07.029.
54. Glaze, W.H., J.W. Kang, and D.H. Chapin, *The Chemistry of Water-Treatment Processes Involving Ozone, Hydrogen-Peroxide and Ultraviolet-Radiation.* Ozone-Science & Engineering, 1987. **9**(4): p. 335-352 https://doi.org/10.1080/01919518708552148.
55. Wang, J.L. and S.Z. Wang, *Reactive species in advanced oxidation processes: Formation, identification and reaction mechanism.* Chemical Engineering Journal, 2020. **401** https://doi.org/10.1016/j.cej.2020.126158.
56. Khan, S.H. and V.K. Yadav, *Advanced Oxidation Processes for Wastewater Remediation: An Overview*, in *Removal of Emerging Contaminants Through Microbial Processes*. 2021. p. 71-93.
57. Wang, J. and R. Zhuan, *Degradation of antibiotics by advanced oxidation processes: An overview.* Sci Total Environ, 2020. **701**: p. 135023 https://doi.org/10.1016/j.scitotenv.2019.135023.
58. Sillanpaa, M., M.C. Ncibi, and A. Matilainen, *Advanced oxidation processes for the removal of natural organic matter from drinking water sources: A comprehensive review.* J Environ Manage, 2018. **208**: p. 56-76 https://doi.org/10.1016/j.jenvman.2017.12.009.
59. von Gunten, U., *Oxidation Processes in Water Treatment: Are We on Track?* Environ Sci Technol, 2018. **52**(9): p. 5062-5075 https://doi.org/10.1021/acs.est.8b00586.
60. Miklos, D.B., et al., *Evaluation of advanced oxidation processes for water and wastewater treatment - A critical review.* Water Res, 2018. **139**: p. 118-131 https://doi.org/10.1016/j.watres.2018.03.042.
61. Chaplin, B.P., *Advantages, Disadvantages, and Future Challenges of the Use of Electrochemical Technologies for Water and Wastewater Treatment*, in *Electrochemical Water and Wastewater Treatment*. 2018. p. 451-494.
62. Oller, I., S. Malato, and J.A. Sanchez-Perez, *Combination of Advanced Oxidation Processes and biological treatments for wastewater decontamination--a review.* Sci Total Environ, 2011. **409**(20): p. 4141-66 https://doi.org/10.1016/j.scitotenv.2010.08.061.
63. Ammar, H.B., et al., *Green electrochemical process for metronidazole degradation at BDD anode in aqueous solutions via direct and indirect oxidation.* Separation and Purification Technology, 2016. **157**: p. 9-16 https://doi.org/10.1016/j.seppur.2015.11.027.
64. De Araújo, K.S., et al., *Advanced oxidation processes: a review regarding the fundamentals and applications in wastewater treatment and industrial wastewater.* Ambiente e Agua - An Interdisciplinary Journal of Applied Science, 2016. **11**(2): p. 387 https://doi.org/10.4136/ambi-agua.1862.
65. Panizza, M., M. Zolezzi, and C. Nicolella, *Biological and electrochemical oxidation of naphthalenesulfonates.* Journal of Chemical Technology and Biotechnology, 2006. **81**(2): p. 225-232 https://doi.org/10.1002/jctb.1396.
66. Chaplin, B.P., *Critical review of electrochemical advanced oxidation processes for water treatment applications.* Environ Sci Process Impacts, 2014. **16**(6): p. 1182-203 https://doi.org/10.1039/c3em00679d.
67. Brillas, E. and C.A. Martinez-Huitle, *Decontamination of wastewaters containing synthetic organic dyes by electrochemical methods. An updated review.* Applied Catalysis B-Environmental, 2015. **166**: p. 603-643 https://doi.org/10.1016/j.apcatb.2014.11.016.
68. Ikehata, K., N.J. Naghashkar, and M.G. Ei-Din, *Degradation of aqueous pharmaceuticals by ozonation and advanced oxidation processes: A review.* Ozone-Science & Engineering, 2006. **28**(6): p. 353-414 https://doi.org/10.1080/01919510600985937.

69. Panizza, M. and G. Cerisola, *Direct and mediated anodic oxidation of organic pollutants.* Chem Rev, 2009. **109**(12): p. 6541-69 https://doi.org/10.1021/cr9001319.
70. Anglada, A., A. Urtiaga, and I. Ortiz, *Contributions of electrochemical oxidation to waste-water treatment: fundamentals and review of applications.* Journal of Chemical Technology and Biotechnology, 2009. **84**(12): p. 1747-1755 https://doi.org/10.1002/jctb.2214.
71. Panizza, M. and G. Cerisola, *Application of diamond electrodes to electrochemical processes.* Electrochimica Acta, 2005. **51**(2): p. 191-199 https://doi.org/10.1016/j.electacta.2005.04.023.
72. Kreysa, G., K.-i. Ota, and R.F. Savinell, *Encyclopedia of Applied Electrochemistry*. 2014.
73. Wu, W.Y., Z.H. Huang, and T.T. Lim, *Recent development of mixed metal oxide anodes for electrochemical oxidation of organic pollutants in water.* Applied Catalysis a-General, 2014. **480**: p. 58-78 https://doi.org/10.1016/j.apcata.2014.04.035.
74. Yu, X., et al., *Recent updates on electrochemical degradation of bio-refractory organic pollutants using BDD anode: a mini review.* Environ Sci Pollut Res Int, 2014. **21**(14): p. 8417-31 https://doi.org/10.1007/s11356-014-2820-0.
75. Muff, J., *Electrochemical Oxidation – A Versatile Technique for Aqueous Organic Contaminant Degradation*, in *Chemistry of Advanced Environmental Purification Processes of Water*. 2014, Elsevier. p. 75-134.
76. Martínez-Huitle, C.A. and L.S. Andrade, *Electrocatalysis in wastewater treatment: recent mechanism advances.* Química Nova, 2011. **34**(5): p. 850-858 https://doi.org/10.1590/s0100-40422011000500021.
77. Santos, I.D., J.C. Afonso, and A.J.B. Dutra, *Behavior of a Ti/RuO2 anode in concentrated chloride medium for phenol and their chlorinated intermediates electrooxidation.* Separation and Purification Technology, 2010. **76**(2): p. 151-157 https://doi.org/10.1016/j.seppur.2010.10.001.
78. Mascia, M., et al., *Kinetics of the electrochemical oxidation of organic compounds at BDD anodes: modelling of surface reactions.* Journal of Applied Electrochemistry, 2006. **37**(1): p. 71-76 https://doi.org/10.1007/s10800-006-9217-9.
79. Martinez-Huitle, C.A., et al., *Single and Coupled Electrochemical Processes and Reactors for the Abatement of Organic Water Pollutants: A Critical Review*. Chem Rev, 2015. **115**(24): p. 13362-407 https://doi.org/10.1021/acs.chemrev.5b00361.
80. Anglada, Á., A. Urtiaga, and I. Ortiz, *Contributions of electrochemical oxidation to waste-water treatment: fundamentals and review of applications.* Journal of Chemical Technology & Biotechnology, 2009. **84**(12): p. 1747-1755 https://doi.org/https://doi.org/10.1002/jctb.2214.
81. Silva, R.G.d., S. Aquino Neto, and A.R.d. Andrade, *Electrochemical degradation of reactive dyes at different DSA® compositions.* Journal of the Brazilian Chemical Society, 2011. **22**(1): p. 126-133 https://doi.org/10.1590/s0103-50532011000100017.
82. Panizza, M., et al., *Anodic oxidation of 2-naphthol at boron-doped diamond electrodes.* Journal of Electroanalytical Chemistry, 2001. **507**(1-2): p. 206-214 https://doi.org/Doi 10.1016/S0022-0728(01)00398-9.
83. Du, X., *A review on the electrochemical treatment of the salty organic wastewater.* IOP Conference Series: Materials Science and Engineering, 2015. **87**: p. 012037 https://doi.org/10.1088/1757-899x/87/1/012037.
84. Chung, C.M., et al., *Alleviation of membrane fouling in a submerged membrane bioreactor with electrochemical oxidation mediated by in-situ free chlorine generation.* Water Res, 2016. **96**: p. 52-61 https://doi.org/10.1016/j.watres.2016.03.041.
85. Chen, G.H., *Electrochemical technologies in wastewater treatment.* Separation and Purification Technology, 2004. **38**(1): p. 11-41 https://doi.org/10.1016/j.seppur.2003.10.006.
86. Radjenovic, J. and D.L. Sedlak, *Challenges and Opportunities for Electrochemical Processes as Next-Generation Technologies for the Treatment of Contaminated Water.* Environ Sci Technol, 2015. **49**(19): p. 11292-302 https://doi.org/10.1021/acs.est.5b02414.
87. Donaghue, A. and B.P. Chaplin, *Effect of select organic compounds on perchlorate formation at boron-doped diamond film anodes.* Environ Sci Technol, 2013. **47**(21): p. 12391-9 https://doi.org/10.1021/es4031672.
88. Liu, W.H., et al., *Advanced treatment of tannery wastewater using the combination of UASB, SBR, electrochemical oxidation and BAF.* Journal of Chemical Technology and Biotechnology, 2017. **92**(3): p. 578-587 https://doi.org/10.1002/jctb.5037.
89. Urtiaga, A.M., et al., *Removal of pharmaceuticals from a WWTP secondary effluent by ultrafiltration/reverse osmosis followed by electrochemical oxidation of the RO concentrate.* Desalination, 2013. **331**: p. 26-34 https://doi.org/10.1016/j.desal.2013.10.010.

90. Wang, J.L. and S.Z. Wang, *Activation of persulfate (PS) and peroxymonosulfate (PMS) and application for the degradation of emerging contaminants.* Chemical Engineering Journal, 2018. **334**: p. 1502-1517 https://doi.org/10.1016/j.cej.2017.11.059.
91. Ike, I.A., et al., *Critical review of the science and sustainability of persulphate advanced oxidation processes.* Chemical Engineering Journal, 2018. **338**: p. 651-669 https://doi.org/https://doi.org/10.1016/j.cej.2018.01.034.
92. Ma, J., et al., *Degradation of benzotriazole by sulfate radical-based advanced oxidation process.* Environ Technol, 2021. **42**(2): p. 238-247 https://doi.org/10.1080/09593330.2019.1625959.
93. Zrinyi, N. and A.L. Pham, *Oxidation of benzoic acid by heat-activated persulfate: Effect of temperature on transformation pathway and product distribution.* Water Res, 2017. **120**: p. 43-51 https://doi.org/10.1016/j.watres.2017.04.066.
94. Furman, O.S., A.L. Teel, and R.J. Watts, *Mechanism of base activation of persulfate.* Environ Sci Technol, 2010. **44**(16): p. 6423-8 https://doi.org/10.1021/es1013714.
95. Fang, G.D., et al., *Sulfate radical-based degradation of polychlorinated biphenyls: effects of chloride ion and reaction kinetics.* J Hazard Mater, 2012. **227-228**: p. 394-401 https://doi.org/10.1016/j.jhazmat.2012.05.074.
96. Fernandes, A., et al., *Pilot scale degradation study of 16 selected volatile organic compounds by hydroxyl and sulfate radical based advanced oxidation processes.* Journal of Cleaner Production, 2019. **208**: p. 54-64 https://doi.org/10.1016/j.jclepro.2018.10.081.
97. Stefan, M.I., *Advanced Oxidation Processes for Water Treatment: Fundamentals and Applications*. 2017: IWA Publishing.
98. Lutze, H.V., et al., *Degradation of perfluorinated compounds by sulfate radicals - New mechanistic aspects and economical considerations.* Water Res, 2018. **129**: p. 509-519 https://doi.org/10.1016/j.watres.2017.10.067.
99. Wang, Y., et al., *Formation of brominated disinfection byproducts from natural organic matter isolates and model compounds in a sulfate radical-based oxidation process.* Environ Sci Technol, 2014. **48**(24): p. 14534-42 https://doi.org/10.1021/es503255j.
100. Kim, D., G.L. Amy, and T. Karanfil, *Disinfection by-product formation during seawater desalination: A review*. Water Res, 2015. **81**: p. 343-55 https://doi.org/10.1016/j.watres.2015.05.040.
101. Moreira, F.C., et al., *Electrochemical advanced oxidation processes: A review on their application to synthetic and real wastewaters.* Applied Catalysis B-Environmental, 2017. **202**: p. 217-261 https://doi.org/10.1016/j.apcatb.2016.08.037.
102. Fujishima, A. and K. Honda, *Electrochemical photolysis of water at a semiconductor electrode.* Nature, 1972. **238**(5358): p. 37-8 https://doi.org/10.1038/238037a0.
103. Koe, W.S., et al., *An overview of photocatalytic degradation: photocatalysts, mechanisms, and development of photocatalytic membrane.* Environ Sci Pollut Res Int, 2020. **27**(3): p. 2522-2565 https://doi.org/10.1007/s11356-019-07193-5.
104. Banerjee, S., et al., *New Insights into the Mechanism of Visible Light Photocatalysis.* J Phys Chem Lett, 2014. **5**(15): p. 2543-54 https://doi.org/10.1021/jz501030x.
105. Hamilton, J.W.J., et al., *Evaluating the Mechanism of Visible Light Activity for N,F-TiO2 Using Photoelectrochemistry.* Journal of Physical Chemistry C, 2014. **118**(23): p. 12206-12215 https://doi.org/10.1021/jp4120964.
106. Brüninghoff, R., *Advanced oxidation processes: materials and technologies for saline wastewater treatment*. 2020, Enschede: University of Twente. p. 199.
107. Domingues, F.S., et al., *Hydrogen peroxide-assisted photocatalytic degradation of textile wastewater using titanium dioxide and zinc oxide.* Environmental Technology, 2019. **40**(10): p. 1223-1232 https://doi.org/10.1080/09593330.2017.1418913.
108. Bruninghoff, R., et al., *Comparative Analysis of Photocatalytic and Electrochemical Degradation of 4-Ethylphenol in Saline Conditions.* Environ Sci Technol, 2019. **53**(15): p. 8725-8735 https://doi.org/10.1021/acs.est.9b01244.
109. Bahnmuller, S., et al., *Degradation rates of benzotriazoles and benzothiazoles under UV-C irradiation and the advanced oxidation process UV/H2O2.* Water Res, 2015. **74**: p. 143-54 https://doi.org/10.1016/j.watres.2014.12.039.
110. Dhaka, S., et al., *Degradation of ethyl paraben in aqueous medium using advanced oxidation processes: Efficiency evaluation of UV-C supported oxidants.* Journal of Cleaner Production, 2018. **180**: p. 505-513 https://doi.org/10.1016/j.jclepro.2018.01.197.
111. Kilic, M.Y., et al., *Photochemical treatment of tyrosol, a model phenolic compound present in olive mill wastewater, by hydroxyl and sulfate radical-based advanced oxidation processes (AOPs).* J Hazard Mater, 2019. **367**: p. 734-742 https://doi.org/10.1016/j.jhazmat.2018.06.062.

112. Yang, W.B., H.D. Zhou, and N. Cicek, *Treatment of Organic Micropollutants in Water and Wastewater by UV-Based Processes: A Literature Review.* Critical Reviews in Environmental Science and Technology, 2014. **44**(13): p. 1443-1476 https://doi.org/10.1080/10643389.2013.790745.
113. Ocampo-Pérez, R., et al., *Degradation of antineoplastic cytarabine in aqueous phase by advanced oxidation processes based on ultraviolet radiation.* Chemical Engineering Journal, 2010. **165**(2): p. 581-588.
114. Sillanpää, M., M.C. Ncibi, and A. Matilainen, *Advanced oxidation processes for the removal of natural organic matter from drinking water sources: A comprehensive review.* Journal of Environmental Management, 2018. **208**: p. 56-76 https://doi.org/https://doi.org/10.1016/j.jenvman.2017.12.009.
115. Chianese, S., et al., *Ibuprofen degradation in aqueous solution by using UV light.* Desalination and Water Treatment, 2016. **57**(48-49): p. 22878-22886 https://doi.org/10.1080/19443994.2016.1153908.
116. Iovino, P., et al., *Degradation of Ibuprofen in Aqueous Solution with UV Light: the Effect of Reactor Volume and pH.* Water Air and Soil Pollution, 2016. **227**(6): p. 194 https://doi.org/10.1007/s11270-016-2890-3.
117. Liu, Y.S., et al., *Photolysis of benzotriazole and formation of its polymerised photoproducts in aqueous solutions under UV irradiation.* Environmental Chemistry, 2011. **8**(2): p. 174-181 https://doi.org/10.1071/En10141.
118. Avisar, D., Y. Lester, and H. Mamane, *pH induced polychromatic UV treatment for the removal of a mixture of SMX, OTC and CIP from water.* J Hazard Mater, 2010. **175**(1-3): p. 1068-74 https://doi.org/10.1016/j.jhazmat.2009.10.122.
119. Ling, S.Y., et al., *Photodegradation of novel brominated flame retardants (NBFRs) in a liquid system: Kinetics and photoproducts.* Chemical Engineering Journal, 2019. **362**: p. 938-946 https://doi.org/10.1016/j.cej.2019.01.103.
120. Lee, E., H.K. Shon, and J. Cho, *Role of wetland organic matters as photosensitizer for degradation of micropollutants and metabolites.* Journal of Hazardous Materials, 2014. **276**: p. 1-9 https://doi.org/10.1016/j.jhazmat.2014.05.001.
121. Moussavi, G., et al., *Comparing the efficacy of VUV and UVC/S2O82- advanced oxidation processes for degradation and mineralization of cyanide in wastewater.* Chemical Engineering Journal, 2016. **294**: p. 273-280 https://doi.org/10.1016/j.cej.2016.02.113.
122. Amor, C., et al., *Application of Advanced Oxidation Processes for the Treatment of Recalcitrant Agro-Industrial Wastewater: A Review.* Water, 2019. **11**(2): p. 205 https://doi.org/10.3390/w11020205.
123. Daneshvar, N., M.A. Behnajady, and Y. Zorriyeh Asghar, *Photooxidative degradation of 4-nitrophenol (4-NP) in UV/H2O2 process: influence of operational parameters and reaction mechanism.* J Hazard Mater, 2007. **139**(2): p. 275-9 https://doi.org/10.1016/j.jhazmat.2006.06.045.
124. Zoschke, K., H. Bornick, and E. Worch, *Vacuum-UV radiation at 185 nm in water treatment--a review.* Water Res, 2014. **52**: p. 131-45 https://doi.org/10.1016/j.watres.2013.12.034.
125. Furatian, L., *The Use of 185 nm Radiation for Drinking Water Treatment Influence of Major Solutes and Temperature on the Degradation of Trace Organic Contaminants*, in *Chemical and Biological Engineering*. 2017, THE UNIVERSITY OF BRITISH COLUMBIA.
126. Zhang, Q., et al., *Understanding and modeling the formation and transformation of hydrogen peroxide in water irradiated by 254 nm ultraviolet (UV) and 185 nm vacuum UV (VUV): Effects of pH and oxygen.* Chemosphere, 2020. **244**: p. 125483 https://doi.org/10.1016/j.chemosphere.2019.125483.
127. Afzal, A., et al., *Anatoxin-a degradation by Advanced Oxidation Processes: vacuum-UV at 172 nm, photolysis using medium pressure UV and UV/H(2)O(2).* Water Res, 2010. **44**(1): p. 278-86 https://doi.org/10.1016/j.watres.2009.09.021.
128. Chen, Y.J., et al., *Degradation kinetics, mechanism and toxicology of tris(2-chloroethyl) phosphate with 185 nm vacuum ultraviolet.* Chemical Engineering Journal, 2019. **356**: p. 98-106 https://doi.org/10.1016/j.cej.2018.09.007.
129. Yao, H., et al., *Effect of Fe(II/III) on tetracycline degradation under UV/VUV irradiation.* Chemical Engineering Journal, 2017. **308**: p. 193-201 https://doi.org/10.1016/j.cej.2016.09.074.
130. Dodd, M.C., M.O. Buffle, and U. Von Gunten, *Oxidation of antibacterial molecules by aqueous ozone: moiety-specific reaction kinetics and application to ozone-based wastewater treatment.* Environ Sci Technol, 2006. **40**(6): p. 1969-77 https://doi.org/10.1021/es051369x.
131. Xie, P., et al., *Application of vacuum-ultraviolet (VUV) to degrade β-blocker propranolol in aquatic environment: Efficiency, kinetics, pathways and acute toxicity.* Journal of the Taiwan Institute of Chemical Engineers, 2019. **103**: p. 75-84 https://doi.org/10.1016/j.jtice.2019.07.011.
132. Wang, J., et al., *Effect of coagulation pretreatment on membrane distillation process for desalination of recirculating cooling water.* Separation and Purification Technology, 2008. **64**(1): p. 108-115 https://doi.org/10.1016/j.seppur.2008.07.022.

133. Nanda, D., et al., *Effect of solution chemistry on water softening using charged nanofiltration membranes.* Desalination, 2008. **234**(1-3): p. 344-353 https://doi.org/10.1016/j.desal.2007.09.103.
134. Radisav, V., et al., *Reuse of Treated Internal or External Wastewaters in the Cooling Systems of Coal-Based Thermoelectric Power Plants*. 2009, Office of Scientific and Technical Information (OSTI).
135. van Limpt, B. and A. van der Wal, *Water and chemical savings in cooling towers by using membrane capacitive deionization.* Desalination, 2014. **342**: p. 148-155 https://doi.org/10.1016/j.desal.2013.12.022.
136. Kuipers, N., et al., *Techno-economic assessment of boiler feed water production by membrane distillation with reuse of thermal waste energy from cooling water.* Desalination and Water Treatment, 2014. **55**(13): p. 3506-3518 https://doi.org/10.1080/19443994.2014.946722.
137. Greenlee, L.F., et al., *Effect of antiscalants on precipitation of an RO concentrate: metals precipitated and particle characteristics for several water compositions.* Water Res, 2010. **44**(8): p. 2672-84 https://doi.org/10.1016/j.watres.2010.01.034.
138. Sweity, A., Z. Ronen, and M. Herzberg, *Induced organic fouling with antiscalants in seawater desalination.* Desalination, 2014. **352**: p. 158-165 https://doi.org/10.1016/j.desal.2014.08.018.
139. Davood Abadi Farahani, M.H., S.M. Borghei, and V. Vatanpour, *Recovery of cooling tower blowdown water for reuse: The investigation of different types of pretreatment prior nanofiltration and reverse osmosis.* Journal of Water Process Engineering, 2016. **10**: p. 188-199 https://doi.org/10.1016/j.jwpe.2016.01.011.
140. Wagner, T.V., et al., *Benzotriazole removal mechanisms in pilot-scale constructed wetlands treating cooling tower water.* J Hazard Mater, 2020. **384**: p. 121314 https://doi.org/10.1016/j.jhazmat.2019.121314.
141. Garcia-Segura, S., J.D. Ocon, and M.N. Chong, *Electrochemical oxidation remediation of real wastewater effluents - A review.* Process Safety and Environmental Protection, 2018. **113**: p. 48-67 https://doi.org/10.1016/j.psep.2017.09.014.
142. McBeath, S.T., D.P. Wilkinsonb, and N.J.D. Grahama, *Application of boron-doped diamond electrodes for the anodic oxidation of pesticide micropollutants in a water treatment process: a critical review.* Environmental Science-Water Research & Technology, 2019. **5**(12): p. 2090-2107 https://doi.org/10.1039/c9ew00589g.
143. Moreira, F.C., et al., *Electrochemical advanced oxidation processes: A review on their application to synthetic and real wastewaters.* Applied Catalysis B: Environmental, 2017. **202**: p. 217-261 https://doi.org/10.1016/j.apcatb.2016.08.037.
144. Othmani, A., et al., *Coupling anodic oxidation, biosorption and alternating current as alternative for wastewater purification.* Chemosphere, 2020. **249**: p. 126480 https://doi.org/10.1016/j.chemosphere.2020.126480.
145. Wohlmuth da Silva, S., et al., *Electrooxidation Using Nb/BDD as Post-Treatment of a Reverse Osmosis Concentrate in the Petrochemical Industry.* Int J Environ Res Public Health, 2019. **16**(5): p. 816 https://doi.org/10.3390/ijerph16050816.
146. Klidi, N., et al., *Applicability of electrochemical methods to paper mill wastewater for reuse. Anodic oxidation with BDD and TiRuSnO2 anodes.* Journal of Electroanalytical Chemistry, 2018. **815**: p. 16-23 https://doi.org/10.1016/j.jelechem.2018.02.063.
147. Le Luu, T., et al., *Electrochemical oxidation as a post treatment for biologically tannery wastewater in batch reactor.* Water Sci Technol, 2019. **80**(7): p. 1326-1337 https://doi.org/10.2166/wst.2019.380.
148. Gomez-Ruiz, B., et al., *Boron doped diamond electrooxidation of 6:2 fluorotelomers and perfluorocarboxylic acids. Application to industrial wastewaters treatment.* Journal of Electroanalytical Chemistry, 2017. **798**: p. 51-57 https://doi.org/10.1016/j.jelechem.2017.05.033.
149. Garcia-Segura, S., et al., *Removal of organic contaminants from secondary effluent by anodic oxidation with a boron-doped diamond anode as tertiary treatment.* J Hazard Mater, 2015. **283**: p. 551-7 https://doi.org/10.1016/j.jhazmat.2014.10.003.
150. Durán, F.E., et al., *Electrochemical technology for the treatment of real washing machine effluent at pre-pilot plant scale by using active and non-active anodes.* Journal of Electroanalytical Chemistry, 2018. **818**: p. 216-222 https://doi.org/10.1016/j.jelechem.2018.04.029.
151. Fernandes, A., et al., *Review on the electrochemical processes for the treatment of sanitary landfill leachates: Present and future.* Applied Catalysis B-Environmental, 2015. **176**: p. 183-200 https://doi.org/10.1016/j.apcatb.2015.03.052.
152. Fernandes, A., et al., *Electrochemical oxidation of humic acid and sanitary landfill leachate: Influence of anode material, chloride concentration and current density.* Sci Total Environ, 2016. **541**: p. 282-291 https://doi.org/10.1016/j.scitotenv.2015.09.052.

153. Gautam, P., S. Kumar, and S. Lokhandwala, *Advanced oxidation processes for treatment of leachate from hazardous waste landfill: A critical review.* Journal of Cleaner Production, 2019. **237**: p. 117639 https://doi.org/10.1016/j.jclepro.2019.117639.
154. Yu, D., et al., *Electrochemical treatment of organic pollutants in landfill leachate using a three-dimensional electrode system.* Chemosphere, 2020. **243**: p. 125438 https://doi.org/10.1016/j.chemosphere.2019.125438.
155. Brillas, E., I. Sires, and M.A. Oturan, *Electro-Fenton process and related electrochemical technologies based on Fenton's reaction chemistry.* Chem Rev, 2009. **109**(12): p. 6570-631 https://doi.org/10.1021/cr900136g.
156. Shin, Y.U., et al., *Electrochemical oxidation of organics in sulfate solutions on boron-doped diamond electrode: Multiple pathways for sulfate radical generation.* Applied Catalysis B-Environmental, 2019. **254**: p. 156-165 https://doi.org/10.1016/j.apcatb.2019.04.060.
157. Sires, I., et al., *Electrochemical advanced oxidation processes: today and tomorrow. A review.* Environ Sci Pollut Res Int, 2014. **21**(14): p. 8336-67 https://doi.org/10.1007/s11356-014-2783-1.
158. He, Y.P., et al., *Recent developments and advances in boron-doped diamond electrodes for electrochemical oxidation of organic pollutants.* Separation and Purification Technology, 2019. **212**: p. 802-821 https://doi.org/10.1016/j.seppur.2018.11.056.
159. Nidheesh, P.V., et al., *Environmental Applications of Boron-Doped Diamond Electrodes: 1. Applications in Water and Wastewater Treatment.* Chemelectrochem, 2019. **6**(8): p. 2124-2142 https://doi.org/10.1002/celc.201801876.
160. Sillanpää, M. and M. Shestakova, *Introduction*, in *Electrochemical Water Treatment Methods*. 2017, Elsevier. p. 1-46.
161. Brito, C.d.N., et al., *Understanding active chlorine species production using boron doped diamond films with lower and higher sp3/sp2 ratio.* Electrochemistry Communications, 2015. **55**: p. 34-38 https://doi.org/10.1016/j.elecom.2015.03.013.
162. Farhat, A., et al., *Removal of Persistent Organic Contaminants by Electrochemically Activated Sulfate.* Environ Sci Technol, 2015. **49**(24): p. 14326-33 https://doi.org/10.1021/acs.est.5b02705.
163. Lan, Y.D., et al., *On the role of salts for the treatment of wastewaters containing pharmaceuticals by electrochemical oxidation using a boron doped diamond anode.* Electrochimica Acta, 2017. **231**: p. 309-318 https://doi.org/10.1016/j.electacta.2017.01.160.
164. Panizza, M. and G. Cerisola, *Direct And Mediated Anodic Oxidation of Organic Pollutants.* Chemical Reviews, 2009. **109**(12): p. 6541-6569 https://doi.org/10.1021/cr9001319.
165. Cañizares, P., et al., *Measurement of Mass-Transfer Coefficients by an Electrochemical Technique.* Journal of Chemical Education, 2006. **83**(8): p. 1204 https://doi.org/10.1021/ed083p1204.
166. Ajao, V., et al., *Valorization of glycerol/ethanol-rich wastewater to bioflocculants: recovery, properties, and performance.* J Hazard Mater, 2019. **375**: p. 273-280 https://doi.org/10.1016/j.jhazmat.2019.05.009.
167. Huber, S.A., et al., *Characterisation of aquatic humic and non-humic matter with size-exclusion chromatography--organic carbon detection--organic nitrogen detection (LC-OCD-OND).* Water Res, 2011. **45**(2): p. 879-85 https://doi.org/10.1016/j.watres.2010.09.023.
168. Tak, B.Y., et al., *Optimization of color and COD removal from livestock wastewater by electrocoagulation process: Application of Box-Behnken design (BBD).* Journal of Industrial and Engineering Chemistry, 2015. **28**: p. 307-315 https://doi.org/10.1016/j.jiec.2015.03.008.
169. Zou, J., et al., *Electrochemical oxidation of COD from real textile wastewaters: Kinetic study and energy consumption.* Chemosphere, 2017. **171**: p. 332-338 https://doi.org/10.1016/j.chemosphere.2016.12.065.
170. Reyes, C., et al., *Degradation and inactivation of tetracycline by TiO2 photocatalysis.* Journal of Photochemistry and Photobiology a-Chemistry, 2006. **184**(1-2): p. 141-146 https://doi.org/10.1016/j.jphotochem.2006.04.007.
171. Kapałka, A., G. Fóti, and C. Comninellis, *Kinetic modelling of the electrochemical mineralization of organic pollutants for wastewater treatment.* Journal of Applied Electrochemistry, 2007. **38**(1): p. 7-16 https://doi.org/10.1007/s10800-007-9365-6.
172. Scialdone, O., et al., *Electrochemical oxidation of organics in water: role of operative parameters in the absence and in the presence of NaCl.* Water Res, 2009. **43**(8): p. 2260-72 https://doi.org/10.1016/j.watres.2009.02.014.
173. Oliveira, E.M.S., et al., *Performance of (in)active anodic materials for the electrooxidation of phenolic wastewaters from cashew-nut processing industry.* Chemosphere, 2018. **201**: p. 740-748 https://doi.org/10.1016/j.chemosphere.2018.02.037.

174. Ellouze, S., et al., *Ferulic acid treatment by electrochemical oxidation using a BDD anode.* Journal of the Taiwan Institute of Chemical Engineers, 2016. **59**: p. 132-137 https://doi.org/10.1016/j.jtice.2015.09.008.
175. Nidheesh, P.V. and R. Gandhimathi, *Trends in electro-Fenton process for water and wastewater treatment: An overview.* Desalination, 2012. **299**: p. 1-15 https://doi.org/10.1016/j.desal.2012.05.011.
176. Sanly, et al., *A Study on the Removal of Humic Acid Using Advanced Oxidation Processes.* Separation Science and Technology, 2007. **42**(7): p. 1391-1404 https://doi.org/10.1080/01496390701289799.
177. Aquino Neto, S. and A.R. De Andrade, *Electrochemical degradation of glyphosate formulations at DSA® anodes in chloride medium: an AOX formation study.* Journal of Applied Electrochemistry, 2009. **39**(10): p. 1863-1870 https://doi.org/10.1007/s10800-009-9890-6.
178. Garcia-Espinoza, J.D., P. Mijaylova-Nacheva, and M. Aviles-Flores, *Electrochemical carbamazepine degradation: Effect of the generated active chlorine, transformation pathways and toxicity.* Chemosphere, 2018. **192**: p. 142-151 https://doi.org/10.1016/j.chemosphere.2017.10.147.
179. Wang, W.L., et al., *Synergistic effect between UV and chlorine (UV/chlorine) on the degradation of carbamazepine: Influence factors and radical species.* Water Res, 2016. **98**: p. 190-8 https://doi.org/10.1016/j.watres.2016.04.015.
180. Han, J., et al., *Removal of Perchlorate Using Reverse Osmosis and Nanofiltration Membranes.* Environmental Engineering Research, 2012. **17**(4): p. 185-190 https://doi.org/10.4491/eer.2012.17.4.185.
181. Puspitasari, V., et al., *Cleaning and ageing effect of sodium hypochlorite on polyvinylidene fluoride (PVDF) membrane.* Separation and Purification Technology, 2010. **72**(3): p. 301-308 https://doi.org/10.1016/j.seppur.2010.03.001.
182. FAO, *Food and Agriculture Organization of the United Nations (FAO)*. 2016, United Nations Publications.
183. Dos Santos, V.L., et al., *Reuse of refinery's tertiary-treated wastewater in cooling towers: microbiological monitoring.* Environ Sci Pollut Res Int, 2015. **22**(4): p. 2945-55 https://doi.org/10.1007/s11356-014-3555-7.
184. Farhat, A., et al., *Assessment of the impact of chloride on the formation of chlorinated by-products in the presence and absence of electrochemically activated sulfate.* Chemical Engineering Journal, 2017. **330**: p. 1265-1271 https://doi.org/10.1016/j.cej.2017.08.033.
185. Groot, C.K., et al., *Mild desalination of various raw water streams.* Water Science and Technology, 2015. **72**(3): p. 371-376 https://doi.org/10.2166/wst.2015.228.
186. Pramanik, B.K., F.A. Roddick, and L.H. Fan, *Biofiltration of feedwater to control organic fouling of low pressure membranes.* Critical Reviews in Environmental Science and Technology, 2017. **47**(20): p. 1958-1985 https://doi.org/10.1080/10643389.2017.1400855.
187. Wagner, T.V., et al., *Pilot-scale hybrid constructed wetlands for the treatment of cooling tower water prior to its desalination and reuse.* J Environ Manage, 2020. **271**: p. 110972 https://doi.org/10.1016/j.jenvman.2020.110972.
188. Wagner, T.V., et al., *A review on the removal of conditioning chemicals from cooling tower water in constructed wetlands.* Critical Reviews in Environmental Science and Technology, 2018. **48**(19-21): p. 1094-1125 https://doi.org/10.1080/10643389.2018.1512289.
189. GarcÍA, J., et al., *Contaminant Removal Processes in Subsurface-Flow Constructed Wetlands: A Review.* Critical Reviews in Environmental Science and Technology, 2010. **40**(7): p. 561-661 https://doi.org/10.1080/10643380802471076.
190. Grafias, P., et al., *Pilot treatment of olive pomace leachate by vertical-flow constructed wetland and electrochemical oxidation: an efficient hybrid process.* Water Res, 2010. **44**(9): p. 2773-80 https://doi.org/10.1016/j.watres.2010.02.015.
191. Wagner, T.V., et al., *Non-target screening reveals the mechanisms responsible for the antagonistic inhibiting effect of the biocides DBNPA and glutaraldehyde on benzoic acid biodegradation.* J Hazard Mater, 2020. **386**: p. 121661 https://doi.org/10.1016/j.jhazmat.2019.121661.
192. Comninellis, C., et al., *Advanced oxidation processes for water treatment: advances and trends for R&D.* Journal of Chemical Technology and Biotechnology, 2008. **83**(6): p. 769-776 https://doi.org/10.1002/jctb.1873.
193. Skoumal, M., et al., *Mineralization of the biocide chloroxylenol by electrochemical advanced oxidation processes.* Chemosphere, 2008. **71**(9): p. 1718-29 https://doi.org/10.1016/j.chemosphere.2007.12.029.
194. Tatoulis, T., et al., *Treatment of table olive washing water using trickling filters, constructed wetlands and electrooxidation.* Environ Sci Pollut Res Int, 2017. **24**(2): p. 1085-1092 https://doi.org/10.1007/s11356-016-7058-6.

195. Talekar, G.V., et al., *Sanitation of blackwater via sequential wetland and electrochemical treatment.* Npj Clean Water, 2018. **1**(1) https://doi.org/10.1038/s41545-018-0014-x.
196. Wang, C.R., et al., *Pilot-scale electrochemical oxidation combined with constructed wetland system for unconventional surface water treatment.* Journal of Chemical Technology and Biotechnology, 2014. **89**(10): p. 1599-1606 https://doi.org/10.1002/jctb.4464.
197. Del Moro, G., et al., *Landfill leachate treatment: Comparison of standalone electrochemical degradation and combined with a novel biofilter.* Chemical Engineering Journal, 2016. **288**: p. 87-98 https://doi.org/10.1016/j.cej.2015.11.069.
198. Saha, P., et al., *Removal of organic compounds from cooling tower blowdown by electrochemical oxidation: Role of electrodes and operational parameters.* Chemosphere, 2020. **259**: p. 127491 https://doi.org/10.1016/j.chemosphere.2020.127491.
199. He, Y., et al., *Fate and distribution of pharmaceutically active compounds in mesocosm constructed wetlands.* J Hazard Mater, 2018. **357**: p. 198-206 https://doi.org/10.1016/j.jhazmat.2018.05.035.
200. Almendros, G. and J. Dorado, *Molecular characteristics related to the biodegradability of humic acid preparations.* European Journal of Soil Science, 1999. **50**(2): p. 227-236 https://doi.org/DOI 10.1046/j.1365-2389.1999.00240.x.
201. Kahl, S., et al., *Effect of design and operational conditions on the performance of subsurface flow treatment wetlands: Emerging organic contaminants as indicators.* Water Res, 2017. **125**: p. 490-500 https://doi.org/10.1016/j.watres.2017.09.004.
202. Matamoros, V., E. Jover, and J.M. Bayona, *Occurrence and fate of benzothiazoles and benzotriazoles in constructed wetlands.* Water Sci Technol, 2010. **61**(1): p. 191-8 https://doi.org/10.2166/wst.2010.797.
203. de Moura, D.C., et al., *Active chlorine species electrogenerated on Ti/Ru0.3Ti0.7O2 surface: Electrochemical behavior, concentration determination and their application.* Journal of Electroanalytical Chemistry, 2014. **731**: p. 145-152 https://doi.org/10.1016/j.jelechem.2014.08.008.
204. Fajardo, A.S., et al., *Electrochemical oxidation of phenolic wastewaters using a batch-stirred reactor with NaCl electrolyte and Ti/RuO 2 anodes.* Journal of Electroanalytical Chemistry, 2017. **785**: p. 180-189 https://doi.org/10.1016/j.jelechem.2016.12.033.
205. Bergmann, M.E.H., A.S. Koparal, and T. Iourtchouk, *Electrochemical Advanced Oxidation Processes, Formation of Halogenate and Perhalogenate Species: A Critical Review.* Critical Reviews in Environmental Science and Technology, 2014. **44**(4): p. 348-390 https://doi.org/10.1080/10643389.2012.718948.
206. Martínez-Huitle, C.A. and M. Panizza, *Electrochemical oxidation of organic pollutants for wastewater treatment.* Current Opinion in Electrochemistry, 2018. **11**: p. 62-71 https://doi.org/10.1016/j.coelec.2018.07.010.
207. Song, H., et al., *Electrochemical activation of persulfates at BDD anode: Radical or nonradical oxidation?* Water Res, 2018. **128**: p. 393-401 https://doi.org/10.1016/j.watres.2017.10.018.
208. Punturat, V. and K.L. Huang, *Degradation pathways and organic matter transformation of acesulfame potassium electro-oxidation in real water matrices.* Journal of the Taiwan Institute of Chemical Engineers, 2017. **80**: p. 222-230 https://doi.org/10.1016/j.jtice.2017.06.054.
209. Mao, X., et al., *Optimization of electrochemical dechlorination of trichloroethylene in reducing electrolytes.* Water Res, 2012. **46**(6): p. 1847-57 https://doi.org/10.1016/j.watres.2012.01.002.
210. Yao, J., et al., *Differential control of anode/cathode potentials of paired electrolysis for simultaneous removal of chemical oxygen demand and total nitrogen.* Sci Total Environ, 2019. **687**: p. 198-205 https://doi.org/10.1016/j.scitotenv.2019.06.106.
211. Wu, J.L., et al., *[Comparative Study of Benzotriazole Electrochemical Oxidation at Boron-doped Diamond and PbO2 Anodes].* Huan Jing Ke Xue, 2015. **36**(7): p. 2540-6.
212. Tian, Y., et al., *Influence of Electrolyte Concentration and Temperature on the Capacitance of Activated Carbon.* Acta Physico-Chimica Sinica, 2011. **27**(2): p. 479-485 https://doi.org/10.3866/Pku.Whxb20110221.
213. Bhatt, P., et al., *Biodegradation of chlorinated compounds - A review.* Critical Reviews in Environmental Science and Technology, 2007. **37**(2): p. 165-198 https://doi.org/10.1080/10643380600776130.
214. Nozawa-Inoue, M., K.M. Scow, and D.E. Rolston, *Reduction of perchlorate and nitrate by microbial communities in vadose soil.* Appl Environ Microbiol, 2005. **71**(7): p. 3928-34 https://doi.org/10.1128/AEM.71.7.3928-3934.2005.
215. Carlstrom, C.I., et al., *(Per)chlorate-reducing bacteria can utilize aerobic and anaerobic pathways of aromatic degradation with (per)chlorate as an electron acceptor.* mBio, 2015. **6**(2): p. e02287-14 https://doi.org/10.1128/mBio.02287-14.

216. Seibert, D., et al., *Occurrence, statutory guideline values and removal of contaminants of emerging concern by Electrochemical Advanced Oxidation Processes: A review.* Sci Total Environ, 2020. **748**: p. 141527 https://doi.org/10.1016/j.scitotenv.2020.141527.
217. Clematis, D. and M. Panizza, *Electrochemical oxidation of organic pollutants in low conductive solutions.* Current Opinion in Electrochemistry, 2021. **26** https://doi.org/10.1016/j.coelec.2020.100665.
218. dos Santos, A.J., et al., *Recent advances in electrochemical water technologies for the treatment of antibiotics: A short review.* Current Opinion in Electrochemistry, 2021. **26** https://doi.org/10.1016/j.coelec.2020.100674.
219. Hu, Z.Z., et al., *Anodic oxidation of organic pollutants: Anode fabrication, process hybrid and environmental applications.* Current Opinion in Electrochemistry, 2021. **26** https://doi.org/10.1016/j.coelec.2020.100659.
220. Salazar-Banda, G.R., et al., *Developments in electrode materials for wastewater treatment.* Current Opinion in Electrochemistry, 2021. **26** https://doi.org/10.1016/j.coelec.2020.100663.
221. Yang, Y., *Recent advances in the electrochemical oxidation water treatment: Spotlight on byproduct control.* Frontiers of Environmental Science & Engineering, 2020. **14**(5) https://doi.org/10.1007/s11783-020-1264-7.
222. Brillas, E., *Recent development of electrochemical advanced oxidation of herbicides. A review on its application to wastewater treatment and soil remediation.* Journal of Cleaner Production, 2021. **290** https://doi.org/10.1016/j.jclepro.2021.125841.
223. Lan, Y., et al., *On the role of salts for the treatment of wastewaters containing pharmaceuticals by electrochemical oxidation using a boron doped diamond anode.* Electrochimica Acta, 2017. **231**: p. 309-318 https://doi.org/10.1016/j.electacta.2017.01.160.
224. Zhang, C.Y., et al., *The Peculiar Roles of Sulfate Electrolytes in BDD Anode Cells.* Journal of the Electrochemical Society, 2015. **162**(8): p. E85-E89 https://doi.org/10.1149/2.0361508jes.
225. Thiam, A., et al., *Electrochemical advanced oxidation of carbofuran in aqueous sulfate and/or chloride media using a flow cell with a RuO2-based anode and an air-diffusion cathode at pre-pilot scale.* Chemical Engineering Journal, 2018. **335**: p. 133-144 https://doi.org/10.1016/j.cej.2017.10.137.
226. Bruguera-Casamada, C., et al., *The ability of electrochemical oxidation with a BDD anode to inactivate Gram-negative and Gram-positive bacteria in low conductivity sulfate medium.* Chemosphere, 2016. **163**: p. 516-524 https://doi.org/10.1016/j.chemosphere.2016.08.042.
227. Villegas-Guzman, P., et al., *Role of sulfate, chloride, and nitrate anions on the degradation of fluoroquinolone antibiotics by photoelectro-Fenton.* Environ Sci Pollut Res Int, 2017. **24**(36): p. 28175-28189 https://doi.org/10.1007/s11356-017-0404-5.
228. Chen, L., et al., *Electrochemical activation of sulfate by BDD anode in basic medium for efficient removal of organic pollutants.* Chemosphere, 2018. **210**: p. 516-523 https://doi.org/10.1016/j.chemosphere.2018.07.043.
229. Davis, J., J.C. Baygents, and J. Farrell, *Understanding Persulfate Production at Boron Doped Diamond Film Anodes.* Electrochimica Acta, 2014. **150**: p. 68-74 https://doi.org/10.1016/j.electacta.2014.10.104.
230. Serrano, K., et al., *Electrochemical preparation of peroxodisulfuric acid using boron doped diamond thin film electrodes.* Electrochimica Acta, 2002. **48**(4): p. 431-436 https://doi.org/10.1016/S0013-4686(02)00688-6.
231. Ganiyu, S.O., C.A. Martinez-Huitle, and M.A. Oturan, *Electrochemical advanced oxidation processes for wastewater treatment: Advances in formation and detection of reactive species and mechanisms.* Current Opinion in Electrochemistry, 2021. **27** https://doi.org/10.1016/j.coelec.2020.100678.
232. Santos, J.E.L., et al., *Evidence for the electrochemical production of persulfate at TiO2 nanotubes decorated with PbO2.* New Journal of Chemistry, 2018. **42**(7): p. 5523-5531 https://doi.org/10.1039/c7nj02604h.
233. Groenen Serrano, K., *Indirect Electrochemical Oxidation Using Hydroxyl Radical, Active Chlorine, and Peroxodisulfate*, in *Electrochemical Water and Wastewater Treatment*. 2018. p. 133-164.
234. de F. Araújo, K.C., et al., *Sulfate pollution: evidence for electrochemical production of persulfate by oxidizing sulfate released by the surfactant sodium dodecyl sulfate.* Environmental Chemistry Letters, 2018. **16**(2): p. 647-652 https://doi.org/10.1007/s10311-017-0703-6.
235. Bagastyo, A.Y., et al., *Impact of sulfate ion addition on electrochemical oxidation of anaerobically treated landfill leachate using boron-doped diamond anode.* Research on Chemical Intermediates, 2020. **46**(11): p. 4869-4881 https://doi.org/10.1007/s11164-020-04243-3.
236. Devi, L.G., et al., *Effect of chloride and sulfate ions on the advanced photo Fenton and modified photo Fenton degradation process of Alizarin Red S.* Journal of Molecular Catalysis a-Chemical, 2013. **374**: p. 125-131 https://doi.org/10.1016/j.molcata.2013.03.023.

237. Ma, J., et al., *Changes in activation energy and kinetics of heat-activated persulfate oxidation of phenol in response to changes in pH and temperature.* Chemosphere, 2017. **189**: p. 86-93 https://doi.org/10.1016/j.chemosphere.2017.09.051.
238. da Costa, T., et al., *BDD-Electrolysis of Oxalic Acid in Diluted Acidic Solutions.* Journal of the Brazilian Chemical Society, 2019 https://doi.org/10.21577/0103-5053.20190051.
239. Santos, G.O.S., et al., *Understanding the electrolytic generation of sulfate and chlorine oxidative species with different boron-doped diamond anodes.* Journal of Electroanalytical Chemistry, 2020. **857** https://doi.org/10.1016/j.jelechem.2019.113756.
240. Grebel, J.E., J.J. Pignatello, and W.A. Mitch, *Effect of halide ions and carbonates on organic contaminant degradation by hydroxyl radical-based advanced oxidation processes in saline waters.* Environ Sci Technol, 2010. **44**(17): p. 6822-8 https://doi.org/10.1021/es1010225.
241. Jin, Y., et al., *Sulfate Ion Removal from Reverse Osmosis Concentrate Using Electrodialysis and Nano-Filtration in Combination with Ettringite Precipitation*, in *Frontiers in Water-Energy-Nexus—Nature-Based Solutions, Advanced Technologies and Best Practices for Environmental Sustainability*. 2020. p. 407-410.
242. Burgos-Castillo, R.C., et al., *Application of electrochemical advanced oxidation to bisphenol A degradation in water. Effect of sulfate and chloride ions.* Chemosphere, 2018. **194**: p. 812-820 https://doi.org/10.1016/j.chemosphere.2017.12.014.
243. Gokulakrishnan, S., A. Mohammed, and H. Prakash, *Determination of persulphates using N,N-diethyl-p-phenylenediamine as colorimetric reagent: Oxidative coloration and degradation of the reagent without bactericidal effect in water.* Chemical Engineering Journal, 2016. **286**: p. 223-231 https://doi.org/10.1016/j.cej.2015.10.058.
244. Saha, P., et al., *Advanced oxidation processes for removal of organics from cooling tower blowdown: Efficiencies and evaluation of chlorinated species.* Separation and Purification Technology, 2022. **278** https://doi.org/10.1016/j.seppur.2021.119537.
245. Piai, L., et al., *Diffusion of hydrophilic organic micropollutants in granular activated carbon with different pore sizes.* Water Res, 2019. **162**: p. 518-527 https://doi.org/10.1016/j.watres.2019.06.012.
246. García-Espinoza, J.D., M. Zolfaghari, and P. Mijaylova Nacheva, *Synergistic effect between ultraviolet irradiation and electrochemical oxidation for removal of humic acids and pharmaceuticals.* Water and Environment Journal, 2019. **34**(2): p. 232-246 https://doi.org/10.1111/wej.12456.
247. Anson, F.C., *Patterns of ionic and molecular adsorption at electrodes.* Accounts of Chemical Research, 2002. **8**(12): p. 400-407 https://doi.org/10.1021/ar50096a002.
248. Jia, Y., et al., *Chemisorbed Sulfate-Driven Oscillatory Electro-Oxidation of Thiourea on Gold.* Journal of Physical Chemistry C, 2015. **119**(44): p. 24837-24843 https://doi.org/10.1021/acs.jpcc.5b07552.
249. Ghaneian, M.T., et al., *The effect of nitrate as a radical scavenger for the removal of humic acid from aqueous solutions by electron beam irradiation.* Journal of Community Health Research, 2013. **1**(3): p. 134-143.
250. Khongthon, W. and V. Pavarajarn, *Effect of Nitrate and Sulfate Contamination on Degradation of Diuron via Electrochemical Advanced Oxidation in a Microreactor.* Engineering Journal-Thailand, 2016. **20**(5): p. 25-34 https://doi.org/10.4186/ej.2016.20.5.25.
251. Wang, L., et al., *Effects of chloride on electrochemical degradation of perfluorooctanesulfonate by Magneli phase Ti4O7 and boron doped diamond anodes.* Water Res, 2020. **170**: p. 115254 https://doi.org/10.1016/j.watres.2019.115254.
252. Yang, Y., et al., *Comparison of halide impacts on the efficiency of contaminant degradation by sulfate and hydroxyl radical-based advanced oxidation processes (AOPs).* Environ Sci Technol, 2014. **48**(4): p. 2344-51 https://doi.org/10.1021/es404118q.
253. Azizi, O., et al., *Mechanism of perchlorate formation on boron-doped diamond film anodes.* Environ Sci Technol, 2011. **45**(24): p. 10582-90 https://doi.org/10.1021/es202534w.
254. Yang, T., et al., *UV/chlorine process for degradation of benzothiazole and benzotriazole in water: Efficiency, mechanism and toxicity evaluation.* Sci Total Environ, 2021. **760**: p. 144304 https://doi.org/10.1016/j.scitotenv.2020.144304.
255. Nika, M.C., et al., *Chlorination of benzothiazoles and benzotriazoles and transformation products identification by LC-HR-MS/MS.* J Hazard Mater, 2017. **323**(Pt A): p. 400-413 https://doi.org/10.1016/j.jhazmat.2016.03.035.
256. Li, X.R., et al., *Enhanced catalytic oxidation of benzotriazole via peroxymonosulfate activated by CoFe2O4 supported onto nitrogen-doped three-dimensional graphene aerogels.* Chemical Engineering Journal, 2020. **400** https://doi.org/10.1016/j.cej.2020.125897.
257. Linaric, M., M. Markic, and L. Sipos, *High salinity wastewater treatment*. Water Sci Technol, 2013. **68**(6): p. 1400-5 https://doi.org/10.2166/wst.2013.376.

258. Pernetti, M. and L. Di Palma, *Experimental evaluation of inhibition effects of saline wastewater on activated sludge.* Environ Technol, 2005. **26**(6): p. 695-703 https://doi.org/10.1080/09593330.2001.9619509.
259. Lefebvre, O. and R. Moletta, *Treatment of organic pollution in industrial saline wastewater: a literature review.* Water Res, 2006. **40**(20): p. 3671-82 https://doi.org/10.1016/j.watres.2006.08.027.
260. Saha, P., et al., *Cooling tower water treatment using a combination of electrochemical oxidation and constructed wetlands.* Process Safety and Environmental Protection, 2020. **144**: p. 42-51 https://doi.org/10.1016/j.psep.2020.07.019.
261. Foglia, A., et al., *Long-term operation of a pilot-scale anaerobic membrane bioreactor (AnMBR) treating high salinity low loaded municipal wastewater in real environment*. Separation and Purification Technology, 2020. **236** https://doi.org/10.1016/j.seppur.2019.116279.
262. Yan, Z.Q., et al., *Selective separation of chloride and sulfate by nanofiltration for high saline wastewater recycling.* Separation and Purification Technology, 2016. **166**: p. 135-141 https://doi.org/10.1016/j.seppur.2016.04.009.
263. NORMAN. *NORMAN List of Emerging Substances*. 2016 February 2016 [cited 2020 07.07]; Available from: https://www.norman-network.net/?q=node/81.
264. Smit, C.E. and S. Wuijts, *Specific pollutants and drinking water relevant substances in the context of the Water Framework Directive: Selection of potentially relevant substances for the Netherlands*. 2012, National Institute for Public Health and the Environment RIVM: The Netherlands.
265. Lee, J.E., et al., *Degradation kinetics and pathway of 1H-benzotriazole during UV/chlorination process.* Chemical Engineering Journal, 2019. **359**: p. 1502-1508 https://doi.org/10.1016/j.cej.2018.11.026.
266. Wu, J.L., et al., *Degradation of benzotriazole by DBD plasma and peroxymonosulfate: Mechanism, degradation pathway and potential toxicity.* Chemical Engineering Journal, 2020. **384** https://doi.org/10.1016/j.cej.2019.123300.
267. Ding, Y., et al., *Photoelectrochemical activity of liquid phase deposited TiO2 film for degradation of benzotriazole.* J Hazard Mater, 2010. **175**(1-3): p. 96-103 https://doi.org/10.1016/j.jhazmat.2009.09.037.
268. Hollingsworth, J., et al., *Anaerobic biodegradability and methanogenic toxicity of key constituents in copper chemical mechanical planarization effluents of the semiconductor industry.* Chemosphere, 2005. **59**(9): p. 1219-28 https://doi.org/10.1016/j.chemosphere.2004.11.067.
269. Liu, Y.S., et al., *Biodegradation of three selected benzotriazoles under aerobic and anaerobic conditions.* Water Res, 2011. **45**(16): p. 5005-14 https://doi.org/10.1016/j.watres.2011.07.001.
270. Seeland, A., et al., *Acute and chronic toxicity of benzotriazoles to aquatic organisms.* Environ Sci Pollut Res Int, 2012. **19**(5): p. 1781-90 https://doi.org/10.1007/s11356-011-0705-z.
271. Cantwell, M.G., et al., *Source determination of benzotriazoles in sediment cores from two urban estuaries on the Atlantic Coast of the United States.* Mar Pollut Bull, 2015. **101**(1): p. 208-218 https://doi.org/10.1016/j.marpolbul.2015.10.075.
272. Cantwell, M.G., J.C. Sullivan, and R.M. Burgess, *Benzotriazoles*, in *Persistent Organic Pollutants (POPs): Analytical Techniques, Environmental Fate and Biological Effects*. 2015. p. 513-545.
273. Zhang, Y., et al., *Synchronous degradation of aqueous benzotriazole and bromate reduction in catalytic ozonation: Effect of matrix factor, degradation mechanism and application strategy in water treatment.* Sci Total Environ, 2020. **727**: p. 138696 https://doi.org/10.1016/j.scitotenv.2020.138696.
274. Minella, M., et al., *Photocatalytic Transformations of 1H-Benzotriazole and Benzotriazole Derivates.* Nanomaterials (Basel), 2020. **10**(9) https://doi.org/10.3390/nano10091835.
275. Liu, Y., et al., *Cu (II)-doped V2O5 mediated persulfate activation for heterogeneous catalytic degradation of benzotriazole in aqueous solution.* Separation and Purification Technology, 2020. **230** https://doi.org/10.1016/j.seppur.2019.115848.
276. Ghanbari, F., et al., *Oxidative removal of benzotriazole using peroxymonosulfate/ozone/ultrasound: Synergy, optimization, degradation intermediates and utilizing for real wastewater.* Chemosphere, 2020. **244**: p. 125326 https://doi.org/10.1016/j.chemosphere.2019.125326.
277. Ye, J., et al., *Degradation of 1H-benzotriazole using vacuum ultraviolet: a prospective treatment method for micro-pollutants.* Water Sci Technol, 2019. **80**(4): p. 773-783 https://doi.org/10.2166/wst.2019.320.
278. Ma, J., et al., *Degradation of benzotriazole by sulfate radical-based advanced oxidation process.* Environ Technol, 2019: p. 1-10 https://doi.org/10.1080/09593330.2019.1625959.
279. Jorfi, S., et al., *A novel combination of oxidative degradation for benzotriazole removal using TiO2 loaded on FeIIFe2IIIO4@C as an efficient activator of peroxymonosulfate.* Applied Catalysis B: Environmental, 2017. **219**: p. 216-230 https://doi.org/10.1016/j.apcatb.2017.07.035.

280. Felis, E., A. Sochacki, and S. Magiera, *Degradation of benzotriazole and benzothiazole in treatment wetlands and by artificial sunlight.* Water Res, 2016. **104**: p. 441-448 https://doi.org/10.1016/j.watres.2016.08.037.
281. Borowska, E., E. Felis, and J. Kalka, *Oxidation of benzotriazole and benzothiazole in photochemical processes: Kinetics and formation of transformation products.* Chemical Engineering Journal, 2016. **304**: p. 852-863 https://doi.org/10.1016/j.cej.2016.06.123.
282. Ghanbari, F. and M. Moradi, *Application of peroxymonosulfate and its activation methods for degradation of environmental organic pollutants: Review.* Chemical Engineering Journal, 2017. **310**: p. 41-62 https://doi.org/10.1016/j.cej.2016.10.064.
283. Giannakis, S., K.Y.A. Lin, and F. Ghanbari, *A review of the recent advances on the treatment of industrial wastewaters by Sulfate Radical-based Advanced Oxidation Processes (SR-AOPs).* Chemical Engineering Journal, 2021. **406** https://doi.org/10.1016/j.cej.2020.127083.
284. Peng, W., et al., *Non-radical reactions in persulfate-based homogeneous degradation processes: A review.* Chemical Engineering Journal, 2021. **421** https://doi.org/10.1016/j.cej.2020.127818.
285. Xiao, R.Y., et al., *Activation of peroxymonosulfate/persulfate by nanomaterials for sulfate radical-based advanced oxidation technologies.* Current Opinion in Chemical Engineering, 2018. **19**: p. 51-58 https://doi.org/10.1016/j.coche.2017.12.005.
286. Xu, H.D., et al., *Improving PMS oxidation of organic pollutants by single cobalt atom catalyst through hybrid radical and non-radical pathways.* Applied Catalysis B-Environmental, 2020. **263** https://doi.org/10.1016/j.apcatb.2019.118350.
287. Zhang, W., et al., *Impact of Chloride Ions on UV/H2O2 and UV/Persulfate Advanced Oxidation Processes.* Environ Sci Technol, 2018. **52**(13): p. 7380-7389 https://doi.org/10.1021/acs.est.8b01662.
288. Caregnato, P., et al., *Chloride anion effect on the advanced oxidation processes of methidathion and dimethoate: role of Cl2(.-) radical.* Water Res, 2013. **47**(1): p. 351-62 https://doi.org/10.1016/j.watres.2012.10.018.
289. Wu, Y.X., et al., *Modelling study on the effects of chloride on the degradation of bezafibrate and carbamazepine in sulfate radical-based advanced oxidation processes: Conversion of reactive radicals.* Chemical Engineering Journal, 2019. **358**: p. 1332-1341 https://doi.org/10.1016/j.cej.2018.10.125.
290. Yuan, R., et al., *Effects of chloride ion on degradation of Acid Orange 7 by sulfate radical-based advanced oxidation process: implications for formation of chlorinated aromatic compounds.* J Hazard Mater, 2011. **196**: p. 173-9 https://doi.org/10.1016/j.jhazmat.2011.09.007.
291. Wang, Z., et al., *Effects of chloride ions on bleaching of azo dyes by Co2+/oxone reagent: kinetic analysis.* J Hazard Mater, 2011. **190**(1-3): p. 1083-7 https://doi.org/10.1016/j.jhazmat.2011.04.016.
292. Wang, P., et al., *Involvements of chloride ion in decolorization of Acid Orange 7 by activated peroxydisulfate or peroxymonosulfate oxidation.* J Environ Sci (China), 2011. **23**(11): p. 1799-807 https://doi.org/10.1016/s1001-0742(10)60620-1.
293. Wang, Z., et al., *Both degradation and AOX accumulation are significantly enhanced in UV/peroxymonosulfate/4-chlorophenol/Cl− system: two sides of the same coin?* RSC Advances, 2017. **7**(20): p. 12318-12321 https://doi.org/10.1039/c7ra01294b.
294. Fang, C.L., et al., *Monochlorophenols degradation by UV/persulfate is immune to the presence of chloride: Illusion or reality?* Chemical Engineering Journal, 2017. **323**: p. 124-133 https://doi.org/10.1016/j.cej.2017.04.094.
295. Ye, J.S., et al., *Degradation of 1H-benzotriazole using ultraviolet activating persulfate: Mechanisms, products and toxicological analysis.* Chemical Engineering Journal, 2018. **334**: p. 1493-1501 https://doi.org/10.1016/j.cej.2017.11.101.
296. Oh, W.-D., et al., *A novel three-dimensional spherical CuBi 2 O 4 consisting of nanocolumn arrays with persulfate and peroxymonosulfate activation functionalities for 1 H-benzotriazole removal.* Nanoscale, 2015. **7**(17): p. 8149-8158.
297. Lutze, H.V., N. Kerlin, and T.C. Schmidt, *Sulfate radical-based water treatment in presence of chloride: formation of chlorate, inter-conversion of sulfate radicals into hydroxyl radicals and influence of bicarbonate.* Water Res, 2015. **72**: p. 349-60 https://doi.org/10.1016/j.watres.2014.10.006.
298. Qian, Y., et al., *Perfluorooctanoic Acid Degradation Using UV-Persulfate Process: Modeling of the Degradation and Chlorate Formation.* Environ Sci Technol, 2016. **50**(2): p. 772-81 https://doi.org/10.1021/acs.est.5b03715.
299. Hou, S., et al., *Chlorate Formation Mechanism in the Presence of Sulfate Radical, Chloride, Bromide and Natural Organic Matter.* Environ Sci Technol, 2018. **52**(11): p. 6317-6325 https://doi.org/10.1021/acs.est.8b00576.
300. Who, *Chemical hazards in drinking-water: Chlorine dioxide, chlorate and chlorite*. 2005.

301. Peng, L.B., D.Y. Deng, and F.T. Ye, *Efficient oxidation of high levels of soil-sorbed phenanthrene by microwave-activated persulfate: implication for in situ subsurface remediation engineering.* Journal of Soils and Sediments, 2016. **16**(1): p. 28-37 https://doi.org/10.1007/s11368-015-1176-5.
302. Ike, I.A., J.D. Orbell, and M. Duke, *Activation of Persulfate at Waste Heat Temperatures for Humic Acid Degradation.* Acs Sustainable Chemistry & Engineering, 2018. **6**(3): p. 4345-4353 https://doi.org/10.1021/acssuschemeng.7b04840.
303. Gokulakrishnan, S., A. Mohammed, and H. Prakash, *Determination of persulphates using N, N-diethyl-p-phenylenediamine as colorimetric reagent: Oxidative coloration and degradation of the reagent without bactericidal effect in water.* Chemical Engineering Journal, 2016. **286**: p. 223-231.
304. Fang, Z., et al., *Comparison of UV/Persulfate and UV/H2O2 for the removal of naphthenic acids and acute toxicity towards Vibrio fischeri from petroleum production process water.* Sci Total Environ, 2019. **694**: p. 133686 https://doi.org/10.1016/j.scitotenv.2019.133686.
305. Federation, W.E., *Standard Methods For The Examination Of Water And Wastewater*. 21 ed, ed. A.D.E.L.S.C.E.W.R.A.E.G.M.A.H. Franson. 2005, Washington, DC, USA: American Public Health Association (APHA).
306. Anipsitakis, G.P., T.P. Tufano, and D.D. Dionysiou, *Chemical and microbial decontamination of pool water using activated potassium peroxymonosulfate.* Water Res, 2008. **42**(12): p. 2899-910 https://doi.org/10.1016/j.watres.2008.03.002.
307. Anipsitakis, G.P., D.D. Dionysiou, and M.A. Gonzalez, *Cobalt-mediated activation of peroxymonosulfate and sulfate radical attack on phenolic compounds. implications of chloride ions.* Environ Sci Technol, 2006. **40**(3): p. 1000-7 https://doi.org/10.1021/es050634b.
308. Deng, Y. and C.M. Ezyske, *Sulfate radical-advanced oxidation process (SR-AOP) for simultaneous removal of refractory organic contaminants and ammonia in landfill leachate.* Water Res, 2011. **45**(18): p. 6189-94 https://doi.org/10.1016/j.watres.2011.09.015.
309. Buxton, G.V., M. Bydder, and G.A. Salmon, *The reactivity of chlorine atoms in aqueous solution Part II. The equilibrium SO 4-+ Cl-Cl Nsbd+ SO 4 2-.* Physical Chemistry Chemical Physics, 1999. **1**(2): p. 269-273.
310. Yang, S., et al., *Degradation efficiencies of azo dye Acid Orange 7 by the interaction of heat, UV and anions with common oxidants: persulfate, peroxymonosulfate and hydrogen peroxide.* J Hazard Mater, 2010. **179**(1-3): p. 552-8 https://doi.org/10.1016/j.jhazmat.2010.03.039.
311. Zhang, Y., et al., *Degradation of p-aminobenzoic acid by peroxymonosulfate and evolution of effluent organic matter: The effect of chloride ion.* Chemical Engineering Journal, 2021. **411**: p. 128462 https://doi.org/10.1016/j.cej.2021.128462.
312. Hao, J.W., et al., *Activation of peroxymonosulfate by cobalt doped graphitic carbon nitride for ammonia removal in chloride-containing wastewater.* Separation and Purification Technology, 2021. **271**: p. 118858 https://doi.org/10.1016/j.seppur.2021.118858.
313. Betterton, E.A. and M.R. Hoffmann, *Kinetics and Mechanism of the Oxidation of Aqueous Hydrogen-Sulfide by Peroxymonosulfate.* Environmental Science & Technology, 1990. **24**(12): p. 1819-1824 https://doi.org/DOI 10.1021/es00082a005.
314. Lente, G., et al., *One- versus two-electron oxidation with peroxomonosulfate ion: reactions with iron(II), vanadium(IV), halide ions, and photoreaction with cerium(III).* Inorg Chem, 2009. **48**(4): p. 1763-73 https://doi.org/10.1021/ic801569k.
315. Ahmadi, M., F. Ghanbari, and M. Moradi, *Photocatalysis assisted by peroxymonosulfate and persulfate for benzotriazole degradation: effect of pH on sulfate and hydroxyl radicals.* Water Sci Technol, 2015. **72**(11): p. 2095-102 https://doi.org/10.2166/wst.2015.437.
316. Neta, P., R.E. Huie, and A.B. Ross, *Rate Constants for Reactions of Inorganic Radicals in Aqueous-Solution.* Journal of Physical and Chemical Reference Data, 1988. **17**(3): p. 1027-1284 https://doi.org/Doi 10.1063/1.555808.
317. Yang, Y., et al., *Comparison of halide impacts on the efficiency of contaminant degradation by sulfate and hydroxyl radical-based advanced oxidation processes (AOPs).* Environmental science & technology, 2014. **48**(4): p. 2344-2351.
318. Moradi, M. and A. Eslami, *Reductive/oxidative degradation of tetrachloroethene and its transformation products using combination of permeable ZVI column and UV/Fe/peroxydisulfate system: RSM design and synergy effect study.* Journal of Water Process Engineering, 2020. **36**: p. 101288 https://doi.org/10.1016/j.jwpe.2020.101288.
319. Qi, C.D., et al., *Activation of peroxymonosulfate by microwave irradiation for degradation of organic contaminants.* Chemical Engineering Journal, 2017. **315**: p. 201-209 https://doi.org/10.1016/j.cej.2017.01.012.
320. Ball, D.L. and J.O. Edwards, *The kinetics and mechanism of the decomposition of Caro's acid. I.* Journal of the American Chemical Society, 1956. **78**(6): p. 1125-1129.

321. Yang, S.Y., et al., *Use of peroxymonosulfate in wet scrubbing process for efficient odor control.* Separation and Purification Technology, 2016. **158**: p. 80-86 https://doi.org/10.1016/j.seppur.2015.12.010.
322. Lou, X., et al., *Peroxymonosulfate activation by phosphate anion for organics degradation in water.* Chemosphere, 2014. **117**: p. 582-5 https://doi.org/10.1016/j.chemosphere.2014.09.046.
323. Yang, F., et al., *Peroxymonosulfate/base process in saline wastewater treatment: The fight between alkalinity and chloride ions.* Chemosphere, 2018. **199**: p. 84-88 https://doi.org/10.1016/j.chemosphere.2018.02.023.
324. Lou, X.Y., et al., *Rapid dye degradation with reactive oxidants generated by chloride-induced peroxymonosulfate activation.* Environ Sci Pollut Res Int, 2013. **20**(9): p. 6317-23 https://doi.org/10.1007/s11356-013-1678-x.
325. Anipsitakis, G.P. and D.D. Dionysiou, *Radical generation by the interaction of transition metals with common oxidants.* Environ Sci Technol, 2004. **38**(13): p. 3705-12 https://doi.org/10.1021/es035121o.
326. Norman, R., P. Storey, and P. West, *Electron spin resonance studies. Part XXV. Reactions of the sulphate radical anion with organic compounds.* Journal of the Chemical Society B: Physical Organic, 1970: p. 1087-1095.
327. Ji, Y.F., et al., *Heat-activated persulfate oxidation of atrazine: Implications for remediation of groundwater contaminated by herbicides.* Chemical Engineering Journal, 2015. **263**: p. 45-54 https://doi.org/10.1016/j.cej.2014.10.097.
328. Liang, C.J. and H.W. Su, *Identification of Sulfate and Hydroxyl Radicals in Thermally Activated Persulfate.* Industrial & Engineering Chemistry Research, 2009. **48**(11): p. 5558-5562 https://doi.org/10.1021/ie9002848.
329. Ding, Y., et al., *Nonradicals induced degradation of organic pollutants by peroxydisulfate (PDS) and peroxymonosulfate (PMS): Recent advances and perspective.* Sci Total Environ, 2021. **765**: p. 142794 https://doi.org/10.1016/j.scitotenv.2020.142794.
330. Muller, A., et al., *Identification of ozonation by-products of 4- and 5-methyl-1H-benzotriazole during the treatment of surface water to drinking water.* Water Res, 2012. **46**(3): p. 679-90 https://doi.org/10.1016/j.watres.2011.11.033.
331. Fang, G.-D., et al., *Sulfate radical-based degradation of polychlorinated biphenyls: Effects of chloride ion and reaction kinetics.* Journal of Hazardous Materials, 2012. **227-228**: p. 394-401 https://doi.org/https://doi.org/10.1016/j.jhazmat.2012.05.074.
332. Yuan, R.X., et al., *Photocatalytic degradation and chlorination of azo dye in saline wastewater: Kinetics and AOX formation.* Chemical Engineering Journal, 2012. **192**: p. 171-178 https://doi.org/10.1016/j.cej.2012.03.080.
333. Yusuf, M., *Handbook of Textile Effluent Remediation*. 2018: Pan Stanford.
334. Fang, C., et al., *Enhanced AOX accumulation and aquatic toxicity during 2,4,6-trichlorophenol degradation in a Co(II)/peroxymonosulfate/Cl(-) system.* Chemosphere, 2016. **144**: p. 2415-20 https://doi.org/10.1016/j.chemosphere.2015.11.030.
335. Chaabane, H., et al., *Photodegradation of sulcotrione in various aquatic environments and toxicity of its photoproducts for some marine micro-organisms.* Water Research, 2007. **41**(8): p. 1781-1789 https://doi.org/10.1016/j.watres.2007.01.009.
336. Tortajada, C., *Contributions of recycled wastewater to clean water and sanitation Sustainable Development Goals.* Npj Clean Water, 2020. **3**(1) https://doi.org/10.1038/s41545-020-0069-3.
337. Goh, P.S., et al., *Membrane fouling in desalination and its mitigation strategies.* Desalination, 2018. **425**: p. 130-155 https://doi.org/10.1016/j.desal.2017.10.018.
338. Mouamfon, M.V.N., et al., *Photodegradation of Sulfamethoxazole Applying UV- and VUV-Based Processes.* Water Air and Soil Pollution, 2011. **218**(1-4): p. 265-274 https://doi.org/10.1007/s11270-010-0639-y.
339. Zhang, W.X., et al., *Membrane fouling in photocatalytic membrane reactors (PMRs) for water and wastewater treatment: A critical review.* Chemical Engineering Journal, 2016. **302**: p. 446-458 https://doi.org/10.1016/j.cej.2016.05.071.
340. Ganiyu, S.O., et al., *Coupling of membrane filtration and advanced oxidation processes for removal of pharmaceutical residues: A critical review.* Separation and Purification Technology, 2015. **156**: p. 891-914 https://doi.org/10.1016/j.seppur.2015.09.059.
341. Zhang, J.H., et al., *Influence of pre-treatment combinations on RO membrane fouling.* Desalination, 2016. **393**: p. 120-126 https://doi.org/10.1016/j.desal.2016.02.020.
342. Anipsitakis, G.P., T.P. Tufano, and D.D. Dionysiou, *Chemical and microbial decontamination of pool water using activated potassium peroxymonosulfate.* Water Research, 2008. **42**(12): p. 2899-2910 https://doi.org/https://doi.org/10.1016/j.watres.2008.03.002.

343. Park, M., et al., *Pre-ozonation for high recovery of nanofiltration (NF) membrane system: Membrane fouling reduction and trace organic compound attenuation.* Journal of Membrane Science, 2017. **523**: p. 255-263 https://doi.org/10.1016/j.memsci.2016.09.051.
344. Yen, H.Y., *Fouling Inhibition of Membrane Separation by H2O2/UV Pre-oxidation for Color Filter Effluent Reuse.* Ozone: Science & Engineering, 2015. **38**(2): p. 163-171 https://doi.org/10.1080/01919512.2015.1095633.
345. Gonzalez-Olmos, R., A. Penades, and G. Garcia, *Electro-oxidation as efficient pretreatment to minimize the membrane fouling in water reuse processes.* Journal of Membrane Science, 2018. **552**: p. 124-131 https://doi.org/10.1016/j.memsci.2018.01.041.
346. Liu, B., et al., *Membrane Fouling and Rejection of Organics during Algae-Laden Water Treatment Using Ultrafiltration: A Comparison between in Situ Pretreatment with Fe(II)/Persulfate and Ozone.* Environ Sci Technol, 2018. **52**(2): p. 765-774 https://doi.org/10.1021/acs.est.7b03819.
347. Varanasi, L., et al., *Transformations of dissolved organic matter induced by UV photolysis, Hydroxyl radicals, chlorine radicals, and sulfate radicals in aqueous-phase UV-Based advanced oxidation processes.* Water Res, 2018. **135**: p. 22-30 https://doi.org/10.1016/j.watres.2018.02.015.
348. Pisarenko, A.N., et al., *Investigation of the use of Chlorine Based Advanced Oxidation in Surface Water: Oxidation of Natural Organic Matter and Formation of Disinfection Byproducts.* Journal of Advanced Oxidation Technologies, 2013. **16**(1): p. 137-150.
349. Lamsal, R., M.E. Walsh, and G.A. Gagnon, *Comparison of advanced oxidation processes for the removal of natural organic matter.* Water Res, 2011. **45**(10): p. 3263-9 https://doi.org/10.1016/j.watres.2011.03.038.
350. Moradi, M. and G. Moussavi, *Investigation of chemical-less UVC/VUV process for advanced oxidation of sulfamethoxazole in aqueous solutions: Evaluation of operational variables and degradation mechanism.* Separation and Purification Technology, 2018. **190**: p. 90-99 https://doi.org/10.1016/j.seppur.2017.08.006.
351. Hirun-Utok, C. and S. Phattarapattamawong, *Degradation and transformation of natural organic matter accountable for disinfection byproduct formations by UV photolysis and UV/chlor(am)ine.* Water Sci Technol, 2019. **79**(5): p. 929-937 https://doi.org/10.2166/wst.2018.496.
352. Carneiro, J.T., et al., *Toward a Physically Sound Structure-Activity Relationship of TiO2-Based Photocatalysts.* Journal of Physical Chemistry C, 2010. **114**(1): p. 327-332 https://doi.org/10.1021/jp906395w.
353. Yang, L., et al., *A Green Method to Determine VUV (185 nm) Fluence Rate Based on Hydrogen Peroxide Production in Aqueous Solution.* Photochem Photobiol, 2018. **94**(4): p. 821-824 https://doi.org/10.1111/php.12913.
354. Scholes, M.L., M.N. Schuchmann, and C. von Sonntag, *Enhancement of radiation-induced base release from nucleosides in alkaline solution: essential role of the O.- radical.* Int J Radiat Biol, 1992. **61**(4): p. 443-9 https://doi.org/10.1080/09553009214551191.
355. Raes, S.M.T., et al., *Water-Based Synthesis of Hydrophobic Ionic Liquids [N8888][oleate] and [P666,14][oleate] and their Bioprocess Compatibility.* ChemistryOpen, 2018. **7**(11): p. 878-884 https://doi.org/10.1002/open.201800187.
356. Zhu, S., et al., *Degradation of carbamazepine by vacuum-UV oxidation process: Kinetics modeling and energy efficiency.* J Hazard Mater, 2019. **368**: p. 178-185 https://doi.org/10.1016/j.jhazmat.2019.01.043.
357. Särkkä, H., A. Bhatnagar, and M. Sillanpää, *Recent developments of electro-oxidation in water treatment — A review.* Journal of Electroanalytical Chemistry, 2015. **754**: p. 46-56 https://doi.org/10.1016/j.jelechem.2015.06.016.
358. Wacławek, S., et al., *Chemistry of persulfates in water and wastewater treatment: A review.* Chemical Engineering Journal, 2017. **330**: p. 44-62 https://doi.org/10.1016/j.cej.2017.07.132.
359. Lee, M.Y., et al., *Enhancement effect among a UV, persulfate, and copper (UV/PS/Cu2+) system on the degradation of nonoxidizing biocide: The kinetics, radical species, and degradation pathway.* Chemical Engineering Journal, 2020. **382**: p. 122312 https://doi.org/10.1016/j.cej.2019.122312.
360. Nosaka, Y. and A.Y. Nosaka, *Generation and Detection of Reactive Oxygen Species in Photocatalysis.* Chem Rev, 2017. **117**(17): p. 11302-11336 https://doi.org/10.1021/acs.chemrev.7b00161.
361. Arany, E., et al., *Degradation of naproxen by UV, VUV photolysis and their combination.* J Hazard Mater, 2013. **262**: p. 151-7 https://doi.org/10.1016/j.jhazmat.2013.08.003.
362. Moser, P.B., et al., *Removal of organic matter of electrodialysis reversal brine from a petroleum refinery wastewater reclamation plant by UV and UV/H202 process.* J Environ Sci Health A Tox Hazard Subst Environ Eng, 2018. **53**(5): p. 430-435 https://doi.org/10.1080/10934529.2017.1409580.

363. Wang, T., et al., *Self-sensitized photodegradation of benzisothiazolinone by low-pressure UV-C irradiation: Kinetics, mechanisms, and the effect of media.* Separation and Purification Technology, 2017. **189**: p. 419-424 https://doi.org/10.1016/j.seppur.2017.08.031.
364. Iovino, P., et al., *Photodegradation of diclofenac in wastewaters.* Desalination and Water Treatment, 2017. **61**: p. 293-297 https://doi.org/10.5004/dwt.2016.11063.
365. Luo, S., et al., *UV direct photolysis of sulfamethoxazole and ibuprofen: An experimental and modelling study.* J Hazard Mater, 2018. **343**: p. 132-139 https://doi.org/10.1016/j.jhazmat.2017.09.019.
366. Li, W., et al., *Enhanced kinetic performance of peroxymonosulfate/ZVI system with the addition of copper ions: Reactivity, mechanism, and degradation pathways.* J Hazard Mater, 2020. **393**: p. 122399 https://doi.org/10.1016/j.jhazmat.2020.122399.
367. Imoberdorf, G. and M. Mohseni, *Degradation of natural organic matter in surface water using vacuum-UV irradiation.* J Hazard Mater, 2011. **186**(1): p. 240-6 https://doi.org/10.1016/j.jhazmat.2010.10.118.
368. García, A.-M., et al., *Separation and Characterization of NOM Intermediates Along AOP Oxidation*, in *Applications of Advanced Oxidation Processes (AOPs) in Drinking Water Treatment*, A. Gil, L.A. Galeano, and M.Á. Vicente, Editors. 2017, Springer International Publishing: Cham. p. 99-132.
369. Geng, P. and G. Chen, *Antifouling ceramic membrane electrode modified by Magnéli Ti 4 O 7 for electro-microfiltration of humic acid.* Separation and Purification Technology, 2017. **185**: p. 61-71 https://doi.org/10.1016/j.seppur.2017.05.023.
370. Chen, L., et al., *Biological performance and fouling mitigation in the biochar-amended anaerobic membrane bioreactor (AnMBR) treating pharmaceutical wastewater.* Bioresour Technol, 2020. **302**: p. 122805 https://doi.org/10.1016/j.biortech.2020.122805.
371. Abdikheibari, S., et al., *Natural organic matter removal and fouling resistance properties of a boron nitride nanosheet-functionalized thin film nanocomposite membrane and its impact on permeate chlorine demand.* Journal of Water Process Engineering, 2020. **34**: p. 101160 https://doi.org/10.1016/j.jwpe.2020.101160.
372. El Kateb, M., et al., *Electrochemical advanced oxidation processes using novel electrode materials for mineralization and biodegradability enhancement of nanofiltration concentrate of landfill leachates.* Water Res, 2019. **162**: p. 446-455 https://doi.org/10.1016/j.watres.2019.07.005.
373. Sen Kavurmaci, S. and M. Bekbolet, *Tracing TiO2 photocatalytic degradation of humic acid in the presence of clay particles by excitation–emission matrix (EEM) fluorescence spectra.* Journal of Photochemistry and Photobiology A: Chemistry, 2014. **282**: p. 53-61 https://doi.org/10.1016/j.jphotochem.2014.03.011.
374. Li, K., et al., *Membrane fouling in an integrated adsorption-UF system: effects of NOM and adsorbent properties.* Environmental Science-Water Research & Technology, 2020. **6**(1): p. 78-86 https://doi.org/10.1039/c9ew00843h.
375. Lakowicz, J.R., *Plasmonics in Biology and Plasmon-Controlled Fluorescence.* Plasmonics, 2006. **1**(1): p. 5-33 https://doi.org/10.1007/s11468-005-9002-3.
376. Beggs, K.M.H., R.S. Summers, and D.M. McKnight, *Characterizing chlorine oxidation of dissolved organic matter and disinfection by-product formation with fluorescence spectroscopy and parallel factor analysis.* Journal of Geophysical Research-Biogeosciences, 2009. **114**(G4) https://doi.org/10.1029/2009jg001009.
377. Moradi, M., et al., *Synthesis of novel Ag-doped S-MgO nanosphere as an efficient UVA/LED-activated photocatalyst for non-radical oxidation of diclofenac: Catalyst preparation and characterization and photocatalytic mechanistic evaluation.* Applied Catalysis B-Environmental, 2020. **260**: p. 118128 https://doi.org/10.1016/j.apcatb.2019.118128.
378. Barbari, K., et al., *Photocatalytically-assisted electrooxidation of herbicide fenuron using a new bifunctional electrode PbO2/SnO2-Sb2O3/Ti//Ti/TiO2.* Chemosphere, 2018. **203**: p. 1-10 https://doi.org/10.1016/j.chemosphere.2018.03.126.
379. Dryer, D.J., G.V. Korshin, and M. Fabbricino, *In situ examination of the protonation behavior of fulvic acids using differential absorbance spectroscopy.* Environ Sci Technol, 2008. **42**(17): p. 6644-9 https://doi.org/10.1021/es800741u.
380. Moussavi, G., E. Fathi, and M. Moradi, *Advanced disinfecting and post-treating the biologically treated hospital wastewater in the UVC/H2O2 and VUV/H2O2 processes: Performance comparison and detoxification efficiency.* Process Safety and Environmental Protection, 2019. **126**: p. 259-268 https://doi.org/10.1016/j.psep.2019.04.016.
381. Quici, N., et al., *Vacuum-UV-photolysis of aqueous solutions of citric and gallic acids.* Journal of Photochemistry and Photobiology a-Chemistry, 2008. **197**(2-3): p. 306-312 https://doi.org/10.1016/j.jphotochem.2008.01.008.

382. Fan, Y., et al., *Kinetic and mechanistic investigations of the degradation of sulfamethazine in heat-activated persulfate oxidation process.* J Hazard Mater, 2015. **300**: p. 39-47 https://doi.org/10.1016/j.jhazmat.2015.06.058.
383. Gu, X.G., et al., *Oxidation of 1,1,1-Trichloroethane Stimulated by Thermally Activated Persulfate.* Industrial & Engineering Chemistry Research, 2011. **50**(19): p. 11029-11036 https://doi.org/10.1021/ie201059x.
384. Waldemer, R.H., et al., *Oxidation of chlorinated ethenes by heat-activated persulfate: kinetics and products.* Environ Sci Technol, 2007. **41**(3): p. 1010-5 https://doi.org/10.1021/es062237m.
385. Cheshme Khavar, A.H., G. Moussavi, and A.R. Mahjoub, *The preparation of TiO2@rGO nanocomposite efficiently activated with UVA/LED and H2O2 for high rate oxidation of acetaminophen: Catalyst characterization and acetaminophen degradation and mineralization.* Applied Surface Science, 2018. **440**: p. 963-973 https://doi.org/10.1016/j.apsusc.2018.01.238.
386. Wang, K.H., et al., *The pH and anion effects on the heterogeneous photocatalytic degradation of o-methylbenzoic acid in TiO2 aqueous suspension.* Chemosphere, 2000. **40**(4): p. 389-94 https://doi.org/10.1016/s0045-6535(99)00252-0.
387. Piscopo, A., D. Robert, and J.V. Weber, *Comparison between the reactivity of commercial and synthetic TiO2 photocatalysts.* Journal of Photochemistry and Photobiology a-Chemistry, 2001. **139**(2-3): p. 253-256 https://doi.org/Doi 10.1016/S1010-6030(01)00381-1.
388. Lutke Eversloh, C., et al., *Electrochemical oxidation of tramadol in low-salinity reverse osmosis concentrates using boron-doped diamond anodes.* Water Res, 2015. **72**: p. 293-304 https://doi.org/10.1016/j.watres.2014.12.021.
389. Deng, Y., et al., *Research on complexation ability, aromaticity, mobility and cytotoxicity of humic-like substances during degradation process by electrochemical oxidation.* Environ Pollut, 2019. **251**: p. 811-820 https://doi.org/10.1016/j.envpol.2019.05.047.
390. Bagastyo, A.Y., et al., *Electrochemical oxidation of reverse osmosis concentrate on boron-doped diamond anodes at circumneutral and acidic pH.* Water Res, 2012. **46**(18): p. 6104-12 https://doi.org/10.1016/j.watres.2012.08.038.
391. Costa, C.R., et al., *Electrochemical oxidation of acid black 210 dye on the boron-doped diamond electrode in the presence of phosphate ions: Effect of current density, pH, and chloride ions.* Electrochimica Acta, 2009. **54**(27): p. 7048-7055 https://doi.org/10.1016/j.electacta.2009.07.027.
392. Yang, F., et al., *An often-overestimated adverse effect of halides in heat/persulfate-based degradation of wastewater contaminants.* Environ Int, 2019. **130**: p. 104918 https://doi.org/10.1016/j.envint.2019.104918.
393. Chen, L.D., et al., *Metal-organic framework-based composite Ni@MOF as Heterogenous catalyst for ethylene trimerization.* Applied Catalysis a-General, 2020. **594**: p. 117457 https://doi.org/10.1016/j.apcata.2020.117457.
394. McDonald, R.I., et al., *Urban growth, climate change, and freshwater availability.* Proc Natl Acad Sci U S A, 2011. **108**(15): p. 6312-7 https://doi.org/10.1073/pnas.1011615108.
395. Oki, T. and S. Kanae, *Global hydrological cycles and world water resources.* Science, 2006. **313**(5790): p. 1068-72 https://doi.org/10.1126/science.1128845.
396. Flörke, M., et al., *Domestic and industrial water uses of the past 60 years as a mirror of socio-economic development: A global simulation study.* Global Environmental Change, 2013. **23**(1): p. 144-156 https://doi.org/10.1016/j.gloenvcha.2012.10.018.
397. Feeley, T.J., et al., *Water: A critical resource in the thermoelectric power industry.* Energy, 2008. **33**(1): p. 1-11 https://doi.org/10.1016/j.energy.2007.08.007.
398. Pan, S.-Y., et al., *Cooling water use in thermoelectric power generation and its associated challenges for addressing water-energy nexus.* Water-Energy Nexus, 2018. **1**(1): p. 26-41 https://doi.org/10.1016/j.wen.2018.04.002.
399. Ahmed, J., Y. Jamal, and M. Shujaatullah, *Recovery of cooling tower blowdown water through reverse osmosis (RO): review of water parameters affecting membrane fouling and pretreatment schemes.* Desalination and Water Treatment, 2020. **189**: p. 9-17 https://doi.org/10.5004/dwt.2020.25639.
400. Wagner, T.V., et al., *Impact of transformation, photodegradation and interaction with glutaraldehyde on the acute toxicity of the biocide DBNPA in cooling tower water.* Environmental Science-Water Research & Technology, 2020. **6**(4): p. 1058-1068 https://doi.org/10.1039/c9ew01018a.
401. Brüninghoff, R., et al., *Electrochemical preparation of defect-engineered titania: Bulk doping versus surface contamination.* Applied Surface Science, 2021. **539**: p. 148136.
402. Scheepers, D., et al., *Asymmetric layer-by-layer polyelectrolyte nanofiltration membranes with tunable retention.* Journal of Polymer Science, 2021. **59**(12): p. 1293-1304 https://doi.org/10.1002/pol.20210166.

403. Scheepers, D., et al., *Influence of charge density and ionic strength on diallyldimethylammonium chloride (DADMAC)-based polyelectrolyte multilayer membrane formation.* Journal of Membrane Science, 2021. **617**: p. 118619 https://doi.org/10.1016/j.memsci.2020.118619.
404. Saha, P., et al., *Advanced oxidation processes for removal of organics from cooling tower blowdown: Efficiencies and evaluation of chlorinated species.* Separation and Purification Technology, 2022. **278**: p. 119537.
405. Bona, A., et al., *Separation of Volatile Fatty Acids from Model Anaerobic Effluents Using Various Membrane Technologies.* Membranes (Basel), 2020. **10**(10): p. 252 https://doi.org/10.3390/membranes10100252.
406. Vymazal, J., *Removal of nutrients in various types of constructed wetlands.* Sci Total Environ, 2007. **380**(1-3): p. 48-65 https://doi.org/10.1016/j.scitotenv.2006.09.014.
407. Vrouwenvelder, J.S., et al., *Phosphate limitation to control biofouling.* Water Res, 2010. **44**(11): p. 3454-66 https://doi.org/10.1016/j.watres.2010.03.026.
408. Li, S., et al., *Impact of reverse nutrient diffusion on membrane biofouling in fertilizer-drawn forward osmosis.* Journal of Membrane Science, 2017. **539**: p. 108-115 https://doi.org/10.1016/j.memsci.2017.05.074.
409. Wiessner, A., et al., *Influence of the redox condition dynamics on the removal efficiency of a laboratory-scale constructed wetland.* Water Res, 2005. **39**(1): p. 248-56 https://doi.org/10.1016/j.watres.2004.08.032.
410. Tong, T.Z., et al., *Mineral scaling in membrane desalination: Mechanisms, mitigation strategies, and feasibility of scaling-resistant membranes.* Journal of Membrane Science, 2019. **579**: p. 52-69 https://doi.org/10.1016/j.memsci.2019.02.049.
411. Al-Amoudi, A.S., *Factors affecting natural organic matter (NOM) and scaling fouling in NF membranes: A review.* Desalination, 2010. **259**(1-3): p. 1-10 https://doi.org/10.1016/j.desal.2010.04.003.
412. Huang, S., et al., *Surface modification of nanofiltration membranes to improve the removal of organic micropollutants: Linking membrane characteristics to solute transmission.* Water Res, 2021. **203**: p. 117520 https://doi.org/10.1016/j.watres.2021.117520.
413. Wang, S.C., et al., *A review of advances in EDCs and PhACs removal by nanofiltration: Mechanisms, impact factors and the influence of organic matter.* Chemical Engineering Journal, 2021. **406**: p. 126722 https://doi.org/10.1016/j.cej.2020.126722.
414. Tang, C.Y., T.H. Chong, and A.G. Fane, *Colloidal interactions and fouling of NF and RO membranes: a review.* Adv Colloid Interface Sci, 2011. **164**(1-2): p. 126-43 https://doi.org/10.1016/j.cis.2010.10.007.
415. Landsman, M.R., D.F. Lawler, and L.E. Katz, *Application of electrodialysis pretreatment to enhance boron removal and reduce fouling during desalination by nanofiltration/reverse osmosis.* Desalination, 2020. **491**: p. 114563 https://doi.org/10.1016/j.desal.2020.114563.
416. Jarusutthirak, C., S. Mattaraj, and R. Jiraratananon, *Influence of inorganic scalants and natural organic matter on nanofiltration membrane fouling.* Journal of Membrane Science, 2007. **287**(1): p. 138-145 https://doi.org/10.1016/j.memsci.2006.10.034.
417. Xu, R., et al., *Influences of temperature on the retention of PPCPs by nanofiltration membranes: Experiments and modeling assessment.* Journal of Membrane Science, 2020. **599**: p. 117817 https://doi.org/10.1016/j.memsci.2020.117817.
418. Liu, Y.L., et al., *Adsorption of pharmaceuticals onto isolated polyamide active layer of NF/RO membranes.* Chemosphere, 2018. **200**: p. 36-47 https://doi.org/10.1016/j.chemosphere.2018.02.088.
419. Kimura, K., et al., *Adsorption of hydrophobic compounds onto NF/RO membranes: an artifact leading to overestimation of rejection.* Journal of Membrane Science, 2003. **221**(1-2): p. 89-101 https://doi.org/10.1016/S0376-7388(03)00248-5.
420. Willet, J., et al., *WaterROUTE: A model for cost optimization of industrial water supply networks when using water resources with varying salinity.* Water Res, 2021. **202**: p. 117390 https://doi.org/10.1016/j.watres.2021.117390.
421. Bianchi, A.B., et al., *Treatment vs. transport: A framework for assessing the trade-offs between on-site desalination and off-site water sourcing for an industrial case study.* Journal of Cleaner Production, 2021. **285**: p. 124901 https://doi.org/10.1016/j.jclepro.2020.124901.
422. Wreyford, J.M., et al., *Modelling framework for desalination treatment train comparison applied to brackish water sources.* Desalination, 2020. **494**: p. 114632 https://doi.org/10.1016/j.desal.2020.114632.
423. Boo, C., et al., *High Performance Nanofiltration Membrane for Effective Removal of Perfluoroalkyl Substances at High Water Recovery.* Environ Sci Technol, 2018. **52**(13): p. 7279-7288 https://doi.org/10.1021/acs.est.8b01040.

424. Douville, H., K. Raghavan, J. Renwick, R. P. Allan, P. A. Arias, M. Barlow, R. Cerezo-Mota, A. Cherchi, T. Y. Gan, J. Gergis, D. Jiang, A. Khan, W. Pokam Mba, D. Rosenfeld, J. Tierney, O. Zolina,, *Water Cycle Changes. In: Climate Change 2021: The Physical Science Basis. Contribution of Working Group I to the Sixth Assessment Report of the Intergovernmental Panel on Climate Change*, in *Chapter 8: Water cycle changes*, V. Masson-Delmotte, P. Zhai, A. Pirani, S. L. Connors, C. Péan, S. Berger, N. Caud, Y. Chen, L. Goldfarb, M. I. Gomis, M. Huang, K. Leitzell, E. Lonnoy, J.B.R. Matthews, T. K. Maycock, T. Waterfield, O. Yelekçi, R. Yu and B. Zhou, Editor. 2021.
425. Abbott, B.W., et al., *Human domination of the global water cycle absent from depictions and perceptions.* Nature Geoscience, 2019. **12**(7): p. 533-+ https://doi.org/10.1038/s41561-019-0374-y.
426. Durack, P.J., *Ocean Salinity and the Global Water Cycle.* Oceanography, 2015. **28**(1): p. 20-31 https://doi.org/10.5670/oceanog.2015.03.
427. UN-Water. "*." Statista, S.I., 24 Feb 2020, . *Annual Industrial Water Demand Worldwide in 2010 and 2050, by Region (in 1,000 Cubic Meters)*. 2020; Available from: https://www-statista-com.ezproxy.library.wur.nl/statistics/1116382/yearly-industrial-water-demand-globally-by-region/.
428. Kansal, S.K. and A. Kumari, *Potential of M. oleifera for the treatment of water and wastewater.* Chem Rev, 2014. **114**(9): p. 4993-5010 https://doi.org/10.1021/cr400093w.
429. Rekhate, C.V. and J.K. Srivastava, *Recent advances in ozone-based advanced oxidation processes for treatment of wastewater- A review.* Chemical Engineering Journal Advances, 2020. **3** https://doi.org/10.1016/j.ceja.2020.100031.
430. von Gunten, U., *Ozonation of drinking water: part II. Disinfection and by-product formation in presence of bromide, iodide or chlorine.* Water Res, 2003. **37**(7): p. 1469-87 https://doi.org/10.1016/S0043-1354(02)00458-X.
431. Sackaria, M. and L. Elango, *Organic micropollutants in groundwater of India-A review.* Water Environ Res, 2020. **92**(4): p. 504-523 https://doi.org/10.1002/wer.1243.
432. Ibrahim, N., S.F.F.S. Zainal, and H.A. Aziz, *Application of UV-Based Advanced Oxidation Processes in Water and Wastewater Treatment*, in *Advanced Oxidation Processes (AOPs) in Water and Wastewater Treatment*. 2019. p. 384-414.
433. Amor, C., et al., *Application of Advanced Oxidation Processes for the Treatment of Recalcitrant Agro-Industrial Wastewater: A Review.* Water, 2019. **11**(2) https://doi.org/10.3390/w11020205.
434. Shestakova, M. and M. Sillanpaa, *Electrode materials used for electrochemical oxidation of organic compounds in wastewater.* Reviews in Environmental Science and Bio-Technology, 2017. **16**(2): p. 223-238 https://doi.org/10.1007/s11157-017-9426-1.
435. Dong, H., W.L. Yu, and M.R. Hoffmann, *Mixed Metal Oxide Electrodes and the Chlorine Evolution Reaction.* Journal of Physical Chemistry C, 2021. **125**(38): p. 20745-20761 https://doi.org/10.1021/acs.jpcc.1c05671.
436. Souza, F.L., et al., *The effect of the sp3/sp2 carbon ratio on the electrochemical oxidation of 2,4-D with p-Si BDD anodes.* Electrochimica Acta, 2016. **187**: p. 119-124 https://doi.org/10.1016/j.electacta.2015.11.031.
437. Wang, Y.H., et al., *Recent advances in electrocatalytic chloride oxidation for chlorine gas production.* Journal of Materials Chemistry A, 2021. **9**(35): p. 18974-18993 https://doi.org/10.1039/d1ta02745j.
438. Czarnetzki, L.R. and L.J.J. Janssen, *Formation of Hypochlorite, Chlorate and Oxygen during Nacl Electrolysis from Alkaline-Solutions at an Ruo2/Tio2 Anode.* Journal of Applied Electrochemistry, 1992. **22**(4): p. 315-324 https://doi.org/Doi 10.1007/Bf01092683.
439. Xiao-Ying Yu, J.R.B., *Hydrogen Peroxide Photolysis in Acidic Aqueous Solutions Containing Chloride Ions. I. Chemical Mechanism.* J. Phys. Chem. A 2003. **107**: p. 1313-1324.
440. Zhou, X.Q., et al., *Nonradical oxidation processes in PMS-based heterogeneous catalytic system: Generation, identification, oxidation characteristics, challenges response and application prospects.* Chemical Engineering Journal, 2021. **410** https://doi.org/10.1016/j.cej.2020.128312.
441. Yang, Y. and J.J. Pignatello, *Participation of the Halogens in Photochemical Reactions in Natural and Treated Waters.* Molecules, 2017. **22**(10) https://doi.org/10.3390/molecules22101684.
442. Oyekunle, D.T., et al., *Impact of chloride ions on activated persulfates based advanced oxidation process (AOPs): A mini review.* Chemosphere, 2021. **280**: p. 130949 https://doi.org/10.1016/j.chemosphere.2021.130949.
443. Chen, D.J., et al., *Photocatalytic degradation of organic pollutants using TiO2-based photocatalysts: A review.* Journal of Cleaner Production, 2020. **268** https://doi.org/10.1016/j.jclepro.2020.121725.
444. Xia, T., et al., *Photocatalytic degradation of organic pollutants by MOFs based materials: A review.* Chinese Chemical Letters, 2021 https://doi.org/10.1016/j.cclet.2021.02.058.
445. Zheng, Z., et al., *Visible-light-driven photoelectrocatalytic activation of chloride by nanoporous MoS2@BiVO4 photoanode for enhanced degradation of bisphenol A.* Chemosphere, 2021. **263**: p. 128279 https://doi.org/10.1016/j.chemosphere.2020.128279.

446. Zhang, Y., et al., *Efficient ammonia removal and toxic chlorate control by using BiVO4/WO3 heterojunction photoanode in a self-driven PEC-chlorine system.* J Hazard Mater, 2021. **402**: p. 123725 https://doi.org/10.1016/j.jhazmat.2020.123725.
447. Marks, R. and K. Doudrick, *Photocatalytic reduction of chlorite in water using bismuth vanadate (BiVO4): effect of irradiance conditions and presence of oxalate on the reactivity and by-product selectivity.* Environmental Science-Water Research & Technology, 2019. **5**(11): p. 2015-2026 https://doi.org/10.1039/c9ew00636b.
448. Thandu, M., C. Comuzzi, and D. Goi, *Phototreatment of Water by Organic Photosensitizers and Comparison with Inorganic Semiconductors.* International Journal of Photoenergy, 2015. **2015**: p. 1-22 https://doi.org/10.1155/2015/521367.
449. Ye, Y., et al., *Homogeneous photosensitized degradation of pharmaceuticals by using red light LED as light source and methylene blue as photosensitizer.* Chemical Engineering Journal, 2017. **316**: p. 872-881 https://doi.org/10.1016/j.cej.2017.02.053.
450. Ye, Y., et al., *Operational parameters affecting MB/Red-light photosensitized degradation of pharmaceuticals.* Journal of Photochemistry and Photobiology a-Chemistry, 2017. **348**: p. 96-101 https://doi.org/10.1016/j.jphotochem.2017.08.013.
451. Guan, S.-H., et al., *A review of photocatalytic materials application on nonylphenol degradation.* Environmental Challenges, 2021. **4** https://doi.org/10.1016/j.envc.2021.100172.
452. Parker, K.M. and W.A. Mitch, *Halogen radicals contribute to photooxidation in coastal and estuarine waters.* Proc Natl Acad Sci U S A, 2016. **113**(21): p. 5868-73 https://doi.org/10.1073/pnas.1602595113.
453. Zhao, J., et al., *The multiple roles of chlorite on the concentrations of radicals and ozone and formation of chlorate during UV photolysis of free chlorine.* Water Res, 2021. **190**: p. 116680 https://doi.org/10.1016/j.watres.2020.116680.
454. Furatian, L., *The Use of 185 nm Radiation for Drinking Water Treatment*, in *Chemical and Biological Engineering*. 2017, THE UNIVERSITY OF BRITISH COLUMBIA.
455. Kishimoto, N., Y. Yamamoto, and S. Nishimura, *Efficacy of vacuum ultraviolet photolysis for bromate and chlorate removal.* Water Science and Technology-Water Supply, 2015. **15**(4): p. 810-816 https://doi.org/10.2166/ws.2015.039.
456. Han, M., M. Jafarikojour, and M. Mohseni, *The impact of chloride and chlorine radical on nitrite formation during vacuum UV photolysis of water.* Sci Total Environ, 2021. **760**: p. 143325 https://doi.org/10.1016/j.scitotenv.2020.143325.
457. Levanov, A.V., et al., *Photochemical oxidation of chloride ion by ozone in acid aqueous solution.* Environ Sci Pollut Res Int, 2015. **22**(21): p. 16554-69 https://doi.org/10.1007/s11356-015-4832-9.
458. Levanov, A.V., et al., *Kinetics of chlorate formation during ozonation of aqueous chloride solutions.* Chemosphere, 2019. **229**: p. 68-76 https://doi.org/10.1016/j.chemosphere.2019.04.105.
459. Levanov, A.V. and O.Y. Isaikina, *Mechanism and Kinetic Model of Chlorate and Perchlorate Formation during Ozonation of Aqueous Chloride Solutions.* Industrial & Engineering Chemistry Research, 2020. **59**(32): p. 14278-14287 https://doi.org/10.1021/acs.iecr.0c02770.
460. Rao, B., et al., *Perchlorate formation by ozone oxidation of aqueous chlorine/oxy-chlorine species: role of ClxOy radicals.* Environ Sci Technol, 2010. **44**(8): p. 2961-7 https://doi.org/10.1021/es903065f.
461. Janssen, L.J.J. and P.D.L. Vanderheyden, *Mechanism of Anodic-Oxidation of Chlorate to Perchlorate on Platinum-Electrodes.* Journal of Applied Electrochemistry, 1995. **25**(2): p. 126-136 https://doi.org/Doi 10.1007/Bf00248169.
462. Zhu, Y., et al., *A critical review on metal complexes removal from water using methods based on Fenton-like reactions: Analysis and comparison of methods and mechanisms.* J Hazard Mater, 2021. **414**: p. 125517 https://doi.org/10.1016/j.jhazmat.2021.125517.
463. Liu, Y.X., S. Shi, and Y. Wang, *Removal of pollutants from gas streams using Fenton (-like)-based oxidation systems: A review.* Journal of Hazardous Materials, 2021. **416** https://doi.org/10.1016/j.jhazmat.2021.125927.
464. O'Dowd, K. and S.C. Pillai, *Photo-Fenton disinfection at near neutral pH: Process, parameter optimization and recent advances.* Journal of Environmental Chemical Engineering, 2020. **8**(5) https://doi.org/10.1016/j.jece.2020.104063.
465. Mousset, E., et al., *Effect of homogeneous Fenton combined with electron transfer on the fate of inorganic chlorinated species in synthetic and reclaimed municipal wastewater.* Electrochimica Acta, 2020. **334** https://doi.org/10.1016/j.electacta.2019.135608.
466. Kishimoto, N., et al., *Effect of oxidation-reduction potential on an electrochemical Fenton-type process.* Chemical Engineering Journal, 2015. **260**: p. 590-595 https://doi.org/10.1016/j.cej.2014.09.056.

467. Ammar, H.B., *Sono-Fenton process for metronidazole degradation in aqueous solution: Effect of acoustic cavitation and peroxydisulfate anion.* Ultrason Sonochem, 2016. **33**: p. 164-169 https://doi.org/10.1016/j.ultsonch.2016.04.035.
468. Babuponnusami, A. and K. Muthukumar, *A review on Fenton and improvements to the Fenton process for wastewater treatment.* Journal of Environmental Chemical Engineering, 2014. **2**(1): p. 557-572 https://doi.org/10.1016/j.jece.2013.10.011.
469. Capodaglio, A.G., *Critical Perspective on Advanced Treatment Processes for Water and Wastewater: AOPs, ARPs, and AORPs.* Applied Sciences-Basel, 2020. **10**(13) https://doi.org/10.3390/app10134549.
470. Mishra, O.P., et al., *Gamma-irradiation produces active chlorine species (ACS) in physiological solutions: Secoisolariciresinol diglucoside (SDG) scavenges ACS - A novel mechanism of DNA radioprotection.* Biochim Biophys Acta, 2016. **1860**(9): p. 1884-97 https://doi.org/10.1016/j.bbagen.2016.05.037.
471. Jiang, B., et al., *Review on electrical discharge plasma technology for wastewater remediation.* Chemical Engineering Journal, 2014. **236**: p. 348-368 https://doi.org/10.1016/j.cej.2013.09.090.
472. Wende, K., et al., *Identification of the biologically active liquid chemistry induced by a nonthermal atmospheric pressure plasma jet.* Biointerphases, 2015. **10**(2): p. 029518 https://doi.org/10.1116/1.4919710.
473. Kondeti, V., et al., *Long-lived and short-lived reactive species produced by a cold atmospheric pressure plasma jet for the inactivation of Pseudomonas aeruginosa and Staphylococcus aureus.* Free Radic Biol Med, 2018. **124**: p. 275-287 https://doi.org/10.1016/j.freeradbiomed.2018.05.083.
474. Haghighat, G., et al., *The role of chloride ions in plasma-activated water treatment processes.* Environmental Science-Water Research & Technology, 2017. **3**(1): p. 156-168 https://doi.org/10.1039/c6ew00308g.
475. Jirásek, V. and P. Lukeš, *Formation of reactive chlorine species in saline solution treated by non-equilibrium atmospheric pressure He/O2 plasma jet*. Plasma Sources Science and Technology, 2019. **28**(3) https://doi.org/10.1088/1361-6595/ab0930.
476. Nikolenko, N.V., et al., *Optimization of Plasma Treatment of Aqueous Sodium Chloride Solutions.* High Energy Chemistry, 2017. **51**(2): p. 122-127 https://doi.org/10.1134/S0018143917020096.
477. Nikolenko, N.V., et al., *Chemical transformations in sodium chloride aqueous solutions under the action of low-temperature contact glow-discharge plasma.* High Energy Chemistry, 2013. **47**(5): p. 262-267 https://doi.org/10.1134/S001814391305007x.
478. Martinez-Pabello, P.U., et al., *Production of nitrates and perchlorates by laser ablation of sodium chloride in simulated Martian atmospheres. Implications for their formation by electric discharges in dust devils.* Life Sci Space Res (Amst), 2019. **22**: p. 125-136 https://doi.org/10.1016/j.lssr.2019.02.007.
479. Lakhian, V. and S.E. Dickson-Anderson, *Reduction of bromate and chlorate contaminants in water using aqueous phase corona discharge*. Chemosphere, 2020. **255**: p. 126864 https://doi.org/10.1016/j.chemosphere.2020.126864.
480. Dehane, A., S. Merouani, and O. Hamdaoui, *Effect of carbon tetrachloride (CCl4) sonochemistry on the size of active bubbles for the production of reactive oxygen and chlorine species in acoustic cavitation field.* Chemical Engineering Journal, 2021. **426** https://doi.org/10.1016/j.cej.2021.130251.
481. Deborde, M. and U. von Gunten, *Reactions of chlorine with inorganic and organic compounds during water treatment-Kinetics and mechanisms: a critical review.* Water Res, 2008. **42**(1-2): p. 13-51 https://doi.org/10.1016/j.watres.2007.07.025.
482. Prutz, W.A., *Interactions of hypochlorous acid with pyrimidine nucleotides, and secondary reactions of chlorinated pyrimidines with GSH, NADH, and other substrates.* Arch Biochem Biophys, 1998. **349**(1): p. 183-91 https://doi.org/10.1006/abbi.1997.0440.
483. Folkes, L.K., L.P. Candeias, and P. Wardman, *Kinetics and mechanisms of hypochlorous acid reactions.* Arch Biochem Biophys, 1995. **323**(1): p. 120-6 https://doi.org/10.1006/abbi.1995.0017.
484. Pattison, D.I. and M.J. Davies, *Absolute rate constants for the reaction of hypochlorous acid with protein side chains and peptide bonds.* Chem Res Toxicol, 2001. **14**(10): p. 1453-64 https://doi.org/10.1021/tx0155451.
485. Reckhow, D.A., P.C. Singer, and R.L. Malcolm, *Chlorination of humic materials: byproduct formation and chemical interpretations.* Environmental science & technology, 1990. **24**(11): p. 1655-1664.
486. Council, N.R., *Drinking Water and Health, Safe Drinking Water Committee, Board on Toxicology and Environmental Health Hazards, Assembly of Life Sciences*. Vol. Volume 2. 1980, Washington, DC:: The National Academies Press.

487. Council, N.R., *Drinking Water and Health, Volume 7: Disinfectants and Disinfectant By-Products.*, in *Drinking Water and Health: Disinfectants and Disinfectant By-Products: Volume 7*. 1987, The National Academies Press.: Washington (DC).
488. Armstrong, D.A., et al., *Standard electrode potentials involving radicals in aqueous solution: inorganic radicals (IUPAC Technical Report).* Pure and Applied Chemistry, 2015. **87**(11-12): p. 1139-1150 https://doi.org/10.1515/pac-2014-0502.
489. Patil, R.S., V.A. Juvekar, and V.M. Naik, *Oxidation of Chloride Ion on Platinum Electrode: Dynamics of Electrode Passivation and its Effect on Oxidation Kinetics.* Industrial & Engineering Chemistry Research, 2011. **50**(23): p. 12946-12959 https://doi.org/10.1021/ie200663a.
490. Wang, W.L., et al., *Degradation of natural organic matter by UV/chlorine oxidation: Molecular decomposition, formation of oxidation byproducts and cytotoxicity.* Water Res, 2017. **124**: p. 251-258 https://doi.org/10.1016/j.watres.2017.07.029.
491. Pati, S.G. and W.A. Arnold, *Reaction rates and product formation during advanced oxidation of ionic liquid cations by UV/peroxide, UV/persulfate, and UV/chlorine.* Environmental Science-Water Research & Technology, 2018. **4**(9): p. 1310-1320 https://doi.org/10.1039/c8ew00254a.
492. Nicoson, J.S., et al., *Kinetics and mechanisms of the ozone/bromite and ozone/chlorite reactions.* Inorg Chem, 2002. **41**(11): p. 2975-80 https://doi.org/10.1021/ic011301s.
493. Siddiqui, M.S., *Chlorine-ozone interactions: Formation of chlorate.* Water Research, 1996. **30**(9): p. 2160-2170 https://doi.org/Doi 10.1016/0043-1354(96)00071-1.
494. Saylor, G.L. and M.J. Kupferle, *The impact of chloride or bromide ions on the advanced oxidation of atrazine by combined electrolysis and ozonation.* Journal of Environmental Chemical Engineering, 2019. **7**(3) https://doi.org/10.1016/j.jece.2019.103105.
495. Hubler, D.K., et al., *Understanding Chlorite and Chlorate Formation Associated with Hypochlorite Generation at Boron Doped Diamond Film Anodes.* Journal of the Electrochemical Society, 2014. **161**(12): p. E182-E189 https://doi.org/10.1149/2.1001412jes.
496. Kang, N., et al., *Perchlorate production by ozone oxidation of chloride in aqueous and dry systems.* Sci Total Environ, 2008. **405**(1-3): p. 301-9 https://doi.org/10.1016/j.scitotenv.2008.07.010.
497. Munichandraiah, N. and S. Sathyanarayana, *Kinetics and Mechanism of Anodic-Oxidation of Chlorate Ion to Perchlorate Ion on Lead Dioxide Electrodes.* Journal of Applied Electrochemistry, 1987. **17**(1): p. 33-48 https://doi.org/Doi 10.1007/Bf01009129.
498. Jung, Y.J., et al., *An investigation of the formation of chlorate and perchlorate during electrolysis using Pt/Ti electrodes: the effects of pH and reactive oxygen species and the results of kinetic studies.* Water Res, 2010. **44**(18): p. 5345-55 https://doi.org/10.1016/j.watres.2010.06.029.
499. *Word Healt Organization; Chlorine Dioxide, Chlorite and Chlorate in Drinking-water https://www.who.int/water_sanitation_health/dwq/chemicals/chlorateandchlorite0505.pdf (accessed Octabor 18, 2021).* 2005.
500. *Word Healt Organization;Perchlorate in Drinking-water https://www.who.int/water_sanitation_health/dwq/chemicals/chlorateandchlorite0505.pdf (accessed Octabor 18, 2021).* 2016.
501. Canonica, S., *Oxidation of aquatic organic contaminants induced by excited triplet states.* Chimia, 2007. **61**(10): p. 641-644 https://doi.org/10.2533/chimia.2007.641.
502. Chuang, Y.H., K.M. Parker, and W.A. Mitch, *Development of Predictive Models for the Degradation of Halogenated Disinfection Byproducts during the UV/H2O2 Advanced Oxidation Process.* Environ Sci Technol, 2016. **50**(20): p. 11209-11217 https://doi.org/10.1021/acs.est.6b03560.
503. Kan, E., et al., *Decomposition of aqueous chlorinated contaminants by UV irradiation with H2O2.* Frontiers of Environmental Science & Engineering, 2015. **9**(3): p. 429-435 https://doi.org/10.1007/s11783-014-0677-6.
504. Pati, S.G. and W.A. Arnold, *Reaction rates and product formation during advanced oxidation of ionic liquid cations by UV/peroxide, UV/persulfate, and UV/chlorine.* Environmental Science: Water Research & Technology, 2018. **4**(9): p. 1310-1320 https://doi.org/10.1039/c8ew00254a.
505. Kang, N., T.A. Anderson, and W.A. Jackson, *Photochemical formation of perchlorate from aqueous oxychlorine anions.* Anal Chim Acta, 2006. **567**(1): p. 48-56 https://doi.org/10.1016/j.aca.2006.01.085.
506. Pan, Y., et al., *Degradation of metronidazole by UV/chlorine treatment: Efficiency, mechanism, pathways and DBPs formation.* Chemosphere, 2019. **224**: p. 228-236 https://doi.org/10.1016/j.chemosphere.2019.02.081.
507. Huang, N., et al., *UV/chlorine as an advanced oxidation process for the degradation of benzalkonium chloride: Synergistic effect, transformation products and toxicity evaluation.* Water Res, 2017. **114**: p. 246-253 https://doi.org/10.1016/j.watres.2017.02.015.

508. Isidro, J., et al., *How to avoid the formation of hazardous chlorates and perchlorates during electro-disinfection with diamond anodes?* J Environ Manage, 2020. **265**: p. 110566 https://doi.org/10.1016/j.jenvman.2020.110566.
509. Yu, H., et al., *Degradation of diclofenac by advanced oxidation and reduction processes: kinetic studies, degradation pathways and toxicity assessments.* Water Res, 2013. **47**(5): p. 1909-18 https://doi.org/10.1016/j.watres.2013.01.016.
510. Velikova, V., I. Yordanov, and A. Edreva, *Oxidative stress and some antioxidant systems in acid rain-treated bean plants - Protective role of exogenous polyamines.* Plant Science, 2000. **151**(1): p. 59-66 https://doi.org/Doi 10.1016/S0168-9452(99)00197-1.
511. Park, K.Y., et al., *Natural organic matter removal from algal-rich water and disinfection by-products formation potential reduction by powdered activated carbon adsorption.* J Environ Manage, 2019. **235**: p. 310-318 https://doi.org/10.1016/j.jenvman.2019.01.080.
512. Pucher, M., et al., *staRdom: Versatile Software for Analyzing Spectroscopic Data of Dissolved Organic Matter in R.* Water, 2019. **11**(11) https://doi.org/10.3390/w11112366.
513. Chen, W., et al., *Molecular-level comparison study on microwave irradiation-activated persulfate and hydrogen peroxide processes for the treatment of refractory organics in mature landfill leachate.* J Hazard Mater, 2020. **397**: p. 122785 https://doi.org/10.1016/j.jhazmat.2020.122785.
514. Chen, W., et al., *Fluorescence excitation-emission matrix regional integration to quantify spectra for dissolved organic matter.* Environ Sci Technol, 2003. **37**(24): p. 5701-10 https://doi.org/10.1021/es034354c.
515. Zhao, Y., et al., *Synergistic oxidation - filtration process analysis of catalytic CuFe2O4 - Tailored ceramic membrane filtration via peroxymonosulfate activation for humic acid treatment.* Water Res, 2020. **171**: p. 115387 https://doi.org/10.1016/j.watres.2019.115387.
516. Ajao, V., et al., *Regeneration and reuse of microbial extracellular polymers immobilised on a bed column for heavy metal recovery.* Water Res, 2020. **171**: p. 115472 https://doi.org/10.1016/j.watres.2020.115472.
517. Li, M., et al., *VUV/UV/Chlorine as an Enhanced Advanced Oxidation Process for Organic Pollutant Removal from Water: Assessment with a Novel Mini-Fluidic VUV/UV Photoreaction System (MVPS).* Environ Sci Technol, 2016. **50**(11): p. 5849-56 https://doi.org/10.1021/acs.est.6b00133.
518. Li, M., et al., *VUV/UV/Chlorine as an Enhanced Advanced Oxidation Process for Organic Pollutant Removal from Water: Assessment with a Novel Mini-Fluidic VUV/UV Photoreaction System (MVPS).* Environmental Science & Technology, 2016. **50**(11): p. 5849-5856 https://doi.org/10.1021/acs.est.6b00133.

Thesis Summary || *Thesis samenvatting*

Thesis Summary

Freshwater is an integral part of the ecosystem that supports human life, agricultural and economic activities. However, freshwater is becoming scarce due to increasing population, economic activity, and climate change. Contamination of freshwater sources by emerging organic (micro)pollutants creates challenges for the ecosystem and human health. The development of industrial activity is accelerating freshwater consumption, and thus, it is essential to close the water cycle by reusing treated wastewater. Cooling towers in the industry are among the largest freshwater consumers and discharge a large volume of saline wastewater, commonly known as cooling tower blowdown water (CTBD). The reuse of CTBD would reduce freshwater consumption and enhance the eco-efficiency and sustainability of industries. However, CTBD contains a complex mixture of salts and organic compounds. The research project described in this thesis was designed to study the advanced oxidation processes (AOPs) to remove the organic compounds (OCs) in this saline condition. In this research, four different AOPs have been studied: electrochemical oxidation, photocatalytic degradation, heat-activated persulfate oxidation, and UVC/vacuum UV process. Particular focus was given to the effectiveness of AOPs in removing the OCs and the influence of chloride ions on the AOPs. The thesis has eight chapters, including an introduction, six experiment result chapters, and a general discussion.

A general introduction about freshwater consumption and the necessity of closing the water cycle to achieve sustainable development goals is described in **Chapter 1**. The possibilities of reusing cooling tower blowdown water within the context of the Water Nexus program is also elaborated in this chapter. A comprehensive overview of cooling tower water quality and quantity is given in this chapter. In addition, current cooling tower water treatment technology is discussed, and the necessity of advanced oxidation processes (AOPs) treatment is also justified. The working principle and the influence of operating parameters on electrochemical oxidation, photocatalytic degradation, heat-activated persulfate oxidation, and UVC/vacuum UV process are discussed. Based on this information the overall objective of this thesis is explained, and the thesis outline is given at the end of **chapter 1**.

The electrochemical oxidation (EO) possibilities and limitations to remove OCs in CTBD are highlighted in **Chapter 2**. EO experiments were carried out with boron-doped diamond (BDD) and Ti/RuO_2 mixed-metal oxide(MMO) anodes in an undivided flat cell in a batch recirculation reaction system. The role of the operational parameters including applied current density (*j*), initial pH, hydrodynamic conditions as recirculation flow rate, and supporting electrolytes were studied. Experimental results show that chemical oxygen demand (COD) and total organic carbon (TOC) removal were almost two times better with the BDD anode than with the MMO. COD and TOC removal was increased with the increase of the *j*-value. However, other operational parameters had a minimal influence on the process performance. Liquid chromatography-organic carbon detection analysis showed that CTBD mainly consists of humic substances. EO with BDD anode at 8.7 mA/cm^2 and neutral pH could mineralize 35% of the humic substances. The rest of the humic substances was partially oxidized to building blocks and low molecular weight compounds. Because of this partial oxidation, COD removal was higher than the TOC removal. A significant amount of chlorinated by-products were formed, including free chlorine, chlorate, perchlorate, and chlorinated organic (AOX). These chlorinated species caused a toxic effect on *Vibrio fischeri* bacteria. Therefore, electrochemical oxidation could be a potential CTBD treatment technique concerning the removal of the OC; however, toxic by-product formation should be considered during application.

Chapters 3 and 4 are focused on overcoming the limitations, improving process efficiency, and minimizing toxic by-product formation during EO of saline wastewater like CTBD.

A hybrid treatment system consisting of vertical flow constructed wetlands (VFCW) and EO with boron-doped diamond (BDD) or mixed metal oxides (MMO) electrodes are studied for the removal of OCs in CTBD in **Chapter 3.** Two treatment scenarios, Scenario 1- VFCW treatment followed by EO (VFCW-EO) and Scenario 2- EO followed by the VFCW treatment (EO-VFCW), are compared. The constructed wetlands were planted with *Phragmites australis* and were operated in batch mode with a three-day retention time. EO of CTBD and VFCW effluent were conducted galvanostatically with a current density of 5.5 mA/cm^2 in the EO-BDD cell and 8.7 mA/cm^2 in the EO-MMO cell for three hours at neutral pH.

The VFCW-EO system (Scenario 1) removed a higher amount of COD, TOC, and benzotriazole than the EO-VFCW (Scenario 2). Again, BDD anode outperforms the MMO, which was similar to chapter 2. VFCW contributes more than half of the OCs removal in the combined system, including 90% BTA removal. However, the subsequent EO resulted in several chlorinated by-products, including chlorinated organic compounds (AOX), chlorate and perchlorate .

In the EO-VFCW system (Scenario 2), OCs removal in the EO system was similar to the standalone EO treatment reported in **Chapter 2**. The subsequent VFCW could not enhance the OCs removal because of the toxic influence of electrochemically treated effluent. The plants' growth and biological activity of the wetland were severely hindered due to the high toxicity. On a positive note, the subsequent VFCW could be able to remove the toxic by-products. Thus, it could be concluded that VFCW could improve the overall OCs and toxic by-products removal, but harmful by-product formation still needs to be dealt with.

The effect of electrolyte composition on EO performance in terms of removal efficiency and toxic by-products formation is described in **Chapter 4**. Benzotriazole (BTA, $C_6H_5N_3$) is used in this study since it is found in the cooling tower water and water bodies in a high concentration. Initially, the influence of electrolyte composition as different Na_2SO_4:$NaNO_3$ ratios was investigated to determine their influence on active sulfate species ($SO_4^{\bullet-}$ and $S_2O_8^{2-}$) formation and formation pathway. Results show that higher Na_2SO_4:$NaNO_3$ ratios promoted the active sulfate species formation via hydroxyl radical-mediated pathway. This pathway was less dominating in electrolytes that only contain sulfate or lower Na_2SO_4:$NaNO_3$ ratios. Excess chemisorption of SO_4^{2-} on the BDD anode hinders the hydroxyl radical formation leading to less active sulfate formation in electrolytes that contain only sulfate. Similar to active sulfate species formation, the EO of benzotriazole was also faster in high Na_2SO_4:$NaNO_3$ or Na_2SO_4:NaCl ratios. Sulfate enriched electrolytes also promoted benzotriazole mineralization, energy consumption, and more importantly, lowered the chlorinated organic compound formation. Liquid chromatography-mass spectrometry (LC-MS) analysis revealed that none of the chlorinated organic compounds were found in the 10:1 Na_2SO_4:NaCl ratio, which were found in other Na_2SO_4:NaCl ratios. Unfortunately, chlorate and perchlorate formation was unavoidable in any Na_2SO_4:NaCl ratios and became more dominating in the 10:1 ratio. Based on the research outcome, it was concluded that

sulfate-enriched electrolytes could be helpful for the electrochemical degradation of organic compounds concerning higher degradation efficiency, low energy consumption, and less chlorinated organic-by-product formation. Nanofiltration could selectively separate the sulfate from waste and produce sulfate-enriched conditions. Thus it could be interesting to combine nanofiltration with electrochemical oxidation to overcome the shortcomings of the EO technique.

Chapters 5 and **6** are focused on alternative AOPs techniques to remove the OCs in presence of chloride. **Chapter 4** indicated that sulfate radical-based AOPs also able to degrade OCs. In addition, **chapters 2, 3, and 4** showed that chlorate and perchlorate formation was unavoidable in EO, especially with BDD anode at higher applied current. Thus, photocatalytic degradation, heat-activated persulfate oxidation, and UVC/vacuum UV AOPs are studied in **chapters 5 and 6** in the presence of chloride ions to elaborate the organic compounds oxidation mechanism and chlorinated by-product formation potential.

Effects of chloride and pH on kinetics, pathways, and chlorinated by-product formation during heat-activated peroxydisulfate and peroxymonosulfate mediated degradation of benzotriazole is studied in **Chapter 5.** Both heat-activated peroxydisulfate and peroxymonosulfate were able to degrade the benzotriazole in the presence and absence of chloride. Peroxydisulfate meditated degradation was faster than peroxymonosulfate meditated degradation in the absence of chloride. It was the opposite in the presence of chloride. Because of radical scavenging by the chloride ions, benzotriazole degradation in peroxydisulfate meditated AOPs was slower. In contrast, the interaction of peroxymonosulfate with chloride ions yielded free chlorine, which promoted faster benzotriazole degradation. pH significantly influenced the peroxymonosulfate mediated AOPs, which was less prominent in peroxydisulfate meditated degradation in both presence and absence of chloride. LC-MS analysis and data analysis with compound discovery software revealed forty-two transformation products (TPs) formed during benzotriazole degradation. This finding helped to elucidate the benzotriazole degradation mechanisms in the presence and absence of chloride. Polymerization, hydroxylation, benzene ring-opening, and carboxylic acid formation were considered the main degradation mechanisms in the absence of chloride. In contrast, chlorination, triazole ring-opening, and nitration were found as additional degradation mechanisms in the presence of chloride. More chlorinated transformation products were detected in

peroxymonosulfate mediated oxidation. Thus the AOX formation and toxicity on *Vibrio fischeri* bacteria were more for the peroxymonosulfate mediated oxidation. Additionally, chlorate was also found in this process, which was undetected in the peroxydisulfate meditated process. This finding indicates that chlorinated by-products formation was influenced by the active chlorine species formed in the system. Free chlorine was the primary precursor of these chlorinated by-products formation. Thus, free chlorine formation should be avoided to minimize the formation of chlorinated by-products, which was achieved in peroxydisulfate meditated oxidation.

Organic compound removal efficiency and chlorinated by-product formation potential in different advanced oxidation processes are compared in **Chapter 6**. The study includes electrochemical oxidation (EO), photocatalytic degradation (PCD), heat-activated peroxydisulfate oxidation, and UVC/vacuum UV (UVC/VUV) processes. Heat-activated peroxydisulfate oxidation could reach more than 95% OCs mineralization from CTBD after 5 h treatment. In comparison, EO, PCD, and UVC/VUV processes could mineralize 50 to 60%. Detailed humic substance analysis elucidated that peroxydisulfate oxidation managed to oxidize the humic substance completely. Still, other processes partly oxidized the humic substance to low molecular substances like building blocks and acids. Interestingly, fluorescence excitation-emission matrices (FEEM) revealed that total fluorescence intensity was removed during EO, whereas the TOC removal was only 50%. Because of partial oxidation and the chlorination of the organic carbon, they lost their fluorescence property. This chlorination was justified by the formation of free chlorine in the EO process. Chlorinated by-products were undetected in PCD, heat-activated peroxydisulfate oxidation, and UVC/VUV processes. These processes also had limited free chlorination formation. Thus, concerning effectiveness and minimum chlorinated by-product formation potential, AOPs could be arranged as heat-activated peroxydisulfate > PCD, UVC/VUV processes> EO for saline water treatment to remove OCs, including humic substances.

A complete technology train to treat the CTBD to reuse was described in **Chapter 7**. Two technology trains were tested. The first one includes wetland, nanofiltration, reverse osmosis, and EO of the nanofiltration concentrate. The second train includes nanofiltration, reverse osmosis, and EO of the nanofiltration concentrate. Technology train performance was evaluated based on salts removal,

benzotriazole removal, TOC removal, nanofiltration flux, and chlorinated by-products formation in the EO. Overall, both the treatment trains were able to reach the water quality required to reuse. In the first train, wetland removed nitrate, ortho-phosphate, and benzotriazole. However, wetland produced more inorganic carbon, which led to higher total carbon concentration in the nanofiltration permeate and increasing fouling in the subsequent nanofiltration system. Divalent ions were removed in the nanofiltration step, but monovalent ions passed through the membrane. The polishing reverse osmosis step removed the rest of the salts and produced desired water quality. The second train performed almost the same as the first train, except benzotriazole passed through the nanofiltration step and was removed in the reverse osmosis step. EO of the nanofiltration concentrated from both trains shows almost the same OCs removal and current efficiency. Compared with the EO of raw CTBD, the EO of nanofiltration concentrated showed better and faster removal efficiency and less chlorinated organic by-product formation. The nanofiltration concentrated had a higher SO_4^{2-}:Cl^- ratio compared with the raw CTBD. Thus the EO performed better for the concentrate. But chlorate and perchlorate formation potential were higher with concentrate, similar to the outcome obtained in **Chapter 4**. The outcome of **Chapter 7** indicated that further research is required to improve the train.

Three main issues are discussed in the general discussion chapter (**Chapter 8)**. **Firstly,** The main outcomes of the research conducted in this thesis are summarized. Overall, research shows that advanced oxidation processes (AOPs) could remove the organic compound from the cooling tower blowdown. However, chlorinated by-production limits the application of electrochemical oxidation. Alternatively, heat-activated peroxydisulfate, photocatalytic degradation, and UVC/VUV processes could effectively remove the organic compound without chlorinated by-product formation. Heat-activated peroxydisulfate could be the most interesting to treat the cooling tower blowdown from an application point of view. Process waste heat from the industry could be used to activate the process and reduce energy consumption. **Secondly,** an overview of the scope of application of AOPs in real water is given**.** AOPs could be integrated into industrial, municipal, and drinking water treatment trains. AOPs could serve as a pre-treatment to break down the non-biodegradable organic compounds or as a barrier to eliminate micropollutants and pathogens during post-treatment. **Finally,** a detailed study of chloride chemistry in all state-of-

the-art AOPs is summarized. Chloride interactions in nine AOPs processes, including four studied in this thesis, are elaborated. It shows that chloride ions had a different interaction with oxidants sources and activators involved in the AOPs. Also, chloride showed specific interaction with the reactive oxidating species (e. g, hydroxyl, sulfate radicals, or ozone atoms) produced during the oxidation process. All those interactions yield different reactive chlorine species. An overview of reactivity of the organic compounds with reactive chloride species is elaborated based on literature. The role of reactive chlorine species in chlorate and perchlorate formation is also discussed. Based on this information, AOPs are grouped into three categories according to their chlorinated by-product formation tendency. This information will help the stakeholders select safe AOPs to remove organic compound saline (waste)water.

Thesis samenvatting

Zoetwater is een integraal onderdeel van het ecosysteem: het ondersteunt menselijk leven, landbouw en economische activiteiten. Toch wordt zoetwater steeds schaarser door toenemende populaties, economische activiteiten en klimaatverandering. Vervuiling van zoetwaterbronnen door opkomende (micro)verontreinigingen resulteert in uitdagingen voor ecosystemen en onze gezondheid. De ontwikkeling van industrie versnelt de consumptie van zoetwater. Daarom is het van vitaal belang om de watercyclus te sluiten door hergebruik van behandeld afvalwater. Industriële koeltorens zijn een van de grootste zoetwater verbruikers en lozen grote volumes zout afvalwater, beter bekend als koeltoren spuiwater (KSW). Het hergebruik van KSW kan zoetwater verbruik verminderen en de eco-efficiëntie en duurzaamheid van industrieën verbeteren. Dit hergebruik is alleen niet eenvoudig, want KSW bevat een complex mengsel van zouten en organische stoffen. Het onderzoeksproject dat in deze thesis beschreven wordt is ontworpen geavanceerde oxidatieprocessen (GOP) te onderzoeken die organische stoffen (OS) kunnen verwijderen in de zoute omstandigheden. In dit onderzoek zijn vier verschillende GOPs bestudeerd: elektrochemische oxidatie, fotokatalytische degradatie, hitte geactiveerde persulfaat oxidatie en het UVC/vacuüm UV-proces. De nadruk ligt op de effectiviteit van GOPs om de OS te verwijderen en de invloed van chloride ionen op de GOPs. De thesis heeft acht hoofdstukken, waaronder een introductie, zes experimentele hoofdstukken en een algemene discussie.

Een algemene introductie over zoetwater verbruik en de noodzaak om de watercyclus te sluiten om de duurzame ontwikkelingsdoelen te kunnen halen wordt in **Hoofdstuk 1** behandeld. De mogelijkheden voor KSW hergebruik binnen het Water Nexus programma wordt ook behandeld in dit hoofdstuk. Een compleet overzicht van KSW kwaliteit en kwantiteit wordt gegeven in dit hoofdstuk. Daarnaast worden de huidige koeltorenwaterbehandelingsprocessen besproken en de noodzaak van GOPs wordt ook aangetoond. Het principe en de invloed van proces parameters op elektrochemische oxidatie, fotokatalytische degradatie, hitte geactiveerde persulfaat oxidatie en het UVC/vacuüm UV proces worden bediscussieerd. Op basis van deze informatie wordt aan het eind van **Hoofdstuk 1** het doel van deze thesis uitgelegd en het overzicht van de thesis gegeven.

De mogelijkheden en limitaties om met elektrochemische oxidatie (EO) OS uit KSW te verwijderen worden belicht in **Hoofdstuk 2**. EO-experimenten werden uitgevoerd met boron-doped diamond (BDD) en Ti/RuO_2 mixed metal oxide (MMO) anodes in een niet gedeelde platte cel in een batch recirculatie systeem. De rol van operationele parameters zoals toegepaste lading dichtheid (*j*), begin pH, hydrodynamische condities zoals recirculatie stroomsnelheid en ondersteunende elektrolyten zijn bestudeerd. Experimentele resultaten laten zien dat chemisch zuurstofverbruik (CZV) en totaal organisch koolstof (TOK) verwijdering bijna twee keer beter waren met de BDD-anode dan met de MMO. COD en TOK-verwijdering nam toe met de toename van de *j*-waarde. De andere operationele parameters hadden minimale invloed op de efficiëntie van het proces. Vloeistofchromatografie gekoppeld aan een organische koolstof meter liet zien dat CTBD vooral bestaat uit humusachtige stoffen. EO met een BDD-anode bij 8.7 mA/cm^2 en neutrale pH was in staat om 35% van de humusachtige stoffen te mineraliseren. De rest van de humusachtige stoffen werden gedeeltelijk geoxideerd tot bouwstoffen en stoffen met lage molecuul massa. Door deze gedeeltelijke oxidatie was de COD-verwijdering hoger dan de TOS-verwijdering. Een significante hoeveelheid gechloreerde bijproducten werden gevormd waaronder elementair chloor, chloraat, perchloraat en gechloreerde organische stoffen (GOS). Deze gechloreerde stoffen hebben een toxisch effect op *Vibrio fischeri* bacteriën. Hierom is elektrochemische oxidatie een potentiële CTBD-behandelingstechniek voor de verwijdering van OS, maar moet de vorming van toxische bijproducten ook in acht worden genomen bij toepassing van deze techniek.

Hoofdstukken 3 en 4 focussen op hoe tijdens EO we de limitaties kunnen minimaliseren, proces efficiëntie kunnen verbeteren en de vorming van toxische bijproducten kunnen minimaliseren tijdens de behandeling van zout afvalwater zoals CTBD.

Een hybride zuiveringssysteem bestaand uit verticaal stromend wetland (VSW) en EO met BDD of MMO-elektrodes worden bestudeerd voor de verwijdering van OS in CTBD in **Hoofdstuk 3**. Twee zuiverings- scenario's, Scenario 1- VFCW-behandeling gevolgd door EO (VFCW-EO) en Scenario 2- EO gevolgd door de VFCW-behandeling (EO-VFCW) zijn vergeleken. De wetlands waren beplant met *Phragmites australis* en werden in batch modus gebruikt met een retentietijd van drie dagen. EO van CTBD en VFCW-effluent werden galvanostatisch uitgevoerd

met een stroomdichtheid van 5.5 mA/cm^2 in de EO-BDD-cel en 8.7 mA/cm^2 in de EO-MMO cel voor 3 uur bij neutrale pH.

Het VFCW-EO-systeem (Scenario 1) verwijderde meer COD, TOS en benzotriazole dan de EO-VFCW (Scenario 2). Net als in **Hoofdstuk 2** presteerden BDD-anodes beter dan de MMO. VFCW draagt bij aan meer dan de helft van de OS-verwijdering in het gecombineerde systeem, inclusief 90% BTA-verwijdering. De daaropvolgende EO resulteerde in een aantal gechloreerde bijproducten waaronder GOS, ClO_3^-, ClO_4^-.

In het EO-VFCW-systeem (Scenario 2) was de verwijdering van OS vergelijkbaar met de op zichzelf staande EO-behandeling in **Hoofdstuk 2**. De daaropvolgende VFCW kon de OS verwijdering niet verbeteren door de toxische invloed van het elektrochemisch behandelde water. De plantgroei en biologische activiteit van het wetland werden sterk beïnvloed door de hoge toxiciteit. Een positief punt dat de erop volgendena-geschakelde VFCW wel toxische bijproducten zou kunnen verwijderen. In conclusie kan VFCW de verwijdering van OS en toxische bijproducten verbeteren, maar moet de vorming van schadelijke bijproducten nog steeds verholpen worden.

Het effect van elektrolyt consumptie op het EO-proces gerelateerd aan behaalde verwijdering en vorming van toxische bijproducten is beschreven in **Hoofdstuk 4**. Benzotriazole (BTA, $C_6H_5N_3$) is in deze studie gebruikt omdat het voor komt in koeltorenwater en waterlichamen in hoge concentraties. Eerst is de invloed van elektrolyt compositie (Na_2SO_4:$NaNO_3$ verhoudingen) onderzocht om de invloed hiervan op actieve de vorming en de tussenproducten van sulfaat ($SO_4^{\bullet-}$ en $S_2O_8^{2-}$) verbindingen vast te stellen. Resultaten laten zien dat een hogere Na_2SO_4:$NaNO_3$ verhouding de vorming van actieve sulfaat verbindingen stimuleert via een hydroxyl radicaal route. Deze route was minder dominant in elektrolyten met alleen sulfaat en lagere Na_2SO_4:$NaNO_3$ verhoudingen. Vergelijkbaar met de vorming van actieve sulfaat verbindingen was de EO van benzotriazole ook sneller voor hoge Na_2SO_4:$NaNO_3$ of Na_2SO_4:NaCl verhoudingen. Sulfaat verrijkte elektrolyten stimuleren ook de mineralisatie van benzotriazole, energie-efficiëntie en nog belangrijker, verlagen de vorming van gechloreerde verbindingen. Vloeistof chromatografie gekoppeld aan massa spectrometrie (LC-MS) analyse toonde aan dat er geen gechloreerde organische verbindingen waren gevonden in de 10:1 Na_2SO_4:NaCl verhouding, maar wel in de andere Na_2SO_4:NaCl verhoudingen.

Helaas kon de vorming van chloraat en perchloraat in geen enkele Na_2SO_4:NaCl verhouding voorkomen worden en werd zelfs meer dominant in de 10:10 verhouding. Op basis van de uitkomsten is geconcludeerd dat sulfaat verrijkte elektrolyten kunnen helpen voor de elektrochemische degradatie van organische verbindingen voor hogere efficiëntie, lager energieverbruik en lagere vorming van gechloreerde organische bijproducten. Nanofiltratie zou op een selectieve manier het sulfaat van het afval kunnen scheiden en sulfaat rijke condities kunnen verzorgen. Hierom kan het interessant zijn om nanofiltratie te combineren met elektrochemische oxidatie om de tekortkomingen van de EO-techniek te verhelpen.

Hoofdstukken 5 en 6 focussen op alternatieve GOP-technieken om OS te verwijderen in de aanwezigheid van chloride. **Hoofdstuk 4** liet zien dat sulfaat radicaal gebaseerde GOPs ook OS kunnen afbreken. Daarnaast lieten **Hoofdstukken 2, 3, en 4** zien dat de vorming van chloraat en perchloraat onvermijdelijk is in EO, vooral met een BDD anode bij hogere stroom. Daarom zijn fotokatalytische afbraak, hitte geactiveerde per-sulfaat afbraak en UVC/vacuüm UV GOPs bestudeerd in **Hoofdstukken 5 en 6** in de aanwezigheid van chloride ionen om verder in te gaan op de oxidatiemechanismen van organische componenten en de vorming van gechloreerde bijproducten.

De effecten van chloride en pH op kinetiek, routes, en vorming van gechloreerde bijproducten tijdens hitte geactiveerde peroxydisulfaat en peroxymonosulfaat gemedieerde afbraak van benzotriazole is bestudeerd in **Hoofdstuk 5**. Hitte geactiveerde peroxydisulfaat en peroxymonosulfaat waren allebei in staat om benzotriazole af te breken zonder de aanwezigheid van chloride. Peroxydisulfaat gemedieerde afbraak was sneller dan peroxymonosulfaat gebaseerde afbraak zonder chloride. Met de aanwezigheid van chloride is het tegenovergestelde waargenomen. Benzotriazole afbraak in peroxydisulfaat gemedieerde GOPs was langzamer door radicaal scavenging door de chloride ionen. Daartegen zorgde de interactie van peroxymonosulfate met chloride ionen voor de vorming van vrije chloor, die de benzotriazole afbraak stimuleerde. pH had een significante invloed op de peroxymonosulfaat gemedieerde GOPs, maar minder invloed op de peroxydisulfaat gemedieerde afbraak in de aanwezigheid en ook in de afwezigheid van chloride. LC-MS-analyse en data-analyse met compound discovery software toonde tweeënveertig transformatieproducten (TPs) die gevormd werden tijdens benzotriazole degradatie. Deze resultaten hielpen om de

afbraakmechanismes van benzotriazole bloot te leggen in de aanwezigheid en afwezigheid van chloride. Polymerisatie, hydroxylatie, opening van benzeen ringen, en de vorming van carboxyl-zuren waren de belangrijkste afbraakmechanismes in afwezigheid van chloride. Aan de andere kant waren chlorering, opening van triazole ringen, en nitratie mechanismes aanvullend gevonden in de aanwezigheid van chloride. In peroxymonosulfaat gemedieerde oxidatie werden meer gechloreerde transformatieproducten gedetecteerd. Daarom was de formatie van GOS en de toxiciteit op *Vibrio fischeri* bacteriën hoger voor de peroxymonosulfaat gemedieerde oxidatie. Daarnaast werd chloraat ook gevonden in dit proces, en niet in het peroxydisulfaat gemedieerde proces. Deze bevinding duidt aan dat de vorming van gechloreerde bijproducten door de aanwezigheid van actieve chloorverbindingen wordt beïnvloed. Vrije chloor was de belangrijkste precursor voor de vorming van deze gechloreerde bijproducten. Daarom moet vorming van vrije chloor vermeden worden om de vorming van gechloreerde bijproducten te minimaliseren. Dit is gelukt in de peroxydisulfaat gemedieerde oxidatie.

Verwijdering van organische stoffen en de vorming van gechloreerde bijproducten zijn vergeleken in **Hoofdstuk 6**. De volgende processen zijn vergeleken: Elektrochemische oxidatie (EO), fotokatalytische degradatie (FKD), hitte-geactiveerde peroxydisulfaat oxidatie en UVC/vacuüm UV (UVC/VUV). Hitte-geactiveerde peroxydisulfaat oxidatie behaalde OS-mineralisatie in het CTBD van meer dan 95% na een behandeling van 5 uur. Ter vergelijking werd in EO, PCD en UVC/VUV 50 tot 60% mineralisatie behaald. Gedetailleerde analyse van de humusachtige componenten toonde aan de peroxydisulfaat oxidatie de humus componenten compleet oxideerde. De andere processen oxideerde de humus componenten gedeeltelijk naar stoffen met een laag moleculair gewicht zoals bouwstenen en zuren. Fluorescentie excitatie-emissie matrices (FEEM) toonde aan dat alle fluoriderende stoffen werden verwijderd tijdens EO terwijl de TOS-verwijdering in dit proces maar 50% was. Door gedeeltelijke oxidatie en het chloreren van OS raakten ze hun fluorerende eigenschappen kwijt. Deze chlorering werd bevestigd door vorming van vrij chloor in het EO proces. Chloreerde bijproducten werden niet gedetecteerd in PCD, hitte-geactiveerde peroxydisulfaat oxidatie, en het UVC/VUV proces. Deze processen hadden ook minimale vorming van vrij chloor. Daarom zijn de GOPs gerangschikt als Hitte-geactiveerde peroxydisulfaat oxidatie > PCD, UVC/VUV > EO gebaseerd op effectiviteit en

minimalisering van de vorming van gechloreerde bijproducten bij de behandeling van zout water om OS zoals humusachtige stoffen te verwijderen.

Een complete technologietrein om KSW te hergebruiken is beschreven in **Hoofdstuk 7.** Twee technologietreinen zijn vergeleken. De eerste bestaat uit: wetland, nanofiltratie, omgekeerde osmose, en EO van het nanofiltratie-concentraat. De tweede trein bestond uit nanofiltratie, omgekeerde osmose en EO van het nanofiltratie-concentraat. De effectiviteit van de technologietrein werd geëvalueerd gebaseerd op verwijdering van zouten, verwijdering van benzotriazole, verwijdering van TOK, nanofultratieflux en vorming van gechloreerde bijproducten in de EO. Beide technologietreinen waren in staat om de geschikte waterkwaliteit voor hergebruik te produceren. In de eerste trein werd nitraat, orthofosfaat en benzotriazole verwijderd door het wetland. Het wetland produceerde meer anorganische koolstof wat resulteerde in een hogere koolstofconcentratie in het nanofiltratie permeaat en hogere fouling van het na-geschakelde nanofiltratie systeem. Divalente ionen werden verwijderd in de nanofiltratie stap, maar monovalente ionen passeerden het membraan. De omgekeerde osmose stap verwijderde de rest van de zouten en zorgde voor de gewenste waterkwaliteit. De tweede trein behaalde bijna dezelfde resultaten als de eerste trein, behalve dat benzotriazole pas in de omgekeerde osmose stap werd verwijderd. EO van het nanofiltratie-concentraat was beter en sneller en zorgde voor minder vorming van gechloreerde bijproducten. Het nanofiltratie-concentraat had een hogere SO_4^{2-}:Cl^- verhouding ten opzichte van het initiële KSW. Daarom behaalde de EO betere resultaten voor het concentraat. Aan de andere kant waren chloraat en perchloraat vorming ook hoger in het concentratie, net als aangetoond in **Hoofdstuk 4**. De uitkomst van **Hoofdstuk 7** toont aan dat meer onderzoek nodig is om de technologietrein verder te verbeteren.

Drie belangrijke uitdagingen zijn besproken in de algemene discussie (**Hoofdstuk 8)**. Als eerste, de belangrijkste resultaten van het onderzoek in deze scriptie. Dit onderzoek laat zien dat GOPs organische componenten van KSW kunnen verwijderen. Vorming van gechloreerde bijproducten beperkt de toepassing van EO. Als alternatief kan hitte-geactiveerde peroxydisulfaat oxidatie, PKD, en UVC/VUV gebruikt worden om organische stoffen te verwijderen zonder de vorming van gechloreerde bijproducten. Hitte-geactiveerde peroxydisulfaat oxidatie zou het meest interessante proces zijn vanuit de toepassing. Afvalwarmte

van de industrie kan gebruikt worden om het proces te activeren en om de energievraag te reduceren. Ten tweede, is een overzicht van de toepassing van GOPs in praktijk water gegeven. GOPs kunnen geïntegreerd worden in industriële-, gemeentelijke- en drinkwaterzuiveringstreinen. GOPs kunnen gebruikt worden als voorzuivering om niet biodegradeerbaar organisch materiaal af te breken of om microverontreinigingen en pathogenen te verwijderen tijdens nazuivering. Als laatst is een gedetailleerde studie van chloride chemie samengevat in alle moderne GOPs. De interacties van chloride in negen GOP-processen, waaronder de vier die in deze scriptie onderzocht zijn, zijn besproken. Het blijkt dat chloride ionen verschillende interacties hebben met bronnen van oxidanten en aktivatoren die betrokken zijn in de GOPs. Daarnaast laat chloride specifieke interacties zien met de reactieve oxiderende stoffen (bijvoorbeeld, hydroxyl, sulfaat radicalen of ozon atomen) die worden gevormd tijdens het oxidatieproces. Al deze interacties komen uit in verschillende reactieve chloor moleculen. Gebaseerd op literatuur is een overzicht van de reactiviteit van de organische stoffen met reactieve chloorstoffen besproken. De rol van reactieve chloorstoffen in de vorming van chloraat en perchloraat is ook bediscussieerd. Gebaseerd op deze informatie zijn de GOPs gegroepeerd in drie categorieën gebaseerd op de verwachtte vorming van gechloreerde bijproducten. Deze informatie zal stakeholders helpen om veilige GOPs te selecteren die organische componenten kunnen verwijderen uit zout (afval)water.

Acknowledgments, About the author, List of publications, and SENSE Diploma

Acknowledgments

An eventful journey comes to an end. I could not finish this long and challenging journey without the help of many people, including my supervisors, colleagues, friends, and, most importantly, my family.

Snigdha, my soulmate, I do not know the proper word to express my gratitude for what you did for the last years, still doing with your severe health condition. You always tried to make sure that I could finish my Ph.D., continue my career, and most importantly, ensure proper care of Somdip, a precious gift from GOD. Your compassion, love, and support are the best gift of my life. I still remember those days when you barely could move, but you pushed me to work and told me that you would take care of yourself and Somdip. Thank you, your sacrifice and encouragement helped me bring my Ph.D. journey to an end. Love you!

Together, a big appropriation goes to my supervisors- Huub and Harry. Without your support and guidance in my professional and personal life, I could not write this text today. Huub, thank you for always providing a positive perspective of my research outcome. Your experience in water treatment and ability to place scientific research in practice helps me think out of the box and direct my research on the right path. I really appreciate your way of providing feedback considering my emotional situation during the AIO meetings. You always said "family first," it helped me feel secure and encouraged me to move on. Your concern and immobilizing all of the resources to help me were remarkable. I am really grateful to you. Harry, such, calm and amicable human being I have ever seen. Thank you so much for all of your motivation, support, and help to become an independent researcher. Whenever I was stacked in my researcher, you were always there with your smart ideas. During my Ph.D., I learned how to approach solving a scientific dilemma from you. At the same time, I learned how to balance work and life. Once, when Somdip was born, you told me, "science could wait, but now you have to be with your family," this gave me strength. I am really thankful to you for your kindness.

I am very lucky to have amazing colleagues (no, I think more than that, like family) at ETE departments. Abiodum, Adi, Adrian, Alaaeldin, Alessio, Alette, Andrea, Andrii, Annemerel, Annemiek, Arnoud, Azie, Baptiste, Bernou, Bingnan, Carlos, casper, Cees, Dainis, Dandan, Darja, David, Delaram, Dilan, Els, Else, Elackiya, Emilius, Fatma, Farzaneh, Grietje, Gunther, Halimat, Hang, Hans, Hardy,

Hooman, Iemke, Ilse, Indra, Ivonne, Jan, Jess, Jessica, Jill, Jinsong, Jiyao, Joeri, Jouke, Justine, Kasper, Katarzyna, Koen, koen wetser, Laura, Lei, Leire, Lucia, Ludovic, Margo, Marjo, Mark, Marko, Maria, Merijn, Miriam, Momo, Nora, Paulina, Philipp, Pim, Renata, Rieks, Rikke, Rosanne, Roxani, Sanne, Sanne raes, Selin, Sha, Shahab, Shiyang, Shokouh, Silvi, Suzanne, Tania, Thomas, Tiemen, Tim, Truong, Victor, Vincent, Viola, Wenbo, Yu, Yujie, Yue, Yvonne, Zhaolu (Sorry, if I forgot someone). You are with me in all my difficult times. I did not feel alone even I was thousands of miles away from my home. Many of you renovated my newly rented house and transferred my stuff when I was with my wife and son. One of many examples of "ETE togetherness." Thank you all. Thanks again to Koen for translating and Annemerel for checking the summary.

The outstanding ETE technical team- Hans, Livio, Ilse, Jean, Katja, Pieter, Julian, Bert, and Vinnie made my time in the lab and modutech smooth and enjoyable. I find you whenever I need to analyze (un)conventional staff. Livio and Pieter, thank you for analyzing many of my samples. Special thanks to Marco Blokland for arranging the analysis at the Wageningen Food Safety Research lab, even during the Covid restriction. Thanks to amazing ETE office personnel- Liesbeth, Anita, Gea, Marjolein, Wies Lisa, Janine for arranging all the official affairs whenever necessary.

Dear Aaron, Yinong, Jiahao, Chenyu, Yicheng, Jiamin, Shakunt - thank you for choosing my research topic for your thesis and contributing to my research. Your hard work reduced my workload and gave me some space to breathe. Dear Mahsa, thank you for not saying "NO" to check my manuscript(s) even though you are super busy. You have been here at ETE only for three months, but we are still in contact. I really enjoy working and discussing science with you; I learn a lot from you. Keep in touch.

Dear Jill and Yu, thank you for being my paranymphs, helping me arrange everything to make the special day of my life more special, smooth, and enjoyable.

I acknowledge the Water Nexus project for funding and giving me the opportunity to work with amazing project partners. Special thanks to Robert Brüninghoff, Benjamin Chatillon, Daniëlle Schepers, Bastian Mei, Guido Mul, Adriaan Jeremiasse, Kitty Nijmeijer, Henk Pool, Albert Janssen, Niels de Groot, Paul Roeleveld and Arjen van Nieuwenhuijzen for all of the collaborations,

meetings, and useful discussions. Henk Pool, Albert Janssen and Niels de Groot, thank you for critical evolution of research output, which helped me to think differently. I also acknowledge shahjalal university of science and technology, Bangladesh for the study leave.

To my Bangladeshi community in Wageningen, thank you for all of your love and support. Kamonashish da & Anita (Mama & Mami of Somdip), it is impossible to list what you did, but thank you for everything. Your presence is a blessing for us. Kabir vai, Ifti vai, Uthpal da, Sazzad, Masud, and Sudip, thank you for making life enjoyable here at Wageningen. I loved the "Vasoman Tong Dokan" where we met, ate, laughed, discussed many socio-political issues of the world, especially about Bangladesh. I am also thankful to Tapos da, Sanjoy da, Rana, Kibria, Nahyan, Tanvir, Souvik, Muktader & Fariha, Mahsina apu, Mahmuda apu, Arif vai, Debasish da, Latiful Vai, Tanvir, Sami & Sharmi, Afia apu, and Faysal. Similarly, I appreciate the help of the Dutch community especially, Arun dai, Puja di, Catharien, and Erik.

আমি আমার প্রিয় পরিবারের প্রতি আমার আন্তরিক কৃতজ্ঞতা প্রকাশ করতে চাই।। বাবা ও মা, তোমাদের প্রতি কৃতজ্ঞতা প্রকাশ করার মতো শব্দ আমার কাছে নেই। তোমাদের যত্ন, ভালবাসা, অনুপ্রেরণা এবং অবিরাম প্রার্থনা আমাকে আজ এখানে নিয়ে এসেছে। আমার সমৃদ্ধি এবং প্রতিষ্ঠার জন্য তোমরা তোমদের সবকিছু ত্যাগ করেছ। তোমরা আমাকে সৎ হতে, ভালোকে অনুসরণ করতে, সাবধানে চিন্তা করতে এবং সমাজ ও দেশের জন্য ভালো করতে শিখিয়েছ। আমি আমার শাশুড়ির কাছেও কৃতজ্ঞ, আমাদের জন্য তার আত্মত্যাগের জন্য। আমি আমার কাকা, কাকি, ভাই, বোন এবং আত্মীয়দের কাছেও কৃতজ্ঞ। আমার অনুপস্থিতিতে আমার বাবা-মায়ের দেখাশুনা করার জন্য। তোমরা সবাই আমার শক্তি। আমি খুব ভাগ্যবান, আমি এই পরিবারে জন্মেছি ।

In the end, I like to thank you all from the bottom of my heart again. Keep in touch. Hope to see you again someday, somewhere.

Stay happy

Pradip

About the author

Pradip Saha was born in December 1983 in Tangail, Bangladesh. He completed his bachelor's in chemical engineering & Polymer Science from Shahjalal University of Science & Technology (SUST), Bangladesh. During his final year of bachelor study, he worked in the application of membrane technology for water and wastewater treatment within a project entitled "INNOWA" endorsed by the European Commission. After completing his bachelor's study, He worked in the Chlor-Alkali industry (Membrane Electrolysis) for two years and one year in a High-pressure boiler water treatment plan. Then in 2010, he started his professional academic career in the CEP department at SUST as a faculty. To enrich his academic career, he pursues a master's degree (general) in Chemical Engineering & Polymer Science from SUST, Bangladesh. In 2014, he started his second master's degree in Environmental Technology at Wageningen University and Research (WUR) with The Netherlands Fellowship Program (NFP) scholarship. As part of his study, he was involved in research on Optimizing biocathodes for acetate production in a Bio-electrochemical System (BES) at the Wetsus-European center of excellence for sustainable water technology, Leeuwarden, Netherlands. Directly after obtaining his master's degree in 2016, he was sleeted for conducting his Ph.D. research in the department of Environmental Technology at WUR, Netherlands, under the NOW Water Nexus program. His PhD is about application of advanced oxidation for the removal of organic pollutants from saline (industrial) wastewater.

List of publications

Part of this thesis:

1. **Saha, Pradip,** Thomas V. Wagner, Jiahao Ni, Alette AM Langenhoff, Harry Bruning, and Huub HM Rijnaarts. "Cooling tower water treatment using a combination of electrochemical oxidation and constructed wetlands." Process Safety and Environmental Protection 144 (2020): 42-51.
2. **Saha, Pradip,** Harry Bruning, Thomas V. Wagner, and Huub HM Rijnaarts. "Removal of organic compounds from cooling tower blowdown by electrochemical oxidation: Role of electrodes and operational parameters." Chemosphere 259 (2020): 127491.
3. **Saha, Pradip,** Yicheng Wang, Mahsa Moradi, Robert Brüninghoff, Gholamreza Moussavi, Bastian Mei, Guido Mul, Huub HM Rijnaarts, and Harry Bruning. "Advanced oxidation processes for removal of organics from cooling tower blowdown: Efficiencies and evaluation of chlorinated species." Separation and Purification Technology 278 (2022): 119537.
4. **Saha, Pradip,** Jiamin Wang, Yinong Zhou, Livio Carlucci, Adriaan W. Jeremiasse, Huub HM Rijnaarts, Harry Bruning,. " Effect of electrolyte composition on electrochemical oxidation: active sulfate formation, benzotriazole degradation, and chlorinated by-products distribution." (submitted, 2021).
5. **Saha, Pradip,** Chenyu Zhou, Mahsa Moradi, Marco Blokland,, Huub HM Rijnaarts, Harry Bruning,. " Heat-activated peroxydisulfate and peroxymonosulfate mediated degradation of benzotriazole: effects of chloride and pH on kinetics, pathways and product toxicity." (in preparation).
6. Thomas V. Wagner, **Saha, Pradip,** Harry Bruning, and Huub HM Rijnaarts. " Lowering the industrial freshwater footprint: A treatment technology train to reuse discharged cooling tower water in the cooling tower itself." (in preparation)

Other publications:

1. Brüninghoff, Robert, Alyssa K. Van Duijne, Lucas Braakhuis, **Pradip Saha,** Adriaan W. Jeremiasse, Bastian Mei, and Guido Mul. "Comparative Analysis of Photocatalytic and Electrochemical Degradation of 4-Ethylphenol in Saline Conditions." Environmental science & technology 53, no. 15 (2019): 8725-8735.
2. Robert Brüninghoff, **Pradip Saha,** Piotr M. Krzywda, Adriaan W. Jeremiasse, Guido Mul, Bastian Mei, Cathodic reduction of oxychlorides in electrooxidized saline water; (in preparation)

Netherlands Research School for the
Socio-Economic and Natural Sciences of the Environment

D I P L O M A

for specialised PhD training

The Netherlands research school for the
Socio-Economic and Natural Sciences of the Environment
(SENSE) declares that

Pradip Saha

born on December 7th 1983 in Tangail, Bangladesh

has successfully fulfilled all requirements of the
educational PhD programme of SENSE.

Wageningen, February 16th 2022

Chair of the SENSE board

Prof. dr. Martin Wassen

The SENSE Director

Prof. Philipp Pattberg

The SENSE Research School has been accredited by the Royal Netherlands Academy of Arts and Sciences (KNAW)

KONINKLIJKE NEDERLANDSE
AKADEMIE VAN WETENSCHAPPEN

The SENSE Research School declares that **Pradip Saha** has successfully fulfilled all requirements of the educational PhD programme of SENSE with a work load of 39.6 EC, including the following activities:

SENSE PhD Courses

- Environmental research in context (2017)
- Research in context activity: 'Organizing WATER NEXUS –Final symposium and Brochure publication '(2021)

Selection of Other PhD and Advanced MSc Courses

- Systematic literature review, Wageningen School of Social Sciences (2017)
- Environmental Electrochemical Engineering, Wageningen University (2021)
- The Essentials of Scientific Writing and Presenting, Wageningen Graduate Schools (2017)
- Reviewing a Scientific Paper, Wageningen Graduate Schools (2016)
- Project and Time Management, Wageningen Graduate Schools (2016)
- Start to teach, Wageningen Graduate Schools (2019)
- Teaching and supervising Thesis students, Wageningen University (2016)
- Scientific Writing, Wageningen Graduate Schools (2018)
- Workshop Scientific Publishing, Wageningen Graduate Schools (2019)

Management and Didactic Skills Training

- Organiser of colloquia in ETE chair group (2016-2017)
- Member of PhD council (2019)
- Teaching in and developing the BSc thesis course 'Environmental Technology Part 1: Design Tools' (2016)
- Supervising one BSc and seven MSc thesis students (2016-2021)
- Teaching in the BSc course 'Basic Technologies for Urban Environmental Management' (2020) and the MSc course 'Managing urban environmental infrastructure' (2021)

Selection of Oral Presentations

- *Electrochemical oxidation and mineralization of cooling tower blowdown water organic compounds.* 25th Topical meeting of The International Society of Electrochemistry, 12-15 May 201, Toledo, Spain
- *Comparison of electrochemical and vacuum ultraviolet (VUV)-based oxidation processes for cooling tower blowdown treatment-a case study.* 12th European symposium on electrochemical engineering, 14-17 June 2021, Leeuwarden, The Netherlands
- *Cooling tower water characterisation and treatment - Dow Benelux, Terneuzen case study*. Industrial Water DECHEMA-Haus, 17 - 19 November 2020, Frankfurt am Main, Germany

SENSE coordinator PhD education

Dr. ir. Peter Vermeulen

This research was financed by the Netherlands Organisation for Scientific Research (NWO), which is partly funded by the Ministry of Economic Affairs and Climate Policy and co-financed by the Netherlands Ministry of Infrastructure and Water Management and partners of the Dutch Water Nexus consortium (project number 14301, Water Nexus 2.3).

Final support from Wageningen University for printing this thesis is gratefully acknowledged.

Cover page concept: Pradip Saha

Cover page design: Zahid Hossain (https://zahidhossaintaniv.wixsite.com/illustrations)

Thesis Layout: Pradip Saha

Printed by ProefschriftMaken, (https://www.proefschriftmaken.nl)